QCD corrections to Higgs observables at hadron colliders

Author(s):
Bühler, Stephan A.

Publication Date:
2013

Permanent Link:
https://doi.org/10.3929/ethz-a-010060807

Diss. ETH No. 21389

QCD Corrections to Higgs observables at hadron colliders

A thesis submitted to attain the degree of

DOCTOR OF SCIENCES of ETH ZÜRICH

(Dr. sc. ETH Zürich)

presented by

Stephan Andreas Bühler

Msc Physik, ETH Zürich
born on 11.05.1985
citizen of Uster ZH

accepted on the recommendation of

Prof. C. Anastasiou, examiner
Prof. T. Becher, co-examiner

2013

"La science, mon garçon, est faite d'erreurs, mais d'erreurs qu'il est bon de commettre, car elles mènent peu à peu à la vérité."

Jules Verne, *Voyage au centre de la terre*

Abstract

The Higgs mechanism as a way to give masses to fundamental particles in a gauge-invariant way was introduced nearly 50 years ago. Ever since, high energy experiments conducted at particle accelerators have looked for evidence of the Higgs boson, until its discovery was finally confirmed by two experiments at the Large Hadron Collider in Geneva in July 2012.

The dominant production mode for Higgs bosons at hadron colliders is the gluon fusion process which accounts for about 90% of the overall rate in the Standard Model of particle physics. At the same time, the gluon fusion cross section is sensitive to possible physics beyond the Standard Model because it is a loop-induced process. Hints for new physics may thus be visible in small deviations of the Higgs production rate from the Standard Model prediction.

The main focus of this thesis is therefore the best possible description of gluon fusion process in the Standard Model of particle physics as well as in generic extensions of it. This goal is achieved in the computer program `iHixs` which incorporates all contributions to gluon fusion through next-to-next-to-leading order in Quantum Chromodynamics and next-to-leading order in the electroweak theory for an arbitrary number of heavy quarks and coupling strengths different from the ones predicted by the Standard Model of particle physics. `iHixs` furthermore allows to properly estimate the various theoretical uncertainties associated with parton distribution functions, the treatment of the Higgs width and the sensitivity to renormalisation and factorisation scales. To properly account for enhanced bottom quark couplings, the next-to-next-to-leading order result for direct bottom quark fusion in Quantum Chromodynamics is included, too.

Using `iHixs`, we give a phenomenological profile of the Higgs boson, investigating the numerical importance of various contributions and check the validity of some approximations that are usually employed in experimental searches.

Based on the observation that the theoretical uncertainty of the next-to-next-to-leading order gluon fusion cross section is still fairly large, we furthermore calculate a part of the cross section at another order higher in the strong coupling, which allows us to estimate the uncertainty of the next order due to renormalisation and factorisation

scales. We find that for some reasonable assumptions, the remaining uncertainty will be below 5%.

Further contents of the thesis consist of the description of the development of the computer code Chaplin which allows for the numerical evaluation of a special class of functions, the so-called harmonic polylogarithms for any complex argument up to weight four in the index vector. The availability of this code simplified the implementation of various features of the code `iHixs` significantly and was developed for this reason. It will be useful in many other applications in high-energy physics, though.

Finally, we briefly present the computation of the fully differential Higgs production cross section through bottom quark fusion, focusing on the method of bare parton distribution functions to cancel infrared divergences associated with initial-state radiation, and provide selected results for a handful of differential observables.

Zusammenfassung

Der Higgs-Mechanismus, welcher es ermöglicht Elementarteilchen eine Masse zu geben ohne dabei die Eichsymmetrie der zugrundeliegenden Theorie zu verletzen, wurde vor fast 50 Jahren gefunden. Seither wurde an verschiedenen Hochenergie-Experimenten an Teilchenbeschleunigern nach Spuren des Higgs-Bosons gesucht, bis seine Entdeckung schliesslich im Juli 2012 von zwei Experimenten am LHC-Beschleuniger in Genf bestätigt wurde.

An Hadron-Beschleunigern wie dem LHC ist der dominierende Produktionsmechanismus für Higgs-Bosonen die Verschmelzung zweier Gluonen zu einem Higgs-Boson, genannt Gluon-Fusion. Er trägt ungefähr 90% zur gesamten Higgs-Produktion im Standardmodell der Teilchenphysik bei. Ausserdem ist der Gluon-Fusion-Prozess wegen seiner Schleifen-Natur empfindlich auf Physik jenseits des Standardmodells. Hinweise auf neue physikalische Phänomene könnten deswegen in einer kleinen Abweichung der Higgs-Produktions-Rate vom der Standardmodell-Vorhersage zu finden sein.

Aufgrund dieser Motivation liegt das Hauptaugenmerk dieser Arbeit auf der bestmöglichen Beschreibung des Gluon-Fusion-Prozesses im Standardmodell der Teilchenphysik und seiner allgemeinen Erweiterungen. Dies wird erreicht in Form eines Computerprogramms namens `iHixs`, welches alle Beiträge zum Gluon-Fusion-Prozess in nächst-zu-nächst-zu-führender störungstheoretischer Ordnung in der Quanten-Chromodynamik und nächst-zu-führender Ordnung in der elektroschwachen Theorie vereint. Der Produktionsquerschnitt kann für eine beliebige Anzahl schwerer Quarks berechnet werden, deren Kopplung zum Higgs-Boson von den Standardmodell-Kopplungen abweichen können. `iHixs` kann ausserdem die theoretische Unsicherheit aufgrund von Partonverteilungsfunktionen, der verschiedenen Möglichkeiten den Higgs-Propagator zu beschreiben und der Abhängigkeit von den nichtphysikalischen Renormierungs- und Faktorisierungs-Skalen berechnen. Um eine vollständige Beschreibung im Falle von verstärkter Kopplung des Bottom-Quarks zum Higgs-Boson zu erreichen wurde ausserdem auch der Prozess der direkten Bottom-Quark-Verschmelzung in nächst-zu-nächst-zu-führender Ordnung der Quanten-Chromodynamik implementiert.

Mithilfe von `iHixs` wird dann ein phänomenologisches Profil des Higgs-Bosons erstellt.

Dabei untersuchen wir den numerischen Einfluss verschiedener Beiträge zum gesamten Wirkungsquerschnitt und überprüfen Vereinfachungen, welche in Experimenten gewöhnlich angewandt werden.

Da die theoretische Unsicherheit des Higgs-Produktions-Wirkungsquerschnitts auch in nächst-zu-nächst-zu-führender Ordnung noch ziemlich gross ist, berechnen wir ausserdem einen Teil der nächst-höheren Ordnung in Quanten-Chromodynamik. Dies ermöglicht es uns, die Skalenabhängigkeit der nächst-höheren Ordnung abzuschätzen. Unter gewissen Annahmen bezüglich der fehlenden Beiträge finden wir eine verbleibende Unsicherheit von weniger als 5%.

Des Weiteren beschreiben wir die Entwicklung des Computerprogramms Chaplin, welches eine spezielle Klasse von mathematischen Funktionen, die sogenannten harmonischen Polylogarithmen, numerisch auszuwerten vermag. Insbesondere kann Chaplin die Polylogarithmen für ein beliebiges komplexes Argument auswerten, wobei Index-Vektoren bis zu einem Gewicht von vier unterstützt sind. Die Verfügbarkeit dieses Codes vereinfachte die Implementierung vieler Bereiche von `iHixs` massiv, und er kann in vielen anderen Rechnungen in der theoretischen Teilchenphysik weiterverwendet werden.

Schliesslich geben wir noch einen kurzen Einblick in eine weitere Rechnung, welche den vollständig differenziellen Higgs-Produktionsquerschnitt durch Bottom-Quark-Fusion beschreibt. Dabei konzentrieren wir uns auf die Methode der nackten Partonverteilungsfunktionen um Infrarot-Divergenzen aus Strahlungskorrekturen des Anfangszustandes aufzuheben, und präsentieren einige Resultate für differenzielle Observablen.

Contents

Contents **v**

List of Figures **ix**

List of Tables **xiii**

1. Introduction **1**

2. Theory **5**

2.1. The Standard Model of particle physics 5
2.2. Lagrangian density of the strong interaction 8
2.3. Perturbative QCD calculations 11
2.3.1. Regularisation 11
2.3.2. Renormalisation 14
2.3.3. Partonic cross sections and the D-dimensional phase-space 18
2.3.4. Hadronic cross section and mass factorisation 20

3. Inclusive Higgs boson hadroproduction at NNLO **25**

3.1. Notation and leading order result 26
3.2. NLO QCD corrections 29
3.2.1. $gg \to H\,(g)$ 30
3.2.2. $q\bar{q} \to Hg$ 32
3.2.3. $qg \to Hq$ 32
3.3. Electroweak contributions 33
3.4. Heavy quark effective theory and NNLO QCD corrections 37
3.4.1. Mixed QCD-electroweak corrections 41
3.4.2. Combining exact and effective corrections 42
3.4.3. Improving the effective theory approach 44
3.5. Higgs propagator treatment 45
3.6. Bottom quark fusion 48

3.7. Description of the program `iHixs` . . . 49
3.7.1. Usage . . . 50
3.7.2. Setting options and variables . . . 50
3.8. Conclusions . . . 54

4. Harmonic polylogarithms and the Chaplin library **57**
4.1. Definition and properties . . . 58
4.1.1. Shuffle algebra . . . 60
4.1.2. Representation as nested sums and values at ± 1 . . . 61
4.1.3. Analytic continuation . . . 62
4.2. The strategy for numerical evaluation . . . 62
4.2.1. Reduction to basis functions and inversion mappings . . . 63
4.2.2. Numerical evaluation of the basis functions . . . 67
4.3. The Chaplin library . . . 69
4.4. Conclusions . . . 70

5. Phenomenology of Higgs production **73**
5.1. Perturbative convergence and scale uncertainty . . . 73
5.2. PDF comparisons . . . 77
5.3. Electroweak contributions . . . 81
5.4. Higgs propagator treatment . . . 82
5.5. Heavy quark effects . . . 85
5.5.1. Effective vs. exact NLO top-only . . . 85
5.5.2. SM bottom quark contributions . . . 88
5.5.3. Top width effects . . . 90
5.5.4. Standard model with a fourth generation . . . 92
5.5.5. Enhanced bottom Yukawa coupling . . . 93
5.6. Conclusions . . . 95

6. QCD Contributions beyond NNLO to gluon fusion **99**
6.1. Higher terms in ϵ of lower-order cross sections . . . 100
6.1.1. Leading and next-to-leading order . . . 100
6.1.2. Integration-by-parts identities . . . 103
6.1.3. The method of reverse unitarity . . . 105
6.1.4. The method of differential equations . . . 107
6.1.5. NNLO master integrals to $\mathcal{O}(\epsilon)$ . . . 111
6.1.6. Double-real master integrals . . . 111

6.1.7. Real-virtual master integrals 127
6.1.8. Double-virtual master integrals 131
6.2. Convolutions of collinear factorisation kernels and lower-order cross sections 132
6.2.1. Convolutions involving delta-terms 134
6.2.2. Convolutions of two plus-distributions 135
6.2.3. Regular convolutions 138
6.2.4. Soft expansion of the convolutions 142
6.3. Numerical results 143
6.3.1. Poles of the N^{3}LO gluon fusion cross section 144
6.3.2. Scale dependence of the N^{3}LO gluon fusion cross section 146
6.4. Conclusions 154

7. Differential Higgs production in bottom quark fusion 157
7.1. Differential Calculations 158
7.1.1. Bare parton distribution functions 161
7.2. Results 163
7.3. Conclusions 167

8. Outlook 169

Appendices 171

A. D-dimensional phase-spaces for Higgs production 173

B. Splitting Kernels 177

C. Re-installing scale dependence and separating scales 181

D. Reduction of HPLs to Basis functions 185
D.1. Weight one and two 185
D.2. Weight three 186
D.3. Weight four 187

Bibliography 195

List of Figures

1.1. Higgs production mechanisms at hadron colliders. (a) Gluon fusion, (b) Vector boson fusion, (c) Higgs strahlung, (d) Associated production. . . . 3

2.1. The strong coupling α_s as a function of the energy scale Q. 17
2.2. A graphical representation of factorisation for the DIS process. 21

3.1. Leading order diagram for the gluon fusion process. 27
3.2. Behaviour of the complex variable x_q. 28
3.3. Sample diagrams for the processes contributing to the NLO QCD corrections to the gluon fusion process. 30
3.4. Two-loop electroweak contributions to Higgs production in gluon fusion. . 33
3.5. One-loop electroweak contributions to the processes $qg \to Hq$ and $q\bar{q} \to Hg$. 35
3.6. Graphical representation of the heavy-quark effective theory. The loop with the heavy quark running inside is absorbed into an effective vertex. . 37
3.7. Branching ratios of the most important Higgs decay channels as a function of the Higgs mass. Figure from ref. [89], obtained with the program `Hdecay`. 45
3.8. Sample diagrams for the bottom quark fusion process. 48

4.1. The different regions of the complex plane in the Chaplin library. 69

5.1. The first three orders of the gluon fusion cross section as a function of the Higgs mass for the 8 (left) and 13 (right) TeV LHC. The bands represent the scale-uncertainty. 74
5.2. Left: The gluon fusion cross section as a function of the centre-of-mass energy of the pp-collider. Right: Scale uncertainty of the first three orders of the gluon fusion cross section with μ_r and μ_f varied simultaneously. . . 75
5.3. Separate dependence on μ_r (left) and μ_f (right) of the gluon fusion cross section for the 8 TeV LHC. 75
5.4. Comparison of the NNLO cross section for different PDF providers at 8 TeV. See text for explanations about the various points. 78

5.5. Comparison of the NNLO cross section for different PDF providers at 13 TeV. See text for explanations about the various points. 79

5.6. Numerical impact of the electroweak corrections as a function of the Higgs mass. Solid line: virtual corrections only, dashed line: virtual plus real corrections. 81

5.7. Numerical impact of the four different schemes for the treatment of the Higgs propagator as a function of the Higgs mass, for the 8 TeV LHC. Top panel: absolute cross section, bottom panel: relative differences. . . . 83

5.8. The normalised invariant mass distribution of the Higgs boson with m_H = 200, 400, 600, 800 GeV, in the default and the Seymour scheme. 84

5.9. The relative difference of the exact and effective NLO cross sections as defined in eq. (5.2), in the $\overline{\mathrm{MS}}$ and OS renormalisation schemes. 85

5.10. The real (solid) and imaginary (dashed) part of the two-loop amplitude $\mathcal{G}^{(2l)}$ in the OS scheme and the scheme dependent piece $\mathcal{F}^{(2l,b)}$. 87

5.11. The exact and effective NLO cross sections for Higgs masses around the $t\bar{t}$-threshold for three different scale choices. Left panel: $\overline{\mathrm{MS}}$ scheme, right panel: OS scheme. 88

5.12. The exact NLO cross sections in all combinations of scheme and scale choice for the whole Higgs mass range. 89

5.13. Impact of bottom quarks on the NNLO Higgs production cross section. Dashed lines: gluon fusion only, solid lines: gluon fusion plus bottom quark fusion. 89

5.14. Top width effects. Left panel: same plot as in fig. 5.9, but with a Γ_t = 2 GeV. Right panel: Relative difference of the NNLO cross section with $\Gamma_t = 0$ and $\Gamma_t = 2\,\mathrm{GeV}$. 91

5.15. Ratio of the NNLO QCD gluon fusion cross section in the SM4 and and the SM as a function of the Higgs mass. 92

5.16. Higgs production cross section for m_H = 125 GeV at the 8 TeV LHC as a function of a variable bottom Yukawa coupling. Left panel: absolute cross sections, right panel: Scale uncertainties 94

6.1. Scale variation of the different orders of the gluon fusion cross section at 8 TeV. μ_f is fixed to m_H and only μ_r is varied. The scaling coefficient K is varied from 0 to 40 to estimate the impact of the unknown N^{3}LO contributions. 149

6.2. Scale variation of the different orders of the gluon fusion cross section at 8 TeV. μ_f and μ_r are varied simultaneously. The scaling coefficient K is varied from 0 to 40. 149
6.3. Scale variation of the different orders of the gluon fusion cross section at 14 TeV. μ_f is fixed to m_H and only μ_r is varied. The scaling coefficient K is varied from 0 to 40. 150
6.4. Scale variation of the different orders of the gluon fusion cross section at 14 TeV. μ_f and μ_r are varied simultaneously. The scaling coefficient K is varied from 0 to 40. 151
6.5. Scale variation of the different orders of the gluon fusion cross section at 8 TeV. In (a) μ_r is varied along the x-axis, while the bars represent variation of μ_f around the central value $m_H/2$. In (b) μ_r is fixed to m_H and only μ_f is varied. The scaling coefficient K is varied from 0 to 40. 151
6.6. Scale variation of the different orders of the gluon fusion cross section at 8 TeV. μ_f is fixed to m_H and only μ_r is varied. K is varied from 0 to 30. Only the gg channel is plotted, and compared to the results obtained with the program `gghiggs` [192]. 152
6.7. 2-D contour plots of the LO, NLO and NNLO cross section at the 8 TeV LHC. The value on the contours is the cross section in picobarns. The x-axis is $\log_2(\mu_f)$, the y-axis $\log_2(\mu_r)$. Our preferred central scale choice is located at (-1,-1). 154
6.8. 2-D contour plots of the approximated N^{3}LO cross section at the 8 TeV LHC. The value on the contours is the cross section in picobarns. The x-axis is $\log_2(\mu_f)$, the y-axis $\log_2(\mu_r)$. Our preferred central scale choice is located at (-1,-1). 155

7.1. Parton distributions for some selected partons, evaluated at a scale typical for the processes described in this thesis. 163
7.2. The Higgs rapidity distribution. The bands describe the uncertainty due to the factorisation scale 164
7.3. The transverse momentum distribution of the Higgs. 165
7.4. Double-differential distribution in rapidity and transverse momentum of the Higgs boson. 166
7.5. The 0-, 1- and 2-jet rate as a function of the p_T used in the jet definition. 167

List of Tables

5.1. Values for the three orders of the cross section and their scale uncertainties for *pp*-colliders at different centre-of-mass energies. 76
5.2. NNLO gluon fusion predictions using different PDF sets and their associated uncertainties for the LHC at 8 and 13 TeV. 80

6.1. Cross sections and scale uncertainties for the 8 TeV LHC. The central scale choice is $\mu_r = \mu_f = m_H/2$, and uncertainties are found by varying the two scales simultaneously by a factor of two. 153

Nomenclature

$\overline{\text{MS}}$ modified Minimal Subtraction scheme

N^{3}LO next-to-next-to-next-to-leading order

BSM Beyond the Standard Model

DGLAP Dokshitzer-Gribov-Lipatov-Altarelli-Parisi

eV Electronvolt

HQET Heavy-quark effective theory

IBP Integration-by-parts

IR Infrared

LHC Large Hadron Collider

LO Leading order

NLO Next-to-leading order

NNLO Next-to-next-to-leading order

OS On-shell scheme

PDF Parton distribution function

QCD Quantum Chromodynamics

QED Quantum Electrodynamics

RGE Renormalisation group equation

SM Standard Model of particle physics

UV Ultraviolet

1. Introduction

The achievements of humankind are manifold. Among them, science, the systematical acquisition and organisation of knowledge, stands out as one of the biggest accomplishments. Since the beginning of civilisation, the quest to observe and consequently explain nature in all its manifestations, as well as passing the acquired knowledge on to further generations has been undertaken by scientists with great success. Science has since branched out into further areas which are not directly related to nature such as sociology or the more abstract study of mathematics and logic, and also philosophy.

Physics is the science of the fundamental constituents of matter and their dynamics. More than in any other natural science, the principle of reductionism which describes an object as the sum of its constituents and their interactions, has been enormously successful, leading to the notion of only few fundamental particles and forces to govern all phenomena observed in nature.

A notable example for reductionism at work is the famous gold-foil experiment by Rutherford conducted in 1909, where it was observed that alpha-particles fired at gold atoms can scatter at very large angles. This led Rutherford to the conclusion that the positive charge of an atom is accumulated in a very small nucleus and shortly thereafter to the proposal of protons and neutrons as building blocks of any atom. The particle content to describe matter thus shrank from many dozens, a fundamental atom for each known element, to just the three constituents protons, neutrons and electrons.

The experiment of Rutherford is notable for another reason. It marks the beginning of experimental particle physics using particle collider experiments. At atomic and subatomic length scales, forces can not be measured directly. Instead, measuring scattering angles and energies of particles emerging from a collision must be interpreted to infer the underlying force of the interaction. Ever since Rutherford, experimental progress in sub-atomic physics has come from scattering experiments almost exclusively.

When later in the 20$^{\text{th}}$ century such collider experiments started to discover a wealth of new, apparently fundamental particles called hadrons, reductionism again proved to be fruitful in the form of the proposal by Gell-Mann and Zweig that protons, neutrons and all the newly found particles were in fact built from the same building blocks themselves, called quarks. Today, we believe that all matter consists of quarks and leptons (the electron and its heavier copies) which are the fundamental constituents of nature.

On the theoretical side, a similar condensation of concepts was successfully achieved. Neglecting the gravitational force for the moment, any interaction among quarks and leptons is described by just two theories, Quantum Chromodynamics (QCD) and electroweak theory which is the unification of Quantum electrodynamics (QED) and the weak nuclear interaction. Starting with the first attempts of Dirac to formulate the revolutionary concepts of Quantum mechanics in a way consistent with the special relativity of Einstein and culminating with the reductionistic realisation of Salam and Weinberg that the electromagnetic and weak forces actually originate from the same fundamental theory, the pair of QCD and the electroweak theory, which is usually called the Standard model (SM) of particle physics, emerged as a very elegant and predictive theory that has been tested to unprecedented precision during the last fifty years in experiments around the world and remains yet to be falsified.

Yet, while one after the other prediction was confirmed by high-energy collider experiments, one crucial feature of the Standard model could not be found for more than forty years, where we are of course talking about the famous Higgs boson, the physical manifestation of the Higgs mechanism which breaks electroweak symmetry and gives the electromagnetic and the weak force their different phenomenology. In order for the Standard model to be theoretically consistent, there has to be at least one Higgs boson, whose mass nevertheless is not constrained by any theoretical considerations.

The Higgs boson was first looked for in earnest at the electron-positron collider LEP at CERN during the 1980s and 1990s. While the LEP experiment in general was a huge success, no traces of the Higgs boson could be found and only a lower limit on its mass could be set. With the knowledge we have today, it is actually conceivable that LEP was tantalisingly close to the Higgs discovery, as its final centre-of-mass energy was just a few Giga-electronvolts (GeV) shy of the energy needed to produce a 125 GeV Higgs boson.

Since accelerating electrons becomes increasingly difficult at high energies due to radiative energy losses, the next generation of experiments chose to collide hadrons, protons to be specific, which allow for much higher collision energies due to their large mass. This led to the construction of the proton-antiproton collider TeVatron at Fermilab at the beginning of the 1990s and the Large hadron collider (LHC) at CERN from 2002 to 2008, and ultimately to the discovery of the Higgs boson at a mass of about 125 GeV as announced on July 4, 2012.

For both the experimental and theoretical particle physics community, the transition

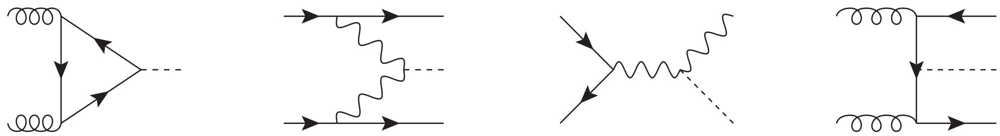

(a) (b) (c) (d)

Figure 1.1.: Higgs production mechanisms at hadron colliders. (a) Gluon fusion, (b) Vector boson fusion, (c) Higgs strahlung, (d) Associated production.

from lepton to hadron colliders had challenging implications, as hadrons are composite objects and generate much messier collider signatures. Computations for hadron colliders are more complicated than their electron-positron counterparts because the colliding protons can not be described in perturbative quantum field theory alone but also need non-perturbative input, and since the initial particles are charged under the strong interaction, QCD processes dominate the physics in these machines.

Most importantly, the strong interaction, as its name hints, has a relatively large coupling constant, which means that perturbation theory in the strong coupling converges much slower than in electroweak processes. Calculating higher-order corrections in perturbative QCD to every process of interest is therefore mandatory to provide reliable predictions for the physics at hadron colliders. The production cross section for SM processes which are already established can be tuned to data in kinematically well understood regions once a collider is up and running, and usually next-to-leading order (NLO) corrections in QCD suffice to describe these processes.

This was obviously not true for the Higgs production rate prior to discovery, which in turn means that we need to understand Higgs production processes at the highest precisions which are computationally accessible. There are multiple ways to produce a Higgs boson at a hadron collider, the most important of which are depicted in the language of Feynman diagrams in figure 1.1. The by far most prolific production mechanism is the gluon fusion process, which accounts for more than half of the total Higgs production rate at the LHC over the whole mass range from 90 GeV to 1 TeV, and for about 90% of the rate for the physical case of the Higgs mass being at 125 GeV.

It was thus clear that the best possible understanding of Higgs production through gluon fusion is absolutely crucial for the discovery of the Higgs and the consequent determination of its properties. This thesis is devoted to this task of providing the best estimate for the gluon fusion production cross section at the LHC, taking into account all relevant contributions. And since any number in science is only meaningful when it comes with an uncertainty, the proper estimation of all theoretical uncertainties for gluon fusion was an equally important goal.

The thesis is organised as follows. In chapter 2, we briefly introduce the Standard model of particle physics and some more specific theoretical techniques that will be used throughout the thesis. In chapter 3, we collect all available fixed-order contributions in perturbative quantum field theory to the gluon fusion process and describe the computer code `iHixs` that combines these results into numerical predictions for the Higgs production rate at hadron colliders. In chapter 4 we briefly meander to the description of a crucial ingredient to the `iHixs` program, the library Chaplin which numerically evaluates a special class of functions, the so-called harmonic polylogarithms (HPLs) for any complex argument. In chapter 5 we draw a phenomenological profile of the Higgs boson using `iHixs`, investigating the impacts of various contributions to gluon fusion on the inclusive cross section. In chapter 6, we provide parts of the next-to-next-to-next-to-leading order ($\mathrm{N^3LO}$) QCD corrections to gluon fusion, going into a bit more calculatory details. The obtained $\mathrm{N^3LO}$ pieces are subsequently used to estimate the uncertainty of the full $\mathrm{N^3LO}$ corrections. Finally, in chapter 7, we shortly present another computation which we performed, the fully differential Higgs production through bottom quark fusion through NNLO QCD. Conclusions are always given per chapter, and we wrap up the thesis with a short outlook in chapter 8.

It is simply stunning how much our knowledge of the world has progressed during the last century, and one can argue that we live in a golden age of particle physics now that the Higgs boson has been discovered and for the first time ever, we have a theoretically consistent[1] model explaining all high-energy physics phenomena. However, it would be nothing short of arrogant to think that we have come close to the final truth regarding our understanding of the fundamental forces of nature. History tells us that every model will eventually be falsified, and perhaps even be considered a mistake by future generations. But this is really and ultimately the way science works, which is why we have chosen the quote [1] on the first page which we translate to English here:

> *"Science, my lad, is made up of mistakes, but they are mistakes which it is useful to make, because they lead little by little to the truth."*

This is true for science as a whole, but even more so for everyday scientific research, as the author had to find out. Still, the urge to understand nature keeps us making these mistakes, and there are few feelings as rewarding as the brief burst of enlightenment when a handful of these mistakes line up to a tiny grain of truth.

[1] Albeit arguably fine-tuned

2. Theory

In this chapter we will introduce the most important theoretical concepts used in this thesis. It is by no means complete, and we kindly refer the reader to the various excellent books which cover the prerequisites like field theory and quantisation of non-abelian gauge theories [2–6], electroweak symmetry breaking [6, 7] or perturbative calculations and particle-physics phenomenology [8–11]. To the physics-inclined reader with no prior knowledge of quantum field theory, we recommend the very accessible book by Zee [12].

We will start with a short section on the Standard model of particle physics and the Higgs mechanism, without going into any detail except for the theory of the strong interaction, which is covered in the second section. The remaining sections of the chapter cover some concepts in perturbative Quantum Chromodynamics (QCD) that will be used in the latter chapters of this thesis.

2.1. The Standard Model of particle physics

The Standard Model of particle physics (SM) unites the description of the electromagnetic, the weak and the strong nuclear interaction using the language of local gauge-field theory.

The particles that constitute matter are described by fermionic fields, and are divided into leptons and quarks. Leptons are only charged under the electromagnetic and the weak force, while quarks are also charged under the strong force and thus take part in all interactions the SM describes. There are three so-called generations (or families) in both the lepton and the quark sector, where each generation consists of an $SU(2)$ doublet,

$$\begin{pmatrix} e^- \\ \nu_e \end{pmatrix} \begin{pmatrix} \mu^- \\ \nu_\mu \end{pmatrix} \begin{pmatrix} \tau^- \\ \nu_\tau \end{pmatrix}, \quad \begin{pmatrix} u \\ d \end{pmatrix} \begin{pmatrix} c \\ s \end{pmatrix} \begin{pmatrix} t \\ b \end{pmatrix}. \tag{2.1}$$

The charged leptons are called the electron, the muon and the tau, each of which is accompanied by a corresponding neutrino. The quarks are called down, up, strange, charm, bottom and top quark. The charged leptons have an electric charge of -1 normalised to the elementary electric charge, while the neutrinos are electrically neutral, which means that they only interact via the weak force. Quarks of the "up" kind (u, c, t) have an electric charge of $+2/3$, while the "down" type quarks (d, s, b) carry $-1/3$ of the elementary electric charge. Notice that the origin of both the number of generations and the fractional charges of the quarks remain a mystery up to the present day, they are not predicted by the SM.

The three interactions are transmitted by bosonic fields, as it is common in quantum field theory. The electromagnetic force is transmitted by the massless photons and couples to all electrically charged particles. It can be described by the Abelian gauge-theory which belongs to the symmetry group $U(1)$. The weak interaction couples to all known matter particles via the massive $W^{\pm}$ and Z^0 bosons, where the force transmitted by the former is sometimes called charged-current interaction, and the one by the latter is referred to as the neutral current interaction. The emission of a W boson turns a charged lepton into a neutrino and an up-type quark into a down-type quark, respectively, and vice versa. The corresponding symmetry group is $SU(2)$.

These two interactions, electromagnetism and the weak nuclear force, actually originate from the same gauge symmetry called electroweak symmetry, which is described by the symmetry group $SU(2) \times U(1)$. In the unified electroweak theory, there are four gauge bosons, called W_1, W_2, W_3 and B, all of which need to be massless due to gauge symmetry.

The full electroweak symmetry then is broken *spontaneously* down to the $U(1)$ symmetry that we observe in nature. Spontaneous symmetry breaking [13,14] always generates massless scalars, so-called Nambu-Goldstone bosons. In the case of electroweak symmetry breaking, there are four Nambu-Goldstone bosons in two $SU(2)$ doublets. Three of these are absorbed by the gauge bosons, giving them their masses. The W_1 and W_2 combine into the charged $W^{\pm}$ and a superposition of W_3 and B becomes the massive Z^0. The remaining combination of W_3 and B stays massless (protected by the unbroken $U(1)$ symmetry), becoming the photon.

Thus, there remains one Nambu-Goldstone scalar, which in turn becomes massive because it has a non-zero vacuum expectation value (VEV). This particle is the Higgs boson. It interacts with the massive vector bosons $W^{\pm}$, Z^0 through the gauged covariant derivative. Furthermore, the Higgs boson can be used to give masses to all matter fields via interaction terms, as gauge-symmetry also forbids explicit mass terms for Dirac-fermions at the Lagrangian level. These couplings are called Yukawa couplings. The phenomenological consequence of this mechanism is that the Higgs boson couples to fermions with a strength proportional to their mass, i.e. the heavier a particle is, the stronger it interacts with the Higgs field.

The application of the theory of spontaneous symmetry breaking which originated in condensed-matter physics to field theory is called the Higgs mechanism, or sometimes, in order to do justice to all scientists involved in its conceiving, Englert–Brout–Higgs–Guralnik–Hagen–Kibble mechanism [15–20]. However, since Higgs arguably was the first person to predict the existence of a massive scalar, the boson is always called Higgs boson.

The application of spontaneous symmetry breaking to the electroweak theory of Glashow [21] was performed by Salam and Weinberg independently in 1967 [22, 23]. After the discovery of the Z boson at CERN which their theory had predicted, the three were jointly awarded the 1979 Nobel prize in physics.

The SM is considered one of the biggest triumphs of modern physics, having emerged as a collaborative effort by a large number of physicists after many years of work. The development of the SM was by no means linear or undisputed, and only after experimental confirmation of some key features like the bottom quark or the massive W and Z bosons, it became the state of the art to describe elementary particles. The formulation of the SM has essentially stayed the same since the mid-seventies of the last century, and has proven to be very resilient. All quantitative tests involving interactions of elementary particles can be explained by the SM, at least within the uncertainties of the respective experiment.

Also the production and decay rates of the recently discovered [24,25] Higgs boson at a mass of 125 GeV, for decades the last missing piece of the SM "jigsaw", are in agreement with the respective predictions by the SM until now, within the statistical uncertainties associated to the various measurements (see e.g. [26]).

Still, there are some questions left open by the SM such as the inclusion of neutrino masses, the nature of dark matter or the inclusion of gravity in the gauge field formalism. Traditionally, also the so-called hierarchy problem which concerns the huge difference in terms of coupling strength between gravity and the electroweak theory has been regarded as a flaw of the SM, but has witnessed a bit of waning interest as of lately. Various extensions of the SM, so-called Beyond the Standard Model (BSM) theories have been worked out in the last 30 years, the most prominent of which are Supersymmetry and various extra-dimensional models. We will not describe any of these BSM scenarios in detail, but briefly touch on the phenomenological impacts of some generic BSM theories on Higgs observables in section 5.5.

2.2. Lagrangian density of the strong interaction

We proceed by giving a slightly more thorough introduction to the theory of the strong interaction, QCD, based on refs. [2, 8]. As mentioned previously, out of the matter constituents, only quarks interact through it. The force-carrying bosons are called gluons and are massless. The underlying symmetry group is $SU(3)$, where 3 is the number of different "colour" charges. Sometimes, we will keep the number of colours arbitrary, i.e. present the features of the theory for the $SU(N_c)$ case. Similarly, the number of flavours which to our current knowledge is equal to 6 will be denoted by N_F. Repeated indices are always implicitly summed over, unless stated otherwise, and we always work in the units where $\hbar = c = 1$.

We proceed by giving the Lagrangian density governing the quark spinor-fields ψ_i and the gluon gauge-field A^a_μ. The full Lagrangian is given by

$$\mathcal{L} = \mathcal{L}_{\text{QCD}} + \mathcal{L}_{\text{gauge}} + \mathcal{L}_{\text{ghost}} \,, \tag{2.2}$$

with

$$\mathcal{L}_{\text{QCD}} = -\frac{1}{4} G^a_{\mu\nu} G^{a,\mu\nu} + \sum_{i=1}^{N_F} \bar{\psi}_i \left(i \not{D} - m_i \right) \psi_i \,, \tag{2.3}$$

where the covariant derivative is given by

$$\not{D} = D_\mu \gamma^\mu = \left(\partial_\mu - i g_s A^a_\mu T^a \right) \gamma^\mu \,, \tag{2.4}$$

and the gluonic field-strength tensor reads

$$G^a_{\mu\nu} = \partial_\mu A^a_\nu - \partial_\nu A^a_\mu - g_s f^{abc} A^b_\mu A^c_\nu \,. \tag{2.5}$$

The two auxiliary parts of the Lagrangian,

$$\mathcal{L}_{\text{gauge}} = \begin{cases} -\frac{1}{2\xi} \left(\partial^\mu A^a_\mu \right)^2 & \text{(covariant)} \\ -\frac{1}{2\xi} \left(n^\mu A^a_\mu \right)^2 & \text{(axial)} \end{cases} \,, \quad \mathcal{L}_{\text{ghost}} = c_a \left(\delta^{ab} \partial^2 + g_s f^{abc} A^c_\mu \partial^\mu \right) c_b \,, \tag{2.6}$$

are needed in order to be able to perform the quantisation of non-Abelian gauge-theories. The fields c_a are called Fadeev-Popov ghosts and have their own Feynman rules. To respect unitarity of the theory, all diagrams involving ghosts have to be added to the QCD diagrams for a given process, in general. However, choosing a certain gauge, the so-called axial gauge, ghost fields are not present, and thus we will not comment further on them.

The Dirac matrices γ^μ obey the anticommutation relation

$$\{\gamma^\mu, \gamma^\nu\} = 2g^{\mu\nu} \,, \tag{2.7}$$

and the generators of the colour algebra in the fundamental representation, which are matrices in the space of spinors, obey the commutation rules

$$\left[T^a, T^b\right] = i f^{abc} T^c \,. \tag{2.8}$$

The fully antisymmetric structure constants f^{abc} furnish a representation of $SU(N_c)$ themselves, in the adjoint representation, by defining $(T^a_A)_{bc} = f^{abc}$. The dimensions of the fundamental and adjoint representation are N_c and $N_c^2 - 1$, respectively. We thus observe that in the QCD case of $N_c = 3$, there are three quarks of each flavour and $3^2 - 1 = 8$ gluons, since the latter live in the adjoint representation as can be seen from their kinetic term (2.5).

The normalisation of the fundamental generators is commonly chosen as

$$\mathrm{Tr}\left(T^a T^b\right) = T_F \delta^{ab} \,, \quad \text{with} \quad T_F = \frac{1}{2} \,, \tag{2.9}$$

which fixes the quadratic Casimir factors for fundamental and adjoint representation,

$$T^a T^a = C_F \mathbf{1}_{N_c \times N_c} \,, \quad T^a_A T^a_A = C_A \mathbf{1}_{(N_c^2-1)\times(N_c^2-1)} \,, \tag{2.10}$$

to

$$C_F = \frac{N_c^2 - 1}{2N_c} \overset{N_c=3}{=} \frac{4}{3} \,, \quad C_A = N_c \overset{N_c=3}{=} 3 \,. \tag{2.11}$$

A local $SU(N_c)$ transformation acts on the quark and gluon fields as

$$\begin{aligned} \psi_i \to U\psi_i \,, \qquad & \bar{\psi}_i \to \bar{\psi}_i U^\dagger \,, \\ A^a_\mu T^a \to U & \left(A^a_\mu T^a + \frac{i}{g_s}\partial_\mu\right) U^\dagger \end{aligned} \tag{2.12}$$

with the transformation U is given by

$$U = \exp\left(i\theta^a(x) T^a\right) \,, \tag{2.13}$$

where $\theta^a(x)$ is an arbitrary vector depending on the spacetime coordinate x. Since the generators T^a are hermitian, U is unitary and it is easily seen that the Lagrangian (2.3) is indeed invariant under local $SU(N_c)$ transformations.

When we calculate collider observables in QCD, we do perturbation theory in the strong coupling, i.e. we expand the desired observable in the coupling constant g_s, provided it is small enough such that perturbation theory is applicable (see section 2.3.2). Since the quantity which enters an observable is always a matrix element (i.e. a sum of Feynman diagrams) *squared*, the variable we expand in is

$$\alpha_s \equiv \frac{g_s^2}{4\pi}\,, \tag{2.14}$$

which we will henceforth call “the strong coupling”.

We conclude the section by giving the Feynman rules for QCD. The gluon propagator in the axial gauge reads

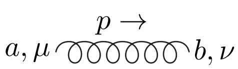

$$= \frac{-i\delta^{ab}}{p^2 + i0}\left(g_{\mu\nu} - \frac{n_\mu p_\nu + n_\nu p_\mu}{n\cdot p} + \frac{(n^2 - \xi p^2)p_\mu p_\nu}{(n\cdot p)^2}\right)\,, \tag{2.15}$$

where the auxiliary vector n may be chosen differently for each gluon. The quark propagator for a quark with mass m is given by

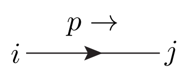

$$= \frac{i\delta_{ij}(\not{p} + m)}{p^2 - m^2 + i0}\,. \tag{2.16}$$

The gauge-vertex is given by

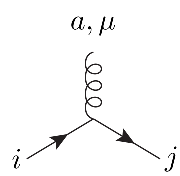

$$= ig_s T^a_{ji}\gamma^\mu\,. \tag{2.17}$$

Finally, the triple and quadruple gluon self-coupling vertices are given by

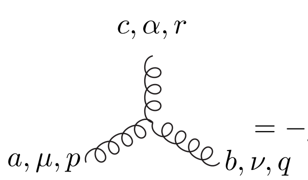

$$= -g_s f^{abc}\left[(p-q)^\alpha g^{\mu\nu} + (q-r)^\mu g^{\nu\alpha} + (r-p)^\nu g^{\alpha\mu}\right]\,, \tag{2.18}$$

where the momenta p, q and r are all taken to be incoming, and

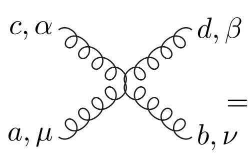

$$= -ig_s^2 \left[\begin{array}{cc} & f^{eac}f^{ebd}(g^{\mu\nu}g^{\alpha\beta} - g^{\mu\beta}g^{\nu\alpha}) \\ + & f^{ead}f^{ebc}(g^{\mu\nu}g^{\alpha\beta} - g^{\mu\alpha}g^{\nu\beta}) \\ + & f^{eab}f^{ecd}(g^{\mu\alpha}g^{\nu\beta} - g^{\mu\beta}g^{\nu\alpha}) \end{array}\right]\,. \tag{2.19}$$

Notice the infinitesimal imaginary part $+i0$ we have added to the propagator denominators, which is required to yield the correct causality properties. We will never write it explicitly again, but it will always be assumed.

2.3. Perturbative QCD calculations

In the previous section, we have presented the Feynman rules for the strong interaction. The notion of Feynman rules relies on the fact that a field theory is well described by a perturbative expansion in a small parameter, namely the coupling constant of the interactions of the theory. It is not *a priori* clear that this is indeed the case for the strong interaction, as its name already suggests strong interactions among the participating particles.

To see that indeed, for the applications considered in the latter chapters of this thesis, perturbation theory is a viable way of calculating observables, we need to introduce the concepts of regularisation and renormalisation.

2.3.1. Regularisation

In calculations in quantum field theory, one soon runs into divergent expressions. The primary textbook example are Feynman diagrams containing loops with less or equal than four powers of the loop momentum in the denominator, e.g.

$$\int \frac{\mathrm{d}^4 k}{(2\pi)^4} \frac{1}{k^2 - m^2}\,, \tag{2.20}$$

where by simple power counting, we find that for $|k| \to \infty$, the denominator is of $\mathcal{O}(|k|^2)$, while the integration measure $\mathrm{d}^4 k$ goes like $\mathcal{O}(|k|^3)$. We thus end up with a divergent integral. This type of divergence, called ultraviolet (UV) divergence because it appears when the momentum of the loop particle becomes much larger than its mass, has historically troubled the people working in the development of quantum field theory. It is resolved by the procedure of renormalisation, which will talk about in the next section.

There is a second kind of divergence, associated with massless particles such as photons or gluons. We can again consider a loop integral as an example,

$$\int \frac{\mathrm{d}^4 k}{(2\pi)^4} \frac{1}{k^2 \left(k - p_1\right)^2 \left(k - p_2\right)^2}\,, \tag{2.21}$$

which corresponds to a 3-point function with inflowing momenta p_1 and $p_2 - p_1$ and a massless particle in the loop. If both momenta are light-like, $p_1^2 = p_2^2 = 0$, the integrand becomes

$$\frac{1}{k^2\,(k^2-2kp_1)\,(k^2-2kp_2)} \xrightarrow{k^2 \ll kp_i} \frac{1}{k^2\,(2kp_1)\,(2kp_2)}\,, \tag{2.22}$$

where we have taken the limit of the loop momentum becoming soft. It is apparent that the denominator vanishes when either $|k| \to 0$ (the soft limit) or when k points along p_1 or p_2, which is called the collinear limit. These divergences are therefore called infrared (IR) divergences. While UV divergences only appear in loop integrals, we encounter IR divergences in phase-space integrations of tree-level diagrams when an external massless particle becomes soft or collinear to another particle.

In fact, it was proven half a decade ago by Kinoshita [27], Lee and Nauenberg [28] that the SM is IR-finite for observables that are inclusive enough. This means that infrared divergences cancel out among different contributions to a physical observable, i.e. when we compute higher order corrections in perturbation theory, IR divergences from so-called virtual corrections (loop diagrams) cancel out with IR divergences from real emission corrections (diagrams with the additional emission of a massless particle). Nevertheless, in intermediate expressions we need to deal with IR singularities and thus need a way to regularise them.

There are numerous ways of regularising UV and IR divergences. For example, to avoid UV singularities, one can introduce a cut-off scale Λ as the upper boundary for the value of the loop momentum [2]. Another traditionally widely-used method is Pauli-Villars regularisation [29], where auxiliary fields with a large mass are introduced to the theory, whose propagators exactly cancel the singular behaviour of the SM particles. Our method of choice to regularise divergences is dimensional regularisation [30], which has become standard practice since its invention. It holds the advantage of preserving all symmetries of the theory in question, in particular gauge symmetry and the associated Ward-identities. The second advantage is that it regularises *both* UV and IR divergences at the same time[1].

The idea is as simple as powerful. We allow the spacetime dimension D which is equal to four, to be any complex number. This analytic continuation is parametrised by the replacement $D = 4 - 2\epsilon$, such that we recover the physical case in the limit $\epsilon \to 0$. Divergences then manifest themselves as poles in ϵ. Note that there are different prescriptions on how to treat the degrees of freedom of external particles within dimensional regularisation schemes, the most common being conventional dimensional regularisation

[1] Formally, the sign of the dimensional regulator ϵ actually has to be negative to regularise IR divergences and positive for UV divergences. Since IR poles cancel out eventually, this distinction if of academic nature only.

(CDR) and dimensional reduction regularisation (DRED)[2]. Throughout this thesis, we choose CDR, where external gluon fields have $D-2$ polarisations and external quarks fields have 2.

As an example, we consider the initial integral from eq. (2.20) in dimensional regularisation, without going into detail about how we perform the D-dimensional integration [2],

$$\begin{aligned}\mu^{4-D}\int\frac{\mathrm{d}^Dk}{(2\pi)^D}\frac{1}{k^2-m^2}&=-\frac{i\Gamma\left(1-\frac{D}{2}\right)m^{D-2}\mu^{4-D}}{(4\pi)^{\frac{D}{2}}}\\&=\frac{im^2}{(4\pi)^2}\left[\frac{1}{\epsilon}+1-\gamma_E-\log\left(\frac{m^2}{\mu^2}\right)+\log(4\pi)+\mathcal{O}(\epsilon)\right],\end{aligned}\tag{2.23}$$

where we have expanded the result in ϵ in the second step, using the expansion of the Gamma-function,

$$\Gamma(1+\epsilon)=1-\gamma_E\epsilon+\mathcal{O}(\epsilon^2)\,,\tag{2.24}$$

as well as its defining property

$$\Gamma(1+z)=z\Gamma(z)\quad\Rightarrow\quad\Gamma(-1+\epsilon)=\frac{\Gamma(1+\epsilon)}{\epsilon(-1+\epsilon)}\,.\tag{2.25}$$

So indeed, we find the divergence to be contained in the pole $1/\epsilon$.

The auxiliary scale μ was introduced rather *ad-hoc* in the above example to keep the mass-dimension of the integral equal to the four-dimensional case. Indeed, since the action

$$S=\int\mathrm{d}^Dx\,\mathcal{L}\,,\tag{2.26}$$

is a dimensionless quantity, we can deduce the mass-dimension of the fermionic and bosonic fields in our Lagrangian from the kinetic terms, and find

$$[\psi_i]=\frac{D-1}{2}\,,\quad\left[A^a_\mu\right]=\frac{D}{2}-1\,.\tag{2.27}$$

This in turn fixes the mass-dimension of the gauge-coupling g to

$$[g]=2-\frac{D}{2}=\epsilon\,.\tag{2.28}$$

Since we ultimately want to expand in the coupling g and keep it dimensionless for this

[2] see for example [31] for a comparison

purpose, we are thus forced to introduce the auxiliary scale μ via

$$g \mapsto g\mu^{\epsilon} . \tag{2.29}$$

The scale μ, often called the *'tHooft mass*, plays a significant role in renormalisation, as we will see now.

2.3.2. Renormalisation

The solution to the issue of UV divergences is the realisation that the fields, masses and coupling constants in the Lagrangian do not correspond to physical observables. The parameters in the Lagrangian have no knowledge of the self-interaction of the theory such as loop corrections to an interaction vertex or a particle propagator. But these self-interactions are inevitably linked to physical, measurable parameters[3]. Thus, they are usually dubbed "bare" parameters and are denoted with a 0-superscript,

$$\mathcal{L} = \mathcal{L}\left(A_{\mu}^{0a}, \psi_i^0, g^0, m_i^0\right) . \tag{2.30}$$

To find the physical parameters in the Lagrangian, one has to split it up in a smart way. All bare parameters are divided into a corresponding physical parameter and a counter-term. The counter-terms are chosen in such a way that when performing perturbation theory with the split-up Lagrangian, the UV divergences (that will still be there, since the same diagrams as when using the bare parameters will be produced) are exactly cancelled by the counter-terms. The renormalisation procedure only works if the theory under consideration is renormalisable, which is determined by the Feynman rules of the theory. The SM is a renormalisable theory.

In QCD, the renormalisation programme results in replacing

$$\begin{gathered} \psi_i^0 = Z_\psi^{1/2}\psi_i, \qquad \bar{\psi}_i^0 = Z_\psi^{1/2}\bar{\psi}_i, \\ A^{0a} = Z_A^{1/2}A^a, \qquad c^0 = Z_c^{1/2}c, \\ m_i^0 = Z_m m_i, \qquad g_s^0 = Z_g g_s \mu^{\epsilon}, \qquad \xi^0 = Z_\xi \xi, \end{gathered} \tag{2.31}$$

where the $Z_i = 1 + \delta Z_i$ are called renormalisation constants and contain the counter-terms δZ_i. Notice that not all renormalisation constants are independent, as they are related by identities obtained from gauge invariance. In the calculations of this thesis, we will only need Z_g and Z_m, which we will provide at the end of the section.

[3] Sloppily put, since in Quantum mechanics "anything that can happen will happen", any measurement of a parameter of a theory includes the whole infinite tower of perturbative corrections that affect it.

While it is clear that all singularities have to be cancelled by the renormalisation constants, one is free to absorb more pieces of the divergent integrals into them. The different choices of how to do this are called different renormalisation schemes. The most common choices are the Minimal subtraction (MS) scheme, the modified Minimal subtraction ($\overline{\text{MS}}$) scheme and the on-shell (OS) scheme. We go back to the regularised result for the divergent integral (2.23) to illustrate the former two,

$$\mu^{4-D}\int\frac{\mathrm{d}^Dk}{(2\pi)^D}\frac{1}{k^2-m^2}=\frac{im^2}{(4\pi)^2}\left[\frac{1}{\epsilon}+1-\gamma_E-\log\left(\frac{m^2}{\mu^2}\right)+\log(4\pi)+\mathcal{O}(\epsilon)\right]. \tag{2.32}$$

In the MS scheme, the counter-terms are chosen to absorb only the $1/\epsilon$ pole, while in the $\overline{\text{MS}}$ scheme, the whole expression

$$\frac{1}{\epsilon}+\log(4\pi)-\gamma_E\,, \tag{2.33}$$

will be cancelled since the logarithm and the Euler-Mascheroni constant are universal factors that always appear in divergent loop integrals. In the "$\overline{\text{MS}}$-philosophy", these (finite) terms do not represent a genuine perturbative contribution to a physical observable. The OS scheme on the other hand defines the counterterm such that the pole of the renormalised propagator is located at the renormalised mass, and is usually only used in perturbative QCD when dealing with massive quarks which have a mass comparable to the typical scales of a high-energy process. We refer to [32] for further reading on renormalisation schemes.

In this thesis, we will use the $\overline{\text{MS}}$ scheme in the renormalisation of the strong coupling throughout. The subtraction of the combination in eq. (2.33) can be achieved by replacing

$$\mu^2\;\mapsto\;\bar{\mu}^2=\frac{e^{\gamma_E}}{4\pi}\mu^2\,. \tag{2.34}$$

In the $\overline{\text{MS}}$ scheme, the renormalised parameters become dependent on the scale μ, i.e. the values of the "constants" of the theory change when they are measured at a different energy scale, which is given by experimental constraints or selection criteria. The dependence can be derived from the relation between bare and renormalised parameters and is termed Renormalisation group equation (RGE). We consider the strong coupling α_s, whose renormalisation constant is given by $Z_\alpha=Z_g^2$,

$$0=\frac{\partial\alpha_s^0}{\partial\log(\mu^2)}=\mu^2\frac{\partial\alpha_s^0}{\partial\mu^2}=\mu^2\frac{\partial}{\partial\mu^2}\left(\mu^{2\epsilon}\left(\frac{e^{\gamma_E}}{4\pi}\right)^{\epsilon}Z_\alpha\alpha_s\right)$$

$$=\mu^2\left(\epsilon(\mu^2)^{\epsilon-1}\left(\frac{e^{\gamma_E}}{4\pi}\right)^{\epsilon}Z_\alpha\alpha_s+\mu^{2\epsilon}\left(\frac{e^{\gamma_E}}{4\pi}\right)^{\epsilon}\left(Z_\alpha+\frac{\partial Z_\alpha}{\partial\alpha_s}\alpha_s\right)\frac{\partial\alpha_s}{\partial\mu^2}\right)\,, \tag{2.35}$$

which yields

$$\frac{\partial\alpha_s}{\partial\log(\mu^2)}=\frac{-\epsilon\alpha_s}{1+\frac{\alpha_s}{Z_\alpha}\frac{\partial Z_\alpha}{\partial\alpha_s}}\equiv\alpha_s\,\beta^{(D)}(\alpha_s)\,, \tag{2.36}$$

where we have defined the D-dimensional Beta-function on the RHS. The Beta-function governs the dependence of the coupling α_s on the renormalisation scale μ. In calculations, the four-dimensional Beta-function $\beta(\alpha_s)$ is used, which is just the limit of $\beta^{(D)}(\alpha_s)$ as $D\to 4$. As is easily checked, the perturbative expansion of $\beta(\alpha_s)$ starts at the first order,

$$\beta(\alpha_s)=-4\pi\sum_{n=0}^{\infty}\beta_n a_s^{n+1}\,,\quad\text{where}\quad a_s\equiv\frac{\alpha_s}{\pi}\,. \tag{2.37}$$

and first three expansion coefficients in the $SU(N_c)$-case read [33, 34]

$$\beta_0=\frac{11}{12}C_A-\frac{1}{3}T_FN_F\,, \tag{2.38}$$

$$\beta_1=\frac{17}{24}C_A^2-\frac{1}{4}C_FT_FN_F-\frac{5}{12}C_AT_FN_F\,, \tag{2.39}$$

$$\begin{aligned}\beta_2=&\frac{2857}{3456}C_A^3+\frac{1}{32}C_F^2T_FN_F-\frac{205}{576}C_FC_AT_FN_F-\frac{1415}{1728}C_A^2T_FN_F\\&+\frac{11}{144}C_FT_F^2N_F^2+\frac{43}{288}C_AT_F^2N_F^2\,,\end{aligned} \tag{2.40}$$

which for QCD becomes

$$\beta_0=\frac{11}{4}-\frac{N_F}{6}\,,\ \beta_1=\frac{51}{8}-\frac{19}{24}N_F\,,\ \beta_2=\frac{2857}{128}-\frac{5033}{1152}N_F+\frac{475}{3456}N_F^2\,. \tag{2.41}$$

Truncating eq. (2.36) at $\mathcal{O}(a_s^2)$ and solving for $a_s(\mu)$ yields

$$a_s(\mu^2)=\frac{a_s(\mu_0)}{1+a_s(\mu_0)\beta_0\log\left(\frac{\mu^2}{\mu_0^2}\right)}\,. \tag{2.42}$$

Since for $N_F<17$, β_0 is larger than zero, the denominator in the equation above is larger than 1 for $\mu>\mu_0$, which means that the coupling α_s becomes smaller the higher the scale μ is chosen. This feature persists when higher orders of the Beta-function are added. Notice that the electromagnetic coupling α_{QED} exhibits the opposite behaviour, for example. This behaviour of the strong coupling is called asymptotic freedom. It was first realised by Gross, Wilczek [35] and Politzer [36], who were jointly awarded the 2004

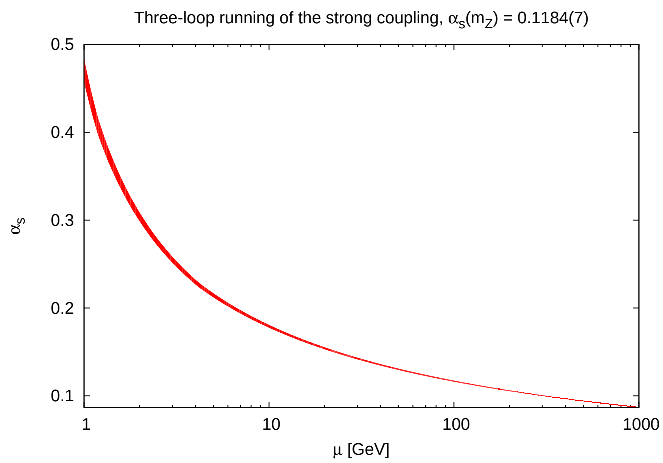

Figure 2.1.: The strong coupling α_s as a function of the energy scale Q.

Nobel prize in physics for their discovery. Asymptotic freedom has been confirmed by a wealth of experimental measurements of the strong coupling covering a vast range of energy scales [37], which follow exactly the running of the strong coupling depicted in figure 2.1 where we took the current world average [38],

$$\alpha_s(m_Z) = 0.1184 \pm 0.0007\,, \tag{2.43}$$

and evolved the coupling using the RGE eq. (2.36). The width of the red curve indicates the uncertainty associated with the initial value at the Z-mass.

Asymptotic freedom, paired with the fact that the value for the strong coupling at $\mu = m_Z \approx 91\,\text{GeV}$ as given in eq. (2.43) is rather small, means that for the energy scales typically probed in the processes described in this thesis, which lie in the ballpark of the Higgs mass of 125 GeV, fixed-order perturbation theory is expected to converge quickly and yield a good approximation to the actual physical observables.

We close this section by giving the expressions for the renormalisation constants of the strong coupling and the quark mass, as we will need it in later chapters.

The renormalisation replacement for the strong coupling in the $\overline{\text{MS}}$ scheme reads

$$\alpha_s^0 = \alpha_s(\mu)\mu^{2\epsilon}\left(\frac{e^{\gamma_E}}{4\pi}\right)^{\epsilon} Z_\alpha\,, \tag{2.44}$$

and the renormalisation constant is, through three-loop order,

$$Z_\alpha = 1 - a_s(\mu)\frac{\beta_0}{\epsilon} + a_s^2(\mu)\left(\frac{\beta_0^2}{\epsilon^2} - \frac{\beta_1}{2\epsilon}\right) + a_s^3(\mu)\left(-\frac{\beta_0^3}{\epsilon^3} + \frac{7\beta_0\beta_1}{6\epsilon} - \frac{\beta_2}{3\epsilon}\right) + \mathcal{O}(a_s^4)\,. \tag{2.45}$$

The renormalisation constant for the quark mass will only be needed to on-loop order. We will compare results in the $\overline{\mathrm{MS}}$ and the OS scheme, which is why we provide both renormalisation constants.

$$Z_m^{\overline{\mathrm{MS}}} = 1 + a_s \frac{\gamma_0}{\epsilon} + \mathcal{O}(a_s^2) = 1 + a_s \frac{1}{\epsilon} + \mathcal{O}(a_s^2)\,, \tag{2.46}$$

where γ_0 is the first expansion coefficient of the so-called anomalous dimension which governs the scale dependence of the $\overline{\mathrm{MS}}$ mass via the RGE

$$\frac{\partial \overline{m}}{\partial \log(\mu^2)} = \gamma(a_s)\overline{m} = \left(-a_s\gamma_0 - a_s^2\gamma_1 - a_s^3\gamma_2 + \mathcal{O}(a_s^4)\right)\overline{m}\,. \tag{2.47}$$

The first three expansion coefficients of the anomalous dimension of the $\overline{\mathrm{MS}}$ quark mass are given by

$$\gamma_0 = 1\,, \quad \gamma_1 = \frac{101}{24} - \frac{5N_F}{6}\,, \quad \gamma_2 = \frac{1249}{64} - \left(\frac{277}{216} + \frac{5\zeta_3}{6}\right)N_F - \frac{35}{1296}N_F^2\,. \tag{2.48}$$

Finally, the one-loop renormalisation constant for the OS quark mass M, which does not depend on a scale, is given by

$$Z_m^{\mathrm{OS}} = 1 + a_s \frac{1}{\epsilon}\left(\frac{\mu^2}{M^2}\right)^{\epsilon}\left(1 + \epsilon^2\frac{\pi^2}{12}\right)\frac{1-2\epsilon/3}{1-2\epsilon}\,. \tag{2.49}$$

2.3.3. Partonic cross sections and the D-dimensional phase-space

With the whole collection of Feynman rules for the SM at hand[4], we can in principle compute the matrix element of any process involving elementary particles.

In processes relevant for the LHC, we always consider processes of the type $1, 2 \to 3, \ldots, n+2$, where particles 1 and 2 are partons (i.e. quarks or gluons) inside the colliding protons, and $3, \ldots, n+2$ are any n final-state SM particles, such as a Higgs boson and additionally radiated partons. We denote the matrix element obtained from adding all Feynman diagrams which contribute to the process by $\mathcal{M}_{2\to n}(\{p_i\},\{m_i\})$, where the sets $\{p_i\}_{i=1,\ldots,n}$ and $\{m_i\}_{i=1,\ldots,n}$ denote all initial- and final-state momenta and masses, respectively (though m_1 and m_2 are always taken to be zero, i.e. the initial states are approximated to be massless). The corresponding squared matrix element with summation over final-state spins and colours and averaging over initial-state spins and colours is written as $|\overline{\mathcal{M}}_{2\to n}(\{p_i\},\{m_i\})|^2$.

The differential partonic cross section for the process under consideration is then given

[4] For a comprehensive list, see for example the appendix of [3].

by [2]

$$\mathrm{d}\sigma(\{p_i\},\{m_i\}) = \frac{1}{2s}\,\mathrm{d}\Phi_n\left(\{p_i\},\{m_i\}\right)\,\left|\overline{\mathcal{M}}_{2\to n}(\{p_i\},\{m_i\})\right|^2 , \tag{2.50}$$

where $s = (p_1 + p_2)^2$ and $\mathrm{d}\Phi_n$ denotes the n-particle phase-space measure,

$$\mathrm{d}\Phi_n\left(\{p_i\},\{m_i\}\right) = \left(\prod_{i=3}^{n+2} \frac{\mathrm{d}^D p_i}{(2\pi)^{D-1}}\delta_+(p_i^2 - m_i^2)\right)\delta^{(D)}\left(p_1 + p_2 - \sum_{i=3}^{n+2} p_i\right)(2\pi)^D , \tag{2.51}$$

with

$$\delta_+(p_i^2 - m_i^2) = \delta(p_i^2 - m_i^2)\theta(p_i^0) , \tag{2.52}$$

to select positive-energy states only. “Differential” in this context means that we retain full knowledge of the momenta of all final-state particles. The inclusive partonic cross section is then simply given by the integral over all final-state momenta, i.e. all information about the final-state kinematics is lost, except the collective four-momentum of the centre-of-mass which is equal to $p_{12} = p_1 + p_2$,

$$\sigma(p_{12},\{m_i\}) = \frac{1}{2s}\int \mathrm{d}\Phi_n\left(\{p_i\},\{m_i\}\right)\,\left|\overline{\mathcal{M}}_{2\to n}(\{p_i\},\{m_i\})\right|^2 . \tag{2.53}$$

As discussed in section 2.3.1 and indicated above, the final-state momenta need to be treated in D dimensions in general, as we have to regularise IR divergences associated with with soft and/or collinear massless final-state particles using dimensional regularisation.

The squared matrix element $|\overline{\mathcal{M}}|^2$ is usually parametrised in terms of the Lorentz invariants $s_{i_1\ldots i_m}$, for which we adopt the convention

$$s_{i_1\ldots i_m} = \left(p_{i_1\ldots i_m}\right)^2 , \tag{2.54}$$

where

$$p_{i_1\ldots i_m} = \tau_{i_1} p_{i_1} + \ldots + \tau_{i_m} p_{i_m} , \text{ with } \quad \tau_i = \begin{cases} +1 & \text{if } i = 1, 2 , \\ -1 & \text{if } i > 2 . \end{cases} \tag{2.55}$$

In this thesis, we will mostly be concerned with the production of one massive particle (a Higgs boson) accompanied by zero, one or two massless partons. The D-dimensional phase-space measures for these cases are provided in appendix A.

2.3.4. Hadronic cross section and mass factorisation

At hadron colliders such as the Fermilab TeVatron or the CERN LHC, the initial-state particles entering scattering processes are not elementary particles but protons or anti-protons. Protons are hadrons, composite objects which consist of quarks and gluons, held together firmly by the strong force and have a mass of approximately 1 GeV. Considering figure 2.1 again, we see that at these low energy scales, we run into the flip-side of asymptotic freedom, i.e. the coupling strength rises strongly as we approach lower energies. The proton is therefore a highly non-perturbative object and cannot be described by perturbative QCD. There is progress in describing hadrons in the framework of lattice QCD, see for example [39] for a review.

This looks like a problem for us since we want to apply perturbation theory to describe processes at the LHC. The solution to this is the parton model and collinear factorisation, developed at the end of the 1960s to describe Deep inelastic scattering (DIS), the scattering of an electron and a proton. For hard scattering processes, i.e. interactions involving a momentum transfer $Q^2 \gg m_p^2$, the proton can be described as a superposition of *free* quarks and gluons, each of them carrying some fraction x of the momentum of the proton. The probability to find a gluon or a quark of a given flavour i with momentum fraction x inside a proton is given by the parton distribution function (PDF) $f_i(x)$.

The crucial point is that all soft, non-perturbative physics is contained in the PDF, which is a universal object. Its values can be extracted in relatively clean experimental conditions such as DIS, and then be used in any process involving colliding protons. Intuitively, one may think of this property, called factorisation, on the level of different wavelengths, or timescales, associated with different energy scales in quantum mechanics. To the soft processes happening inside the proton, a highly energetic, hard scattering is "invisible", since it happens on much shorter timescales. It has to be noted, though, that factorisation has only been proven to be valid for DIS and the Drell-Yann process [40]. In other hadronic processes with two initial protons, it is merely an approximation which has been experimentally proven to be excellent, though. A graphical representation of factorisation is given in figure 2.2 which depicts DIS. The full process is split up in the emission of a parton i from the proton P (lower, round blob) which is universal, i.e. independent of the subsequent hard scattering of i with the photon (upper, square blob), which in turn is independent of origin of i (i.e. independent of the hadron P), and finally the contributions from all partons have to be added by summing over i.

When we split up a process in this way, we introduce new singularities, though. The initial states for the hard scattering amplitude are now quarks and gluons, which can themselves emit massless partons that may become soft and/or collinear to external

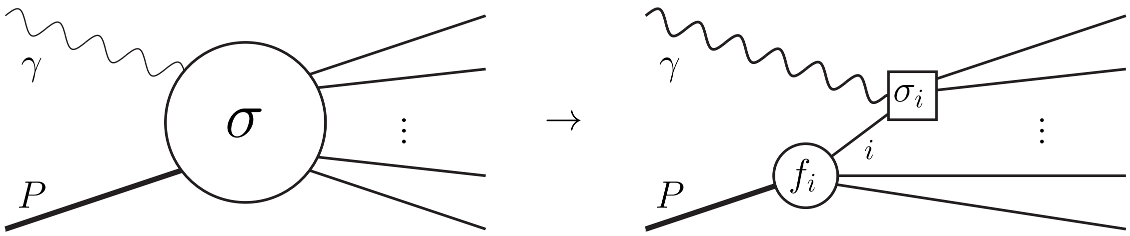

Figure 2.2.: A graphical representation of factorisation for the DIS process.

momenta. As we have seen before, this generates IR singularities. These singularities will not cancel against any other hard contribution, though, as was the case for the usual final-state IR singularities which cancel among real and virtual corrections. But they cancel when the soft piece containing the PDF is added, since it contains the same singularities. They are the price we pay for turning the partons inside the proton into quasi-asymptotic particles. Therefore, we need another renormalisation, rendering the bare PDF and the hard partonic cross section finite. This renormalisation is usually called mass factorisation or collinear factorisation, because it is associated with the IR structure of the theory rather than the UV limit. Here, again, there are different possible ways of absorbing finite pieces of the soft emissions into the PDF, i.e. different factorisation schemes. We always use the $\overline{\text{MS}}$ scheme.

As in the usual UV-renormalisation, collinear factorisation introduces an artificial scale into the objects involved. This scale is called factorisation scale, μ_f. After factorisation, both the PDF and the hard scattering cross section depend on μ_f. The equation governing the scale-dependence of the PDF, i.e. the equivalent of the RGE, is called Dokshitzer-Gribov-Lipatov-Altarelli-Parisi equation, or DGLAP equation, which owes its long name to the fact that Gribov and Lipatov [41], Dokshitzer [42] and Altarelli and Parisi [43] all discovered it independently in the 1970s. It reads

$$\frac{\partial f_i(\mu_f, x)}{\partial \log(\mu_f)} = \left(P_{ij} \otimes f_j(\mu_f)\right)(x) \equiv \int_0^1 \mathrm{d}y \mathrm{d}z\, P_{ij}(y) f_j(\mu_f, z)\, \delta(zy - x)\,, \tag{2.56}$$

where $\otimes$ denotes the convolution operation which is defined on the RHS. Summation over the index j which runs over all quarks, antiquarks and the gluon is implicit. The $P_{ij}(x)$ are the Altarelli-Parisi splitting kernels. They parametrise the probability that a parton j splits into a parton i and a third parton (whose index is not given since it is implicitly clear from the QCD Feynman rules), with i carrying the fraction x of the momentum of j (and thus the third, unlabelled parton carries the momentum fraction

$1-x$). The splitting kernels are purely perturbative objects

$$P_{ij}(x) = \sum_{n=0}^{\infty} a_s^{n+1} P_{ij}^{(n)}(x)\,, \tag{2.57}$$

and can be calculated using usual Feynman-diagrammatic techniques. The leading-order, one-loop kernels were calculated by Altarelli and Parisi in 1977 [43]. We provide the full list of $\overline{\mathrm{MS}}$-splitting kernels used in the calculations of this thesis in appendix B.

The importance of the DGLAP eq. (2.56) can hardly be overstated, since it allows us to relate PDFs at vastly different scales by purely perturbative means. The dependence of the PDFs on x can not be predicted by perturbative QCD, as we have argued. But using eq. (2.56), we can measure the distributions in x at some specific energy scale, e.g. DIS at moderate centre-of-mass energies which allow for clean experimental signatures, and then evolve the distributions to the energy scales appropriate for the physical process under consideration. Were it not for the DGLAP equation, we would have to measure the structure of the proton at every energy scale anew. The factorisation scale μ_f and the renormalisation scale μ_r are usually considered independent and are often varied separately for estimates of the scale-dependence of a fixed-order perturbative result. This scale dependence is used as an estimate for the remaining theoretical uncertainty, although the prescriptions how to vary the scales are often chosen *ad-hoc* and may change the quoted uncertainties significantly. For computational details on how to separate the factorisation and renormalisation scales, see section 6.3.2.

We still have to give a formula for the hadronic cross section, as well as for the process of mass factorisation. The (inclusive) hadronic cross section for a proton-proton collision is given by

$$\sigma(P_1, P_2, \mu_f, \mu_r) = \int_0^1 \mathrm{d}x_1 \mathrm{d}x_2\, f_i(\mu_f, x_1)\, f_j(\mu_f, x_2)\, \sigma_{ij}(p_{12}, \mu, \mu_f)\,, \tag{2.58}$$

where again, summation over the parton indices i and j is implicit. σ_{ij} is the renormalised and mass-factorised partonic cross section with incoming momenta $p_i = x_i P_i$, where P_1 and P_2 are the proton momenta. In a usual collider experiment, we have $\vec{P}_1 = -\vec{P}_2$ and due to rotational symmetry, the hadronic cross section only depends on the scalar variable $S = (P_1 + P_2)^2$, the total centre-of-mass energy squared, which at the LHC currently corresponds to $(8\,\mathrm{TeV})^2$, and additional external scales such as the masses of final-state particles. In the specific case of Higgs production, where we have just the Higgs mass as an external scale, the total hadronic cross section can be written as

(suppressing the scale-dependence for the time being)

$$\sigma(\tau) = \int_0^1 \mathrm{d}x_1 \mathrm{d}x_2 \, f_i(x_1) \, f_j(x_2) \, \sigma_{ij} \left(z = \frac{\tau}{x_1 x_2} \right) \Theta(x_1 x_2 - \tau) \, , \tag{2.59}$$

where we have defined the two dimensionless variables

$$\tau \equiv \frac{m_H^2}{S} \quad \text{and} \quad z = \frac{m_H^2}{s} = \frac{m_H^2}{x_1 x_2 S} = \frac{\tau}{x_1 x_2} \, , \tag{2.60}$$

with $s = p_{12}^2$ the partonic centre-of-mass energy. The Theta-function in eq. (2.59) reflects the fact that s has to be at least m_H^2. This kinematic constraint is usually absorbed into σ_{ij}, but we chose to write it explicitly for the following manipulation,

$$\begin{aligned}
\sigma(\tau) =& \int_0^1 \mathrm{d}x_1 \mathrm{d}x_2 \mathrm{d}z \, f_i(x_1) \, f_j(x_2) \, \sigma_{ij}(z) \, \delta \left(z - \frac{\tau}{x_1 x_2} \right) \\
=& \int_0^1 \mathrm{d}x_1 \mathrm{d}x_2 \mathrm{d}z \, f_i(x_1) \, f_j(x_2) \, \sigma_{ij}(z) \, x_1 x_2 \delta \left(x_1 x_2 z - \tau \right) \\
=& \tau \int_0^1 \mathrm{d}x_1 \mathrm{d}x_2 \mathrm{d}z \, f_i(x_1) \, f_j(x_2) \, \frac{\sigma_{ij}(z)}{z} \delta \left(x_1 x_2 z - \tau \right) \\
=& \tau \left(f_i \otimes f_j \otimes \frac{\sigma_{ij}(z)}{z} \right) (\tau) \, ,
\end{aligned} \tag{2.61}$$

i.e. we are able to write the total hadronic cross section as a triple convolution. This form makes it straightforward to derive the mass factorisation formula for the partonic cross section.

The relation between bare and factorised PDFs is given by

$$f_i(\mu_f, x) = \left(\Gamma_{ij}(\mu_f) \otimes f_j^0 \right) (x) \, , \tag{2.62}$$

where Γ_{ij} is the collinear counterterm kernel, the equivalent of the renormalisation constant in the UV-renormalisation case. It is a function of the splitting kernels and reads, through three-loop order,

$$\begin{aligned}
\Gamma_{ij}(\mu, x) =& \, \delta_{ij} \delta(1-x) - a_s(\mu) \frac{P_{ij}^{(0)}(x)}{\epsilon} \\
&+ a_s^2(\mu) \Bigg\{ - \frac{1}{2\epsilon} P_{ij}^{(1)}(x) + \frac{1}{2\epsilon^2} \left[\left(P_{ik}^{(0)} \otimes P_{kj}^{(0)} \right)(x) + \beta_0 P_{ij}^{(0)}(x) \right] \Bigg\} \\
&+ a_s^3(\mu) \Bigg\{ - \frac{1}{6\epsilon^3} \Big[\left(P_{ik}^{(0)} \otimes P_{kl}^{(0)} \otimes P_{lj}^{(0)} \right)(x) + 3\beta_0 \left(P_{ik}^{(0)} \otimes P_{kj}^{(0)} \right)(x)
\end{aligned}$$

$$+ 2\beta_0^2 P_{ij}^{(0)}(x)\Big] + \frac{1}{12\epsilon^2}\Big[3\left(P_{ik}^{(0)} \otimes P_{kj}^{(1)}\right)(x) + 3\left(P_{ik}^{(1)} \otimes P_{kj}^{(0)}\right)(x)$$

$$+ 4\beta_1 P_{ij}^{(0)}(x) + 4\beta_0 P_{ij}^{(1)}(x)\Big] - \frac{1}{3\epsilon}P_{ij}^{(2)}(x)\Bigg\} + \mathcal{O}(a_s^4)\,. \tag{2.63}$$

We have argued before that initial-state collinear divergences are an artifact of the factorisation of a full hadronic cross section into a soft PDF and a hard partonic cross section. In other words, we obtain the identical, finite hadronic cross section if we either use bare PDFs and a non-mass-factorised partonic cross section, or the finite mass-factorised equivalents. In the former case, all ingredients going into the convolution in eq. (2.61) are divergent, but the poles cancel completely. If we denote by $\hat{\sigma}$ the partonic cross section before mass-factorisation, this equivalence reads

$$\begin{aligned}\sigma(\tau) =&\tau\left(f_i^0 \otimes f_j^0 \otimes \frac{\hat{\sigma}_{ij}(z)}{z}\right)(\tau)\\ =&\tau\left(f_i \otimes f_j \otimes \frac{\sigma_{ij}(z)}{z}\right)(\tau)\,.\end{aligned} \tag{2.64}$$

If we now use eq. (2.62) to replace finite PDFs with bare ones, we find (using the fact that a multiple convolution is completely symmetric in its arguments)

$$\begin{aligned}\sigma(\tau) =&\tau\left(f_i^0 \otimes f_j^0 \otimes \frac{\hat{\sigma}_{ij}(z)}{z}\right)(\tau)\\ =&\tau\left(\Gamma_{ik} \otimes f_k \otimes \Gamma_{jl} \otimes f_l \otimes \frac{\sigma_{ij}(z)}{z}\right)(\tau)\\ =&\tau\left(f_i^0 \otimes f_j^0 \otimes \Gamma_{ki} \otimes \Gamma_{lj} \otimes \frac{\sigma_{kl}(z)}{z}\right)(\tau)\end{aligned} \tag{2.65}$$

which leads to the desired relation between the partonic cross section before and after mass factorisation,

$$\frac{\hat{\sigma}_{ij}(x)}{x} = \left(\Gamma_{ki} \otimes \Gamma_{lj} \otimes \frac{\sigma_{kl}(z)}{z}\right)(x)\,. \tag{2.66}$$

Since we eventually always want to calculate hadronic cross sections and like the convolution expression eq. (2.61), we will henceforth absorb the factor of $1/z$ into the partonic cross section σ_{ij}, i.e. eq. (2.50) will include a factor of $1/z$ on the RHS. Thus, the hadronic cross section and the mass factorisation equation simply read

$$\sigma(\tau) = \tau\left(f_i \otimes f_j \otimes \sigma_{ij}\right)(\tau)\,, \quad \text{and} \quad \hat{\sigma}_{ij}(x) = \left(\Gamma_{ki} \otimes \Gamma_{lj} \otimes \sigma_{kl}\right)(x)\,. \tag{2.67}$$

3. Inclusive Higgs boson hadroproduction at NNLO

As mentioned in the introduction the gluon fusion process is by far the most prolific Higgs production process at the LHC. There are final-state configurations which are dominated by other production processes, for example the final state with three charged leptons which selects the associated production process [44]. These configurations are chosen specifically for this reason, i.e. to probe sub-leading production channels and isolate a different coupling of the Higgs boson.

Yet, to this date, all Higgs signals observed at the LHC with enough statistical significance to claim a discovery are based on the gluon fusion channel, it is in this sense the only established production mechanism for a Higgs boson.

We proceed by giving a short chronological account of the calculations contributing to the gluon fusion cross section.

In 1975, Ellis, Gaillard and Nanopoulos published their seminal paper “A phenomenological profile of the Higgs boson” [45], where in a heroic effort, all production and decay processes for the Higgs boson were calculated. However, the authors missed out on the loop-induced coupling of the Higgs to gluons. Wilczek pointed out this flaw in 1977 [46], but he only considered the coupling to be important in decays of the Higgs. Finally, Georgi, Glashow, Machacek and Nanopoulos understood the importance of the gluon coupling as a production mechanism and computed the leading-order (LO) cross section [47].

The beginning of the 1990s witnessed the computation of the next-to-leading order (NLO) QCD corrections [48, 49] in the five-flavour heavy-quark effective theory (HQET) which we will introduce in section 3.4. About five years later, the NLO QCD corrections in the full theory were completed [50], which allowed to validate the good approximation yielded by the HQET. While the original publication [50] contained some integral expressions that could only be evaluated numerically, later publications simplified the NLO QCD result to a form with no integrations left, using the language of harmonic polylogarithms [51–53].

At the beginning of the new millennium, the next-to-next-to-leading order (NNLO) QCD corrections in HQET were computed, first in an expansion around the threshold limit [54, 55] and subsequently in the full kinematics [56, 57].

The following years saw the completion of NLO electroweak corrections [58] in the full theory, mixed QCD-electroweak corrections [59] in the HQET, as well as power-corrections in $1/m_t$ to the infinite-top-mass approximation of the HQET [60, 61].

Furthermore, beyond fixed-order perturbation theory, resummation results have been calculated to next-to-next-to-leading logarithmic (NNLL) accuracy for soft gluon resummation [62] and in the soft-collinear-effective theory framework [63].

The aim of this chapter is to give a quick, yet comprehensive overview of all available fixed-order contributions and how to combine them in a consistent way. This combination was performed in the computer program `iHixs` [64] which we will present at the end of the chapter. Please note that few of the contents of this chapter represent original work of the author, but the key challenge was rather the gathering and combining of previously calculated work.

Wherever possible, we will consider a Higgs boson with interactions that are more general than in the SM, described by the Feynman rules

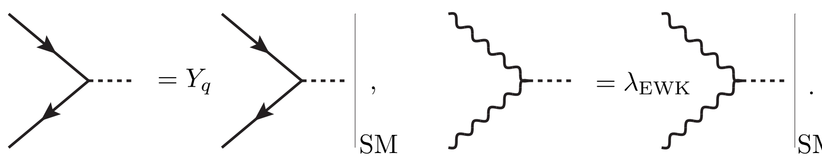

(3.1)

The H-q-$\bar{q}$ vertex is the product of an arbitrary, flavour-dependent factor Y_q and the analogous Feynman rule in the Standard Model. The Standard Model Feynman rules for the H-W-W and H-Z-Z vertices are rescaled by a global factor λ_{ewk}. We did not find it necessary to introduce a separate rescaling factor for the W and Z boson vertices, as the ratio of the coefficients of the corresponding operators is fixed by the custodial symmetry and very tightly constrained by electroweak precision tests [65].

Furthermore, the number of quark flavours is kept arbitrary whenever possible, allowing to calculate predictions for Higgs production in theories with additional heavy flavours.

3.1. Notation and leading order result

The leading order diagram for the process $gg \to H$ is displayed in figure 3.1, where the fermion in the loop represents any quark. In the SM the coupling of the Higgs to

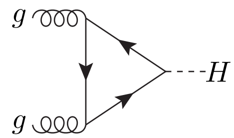

Figure 3.1.: Leading order diagram for the gluon fusion process.

fermions is proportional to the mass of the respective fermion,

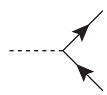

$$= -i\frac{m_f}{v} H\bar{\psi}_f\psi_f \,, \tag{3.2}$$

which means that the bulk of the cross section in the SM is generated by the top quark running in the loop, since it has by far the largest mass of all quarks.

We expand the gluon fusion cross section as

$$\sigma_{ij}(z,\mu_f,\mu_r) = \frac{G_f\pi}{288\sqrt{2}} \sum_{p=0}^{\infty} a_s(\mu_r)^{2+p}\, \eta_{ij}^{(p)}\left(z,\mu_f,\mu_r\right) \,, \tag{3.3}$$

and introduce the two dimensionless variables τ_q and x_q,

$$\tau_q \equiv \frac{4m_q(m_q - i\Gamma_q)}{m_H^2} \,, \quad x_q = \frac{\sqrt{1-\tau_q}-1}{\sqrt{1-\tau_q}+1} \,. \tag{3.4}$$

Observe that we allow for a non-zero width Γ_q for the quarks, implemented through the complex mass scheme [66–68] which accounts for width-effects in a gauge-invariant way. For $\Gamma_q = 0$, the variable τ_q becomes real. The corresponding behaviour of x_q is depicted in figure 3.2. x_q is real and negative if τ_q is smaller than 1, and becomes exactly -1 on threshold ($2m_q = m_h$). For values below threshold (i.e. when the Higgs is lighter than twice the quark mass), x_q becomes complex and runs along the unit circle. The limit of an infinitely heavy quark or, equivalently, a massless Higgs corresponds to the limit $x_q \to 1$. When the width Γ_q is taken to be non-zero, the curve describing x_q moves inside the unit circle, and the behaviour around the threshold $\tau_q = 1$ is smoothened out.

The LO cross section is found to be

$$\eta_{gg}^{(0)}(z) = \left|\sum_q Y_q\tau_q\frac{3}{2}A(\tau_q)\right|^2 \delta(1-z) \,, \tag{3.5}$$

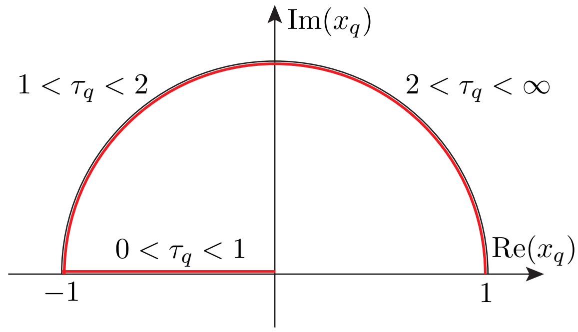

Figure 3.2.: Behaviour of the complex variable x_q.

where the amplitude $A(\tau_q)$ reads

$$A(\tau_q) = 1 - \frac{1}{2}\frac{(1+x_q)^2}{(1-x_q)^2}\mathrm{H}_{0,0}(x_q)\,. \tag{3.6}$$

The sum in eq. (3.5) runs over all N_F quark flavours, and Y_q is the scaling factor of the Yukawa coupling w.r.t the SM value which we introduced at the end of the previous section.

The function $\mathrm{H}_{0,0}(x)$ is the first harmonic polylogarithm (HPL) that we encounter. This class of functions appears naturally in perturbative QCD calculations. The special case appearing here can be written in terms of the classical (complex) logarithm,

$$\mathrm{H}_{0,0}(x) = \frac{1}{2}\log^2(x)\,. \tag{3.7}$$

For the general definition of HPLs and more information on their properties, we refer to chapter 4.

Note that the quantity $\tau_q \frac{3}{2} A(\tau_q)$ has the simple limits

$$\lim_{\tau_q\to\infty} \tau_q \frac{3}{2} A(\tau_q) = 1 \quad \lim_{\tau_q\to 0} \tau_q \frac{3}{2} A(\tau_q) = 0\,. \tag{3.8}$$

We observe that the LO cross section $\eta_{gg}^{(0)}$ is proportional to $\delta(1-z)$, due to the $2\to 1$ phase-space. There are no other particles besides the Higgs to carry away momentum, thus the partonic centre-of-mass energy $\sqrt{\hat{s}}$ must be equal to m_H, which corresponds to $z = 1$. While this will be the case for all higher-order virtual corrections as well, the contributions from real-emission diagrams have a non-trivial dependence on z.

In particular, there are terms proportional to $(1-z)^{-1+k\epsilon}$ for some integer k, which diverge in the limit $z \to 1$ when ϵ is taken to zero. To extract the singularities associated with these terms, one applies the following trick, called plus-expansion,

$$\begin{aligned}\int_0^1 \mathrm{d}x\, x^{-1+k\epsilon} f(x) &= f(0)\int_0^1 \mathrm{d}x\, x^{-1+k\epsilon} + \int_0^1 \mathrm{d}x\, x^{-1+k\epsilon}(f(x)-f(0)) \\ &= \frac{f(0)}{k\epsilon} + \sum_{n=0}^{\infty}\left(\frac{k\epsilon}{n!}\right)^n \int_0^1 \mathrm{d}x\, \log^n(x)\left(\frac{f(x)-f(0)}{x}\right) ,\end{aligned} \tag{3.9}$$

where the function $f(x)$ is assumed to be smooth and finite at $x=1$. The denominator in the integral thus vanishes at $x=1$ and renders the singularity integrable. The trick can be written independently of the regular function f in the sense of distributions,

$$x^{-1+k\epsilon} = \frac{\delta(1-z)}{k\epsilon} + \sum_{n=0}^{\infty}\left(\frac{k\epsilon}{n!}\right)^n \left[\frac{\log^n(x)}{x}\right]_+ = \frac{\delta(1-z)}{k\epsilon} + \sum_{n=0}^{\infty}\left(\frac{k\epsilon}{n!}\right)^n \mathcal{D}_n(x)\, , \tag{3.10}$$

where we have provided both common notations for the plus-distribution which is defined via its action on a regular test function f,

$$\int_0^1 \mathrm{d}x\, \mathcal{D}_n(x) f(x) = \int_0^1 \mathrm{d}x\, \frac{\log^n(x)}{x}\left[f(x)-f(0)\right] . \tag{3.11}$$

In our case, $x = \bar{z} \equiv 1-z$. In this way, all IR divergences can be extracted from real-emission diagrams and cancel when added to the virtual corrections, according to the KLN theorem mentioned in section 2.3.1. Thus, the general cross section at higher orders will be a superposition of three types of contributions, delta-, plus- and regular contributions,

$$\eta_{ij}^{(p)}(z,\mu_f,\mu_r) = \eta_{ij;\delta}^{(p)}(\mu_f,\mu_r)\,\delta(1-z) + \eta_{ij;+}^{(p)}(z,\mu_f,\mu_r) + \eta_{ij;R}^{(p)}(z,\mu_f,\mu_r)\, , \tag{3.12}$$

with

$$\eta_{ij;+}^{(p)}(z,\mu_r,\mu_f) = \sum_{n=0}^{\infty} \eta_{ij;+}^{(p),n}(\mu_f,\mu_r)\,\mathcal{D}_n(1-z)\, , \tag{3.13}$$

and $\eta_{ij;R}^{(p)}$ contains all terms which do not diverge as $z \to 1$.

3.2. NLO QCD corrections

At the next order in QCD, there are on the one hand two-loop diagrams for the $gg \to H$ process and the one-loop diagrams for the process $gg \to Hg$, and on the other hand, new partonic channels open up via the processes $qg \to Hq$ and $q\bar{q} \to Hg$. We show a sample diagram for every process in figure 3.3.

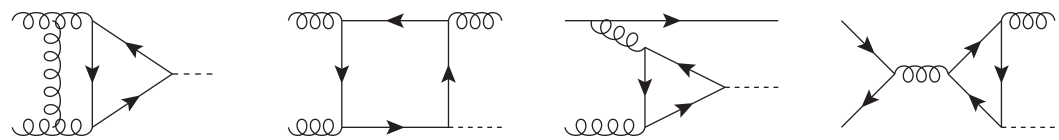

(a) $gg \to H$ (b) $gg \to Hg$ (c) $qg \to Hq$ (d) $q\bar{q} \to Hg$

Figure 3.3.: Sample diagrams for the processes contributing to the NLO QCD corrections to the gluon fusion process.

We proceed by giving the results for the separate partonic channels. Wherever the expressions are deemed too long to be provided in the main text, we refer to appendices or publicly available references on the Internet.

3.2.1. $gg \to H\,(g)$

The δ-part of the NLO correction to the gluon gluon sub-process can be written as

$$\eta^{(1)}_{gg;\delta} = |B|^2 \left[2\beta_0 \log\left(\frac{\mu_r^2}{\mu_f^2}\right) + \pi^2 \right] + 2\mathrm{Re}\left[B \sum_q V_q(\tau_q)^* \right] , \tag{3.14}$$

where

$$B \equiv \sum_q Y_q \tau_q \frac{3}{2} A(\tau_q) \, , \tag{3.15}$$

is the LO coefficient, and

$$V_q(\tau_q) = Y_q \frac{3}{8} M^{(1)}_{f,\mathrm{fin}}(\tau_q) = -Y_q \frac{3}{2} \mathcal{G}_i^{2l} \, , \tag{3.16}$$

with the limit

$$\lim_{\tau_q \to \infty} V_q(\tau_q) = \frac{11}{4} \, . \tag{3.17}$$

The amplitude $M^{(1)}_{f,\mathrm{fin}}(\tau_q)$ can be found in eq. (7.4) of ref. [53] and $\mathcal{G}^{(2l)}_{1/2}$[1] can be found in eqs. (26-30) of ref. [52]. The former expressions are only valid when the variable x_q is on the unit circle for quark masses higher than half of the Higgs mass, i.e. when we set the quark width to zero, because it is parametrised in the variable θ, where $x = \exp(i\theta)$. The latter formula, on the other hand, is given in terms of HPLs with general complex argument x_q. Thus, we chose to use the latter formula in our implementation in `iHixs`.

[1] To be precise, the virtual amplitude V_q as we denote it above corresponds only to the first line of eq. (27) in ref. [52], i.e. without dividing the bracketed expression with the Born amplitude and without adding the hermitian conjugate.

This necessitated the ability to numerically evaluate any HPL up to weight 4 for complex arguments, which in turn led to the development of the library CHAPLIN, which we describe in chapter 4. The authors of [52] actually provide the two-loop amplitude $\mathcal{G}_i^{2l}$ for the two cases of the heavy quark renormalised in the $\overline{\mathrm{MS}}$ or the on-shell scheme.

The difference between the two schemes can be quantified as

$$\mathcal{G}_{1/2}^{(2l),\mathrm{OS}}(x) - \mathcal{G}_{1/2}^{(2l),\overline{\mathrm{MS}}}(x) \propto \left(\frac{4}{3} + \log\left(\frac{\mu_r^2}{m_t^2}\right)\right) \mathcal{F}_{1/2}^{(2l,b)}(x)\,, \tag{3.18}$$

where $\mathcal{F}_{1/2}^{(2l,b)}$ is the derivative of the Born amplitude w.r.t the quark mass. The scale-dependent logarithm is present in the $\overline{\mathrm{MS}}$ amplitude and missing in the OS one. The origin of this specific difference is found in the two renormalisation constants we have provided in eqs. (2.46) and (2.49), respectively. While they obviously have to cancel the same poles, the finite $\mathcal{O}(\epsilon^0)$ parts of the constants differ by

$$Z_m^{\mathrm{OS}} - Z_m^{\overline{\mathrm{MS}}} = a_s \left[\frac{4}{3} + \log\left(\frac{\mu^2}{m_t^2}\right) + \mathcal{O}(\epsilon)\right]\,, \tag{3.19}$$

which is easily obtained by expanding the OS renormalisation constant in ϵ.

We have implemented both schemes in `iHixs`[2] and will probe the sensitivity to the choice in chapter 5.5.

The plus-distribution part is

$$\eta_{gg;+}^{(1)} = |B|^2 \left[-6\log\left(\frac{\mu_f^2}{m_H^2}\right)\mathcal{D}_0(1-z) + 12\mathcal{D}_1(1-z)\right]\,, \tag{3.20}$$

and the regular part of the NLO gluon-gluon-correction is

$$\begin{aligned}\eta_{gg;R}^{(1)} =& |B|^2\left\{2\left[p_{gg}^{(r)}(z)\log\left(\frac{(1-z)^2}{z}\right) - 3\log\left(\frac{z}{1-z}\right)\right] - 2\log\left(\frac{\mu_f^2}{m_H^2}\right)p_{gg}^{(r)}(z)\right\} \\ &+ \int_0^1 \mathrm{d}\lambda\, \frac{3}{z(1-z)\lambda(1-\lambda)}\left\{\frac{z^4}{2}\sum_{j=1}^{4}\left|\sum_q A_{gggH}^{jq}(\tau_q,\lambda)\right|^2 - (1-z+z^2)^2|B|^2\right\},\end{aligned} \tag{3.21}$$

[2]This choice was actually not included in the original `iHixs` program, but was added from the latest version 1.3.3 on.

with $p_{gg}^{(r)}(z)$ the regular part of the gluon splitting kernel (see appendix B)

$$p_{gg}^{(r)}(z) = 3\left(\frac{1}{z} + z(1-z) - 2\right) . \tag{3.22}$$

The form factors $A_{gggH}^{jq}(\tau_q)$ can be found in the Appendix B.2. of [64]. Notice that in the second line, the sum of the terms in the curly bracket vanishes fast enough in both limits $\lambda \to 0$ and $\lambda \to 1$, and thus the apparently divergent integral over λ is actually finite.

3.2.2. $q\bar{q} \to Hg$

The $q\bar{q}$ initial state starts contributing to the total cross section at order a_s^3 in QCD. There are no soft (δ- or plus-) terms, which is obvious from the fact that there are no corresponding $2 \to 1$ diagrams in the soft limit where the radiated parton is not observed,

$$\eta_{q\bar{q};\delta}^{(1)} = \eta_{q\bar{q};+}^{(1)} = 0 . \tag{3.23}$$

The regular contributions read

$$\eta_{q\bar{q};R}^{(1)} = \frac{32}{27}\frac{(1-z)^3}{z}\left|\sum_q Y_q \tau_q A_{q\bar{q}gH}(z)\right|^2 , \tag{3.24}$$

with $A_{q\bar{q}gH}(z)$ given in eq. (B.5) of [64].

3.2.3. $qg \to Hq$

The gluon-quark initial state also contributes at order a_s^3. Analogous to the $q\bar{q}$-channel, there are no soft terms,

$$\eta_{qg;\delta}^{(1)} = \eta_{qg;+}^{(1)} = 0 , \tag{3.25}$$

and

$$\begin{aligned}\eta_{qg;R}^{(1)} =& \left\{ |B|^2 \left[\frac{C_F}{2} z - p_{gq}(z)\log\left(\frac{z}{(1-z)^2}\right) - p_{gq}(z)\log\left(\frac{\mu_f^2}{m_H^2}\right)\right]\right. \\ &\left. + \int_0^1 d\lambda \frac{1}{(1-\lambda)_+}\left[\left|\sum_q Y_q \tau_q A_{q\bar{q}gH}(y_\lambda)\right|^2 \frac{1+(1-z)^2\lambda}{z}\right]\right\}\end{aligned} \tag{3.26}$$

with

$$y_\lambda = \frac{-z}{(1-z)(1-\lambda)} , \tag{3.27}$$

(a) (b)

Figure 3.4.: Two-loop electroweak contributions to Higgs production in gluon fusion.

and the LO splitting-kernel for a gluon splitting into a $q\bar{q}$-pair (see appendix B),

$$p_{gq}(z) = P_{gq}^{(0)}(z) = \frac{2}{3}\frac{1+(1-z)^2}{z}\,. \tag{3.28}$$

3.3. Electroweak contributions

Two-loop electroweak contributions to the process $gg \to H$ may either arise as genuine $\mathcal{O}(\alpha)$ corrections to the LO diagram from figure 3.1, as depicted in figure 3.4 (a), or via diagrams fusing two vector bosons into a Higgs boson via the respective coupling, depicted in figure 3.4 (b). Neglecting the difference of the Higgs couplings in the two processes, both of them are of the same perturbative order, $\mathcal{O}(\alpha_s^2\alpha)$ when interfered with the Born diagram.

A first computation considered only a gauge-invariant subset of diagrams of the type depicted in fig. 3.4 (b) where the quark propagating in the loop is considered massless [69]. The result for the amplitude is given in terms of a set of polylogarithms which the authors call generalised harmonic polylogarithms (GPLs). These functions can be remapped into harmonic polylogarithms with more complicated (complex) arguments [70].

In ref. [71], the two-loop contributions of type (a) and (b) involving top quarks were found in the limit $m_H \ll 2m_W$, using the background-field method. Finally, the full result for the two-loop electroweak contributions was computed in references [58, 72] for the full mass-range of the Higgs boson. The authors deal with singularities arising at thresholds such as $m_H = 2m_W$ or $m_H = 2m_t$ by using the complex mass scheme. There are no analytic results provided, but the authors of ref. [72] were so kind as to provide us with a grid file containing the numerical impact of the electroweak corrections, parametrised in the variable

$$\delta_{\mathrm{EWK}} = \left.\frac{\sigma^{\mathrm{born}}_{\mathrm{EWK+QCD}}}{\sigma^{\mathrm{born}}_{\mathrm{QCD}}}\right|_{\text{top only}} - 1 = \left|1 + \frac{\mathcal{M}_{ggh,\mathrm{EWK}}}{\frac{3}{2}\tau_q A\left(\tau_{top}\right)}\right|^2 - 1\,, \tag{3.29}$$

which parametrises the increase or decrease, respectively, of the $\mathcal{O}(\alpha_s^2\alpha)$ cross section over the LO QCD $\mathcal{O}(\alpha_s^2)$ one.

The inclusion of the virtual electroweak contributions in the partonic cross section (3.3) can be realised in different ways, depending on the factorisation scheme chosen[3]. In ref. [72], two factorisation schemes are presented:

1. Complete factorisation:

$$\sigma^{(0)} G_{ij} \;\to\; \sigma^{(0)}(1+\delta_{\rm EWK}) G_{ij}\,. \tag{3.30}$$

2. Partial factorisation:

$$\sigma^{(0)} G_{ij} \;\to\; \sigma^{(0)}\left[G_{ij} + a_s^2 \delta_{\rm EWK} G_{ij}^{(0)}\right]\,, \tag{3.31}$$

where we have intermediately adopted the notation of ref. [72],

$$\sigma_{ij} = \sigma^{(0)} G_{ij}\,, \quad \text{with} \quad G_{ij} = \sum_{n=0}^{\infty} a_s^{n+2} G_{ij}^{(0)}\,, \quad \text{s.t.} \quad G_{gg}^{(0)} = \delta(1-z)\,, \tag{3.32}$$

which means that

$$\sigma^{(0)} = \frac{G_f \pi}{288\sqrt{2}} \left| \sum_q \tau_q \frac{3}{2} A(\tau_q) \right|^2 . \tag{3.33}$$

The complete factorisation scheme results in an overall rescaling of the result, i.e. one believes that the electroweak contributions will be of the same size at all higher orders in QCD. When opting for the partial factorisation scheme, they are simply treated as a perturbative correction in α. The partial factorisation scheme results in a smaller numerical effect, since QCD corrections in gluon fusion are large. In the case of `iHixs` we chose a different way of including the leading electroweak corrections contained in $\delta_{\rm EWK}$, for which we first have to introduce the framework of effective theories. Please see section 3.4.3 for details.

In addition to the two-loop electroweak contributions, there are also diagrams involving electroweak vector bosons that contribute to the real-radiation processes $qg \to Hq$ and $q\bar{q} \to Hg$, depicted in figure 3.5. When interfered with the corresponding pure QCD diagrams of fig. 3.3, these contributions are of $\mathcal{O}(\alpha_s^2\alpha)$, too.

These contributions were calculated and studied in references [73] and [74], where the latter also included massive bottom quark effects. We repeated the calculation during

[3] The use of the word factorisation here is not related to collinear/mass factorisation.

(a) (b)

Figure 3.5.: One-loop electroweak contributions to the processes $qg \to Hq$ and $q\bar{q} \to Hg$.

the construction of `iHixs`, using the generalised Feynman rules (3.1). The contributions to the cross section read[4]

$$\begin{aligned}\eta^{(0)\mathrm{EWK}}_{q\bar{q};R} =&\lambda_{\mathrm{EWK}}\frac{8}{3}\frac{1-z}{z}\sum_q \sum_{X\in\{W_i,Z_i,H\}}\mathrm{Re}\Bigg\{\tau_q A_{qqgH}(z)c_{X,q}\cdot\\ &\left[\mathcal{F}^*_{1,X,q}(s_{13},s_{23},s_{12})\frac{s_{13}^2}{s_{12}}+\mathcal{F}^*_{2,X,q}(s_{13},s_{23},s_{12})\frac{s_{23}^2}{s_{12}}\right]\Bigg\} \qquad (3.34)\end{aligned}$$

where $A_{q\bar{q}gH}(z)$ given in appendix B of ref. [64]. The sum over X runs over all W and Z-like bosons in the model, as well as over the Higgs boson (replace the wiggled line by a dashed line in figure 3.5), while the sum over q runs over all heavy quarks as before. The coupling $c_{X,q}$ contains Kronecker delta symbols which select specific initial state quarks, depending on X, as explained below.

- Z loops: For the initial state quarks $q \in \{u,d,c,s,b\}$ we have the following couplings

$$\begin{aligned}\lambda_Z =&2\\ c_{Z,q} =&(\delta_{qu}+\delta_{qc})(v_{Z,u}^2+a_{Z_u}^2)+(\delta_{qd}+\delta_{qs}+\delta_{qb})(v_{Z,d}^2+a_{Z_d}^2)\\ v_{Z,u} =&\frac{g_W}{c_W}(\frac{1}{2}-\frac{4}{3}s_W^2) \quad , \quad a_{Z,u}=\frac{g_W}{2c_W}\\ v_{Z,d} =&\frac{g_W}{c_W}(-\frac{1}{2}+\frac{2}{3}s_W^2) \quad , \quad a_{Z,d}=\frac{g_W}{2c_W}\,, \qquad (3.35)\end{aligned}$$

  where $c_W = \cos\theta_W$ and $s_W = \sin\theta_W$ denote the cosine and sine of the weak mixing angle, also known as *Weinberg angle* and $g_W = 4\pi\sqrt{\alpha}$ is the weak coupling.

  The form factor is identical for all initial state quarks and yields

$$\mathcal{F}_1^{Z_q} = -\,m_z^2 A_{ewk}\left(s_{13},s_{23},s_{12},Q,m_z\right)$$

[4] The (0) superscript is chosen because these contributions are of $\mathcal{O}(a_s^2)$, like the LO QCD process.

$$\mathcal{F}_2^{Z_q} = -\, m_z^2 A_{ewk}\left(s_{23}, s_{13}, s_{12}, Q, m_z\right) \tag{3.36}$$

with $A_{ewk}(s,t,u,m_h,m_z)$ given in appendix B of [64].

- W loops: The couplings are given by

$$\lambda_W = 2, \quad c_{W,q} = (v_{W,q}^2 + a_{W,q}^2), \quad v_{W,q} = \frac{g_W}{\sqrt{2}}, \quad a_{W,q} = \frac{g_W}{\sqrt{2}}, \tag{3.37}$$

$$\begin{aligned}
\mathcal{F}_1^W =& -\, m_w^2 A_{ewk}\left(s_{13}, s_{23}, s_{12}, Q^2, m_w\right) \sum_L \delta_{qL} - m_w^2 A_{ewk}^{m_t}\left(s_{13}, s_{23}, s_{12}\right) \delta_{qb} \\
\mathcal{F}_2^W =& -\, m_w^2 A_{ewk}\left(s_{23}, s_{13}, s_{12}, Q^2, m_w\right) \sum_L \delta_{qL} - m_w^2 A_{ewk}^{m_t}\left(s_{23}, s_{13}, s_{12}\right) \delta_{qb}
\end{aligned} \tag{3.38}$$

where L sums over all light quark states u, d, c, s. Note that here we have summed over the internal light quark flavors. This yields a CKM coefficient of

$$\sum_{j=1,2} |V_{ij}|^2 \approx 1 \quad \text{for} \quad \text{i} = 1, 2 \tag{3.39}$$

Measurements show this to be true to about 1 in 10000, so it is a good enough approximation to make.
For $q = b$, we have to take the internal quark to be a top. The couplings are unchanged if we use that $|V_{33}|^2 \approx 1$, which is also a good approximation to make. The form factor $A_{ewk}^{m_t}\left(s,t,u\right)$ is given in appendix B of [64].

- Higgs in the loop: In the standard model this gives a non negligible contribution for $q = b$, other quarks may be considered as well if their Yukawas are enhanced. The couplings are given by

$$\lambda_H = 3, \quad c_{H,q} = \delta_{qb}(v_{H,q}^2 + a_{H,q}^2), \quad v_{H,q} = \frac{m_q Y_q}{v}, \quad a_{H,q} = 0, \tag{3.40}$$

and the form factors which are also found in appendix B of [64], are

$$\begin{aligned}
\mathcal{F}_1^H =& -\, m_h^2 A_H\left(s_{13}, s_{23}, s_{12}\right) \\
\mathcal{F}_2^H =& -\, m_h^2 A_H\left(s_{23}, s_{13}, s_{12}\right).
\end{aligned} \tag{3.41}$$

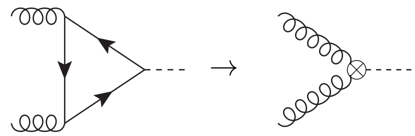

Figure 3.6.: Graphical representation of the heavy-quark effective theory. The loop with the heavy quark running inside is absorbed into an effective vertex.

3.4. Heavy quark effective theory and NNLO QCD corrections

As we have seen from the previous two sections, the gluon fusion process starts at the one-loop level since there is no direct coupling of the massless gluon to the Higgs boson. The NLO corrections presented in the previous section were already quite involved, as they require the calculation of two-loop integrals with different mass-scales.

But in the process of computing the NLO QCD corrections, it had been realised that for Higgs masses which are relatively light compared to the masses of the fermions which couple the Higgs to gluons, the limit of infinitely heavy quark masses yields a good approximation to the full result at LO [48, 75].

This approximation yields significant simplifications for higher-order computations when formulated in the language of an effective field theory. An effective field theory is a low-energy approximation of a larger theory, valid up to a certain scale Λ. Fields which are heavier than Λ decouple (they are too heavy to be produced and propagate) from the theory in this low-energy limit and can be “integrated out” from loop diagrams. All effects of the heavy states are then contained in the couplings of the effective theory.

In the case of SM Higgs production in gluon fusion, the top quark is the only heavy state which is integrated out into the effective coupling of the Higgs boson to two gluons which is called a Wilson coefficient and is usually denoted by C_1. The calculation of the SM Wilson coefficient has been carried out to five-loop accuracy [75–78], which would be enough to calculate the gluon fusion process to N^{4}LO accuracy.

BSM scenarios usually feature more heavy coloured particles, which can equally be absorbed into the Wilson coefficient. The effective theory language thus provides an ideal tool to deal with new physics models, since the only part that changes w.r.t the SM is the coupling C_1, but the rest of the partonic cross sections stays the same. The Wilson coefficient C_1 has been calculated to three-loop accuracy in the minimal supersymmetric Standard Model (MSSM) [79] as well as in models involving additional heavy quarks with SM-like couplings [80] or arbitrary couplings [81]. We have implemented the latter in `iHixs`, and will present it below for completeness.

Going into the details of deriving the effective theory formulation and calculating the Wilson coefficient C_1 would be beyond the scope of this thesis. We refer to the review [82] for technical details and just write out the effective Lagrangian below. Note that the relation of theory parameters such as the strong coupling α_s or the masses of lighter particles in the full and the effective theory are not trivial, and one has to pay attention which of the two expressions are expanded in.

We split the full original Lagrangian into a part containing all n_l light flavours and the part containing the n_h heavy quark fields,

$$\mathcal{L} = \mathcal{L}_{\text{QCD}}^{n_l} + \sum_{i=1}^{n_h} \bar{\psi}_i \left(i\not{D} - m_i \right) \psi_i - Y_i \frac{m_i}{v} H \bar{\psi}_i \psi_i \,, \tag{3.42}$$

where Y_i again parametrises the rescaling of the Yukawa coupling for the heavy quark field ψ_i from its SM value.

After integrating out the heavy quarks, the effective Lagrangian reads

$$\mathcal{L}^{\text{eff}} = \mathcal{L}_{\text{QCD}}^{n_l,\text{eff}} - \frac{1}{4v}\, C_1\, H G^{a,\mu\nu} G^a_{\mu\nu} \,, \tag{3.43}$$

where $G^a_{\mu\nu}$ denotes the gluonic field-strength tensor and $\mathcal{L}_{\text{QCD}}^{n_l,\text{eff}}$ has the exact same form as $\mathcal{L}_{\text{QCD}}^{n_l}$ but in terms of the parameters of the n_l-flavour low-energy theory.

The Lagrangian above is given in terms of bare fields and couplings, where we have suppressed the "0"-superscripts. The Wilson coefficient C_1 has to renormalised as well,

$$C_1^0 = Z_1(\mu)\, C_1(\mu) \,, \tag{3.44}$$

with

$$Z_1(\mu) = \frac{1}{1 - \beta(\mu)/\epsilon} = 1 - a_s \frac{\beta_0}{\epsilon} + a_s^2 \left(\frac{\beta_0^2}{\epsilon^2} - \frac{\beta_1}{\epsilon} \right) + a_s^3 \left(-\frac{\beta_0^3}{\epsilon^3} + \frac{2\beta_0\beta_1}{\epsilon^2} - \frac{\beta_2}{\epsilon} \right), \tag{3.45}$$

where the β_i are the expansion coefficients of the Beta-function in the n_l-flavour theory. From here on, we will abandon the variable n_l again in favour of the variable N_F, i.e. as before, N_F will denote the number of active flavours. Whether we are in the full or in the effective theory is always clear from context.

The full three-loop result for the renormalised Wilson coefficient in the case of many heavy quarks with arbitrary Yukawa coupling rescalings reads [81]

$$
\begin{aligned}
C_1(\mu) = &-\frac{1}{3}a_s(\mu)\Upsilon_0 - \frac{11}{12}a_s^2(\mu)\Upsilon_0 - \frac{1}{3}a_s^3(\mu)\Bigg\{-N_F\left(\frac{67}{96}\Upsilon_0 + \frac{2}{3}\Upsilon_1\right) \\
&+\Upsilon_0\left(\frac{1877}{192} - \frac{77}{576}n_h + \frac{113}{96}L_1 + \frac{3}{8}L_2\right) - \Upsilon_1\left(\frac{19}{8} + \frac{113}{96}n_h + \frac{3}{4}L_1\right) + \frac{3}{8}n_h\Upsilon_2 \\
&+\sum_{\substack{1\le i<n_h \\ i<j\le n_h}}\Bigg[(Y_i - Y_j)\left(\frac{57}{128}\left(\frac{m_i^2}{m_j^2} - \frac{m_j^2}{m_i^2}\right) + \left(\frac{57}{128}\frac{m_i^2}{m_j^2} + \frac{57}{128}\frac{m_j^2}{m_i^2} + \frac{43}{32}\right)\log\left(\frac{m_i}{m_j}\right)\right. \\
&\quad\left. + \frac{57}{256}\frac{m_i^6 + m_j^6}{m_i^2 m_j^2\left(m_i^2 - m_j^2\right)}\log^2\left(\frac{m_i}{m_j}\right)\right) \\
&\quad - \log^2\left(\frac{m_i}{m_j}\right)\left(\frac{73}{256}\left(Y_i + Y_j\right) + \frac{23}{128}\frac{Y_i m_i^2 - Y_j m_j^2}{m_i^2 - m_j^2}\right. \\
&\quad + \frac{3}{512}\left(m_i^2 - m_j^2\right)\frac{19m_i^4 + 24m_i^2m_j^2 + 19m_j^4}{m_i^3 m_j^3}\left(Y_j\log\left(\frac{m_j - m_i}{m_j + m_i}\right) - Y_i\log\left(\frac{m_i - m_j}{m_i + m_j}\right)\right)\Bigg) \\
&\quad - \frac{3}{1024}\frac{19m_i^6 + 5m_i^4m_j^2 - 5m_i^2m_j^4 - 19m_j^6}{m_i^3 m_j^3} \\
&\quad\cdot\Bigg(8Y_i\mathrm{Li}_3\left(\frac{m_j}{m_i}\right) - 8Y_j\mathrm{Li}_3\left(\frac{m_i}{m_j}\right) - Y_i\mathrm{Li}_3\left(\frac{m_j^2}{m_i^2}\right) + Y_j\mathrm{Li}_3\left(\frac{m_i^2}{m_j^2}\right) \\
&\quad - 2\log\left(\frac{m_i}{m_j}\right)\left(Y_i\mathrm{Li}_2\left(\frac{m_j^2}{m_i^2}\right) + Y_j\mathrm{Li}_2\left(\frac{m_i^2}{m_j^2}\right) - 4Y_i\mathrm{Li}_2\left(\frac{m_j}{m_i}\right) - 4Y_j\mathrm{Li}_2\left(\frac{m_i}{m_j}\right)\right)\Bigg)\Bigg]\Bigg\}\,,
\end{aligned}
\tag{3.46}
$$

where we have defined

$$
\begin{aligned}
L_1 &= \sum_{i=1}^{n_h}\log\left(\frac{m_i}{\mu}\right) \quad , \quad L_2 = \sum_{i=1}^{n_h}\log^2\left(\frac{m_i}{\mu}\right) \quad , \\
\Upsilon_0 &= \sum_{i=1}^{n_h} Y_i\,, \quad \Upsilon_1 = \sum_{i=1}^{n_h} Y_i\log\left(\frac{m_i}{\mu}\right)\,, \quad \Upsilon_2 = \sum_{i=1}^{n_h} Y_i\log^2\left(\frac{m_i}{\mu}\right)\,,
\end{aligned}
\tag{3.47}
$$

and Li_2 is the dilogarithm function (see chapter 4). If all $Y_i = 1$ we recover the Wilson coefficient for n_h heavy quarks with Standard Model-like Yukawa interactions of [80],

$$
C_1 = -\frac{a_s}{3}\left\{n_h + a_s\frac{11}{4}n_h - a_s^2\left[-\frac{1877}{192}n_h + \frac{77}{576}n_h^2 + \frac{19}{8}L_1 + N_F\left(\frac{67}{96}n_h + \frac{2}{3}L_1\right)\right]\right\}\,,
\tag{3.48}
$$

and for $n_h = 1$, we find the SM result [76–78] where we also give the four-loop contributions,

$$C_1 = -\frac{a_s}{3}\Bigg\{1 + a_s\frac{11}{4} + a_s^2\left[\frac{2777}{288} - \frac{19}{8}L_t + N_F\left(-\frac{67}{96} - \frac{2}{3}L_t\right)\right] \tag{3.49}$$

$$+ a_s^3\Bigg[\left(-\frac{6865}{31104} - \frac{77}{864}L_t - \frac{2}{9}L_t^2\right)N_F^2 \tag{3.50}$$

$$+\left(\frac{23}{8}L_t^2 - \frac{55}{27}L_t + \frac{40291}{20736} - \frac{110779}{13824}\zeta_3\right)N_F \tag{3.51}$$

$$-\frac{2892659}{41472} + \frac{897943}{9216}\zeta_3 + \frac{209}{16}L_t^2 - \frac{1733}{144}L_t\Bigg] + \mathcal{O}(a_s^4)\Bigg\}\,, \tag{3.52}$$

with $L_t = \log(m_t/\mu)$.

The cross section for Higgs production in the effective theory is then given by

$$\sigma_{ij}^{\text{eff}}(z,\mu_f,\mu_r) = \frac{G_F\pi}{32\sqrt{2}}|C_1(\mu_r)|^2\sum_{n=0}^{\infty}a_s^n(\mu_r)\Delta_{ij}^{(n)}(z,\mu_f,\mu_r)\,, \tag{3.53}$$

with the LO cross section now simply

$$\Delta_{ij}^{(0)}(z,\mu_f,\mu_r) = \delta_{ig}\delta_{jg}\delta(1-z)\,, \tag{3.54}$$

and the NLO corrections [48, 56]

$$\begin{aligned}\Delta_{gg}^{(1)}(z,\mu_f,\mu_r) = &\left(\pi^2 + 2\beta_0(L_r - L_f)\right)\delta(1-z) - 6L_f\mathcal{D}_0(1-z) + 12\mathcal{D}_1(1-z)\\ &+ 6\left(z^2 - z + 2 - \frac{1}{z}\right)L_f - \frac{11}{2}\frac{(1-z)^3}{z}\\ &- \frac{6}{1-z}\left(z^3 - 2z^2 + 3z - 2 + \frac{1}{z}\right)\log(z)\\ &- 12\left(z^2 - z + 2 - \frac{1}{z}\right)\log(1-z)\,,\end{aligned} \tag{3.55}$$

$$\Delta_{qg}^{(1)}(z,\mu_f,\mu_r) = \frac{2}{3}\left(2 - z - \frac{2}{z}\right)\left(L_f + \log(z) - 2\log(1-z)\right) + 2 - \frac{x}{3} - \frac{1}{x}\,, \tag{3.56}$$

$$\Delta_{q\bar{q}}^{(1)}(z,\mu_f,\mu_r) = \frac{32}{27}\frac{(1-z)^3}{z}\,, \tag{3.57}$$

where

$$L_f = \log\left(\frac{\mu_f^2}{m_H^2}\right)\,,\quad L_r = \log\left(\frac{\mu_r^2}{m_H^2}\right)\,. \tag{3.58}$$

It can be verified straightforwardly that the effective cross section above indeed is the limit of the exact NLO QCD result given in section 3.2. This is seen most easily in the coefficient of $\delta(1-z)$. Taking $\tau_q \to \infty$ in eq. (3.14) using eq. (3.17), we recover the a_s^3-coefficient of the effective cross section (3.53),

$$\begin{aligned}&\frac{G_F\pi}{32\sqrt{2}}\left(\left|C_1^{(0)}\right|^2\left(\pi^2+2\beta_0(L_r-L_f)\right)+2\mathrm{Re}\left(C_1^{(0)}C_1^{(1)*}\right)\right)\\=&\frac{G_F\pi\Upsilon_0^2}{288\sqrt{2}}\left(\pi^2+2\beta_0(L_r-L_f)+\frac{11}{2}\right).\end{aligned}\tag{3.59}$$

In the effective theory formulation, the NNLO QCD corrections were computed in ref. [56]. Due to double-real-radiation corrections, there are two additional channels opening up at this order, the qq initial state with two identical quarks, and the qQ channel where Q denotes a quark of different flavour than q (i.e. $q \neq Q \neq \bar{q}$). The regular parts of the results consist of HPLs of up to weight 4 with the real argument z. The analytic formulae of the NNLO results can be found in chapter IV of [56], but one has to pay attention that the $\eta_{ij}^{(n)}$ provided there differ from our $\Delta_{ij}^{(n)}$ by a factor of $1/z$ and also include the expansion of the Wilson coefficient C_1. For the analytic expressions in our conventions, we refer to the ancillary file `sigma.mpl` of the arXiv submission [83].

3.4.1. Mixed QCD-electroweak corrections

To obtain a quantitative idea about which factorisation scheme for the electroweak corrections (see section 3.3) is closest to reality, the authors of ref. [59] computed the mixed QCD-electroweak contributions to the gluon fusion process, i.e. diagrams of $\mathcal{O}(\alpha_s^3\alpha)$. A sample diagram would be any of the two diagrams in figure 3.4 with an additional gluon loop. A calculation in the full theory is unfeasible for the time being, therefore the authors of ref. [59] resorted to an effective theory where the W boson is integrated out. Formally, this theory is only valid in the (unphysical) region $m_H < m_W$, but there is reason to believe that the K-factor (i.e. the ratio of NLO and LO result) is well-approximated to much higher masses, since this was observed in the case of the effective theory with the top quark integrated out.

In this framework, we denote the Wilson coefficient C_1 as

$$C_1 = -\frac{a_s}{3}\left\{1+\kappa_{\mathrm{EWK}}\left[1+a_sC_{1w}+a_s^2C_{2w}\right]+a_sC_{1q}+a_s^2C_{2q}\right\},\tag{3.60}$$

where

$$\kappa_{\mathrm{EWK}} = \frac{3\alpha}{16\pi s_W^2}\left\{\frac{2}{c_W^2}\left[\frac{5}{4}-\frac{7}{3}s_W^2+\frac{22}{9}s_W^4\right]+4\right\},\tag{3.61}$$

is the limit of the two-loop light-fermion contributions from [69] for $m_W \to \infty$, and s_W and c_W denote the sine and cosine of the weak mixing angle, respectively. C_{1q} and C_{2q} denote the expansion coefficients of the pure QCD Wilson coefficient from the previous section. For the complete factorisation scheme to hold, we would need $C_{1w} = C_{1q}$ and $C_{2w} = C_{2q}$.

The result the authors of ref. [59] find is

$$C_{1w} = \frac{7}{6}, \quad \text{as opposed to} \quad C_{1q} = \frac{11}{4}, \tag{3.62}$$

in the SM. So, clearly, complete factorisation overestimates the impact of the electroweak corrections, at least at this order in QCD. The four-loop[5] contribution C_{2w} was not computed, but shown to have no big numerical impact when varied from -30 to 30. However, adapting the pattern of successive corrections found in the pure QCD corrections to the known first two orders of the electroweak corrections yields an estimate of $C_{2w} \sim 10$, which is what we have implemented in `iHixs`.

3.4.2. Combining exact and effective corrections

One should of course only resort to an effective theory formulation when the corresponding calculation in the full theory is not available, such as the NNLO QCD and mixed QCD-electroweak corrections in the present case. For all other contributions to the cross section, the full results should be used. When merging the exact and effective pieces of the cross section, we have to avoid double-counting, though.

We match the effective theory and full theory perturbative expansions as follows. Let us assume that we can compute the contributions to the cross section exactly through some perturbative order for only some of the heavy particles which contribute to Higgs production amplitudes:

$$\sigma_{\text{partial}} = \sigma^{(0)}_{\text{partial}} + a_s \sigma^{(1)}_{\text{partial}} + a_s^2 \sigma^{(2)}_{\text{partial}} + \dots \tag{3.63}$$

and the corresponding effective theory formulation for these contributions reads

$$\sigma_{\text{partial,eff}} = \left| C_0^{\text{partial}} + C_1^{\text{partial}} a_s + C_2^{\text{partial}} a_s^2 + \dots \right|^2 \left[\eta_0 + a_s \eta_1 + a_s^2 \eta_2 + \dots \right], \tag{3.64}$$

[5]Beware of the notation again, which labels the expansion coefficients according to their order in the strong coupling only. However, the additional electroweak coupling means that C_{iw} is one loop-order higher than C_{iq}.

We then write the cross-section as

$$\sigma = \sum_{n=0}^{\infty} a_s^n \left[\sigma^{(n)}_{\text{partial}} \Theta(n \le N) + \delta\sigma_{\text{eff}}\right] \tag{3.65}$$

where N is the last perturbative order that the partial contributions are known in the full theory and

$$\delta\sigma^{(0)}_{\text{eff}} = \left\{|C_0|^2 - \Theta(0 \le N)\left|C_0^{\text{partial}}\right|^2\right\}\eta_0, \tag{3.66}$$

$$\begin{aligned}\delta\sigma^{(1)}_{\text{eff}} = &\left\{|C_0|^2 - \Theta(1 \le N)\left|C_0^{\text{partial}}\right|^2\right\}\eta_1 \\ &+ \left\{2\text{Re}\left(C_0 C_1^*\right) - \Theta(1 \le N) 2\text{Re}\left(C_0^{\text{partial}} C_1^{\text{partial}*}\right)\right\}\eta_0,\end{aligned} \tag{3.67}$$

$$\begin{aligned}\delta\sigma^{(2)}_{\text{eff}} = &\left\{|C_0|^2 - \Theta(2 \le N)\left|C_0^{\text{partial}}\right|^2\right\}\eta_2 \\ &+ \left\{2\text{Re}\left(C_0 C_1^*\right) - \Theta(2 \le N) 2\text{Re}\left(C_0^{\text{partial}} C_1^{\text{partial}*}\right)\right\}\eta_1 \\ &+ \left(\left\{|C_1|^2 - \Theta(2 \le N)\left|C_1^{\text{partial}}\right|^2\right\}\right. \\ &\left.+ \left\{2\text{Re}\left(C_0 C_2^*\right) - \Theta(2 \le N) 2\text{Re}\left(C_0^{\text{partial}} C_2^{\text{partial}*}\right)\right\}\right)\eta_0.\end{aligned} \tag{3.68}$$

In our process of gluon fusion including many heavy quarks and electroweak corrections, using the Feynman rules of eq. (3.1), this means that

$$C_0 = \kappa_{\text{QCD}} \cdot 1 + \kappa_{\text{EWK}} \cdot 1 \tag{3.69}$$

$$C_1 = \kappa_{\text{QCD}} \cdot \frac{11}{4} + \kappa_{\text{EWK}} \cdot \frac{7}{6} \tag{3.70}$$

$$C_2 = \kappa_{\text{QCD}} \cdot C_{2q} + \kappa_{\text{EWK}} \cdot C_{2w}\,. \tag{3.71}$$

where we have factorised the quantity

$$\kappa_{\text{QCD}} = \sum_{q \in \text{heavy}} Y_q = \Upsilon_0\,, \tag{3.72}$$

from the Wilson coefficient (3.46).

The QCD-corrections are known up to NLO, i.e. $N = 1$, which means we need to subtract the quantities

$$C_0^{\text{partial}} = \kappa_{\text{QCD}} \cdot 1 \tag{3.73}$$

$$C_1^{\text{partial}} = \kappa_{\text{QCD}} \cdot \frac{11}{4}\,. \tag{3.74}$$

The second-order merging prescription (3.68) is not needed.

3.4.3. Improving the effective theory approach

When comparing the LO and NLO QCD results for gluon fusion in both the full and the effective theory, it was observed that the effective theory works much better for the K-factor (the ratio $\sigma_{\mathrm{NLO}}/\sigma_{\mathrm{LO}}$) rather than the absolute cross section. This can be understood by the observation that at NLO, all real and virtual amplitudes in the soft or collinear limit have the same dependence on the masses of the heavy quarks as at leading order. It seems that the factorisation of the cross section in the infrared limit closely resembles the factorisation of the cross section in the limit of infinitely heavy massive particles. Finite quark-mass effects are important for hard radiation terms, but these are expected to have a typical perturbative expansion where an α_s suppression occurs from one order to the other.

We can thus improve on the effective theory approximation by making the replacement

$$\kappa_{\mathrm{QCD}} \to \sum_{q \,\in\, \mathrm{heavy}} Y_q \frac{3}{2} \tau_q A(\tau_q)\,, \tag{3.75}$$

and

$$\kappa_{\mathrm{EWK}} \to \lambda_{\mathrm{EWK}}\, \mathcal{M}_{ggh,\mathrm{EWK}} \left(m_H^2, M_W^2, M_Z^2, \ldots \right)\,, \tag{3.76}$$

where $\mathcal{M}_{ggh,\mathrm{EWK}}$ is the full two-loop electroweak amplitude for $gg \to H$ from [58, 72] which we discussed in section 3.3. In other words, we rescale the Wilson coefficients of the effective theory with their respective *exact* leading-order amplitude.

As previously mentioned, we were given a data file containing values for the quantity δ_{EWK} as defined in eq. (3.29). Thus, we can achieve the rescaling from eq. (3.76) by substituting[6]

$$\kappa_{\mathrm{EWK}} \to \lambda_{\mathrm{EWK}} \frac{3}{2} \tau_q A\left(\tau_{top}\right) \times \sqrt{1 + \delta_{\mathrm{EWK}}} - 1. \tag{3.77}$$

Notice that we make a small error here as we rescale the entirety of electroweak contributions with the rescaling factor λ_{EWK}, as the virtual diagrams including massive quarks as depicted in figure 3.4 (a) are not proportional to this coupling. The error, however is small, especially for light Higgs masses where the electroweak corrections are dominated by the light quark loops of figure 3.4 (b).

[6] Solving eq. (3.29) for $\mathcal{M}_{ggh,\mathrm{EWK}}$

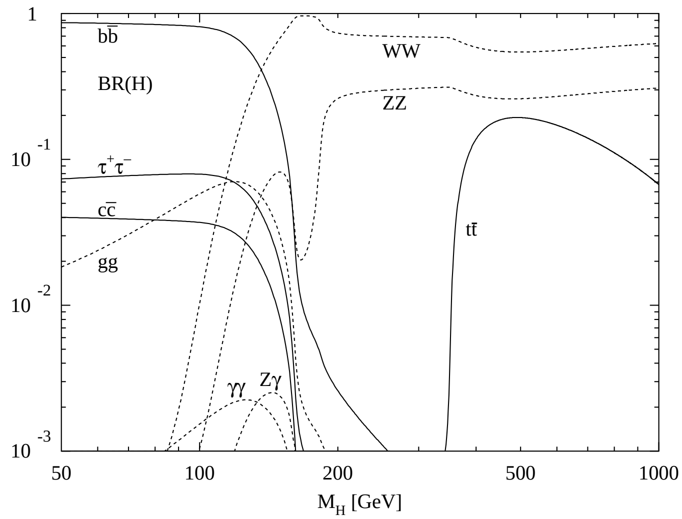

Figure 3.7.: Branching ratios of the most important Higgs decay channels as a function of the Higgs mass. Figure from ref. [89], obtained with the program `Hdecay`.

3.5. Higgs propagator treatment

The better part of the work contained in this thesis was done during the dark ages before July 4$^{\text{th}}$ 2012, i.e. before the mass of the Higgs boson was known to be approximately 125 GeV. When the TeVatron [84] and later the LHC [85,86] started ruling out SM Higgs bosons over a wide range of intermediate masses, the prospect of a heavy Higgs with a mass above 400 GeV started looking more and more likely.

Thus, a fair amount of effort was dedicated to studies of Higgs width effects during the development of `iHixs`, which stirred some discussions in the community on the Higgs width treatment and led to a number of publications at the beginning of 2012 (e.g. [87] or chapter 15 of the report [88]). Since the discovery of the Higgs, excitement has cooled down, yet the discussion is still interesting in the light of a potential second, heavier Higgs which is a feature of virtually any BSM model.

Also, the effects of performing an actual integration over a Breit-Wigner-like line shape instead of just taking the Higgs to be on-shell are enhanced when one is interested in a certain final state the Higgs decays into. Especially for light Higgs masses, the decay branching ratios depend strongly on the mass due to the crossing of kinematic thresholds, as can be seen in figure 3.7 which was taken from ref. [89]. Thus, when the branching ratio is obtained at a non-zero virtuality of the Higgs, its value may differ significantly from the the one at the nominal Higgs mass.

In `iHixs` we compute the partonic cross section for resonant production and subsequent decay of a Higgs boson into a final-state $\{H_{\text{final}}\}$ in the s-channel approximation, by performing an integration over the invariant mass of the Higgs decay products,

$$\sigma_{ij\to\{H_{\text{final}}\}+X}(\hat{s}) = \int_{Q_a^2}^{Q_b^2} dQ^2 \frac{Q\Gamma_H(Q)}{\pi} \frac{\sigma_{ij\to H}(\hat{s},Q^2)\text{Br}_{H\to\{H_{\text{final}}\}}(Q)}{\Delta_H\left(Q,m_H\right)}, \tag{3.78}$$

i.e. as mentioned above, both the production cross section $\sigma_{ij\to H}$ and the decay branching ratio $\text{Br}_{H\to\{H_{\text{final}}\}}$ are evaluated using the Higgs virtuality Q instead of the Higgs mass m_H. The respective branching ratios for a given Higgs mass were obtained with the program `Hdecay` [89] and stored in a data file. The boundaries of integration, Q_a^2 and Q_b^2 are usually defined by the experimental setup and kinematics. They may in principle be approximated by $Q_a = 0$ and $Q_b = \infty$ for most cases, since the line shape we integrate over will always be peaked at $Q = m_H$ and fall off reasonably fast when going off resonance.

The total inclusive cross-section corresponds to summing over all Higgs boson final states,

$$\sum_{\text{final}} \text{Br}_{H\to\{H_{\text{final}}\}}(Q) = 1. \tag{3.79}$$

The function Δ_H arises from s-channel Higgs propagator diagrams and it diverges at leading order in perturbation theory for $Q \to m_H$. A Dyson-resummation of dominant Feynman diagrams in this limit at all orders in perturbation theory is necessary in order to obtain a sensible finite result.

We have implemented four different schemes for the treatment of the propagator Δ_H in `iHixs`:

- **Zero width approximation** (ZWA):

$$\frac{1}{\Delta_H\left(Q,m_H\right)} \to \frac{\pi}{m_H\Gamma_H(m_H)}\delta\left(Q^2-m_H^2\right) \tag{3.80}$$

  In this scheme which has traditionally been used in every study on Higgs production and decay, there is no actual integration, i.e. the production and decay probabilities are evaluated at the nominal Higgs mass m_H. It should be an adequate treatment for a light Higgs boson where the width of the Higgs boson is very small in comparison to its mass.

- **Naive Breit-Wigner** (BW):

$$\frac{1}{\Delta_H\left(Q,m_H\right)} = \frac{1}{(Q^2-m_H^2)^2+m_H^2\Gamma_H^2(m_H)} \tag{3.81}$$

This corresponds to resumming leading width contributions for $Q \sim m_H$. The scheme is also called fixed-width scheme since the Higgs width is always evaluated at m_H.

- **Breit-Wigner with running width**:

$$\frac{1}{\Delta_H\left(Q, m_H\right)}=\frac{1}{(Q^2-m_H^2)^2+Q^2\Gamma_H^2(Q)} \tag{3.82}$$

This scheme is similar to the naive Breit-Wigner scheme, except for the fact that the width-part of the propagator is evaluated at the virtuality Q.

- **Seymour scheme**:

$$\frac{1}{\Delta_H(Q, m_H)}=\frac{m_H^4/Q^4}{(Q^2-m_H^2)^2+\Gamma_H^2(m_H^2)\frac{Q^4}{m_H^2}} \tag{3.83}$$

This scheme is a prescription to account for signal-background interference effects at the high energy limit and finite width resummation simultaneously. It is derived in ref. [90] for the process $pp \to H \to VV$ ($V = W$ or Z), whose signal-background interference with continuum vector boson pair production is found in an effective theory using the Goldstone equivalence theorem. The author of [90] finds that the bulk of the signal-background interference effects can be absorbed into a modification of the Higgs propagator,

$$\frac{i}{Q^2-m_H^2} \;\to\; \frac{i\frac{m_H^2}{Q^2}}{Q^2-m_H^2+i\Gamma_H(m_H^2)\frac{Q^2}{m_H}}, \tag{3.84}$$

which results in the Δ_H given above. This scheme is designed to interpolate smoothly between two limits which are well described either by resummation or by fixed-order perturbation theory: the resonant region $Q \sim m_H$ and the high energy limit $Q \gg m_H$.

The validity of the Seymour scheme was investigated at the differential level in ref. [91], where the signal-background interference in the process $gg \to H \to WW$ was fully calculated at leading order in QCD. In figure 8 of [91], the comparison is shown. The authors find that indeed, the approximation (3.84) captures a significant amount of the signal-background interference, but generally fails to properly describe differential distributions. Interestingly, while one generally thinks of signal-background interference effects to be only relevant if the width of a particle becomes comparable to its mass, the

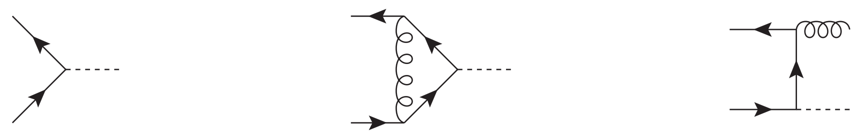

(a) LO (b) NLO virtual (c) NLO real

Figure 3.8.: Sample diagrams for the bottom quark fusion process.

authors of the reference above, as well as those of other publications [92, 93] find that in the case of $gg \to H \to WW$ interfered with the direct $gg \to WW$ process, signal-background interference effects can be as large as 10% at the inclusive level even for a 120 GeV Higgs with a very small width. A careful choice of selection cuts in differential variables can suppress this phenomenon below the per cent level, though.

We have to admit that neither of the options on the treatment of the Higgs line shape we have given above are on completely solid theoretical grounds and in general violate gauge-invariance, as has been pointed out for example in references [68, 94]. An apparently consistent recipe is "complex pole scheme" presented in ref. [68] and compared to other schemes in ref. [87]. The proposal is to replace the squared Higgs mass anywhere it appears with the complex pole s_H which is the solution of the equation

$$s_H - M_H^2 + \Sigma_{HH}(s_H)\,, \tag{3.85}$$

where M_H is the renormalised Higgs mass and Σ_{HH} the Dyson-resummed self-energy of the Higgs

It was not clear to us how to consistently apply this scheme, though, since the Higgs mass enters all invariants parametrising the phase-space integral, which is a manifestly real object. When the light Higgs hypothesis emerged as the reality, we abandoned further investigations of the Higgs line shape.

3.6. Bottom quark fusion

Although we have argued that gluon fusion is the dominant process for Higgs production at hadron colliders, we also decided to consider the direct annihilation of two bottom quarks into a Higgs boson, as depicted in figure 3.8 (a).

The reason for the inclusion lies in the large enhancement of the bottom quark fusion cross section when the Yukawa coupling modifier Y_b is chosen to be large, which is a common feature of a wealth of BSM models, the most prominent of which is the minimal supersymmetric Standard model (MSSM) with large $\tan\beta$ [95].

The $b\bar{b} \to H$ process as we are describing it above only exists in the five-flavour scheme (5FS), also called variable-flavour scheme (VFS), where the bottom quark is considered a part of the proton. Contrarily, in the four-flavour or fixed-flavour scheme (4FS or FFS), the bottom quark is considered too heavy to be found in the proton and can only be produced perturbatively, by gluon splittings. In the 4FS the inclusive cross section develops large logarithms $\sim \log(m_b/m_H)$ due to the collinear production of b-quarks which is regulated by the bottom mass. In the 5FS these logarithms are re-summed to all orders by the DGLAP evolution inside the bottom PDFs, for all scales up to the factorisation scale adopted in the calculation. The leading-order process for Higgs production through bottom quark fusion in the 4FS is $gg \to b\bar{b}H$, i.e. two gluons split into a pair of $b\bar{b}$-pairs, half of which fuse into a Higgs.

Bottom quark annihilation has been the subject of much theoretical discussion in the last decade due to this scheme dependence in treating the initial state bottom quarks. Bottom quarks lie in an intermediate mass range between the non-perturbative regime of the proton mass and the typical scale of a hard scattering event at the LHC. The improved convergence of the perturbative expansion is an advantage of the 5FS approach, but at the same time it makes the 5FS prediction very sensitive to the choice of factorisation scale. It has been realized that if the factorisation scale is set to low values $\sim m_H/4$, both the 5FS and the 4FS predictions for the inclusive cross sections agree with each other within their respective uncertainties [96–98], and there is an open discussion as to how one would combine information from both approaches [99,100]. Ref. [100] arrives at the conclusion that the 5FS framework is better suited for inclusive calculations, which is why for our purposes in `iHixs`, we simply use the 5FS NNLO QCD result which was published in ref. [101].

The only modifications we had to apply to the analytic formulae found in appendix A of [101] were the multiplication of the partonic cross sections with the Yukawa coupling rescaling Y_b^2, as well as a reconstruction of the exact dependence on renormalisation and factorisation scale, because the partonic cross sections were only provided for $\mu_r = \mu_f = m_H$. This was achieved with the method we describe in appendix C.

3.7. Description of the program `iHixs`

To conclude the chapter, we give a description of the program `iHixs` which we wrote to yield numerical results for the processes we described in the previous sections. It is written in the `Fortran` language (except for a `C++` wrapper to read in the parameters for a given run) which, despite its penchant to compile even in the presence of horrendous programming errors and complete lack of readability is still immensely popular in the high-energy physics community.

The core of the program consists of a Monte-Carlo integration routine which performs the integration over the variables x_1 and z (c.f. eq. (2.59). x_2 is derived from these two), as well as the Breit-Wigner integration over Q (c.f. eq. (3.78)) unless we employ the zero-width approximation, and the variable λ which appears in the regular pieces of the NLO QCD corrections of section 3.2. The integration is carried out by the VEGAS algorithm implemented in the CUBA-library [102].

Further libraries that are used include the package `OneLOop` [103, 104] for the evaluation of one-loop scalar integrals with complex masses, the LHAPDF-library [105] which provides a universal interface to incorporate different PDF sets, and the library CHAPLIN to evaluate HPLs of up to weight 4 numerically for arbitrary complex arguments (see chapter 4).

The code may be downloaded from the website

$$\text{http://www.phys.ethz.ch/\~{}pheno/ihixs}\,. \tag{3.86}$$

Installation instructions are found in the `README` file.

3.7.1. Usage

The various features of `iHixs` are controlled by an input `runcard`, a text file that is edited by the user. To run with a given `runcard` as input type in the installation directory:

```
./ihixs -i runcard_name -o output_filename
```

When no `runcard` is given, the program runs on the default card (called ‘runcard’) in the installation directory. When no output filename is given, the program writes the output into `runcard_name.out`.

The output consists of the total cross sections per perturbative order in QCD, together with the corresponding Monte-Carlo uncertainties and the PDF errors. Those are set to zero if no PDF uncertainty is requested in the `runcard`. The input `runcard` is also appended.

3.7.2. Setting options and variables

In the `runcard` anything after a hash symbol,‘#’, is considered as a comment and is ignored. The following options are available:

- `pdf_provider` : Sets the PDF grid used. The user can choose between the MSTW08 [106], ABKM09 [107], GJR09 [108], ABM11 [109], NNPDF21 [110], CT10 [111] and NNPDF23 [112] sets. Within the MSTW PDFs there is also the option to switch confidence level from 68% to 90% and to use the MSTW grids with the strong coupling constant varied by one standard deviation from the best fit value. The exact filenames of the available grids are stated in the default `runcard`.

- `effective_theory_flag` : Set to 0 for the exact LO and NLO QCD effects and HQET approximation for NNLO. Set to 1 for the improved HQET approximation through LO, NLO, NNLO.

- `no_error_flag`: Set to 0 to calculate with PDF uncertainty, set to 1 to calculate without PDF uncertainty.

- `collider`: Set to 'LHC' or 'TEVATRON'

- `Etot`: The total centre-of-mass collider energy. This option is ignored if the collider chosen above is TeVatron and the energy is set to 1.96 TeV.

- `mhiggs`: The nominal mass of the Higgs boson.

- `higgs_width_scheme` : Set to 0 for the default finite width scheme, to 1 for the Seymour scheme and to 2 for the running-width scheme. For a description of these schemes see section 3.5.

- `higgs_width_grid`: The path of the file with the grid for the width of the Higgs, and the branching ratios to $\gamma\gamma$, WW, ZZ and $b\bar{b}$ as a function of m_H. If no path is set the default grid is used, `HdecayGrid.dat`, constructed with `Hdecay v.3.532` [89]with arguments that can be read in the header of the file. If the user supplies a grid file of his own, operating requirements are that the maximum number of grid points cannot exceed 16200, that the first three lines of the file are reserved for comments (so they are not read) and that the format of each line is respected, i.e. that the data is given in the order m_H, Γ_H, $\mathrm{BR}_{\gamma\gamma}$, BR_{WW}, BR_{ZZ}, $\mathrm{BR}_{b\bar{b}}$.

- `min_mh` : Sets a minimum in the invariant mass of the Higgs boson. This allows the user to study the total cross section in the presence of kinematical cuts.

- `max_mh` : Sets a maximum in the invariant mass of the Higgs boson.

- `bin_flag` : Set to 1 to produce files with the bin-integrated Higgs invariant mass. Set to 0 not to produce it. The data files produced contain the cross section per bin, with the bin size set to 1 GeV, from 30 to 2000 GeV at LO, NLO and NNLO. The files are named '`masshisto$`m_H`.$order`', so e.g. for $m_H = 200$ GeV the NLO file will be '`masshisto200.1` '.

- `muf/mhiggs` : The ratio of the factorisation scale and the Higgs mass.

- `mur/mhiggs` : The ratio of the renormalisation scale and the Higgs mass.

- `DecayMode`: Set to `no_width` for the zero width approximation total cross section, to '`total`' for finite width total cross section, or to the decay modes '`gamma gamma`', '`ZZ`', '`WW`', '`b b-bar`'.

- `ProductionMode`: Set to '`gg`' for gluon fusion or to '`bb`' for bottom quark fusion.

- `K_ewk`: This is a global rescaling factor for all electroweak corrections. Set to 0.0 to switch them off.

- `K_ewk_real`: Set to 0.0 to switch the electroweak corrections to $H + j$ off.

- `K_ewk_real_b`: Set to 0.0 to switch the electroweak corrections to $H + j$ that include diagrams with massive quarks or Higgs boson in the loop, off.

- `m_top`: The mass of the top quark.

- `Gamma_top`: The width of the top quark.

- `Y_top` : Rescaling factor for the SM Yukawa coupling of the top quark. Note that this can be set to an arbitrarily small positive value, but not to 0.0 exactly.

- `scheme_top`: Set to 0 to use the $\overline{\text{MS}}$ scheme for the top mass renormalisation and to 1 for the on-shell scheme. In the case of the $\overline{\text{MS}}$ scheme, the mass input from above is interpreted as $\overline{m}_t(\overline{m}_t)$, i.e. the $\overline{\text{MS}}$ top mass at its own scale and run to $\overline{m}_t(\mu_r)$ from there.

- `m_bot`: The mass of the bottom quark.

- `Gamma_bot`: The width of the bottom quark.

- `Y_bot`: Rescaling factor for the SM Yukawa coupling of the bottom quark.

- `scheme_bottom`: Set to 0 to use the $\overline{\text{MS}}$ scheme for the bottom mass renormalisation and to 1 for the on-shell scheme. In the $\overline{\text{MS}}$ case, the mass interpreted as $\overline{m}_t(10\,\text{GeV})$.

- `heavy quark`: Optional extra quarks in the model. The argument of this option should be formatted as $m_Q : \Gamma_Q : Y_Q : s_Q$ where Y_Q is the rescaling factor from a SM-like Yukawa coupling m_Q/v and s_Q parametrises the scheme-choice like for the top quark. For example, adding an extra 300GeV quark with width 1.2GeV, a Yukawa coupling that is $5.7\frac{m_Q}{v}$ and renormalisation in the on-shell scheme, the user should type:

  ‘`heavy quark = 300.0 :  1.2 :  5.7 :  1`’

- `m_Z`: The mass of the Z boson.

- `Gamma_Z`: The width of the Z boson

- `m_W`: The mass of the W boson

- `Gamma_W`: The width of the W boson

- `epsrel`: Sets the relative Monte-Carlo integration error.

- `epsabs`: Sets the absolute Monte-Carlo integration error.

- `nstart` : Sets the number of points per Vegas iteration.

- `nincrease`: Sets the number of points by which the number of points per iteration increases

- `mineval`: Sets the minimum number of points before ending the Monte-Carlo integration

- `maxeval`: Sets the maximum number of points after which the integration ends.

- `adapt to central only`: Set to 0 to force Vegas to adapt to all integrand. Set to 1 to adapt to the central integrand only. This is useful when running with PDF errors. Then each member of the PDF grid is treated as a separate integral. Adapting to the central only assumes that the peak structures of all integrals is similar which is a good approximation, and saves some CPU time.

- `vegas_verbose`: Set to 0 for silent Vegas output. Set to 2 to have information about each iteration printed in the standard output (the console).

Further information and a version history of the program can be found on the website (3.86).

3.8. Conclusions

We have introduced the processes of gluon fusion and bottom quark fusion, with an emphasis on the former one. The framework we are working in are the generalised Feynman rules of eq. (3.1) which allow each quark to have a Yukawa coupling different from the SM strength, and also the coupling of the Higgs to vector bosons can be rescaled.

The perturbative expansion of the inclusive cross section starts at the one-loop level, where heavy quarks propagating in a loop create the coupling of the gluons to the Higgs. The LO amplitude (3.6) is given by a simple squared logarithm in the variable x_q which is in general complex.

The NLO QCD corrections consist of two-loop virtual corrections to the LO diagrams and real-radiation contributions for which two new partonic channels open up, the qg and the $q\bar{q}$ channel. All contributions to the NLO cross section are known analytically, the most complicated pieces being the weight-four harmonic polylogarithms of the virtual corrections, which have the complex x_q as an argument.

Electroweak corrections to gluon fusion arise in three ways. There are two kinds of contributions at the two-loop level, through light quark loops and subsequent fusion of two electroweak gauge bosons into a Higgs boson, or via the massive quark diagrams of figure 3.4. Furthermore, there are electroweak contributions to the real-radiation processes $qg \to Hq$ and $q\bar{q} \to Hg$. Out of the three types of contributions, we only lack an analytical expression for the virtual massive quark contributions. Since virtual corrections are independent of parton luminosities, we can still implement the full virtual electroweak corrections through a data-file containing the enhancement factor δ_{EWK} as defined in eq. (3.29), which was kindly provided to us by the authors of ref. [72].

Beyond the NLO QCD and electroweak corrections, one has to resort to effective theory approximations. In the case of QCD corrections, this amounts to integrating out the heavy quark degrees of freedom. We have implemented the Wilson coefficient for the effective coupling of gluons to the Higgs boson for an arbitrary number of heavy quarks with couplings different from their SM values as given in eq. (3.46), and the corresponding partonic cross sections in the effective theory.

In the framework of effective theories, also the mixed QCD-electroweak corrections can be approximated, at least the contributions coming from light quark loops. The heavy degrees of freedom integrated out are the electroweak gauge bosons. The four-loop mixed QCD-electroweak corrections are unknown, but have been found to be numerically insignificant.

In sections 3.4.2 and 3.4.3 we explain how we combine the exact and effective theory cross sections to avoid double-counting, and define our improved effective theory approximation, which essentially consists of rescaling the Wilson coefficients with the exact LO amplitude for the respective process.

The different schemes to treat off-shell effects of the Higgs are given in section 3.5. All except the zero-width approximation include an integration over some Breit-Wigner-like distribution, the form of which depends on the scheme chosen. The Seymour-scheme in particular differs from the other approaches inasmuch as it seeks to emulate signal-background interference effects in the $gg \to H \to VV$ process.

The bottom quark fusion process is presented rather briefly in section 3.6, as we have straightforwardly implemented the NNLO QCD cross sections, with the appropriate rescaling factors due to our generalised Feynman rules.

Finally, the `iHixs` program is described in some detail in section 3.7 to showcase its various features.

4. Harmonic polylogarithms and the Chaplin library

When computing higher-order corrections in perturbative QCD, one invariably encounters a class of functions called polylogarithms, which can be thought of as a generalisation of the ordinary logarithm. The simplest and most important example is the dilogarithm function Li_2, which appeared in mathematical works of the 17^{th} century [113], already. The first proper studies on it are often accredited to Leonhard Euler who investigated the function in the 1760s, although apparently his work is predated by the one of Landen [113]. The British mathematician William Spence [114] then conducted comprehensive studies on the dilogarithm at the beginning of the 19^{th} century, deriving important identities for argument transformations and extended the class of functions under consideration to the classical polylogarithms Li_n. Thus, the dilogarithm is often referred to as “Spence's function”.

Nielsen [115] further extended the set of polylogarithms, allowing for two integer indices. Starting at the end of the previous century, various two-loop computations necessitated a further generalisation, leading to the notions of harmonic polylogarithms [116], two-dimensional harmonic polylogarithms [117,118], cyclotomic harmonic polylogarithms [119] or the previously mentioned generalised harmonic polylogarithms found in the electroweak corrections to gluon fusion [69]. All these classes of functions are subsets of the multiple polylogarithms introduced by Goncharov during the 1990s [120–122].

For all processes considered in this thesis, the subset of harmonic polylogarithms proved sufficient to parametrise all results. As mentioned in sections 3.1 and 3.2, the argument of the HPLs may be a complex number, though. When writing a Monte-Carlo integration code such as `iHixs`, we thus need to be able to evaluate HPLs numerically for any complex argument. Furthermore, since the same numerical code should also be useful in Monte-Carlo codes that generate differential distributions, where 1) the integrand usually has to be evaluated many millions of times and 2) there are big cancellations among various contributions at the numerical level, the numerical implementation should also be fast and precise.

While there are existing numerical implementations of HPLs, none of them fulfilled all the criteria above. The `Fortran` code `hplog` [123] is fast and precise but restricted to real arguments. The MATHEMATICA package HPL [124, 125] allows for complex arguments but is hard to interface with a computer program dynamically, and also not fast enough for repeated evaluations. Finally, the `C++` library GiNaC contains an implementation of general multiple polylogarithms for any complex argument [126], but its speed is not sufficient for many repeated evaluations, either.

This led to the development of the CHAPLIN (the obvious acronym for "Complex Harmonic PolyLogarithms In fortraN") library, a code which allows to evaluate HPLs up to weight four (we will define the weight of a polylogarithm in a moment) for arbitrary complex arguments.

We will first define the class of harmonic polylogarithms and point out some of their properties, show how we can reduce a general HPL to a superposition of basis functions and then provide algorithms to evaluate the basis functions for arbitrary complex argument. The library CHAPLIN is presented at the end of the chapter.

4.1. Definition and properties

We start by defining the classical polylogarithms,

$$\mathrm{Li}_n(x) = \int_0^x \mathrm{d}t\, \frac{\mathrm{Li}_{n-1}(t)}{t}\,, \quad \text{with} \quad \mathrm{Li}_1(x) = -\log(1-x)\,. \tag{4.1}$$

The extension to harmonic polylogarithms is performed by allowing for the three different denominator functions (also called "weight" functions)

$$f_{-1}(t) = \frac{1}{1+t}\,, \quad f_0(t) = \frac{1}{t}\,, \quad f_1(t) = \frac{1}{1-t}\,, \tag{4.2}$$

and defining recursively

$$\mathrm{H}(a_1,\ldots,a_n;x) = \int_0^x \mathrm{d}t\, f_{a_1}(t)\, \mathrm{H}(a_2,\ldots,a_n;t)\,, \quad \text{for} \quad a_i \in \{-1,0,1\}\,, \tag{4.3}$$

with the initial condition $\mathrm{H}(\,;t) = 1$. For the special case of all a_i being equal to zero where the integral (4.2) is divergent, we simply define

$$\mathrm{H}(\vec{0}_n;x) \equiv \frac{\log^n(x)}{n!}\,, \quad \text{where} \quad \vec{a}_k = (\underbrace{a,\ldots,a}_{n\,\text{times}})\,. \tag{4.4}$$

The definition (4.2) directly fixes the derivative of a HPL,

$$\frac{\mathrm{d}}{\mathrm{d}x}\,\mathrm{H}(a_1,\ldots,a_n;x) = f_{a_1}(x)\mathrm{H}(a_2,\ldots,a_n;x)\,. \tag{4.5}$$

The length of the index vector $\vec{a} = (a_1, \ldots, a_n)$, i.e. the number of indices n is called the *weight* of the polylog. We will often use the more compact notation

$$\mathrm{H}(a_1,\ldots,a_n;x) = \mathrm{H}_{a_1,\ldots,a_n}(x)\,, \tag{4.6}$$

and also the so-called “m”-notation, where the number of indices equal to zero to the left of a non-zero index plus one is multiplied to that non-zero index, and the 0-indices are subsequently omitted. To illustrate this slightly convoluted statement, we give an example,

$$\mathrm{H}(\underbrace{0,0}_{3-1},-1,\underbrace{0}_{2-1},1;x) = \mathrm{H}_{-3,2}(x)\,. \tag{4.7}$$

In this notation, the weight of the polylogarithm is given by the sum of the absolute values of all indices. The relation of HPLs to Nielsen polylogs [115] which are defined as

$$\mathrm{S}_{n,p}(x) = \frac{(-1)^{n+p-1}}{(n-1)!p!}\int_0^1 \mathrm{d}t\,\frac{\log^{n-1}(t)\log^p(1-xt)}{t}\,, \tag{4.8}$$

is given by

$$\mathrm{S}_{n,p}(x) = \mathrm{H}(\vec{0}_n,\vec{1}_p;x)\;. \tag{4.9}$$

While it is in general not possible to obtain a closed form in terms of elementary functions for a given HPL of higher weight, there are the special cases similar to eq. (4.4),

$$\mathrm{H}(\pm\vec{1}_n;x) = (\mp 1)^n\frac{\log^n(1\mp x)}{n!}\,,\quad \text{and}\quad \mathrm{H}(\vec{0}_{n-1},1;x) = \mathrm{Li}_n(x)\,. \tag{4.10}$$

There are 3^k different HPLs for a given weight k. There is a wealth of relations among HPLs which allows one to define a certain set of basis functions for each weight and reduce all HPLs of the corresponding weight to a linear combination of these basis functions. Actually, we will see that up to weight three, the only basis function we need are the ordinary logarithm and the classical polylogs, with a certain set of arguments. Starting from weight four, this is no longer possible and genuine new functions will appear.

4.1.1. Shuffle algebra

From the definition in eq. (4.2), it is clear that unless $(a_1, \ldots, a_n) = \vec{0}_n$,

$$\mathrm{H}(a_1, \ldots, a_n; 0) = 0 \,. \tag{4.11}$$

Similarly to the divergence of $\mathrm{H}(\vec{0}_n; x)$ at $x = 0$, HPLs with a leftmost index equal to ± 1 diverge at $x = \pm 1$ unless all other indices are equal to zero. These divergences can be made apparent by exploiting the shuffle-algebra structure that HPLs satisfy. The shuffle product of two vectors $\vec{n}$ and $\vec{m}$ is defined as the sum of all permutations of the elements of $\vec{n}$ and $\vec{m}$ where the order of elements coming from *the same* vector is not changed. Again, we illuminate this statement with an example,

$$\begin{aligned}(a,b,c)\,\Delta\,(d,e) =&(a,b,c,d,e) + (a,b,d,c,e) + (a,d,b,c,e)\\ &+(d,a,b,c,e) + (a,b,d,e,c) + (a,d,b,e,c)\\ &+(d,a,b,e,c) + (a,d,e,b,c) + (d,a,e,b,c)\\ &+(d,e,a,b,c)\end{aligned} \tag{4.12}$$

The shuffle algebra of HPLs relates the product of two HPLs of equal argument to the sum of all HPLs with indices in the shuffle product of the original two index vectors,

$$\mathrm{H}(\vec{a}; x)\,\mathrm{H}(\vec{b}; x) = \sum_{\vec{c}\,\in\,\vec{a}\Delta\vec{b}} \mathrm{H}(\vec{c}; x) \,. \tag{4.13}$$

The shuffle algebra structure is actually a property of any function defined via iterated integrals, and can easily be proven by iteratively dividing up the integration region $\int_0^x \mathrm{d}t_1 \mathrm{d}t_2$ into a lower and an upper triangle,

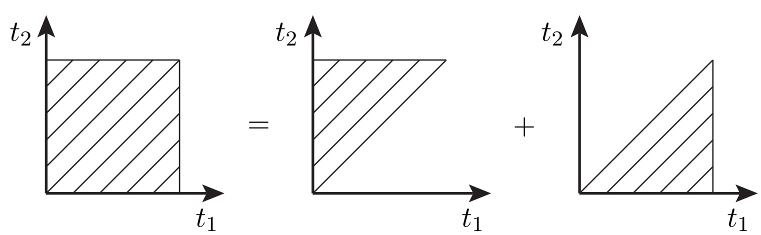

which means, denoting $(a_2, \ldots, a_n) = \hat{\vec{a}}$ and $(b_2, \ldots, b_n) = \hat{\vec{b}}$

$$\begin{aligned}\mathrm{H}(\vec{a}; x)\,\mathrm{H}(\vec{b}; x) &= \int_0^x \mathrm{d}t_1 \mathrm{d}t_2\, f_{a_1}(t_1) f_{b_1}(t_2) \mathrm{H}(\hat{\vec{a}}; t_1)\mathrm{H}(\hat{\vec{b}}; t_2)\\ &= \int_0^x \mathrm{d}t \left[f_{a_1}(t)\mathrm{H}(\hat{\vec{a}}; t)\mathrm{H}(\vec{b}; t) + f_{b_1}(t)\mathrm{H}(\vec{a}; t)\mathrm{H}(\hat{\vec{b}}; t)\right] .\end{aligned} \tag{4.14}$$

Repeating the same step for the $\int_0^t \mathrm{d}u_1 \mathrm{d}u_2$ integration and all further nested integrations, we see that we can pull out all weight functions and mix their order freely, except for the ones coming from the same index vector.

If we now consider, for example, the HPL $\mathrm{H}(1,0,1;x)$, we can use the shuffle algebra to pull out the logarithmic divergence at $x=1$,

$$\mathrm{H}(1,0,1;x) = \mathrm{H}(1;x)\mathrm{H}(0,1;x) - 2\mathrm{H}(0,1,1;x) = -\log(1-x)\mathrm{Li}_2(x) - 2\mathrm{H}_{2,1}(x)\,, \quad (4.15)$$

where the second term on the RHS is finite at $x=1$.

4.1.2. Representation as nested sums and values at ± 1

While we usually define a HPL via nested integrals, there exists a second definition of HPLs as nested sums [121], valid for $|x| < 1$,

$$\begin{aligned}&\mathrm{H}(\underbrace{0,\ldots,0}_{m_k-1},1,\underbrace{0,\ldots,0}_{m_{k-1}-1},a_{k-1}\ldots,\underbrace{0,\ldots,0}_{m_1-1},a_1;x)\\ &= (-1)^{k+p}\mathrm{Li}_{m_1,\ldots,m_k}(\frac{a_2}{a_1},\frac{a_3}{a_2},\ldots,\frac{a_{k-1}}{a_{k-2}},\frac{1}{a_{k-1}},x)\,,\end{aligned} \quad (4.16)$$

where p is the number of $+1$ indices among the a_i and

$$\mathrm{Li}_{m_1,\ldots,m_k}(x_1,\ldots,x_k) = \sum_{n_k=1}^{\infty} \frac{x_k^{n_k}}{n_k^{m_k}} \sum_{n_{k-1}=1}^{n_k-1} \cdots \sum_{n_1=1}^{n_2-1} \frac{x_1^{n_1}}{n_1^{m_1}}\,. \quad (4.17)$$

HPLs with their rightmost index equal to zero have to be rewritten as a sum of other HPLs using the shuffle algebra. Having the leftmost non-zero index equal to +1 and not -1 can be achieved via the identity

$$\mathrm{H}(a_1,\ldots,a_n;x) = (-1)^p \mathrm{H}(-a_1,\ldots,-a_n;-x)\,, \quad (4.18)$$

which is easily obtained from the integral definition (4.2) by mapping $t \to -t$. The exponent p is the number of non-zero indices among the a_i.

As the notation already suggests, we recover the classical polylogarithms for the case $k=1$, and their sum-representation just reads

$$\mathrm{Li}_n(x) = \sum_{k=1}^{\infty} \frac{x^k}{k^n}\,, \quad (4.19)$$

which immediately gives us the relation between classical polylogarithms at $x=1$ and the Riemann zeta values,

$$\mathrm{Li}_n(1) = \zeta_n \quad \text{for} \quad n \geq 2\,. \tag{4.20}$$

In general the value of a HPL at $x = \pm 1$ is thus given by alternating multiple zeta values,

$$\zeta(m_1, \ldots, m_n; \sigma_1, \ldots, \sigma_n) = \sum_{k_1 > k_2 > \ldots > k_n > 0} \frac{\sigma_1^{k_1} \sigma_2^{k_2} \cdots \sigma_n^{k_n}}{k_1^{m_1} k_2^{m_2} \cdots k_n^{m_n}}\,, \tag{4.21}$$

where $\sigma_i = \pm 1$, which up to weight four can be written as combinations of ordinary zeta values, factors of $\log(2)$ and the constant $\mathrm{Li}_4(1/2)$ in the non-divergent cases.

4.1.3. Analytic continuation

The integral definition (4.2) is valid for any complex number x unless we are sitting on a divergence. To keep the functions single-valued, one needs to introduce branch cuts. At weight one, we analytically continue the HPLs according to the usual prescription for the principal branch of the complex logarithm, i.e. we place the branch cut on the real axis,

$$\begin{aligned}
\mathrm{H}_{-1}(x + i\epsilon) &= \log(|1 + x|) + i\pi && \text{for} \quad x \in \mathbb{R},\ x < -1\,,\\
\mathrm{H}_{0}(x + i\epsilon) &= \log(|x|) + i\pi && \text{for} \quad x \in \mathbb{R},\ x < 0\,,\\
\mathrm{H}_{1}(x + i\epsilon) &= -\log(|1 - x|) + i\pi && \text{for} \quad x \in \mathbb{R},\ x > 1\,.
\end{aligned} \tag{4.22}$$

These prescriptions then define the analytic continuation for any higher-weight HPL. A general HPL with mixed indices has branch cuts for $-\infty < x < 0$ and $1 < x < \infty$ on the real axis, i.e. all HPLs are real-valued on the interval $(0, 1)$.

4.2. The strategy for numerical evaluation

There are many more functional identities among HPLs than just the shuffle relations or eq. (4.18), for example the well-known "mirror" relation

$$\mathrm{Li}_2(1 - x) = -\mathrm{Li}_2(x) + \zeta_2 - \log(1 - x)\log(x)\,, \tag{4.23}$$

or the inversion relation

$$\mathrm{Li}_2\left(\frac{1}{x}\right) = -\mathrm{Li}_2(x) - \zeta_2 - \mathrm{H}_{0,0}(-x)\,. \tag{4.24}$$

The derivation of such identities involving different arguments is quite tricky using the integral definition of the HPLs, especially when going to higher weights. Yet, we exactly want to exploit all possible identities to reduce an arbitrary HPL up to weight four to a superposition of a certain set of basis functions. The task of numerical evaluation of the HPLs then becomes the numerical evaluation of the basis functions.

In recent years, a very efficient way of obtaining all identities among polylogarithms has been developed. It goes under the name of symbol calculus [127–130]. Symbol calculus enables us to perform a two-step programme to find an efficient way to numerically evaluate HPLs for arbitrary arguments.

In the first step, we use it to identify a certain set of basis functions which span the space of all HPLs up to weight four, and find the expressions for all HPLs in terms of these basis functions. In the second step, we derive inversion mappings of the type (4.24) for all basis functions, i.e. we can map any argument outside the unit disc into it.

Finally, inside the unit disc, we know that we can expand polylogarithms and thus also our basis functions in a series, for example via eq. (4.17), to be able to perform an evaluation. Actually, the series employed will depend on the location of the argument z in the unit disc to ensure the best possible convergence.

We will lay out these three steps (reduction to basis functions, inversion relations for basis functions, series expansion of basis functions inside the unit disc) in the following sections. The first two steps have been derived and published in a dedicated publication [129] with more emphasis on the technicalities associated with symbol calculus. We will therefore be rather brief on these topics.

4.2.1. Reduction to basis functions and inversion mappings

At the heart of the symbol calculus is the so-called *symbol map*, a linear map that associates to a HPL of weight n a tensor of rank n. As an example, the tensor associated to the classical polylogarithm $\mathrm{Li}_n(z) = \mathrm{H}(\vec{0}_{n-1}, 1; z)$ reads,

$$\mathcal{S}(\mathrm{Li}_n(z)) = -(1-z) \otimes \underbrace{z \otimes \ldots \otimes z}_{(n-1)\text{ times}} . \tag{4.25}$$

Furthermore, the symbol maps products that appear inside the tensor product to a sum of tensors,

$$\ldots \otimes (X \cdot Y) \otimes \ldots = \ldots \otimes X \otimes \ldots + \ldots \otimes Y \otimes \ldots . \tag{4.26}$$

It is conjectured that all the functional identities among (multiple) polylogarithms are mapped under the symbol map $\mathcal{S}$ to algebraic relations among the tensors. Hence, the symbol calculus provides an effective way to resolve all the functional equations among a certain class of polylogarithms.

In Ref. [129], the symbol map was used to obtain a set of basis functions through which all HPLs up to weight four can be expressed. The basis functions obtained read,

- for weight one,

$$\mathcal{B}_1^{(1)}(z) = \ln z, \quad \mathcal{B}_1^{(2)}(z) = \ln(1-z), \quad \mathcal{B}_1^{(3)}(z) = \ln(1+z)\,, \tag{4.27}$$

- for weight two,

$$\mathcal{B}_2^{(1)}(z) = \mathrm{Li}_2(z), \quad \mathcal{B}_2^{(2)}(z) = \mathrm{Li}_2(-z), \quad \mathcal{B}_2^{(3)}(z) = \mathrm{Li}_2\left(\frac{1-z}{2}\right)\,, \tag{4.28}$$

- for weight three,

$$\begin{aligned}
&\mathcal{B}_3^{(1)}(z) = \mathrm{Li}_3(z), && \mathcal{B}_3^{(2)}(z) = \mathrm{Li}_3(-z), && \mathcal{B}_3^{(3)}(z) = \mathrm{Li}_3(1-z),\\
&\mathcal{B}_3^{(4)}(z) = \mathrm{Li}_3\left(\frac{1}{1+z}\right), && \mathcal{B}_3^{(5)}(z) = \mathrm{Li}_3\left(\frac{1+z}{2}\right), && \mathcal{B}_3^{(6)}(z) = \mathrm{Li}_3\left(\frac{1-z}{2}\right),\\
&\mathcal{B}_3^{(7)}(z) = \mathrm{Li}_3\left(\frac{1-z}{1+z}\right), && \mathcal{B}_3^{(8)}(z) = \mathrm{Li}_3\left(\frac{2z}{z-1}\right)\,,
\end{aligned} \tag{4.29}$$

- for weight four,

$$\begin{aligned}
&\mathcal{B}_4^{(1)}(z) = \mathrm{Li}_4(z), && \mathcal{B}_4^{(2)}(z) = \mathrm{Li}_4(-z), && \mathcal{B}_4^{(3)}(z) = \mathrm{Li}_4(1-z),\\
&\mathcal{B}_4^{(4)}(z) = \mathrm{Li}_4\left(\frac{1}{1+z}\right), && \mathcal{B}_4^{(5)}(z) = \mathrm{Li}_4\left(\frac{z}{z-1}\right), && \mathcal{B}_4^{(6)}(z) = \mathrm{Li}_4\left(\frac{z}{z+1}\right),\\
&\mathcal{B}_4^{(7)}(z) = \mathrm{Li}_4\left(\frac{1+z}{2}\right), && \mathcal{B}_4^{(8)}(z) = \mathrm{Li}_4\left(\frac{1-z}{2}\right), && \mathcal{B}_4^{(9)}(z) = \mathrm{Li}_4\left(\frac{1-z}{1+z}\right),\\
&\mathcal{B}_4^{(10)}(z) = \mathrm{Li}_4\left(\frac{z-1}{z+1}\right), && \mathcal{B}_4^{(11)}(z) = \mathrm{Li}_4\left(\frac{2z}{z+1}\right), && \mathcal{B}_4^{(12)}(z) = \mathrm{Li}_4\left(\frac{2z}{z-1}\right),\\
&\mathcal{B}_4^{(13)}(z) = \mathrm{Li}_4\left(1-z^2\right), && \mathcal{B}_4^{(14)}(z) = \mathrm{Li}_4\left(\frac{z^2}{z^2-1}\right), && \mathcal{B}_4^{(15)}(z) = \mathrm{Li}_4\left(\frac{4z}{(z+1)^2}\right)\,.
\end{aligned} \tag{4.30}$$

All harmonic polylogarithms up to weight three can be expressed through the basis functions in eqs. (4.27 - 4.30). Starting from weight four, we need to extend the set of functions by adjoining three new elements to the basis,

$$\begin{gathered}\mathcal{B}_4^{(16)}(z) = \mathrm{Li}_{2,2}(-1, z), \quad \mathcal{B}_4^{(17)}(z) = \mathrm{Li}_{2,2}\left(\frac{1}{2}, \frac{2z}{z+1}\right), \\ \mathcal{B}_4^{(18)}(z) = \mathrm{Li}_{2,2}\left(\frac{1}{2}, \frac{2z}{z-1}\right), \end{gathered} \tag{4.31}$$

where $\mathrm{Li}_{2,2}$ denotes a two-variable multiple polylogarithm that cannot be expressed through classical polylogarithms only,

$$\mathrm{Li}_{2,2}(z_1, z_2) = \sum_{n_1=1}^{\infty} \sum_{n_2=1}^{n_1-1} \frac{z_1^{n_1}}{n_1^2} \frac{z_2^{n_2}}{n_2^2} \,. \tag{4.32}$$

For practical purposes we find it more convenient to use a different set of multiple polylogarithms as basis functions than the one used in Ref. [129]. More specifically, we perform a change of basis and replace the functions $\mathcal{B}_4^{(i)}(z)$, for $i = 16, 17, 18$, by the functions $\tilde{\mathcal{B}}_4^{(i)}(z)$, which are directly expressed as HPLs,

$$\begin{aligned} \tilde{\mathcal{B}}_4^{(16)}(z) &= \mathrm{H}(0,1,0,-1;z) = \mathcal{B}_4^{(16)}(-z)\,, \\ \tilde{\mathcal{B}}_4^{(17)}(z) &= \mathrm{H}(0,1,1,-1;z)\,, \\ \tilde{\mathcal{B}}_4^{(18)}(z) &= \mathrm{H}(0,1,1,-1;-z)\,. \end{aligned} \tag{4.33}$$

The mapping from $(\mathcal{B}_4^{(17)}, \mathcal{B}_4^{(18)})$ to $(\tilde{\mathcal{B}}_4^{(17)}, \tilde{\mathcal{B}}_4^{(18)})$ is given in appendix D. The set of the 32 functions $\mathcal{B}_i^{(j)}(z)$ defines a basis through which all HPLs up to weight four can be expressed. As a consequence, any numerical code to evaluate this set of basis functions will automatically be able to evaluate all 120 HPLs up to weight four. Furthermore, as the basis functions only involve the two genuine harmonic polylogarithms $\mathrm{H}_{2,-2}(z)$ and $\mathrm{H}_{2,1,-1}(z)$ besides the ordinary logarithms and the classical polylogarithms $\mathrm{Li}_2(z)$, $\mathrm{Li}_3(z)$ and $\mathrm{Li}_4(z)$, it is enough to have numerical routines for these six functions. In this way we can reduce the problem of evaluating the 120 HPLs up to weight four to only a handful of non-trivial numerical routines.

For the expressions of all HPLs through weight four in terms of the basis functions $\mathcal{B}_i^{(j)}$, we refer to appendix D. Notice that only a minimal set of reduction formulae is given to save space, as all other reductions can be obtained via the shuffle algebra (4.13).

The basis functions as they are defined in eqs. (4.27) through (4.30) are actually only correct in their entirety for $z \in [0, 1]$. All basis functions need to recreate the analytic properties of HPLs as defined in the previous subsection for any complex argument. For most of the basis functions, the definition stays the same, but we need to make two adjustments to the definitions to ensure that they exhibit the same cuts as a HPL.

First, the definition of $\mathcal{B}_4^{(13)}(z)$ valid on the whole complex plane reads [129],

$$\mathcal{B}_4^{(13)}(z) = \begin{cases} \mathrm{Li}_4(1-z^2)\,, & \text{if } \mathrm{Re}(z) > 0 \text{ or } (\mathrm{Re}(z) = 0 \text{ and } \mathrm{Im}(z) \geq 0)\,, \\ \mathrm{Li}_4(1-z^2) - \frac{i\pi}{3}\,\sigma(z)\,\ln^3(1-z^2)\,, & \text{otherwise}\,, \end{cases} \tag{4.34}$$

where

$$\sigma(z) = \mathrm{sign}(\mathrm{Im}(z))\,. \tag{4.35}$$

Second, we note that there is a subtlety in the basis function $\mathcal{B}_4^{(15)}(z)$ when going from the interior to the exterior of the unit disc because $\mathcal{B}_4^{(15)}(z)$ has a branch cut along the unit circle in the complex z-plane. In Ref. [129] it was shown that if we want $\mathcal{B}_4^{(15)}(z)$ to be continuous and real for $z \in [0,1]$, we need to choose the following prescription for $|z| = 1$,

$$\mathcal{B}_4^{(15)}(z) = \mathrm{Li}_4\left(\frac{4z}{(1+z)^2} + i\sigma(z)\varepsilon\right)\,. \tag{4.36}$$

The inversion relations for the basis functions are derived in appendices E and F of ref. [129]. We give the results for weights one and two, but refer to said appendices for the lengthy result for higher weights.

For weight 1, the inversion relations read

$$\begin{aligned} \mathcal{B}_1^{(1)}(x) &= -\mathcal{B}_1^{(1)}\left(\frac{1}{x}\right)\,, \\ \mathcal{B}_1^{(2)}(x) &= -\mathcal{B}_1^{(1)}\left(\frac{1}{x}\right) + \mathcal{B}_1^{(2)}\left(\frac{1}{x}\right) - i\pi\sigma(x)\,, \\ \mathcal{B}_1^{(3)}(x) &= \mathcal{B}_1^{(3)}\left(\frac{1}{x}\right) - \mathcal{B}_1^{(1)}\left(\frac{1}{x}\right)\,, \end{aligned} \tag{4.37}$$

and for weight two, they are

$$\begin{aligned} \mathcal{B}_2^{(1)}(x) =& -i\pi\sigma(x)\mathcal{B}_1^{(1)}\left(\frac{1}{x}\right) - \frac{1}{2}\mathcal{B}_1^{(1)}\left(\frac{1}{x}\right)^2 - \mathcal{B}_2^{(1)}\left(\frac{1}{x}\right) + \frac{\pi^2}{3}\,, \\ \mathcal{B}_2^{(2)}(x) =& -\frac{1}{2}\mathcal{B}_1^{(1)}\left(\frac{1}{x}\right)^2 - \mathcal{B}_2^{(2)}\left(\frac{1}{x}\right) - \frac{\pi^2}{6}\,, \\ \mathcal{B}_2^{(3)}(x) =& -\log(2)\,\mathcal{B}_1^{(1)}\left(\frac{1}{x}\right) - \frac{1}{2}\mathcal{B}_1^{(1)}\left(\frac{1}{x}\right)^2 + \mathcal{B}_1^{(2)}\left(\frac{1}{x}\right)\mathcal{B}_1^{(1)}\left(\frac{1}{x}\right) + \mathcal{B}_2^{(1)}\left(\frac{1}{x}\right) \\ & - \mathcal{B}_2^{(2)}\left(\frac{1}{x}\right) + \mathcal{B}_2^{(3)}\left(\frac{1}{x}\right) - \frac{\pi^2}{4}\,, \end{aligned} \tag{4.38}$$

Notice how the inversion relation for a given basis function $\mathcal{B}_i^{(j)}$ in general involves all other basis functions of the same weight i, as well as combinations of lower-weight basis functions and/or constants. The weight of each summand is always equal to i, though, as the product of a weight-n and a weight-m function is of weight $n+m$, as can be seen in eq. (4.13). The constants π, ζ_n, $\log(2)$ etc. also have a certain weight, as they can be written as polylogarithms evaluated at special points such as $x = \pm 1$ or $x = 1/2$. Since π and $\log(a)$ for an algebraic number $0 \neq a \neq 1$ are of transcendentality one, and it is conjectured that ζ_{2n+1} is of transcendentality $2n+1$, the weight of a polylogarithmic expression is often called transcendental weight or degree of transcendentality[1]. In general, objects appearing in perturbative QCD such as loop integrals do not have a uniform weight, contrarily to what is found in more symmetric theories such as $N = 4$ super-Yang-Mills theory [131].

4.2.2. Numerical evaluation of the basis functions

Having found the basis functions and their inversion mappings, we now need to find a way to evaluate them for arguments within the unit disc of the complex plane. As already mentioned, we would like to find a series expansion for all the basis functions which we then want to truncate after a certain number of summands, assuming that convergence is fast enough.

Let us focus on the easiest case, the dilogarithm Li_2, for the moment. We already know a series expansion for it due to the relation of polylogarithms to nested sums,

$$\mathrm{Li}_2(x) = \sum_{k=1}^{\infty} \frac{x^k}{k^2} \,. \tag{4.39}$$

This expansion only converges reasonably fast only if $|x| \ll 1$, though. A faster-converging expansion for small values of x is given by the “Bernoulli” expansion which has been known for a long time [132, 133]. In this series, the dilogarithm is expanded in the variable $\log(1-x)$,

$$\mathrm{Li}_2(x) = \sum_{k=0}^{\infty} \frac{B_k}{(k+1)!} \left(-\log(1-x)\right)^{k+1} , \tag{4.40}$$

where B_k denotes the k^{th} Bernoulli number, which is defined via the generating series

$$\frac{z}{e^z - 1} = \sum_{n=0}^{\infty} B_n \frac{z^n}{n!} \,. \tag{4.41}$$

[1] Or even just “transcendentality”, although mathematicians may find this an abuse of nomenclature since it is not even proven that ζ_3 is a transcendental number.

Note that $B_{2n+1} = 0$, $\forall n \in \mathbb{N}$. The Bernoulli numbers are related to zeta values via the formula

$$\zeta_0 = B_1 = -\frac{1}{2} \quad \text{and} \quad \zeta_{-n} = -\frac{B_{n+1}}{n+1} \quad \text{for } n \geq 1\,. \tag{4.42}$$

The Bernoulli expansion converges for $\mathrm{Re}(x) < 1/2$, which can be achieved using the identity (4.23). Still, for arguments far from the origin, the convergence is not very fast anymore, and we rather resort to an alternative expansion in the variable $\log(x)$ which was derived in ref. [134],

$$\mathrm{Li}_2(x) = -\log(x)\,\log\left(-\log(x)\right) + \sum_{k=0}^{\infty} \frac{\zeta_k^{(2)}}{k!}\,\log^k(x)\,, \tag{4.43}$$

where $\zeta_k^{(n)}$ denote the shifted zeta values defined as

$$\zeta_n^{(k)} = \begin{cases} \zeta_{k-n}, & \text{if } k-n \neq 1\,, \\ H_{k-1}, & \text{if } k-n = 1\,, \end{cases} \quad , \quad \text{with} \quad H_m = \sum_{n=1}^{m} \frac{1}{n}\,, \tag{4.44}$$

i.e. H_m denotes the m-th harmonic number. This expansion converges fast for $|x| \sim 1$. The derivations of both expansion can be found in ref. [135].

We have therefore found series expansions for the dilogarithm for any region of the unit disc. If the variable x is close to the origin, i.e. $|x| \leq r_{\mathrm{min}}$, we use the Bernoulli expansion to expand in $\log(1-x)$, and if x lies on the annulus $r_{\mathrm{min}} < |x| < 1$ we expand in $\log(x)$. The optimal value of the boundary value r_{min} was determined empirically to be $r_{\mathrm{min}} = 0.3$.

The strategy for the other basis functions Li_3, Li_4, $\mathrm{H}_{2,-2}$ and $\mathrm{H}_{2,1,-1}$ is identical, i.e. we want to find two expansions, one in $\log(1-x)$ and the other in $\log(x)$ for each of them. In chapter 4 of ref. [135], these expansions are all derived, but require the introduction of quite a lot of notation, which is spared the reader here.

In the case of the expansions in $\log(x)$ for $\mathrm{H}_{2,-2}$ and $\mathrm{H}_{2,1,-1}$, we have to distinguish between the cases $\mathrm{Re}(x) \gtrless 0$. For $\mathrm{H}_{2,-2}$, we map one case to the other using the identity

$$\mathrm{H}(0,1,0,-1;x) = -\mathrm{H}(0,-1,0,1;-x) = \mathrm{H}(0,1,0,-1;-x) + (\text{other terms})\ , \tag{4.45}$$

where "(other terms)" consists of classical polylogarithms and logarithms only.

Finally, for $\mathrm{H}_{2,1,-1}$ and the case $\mathrm{Re}(x) < 0$, we employ a second expansion in the variable $\log(-x)$.

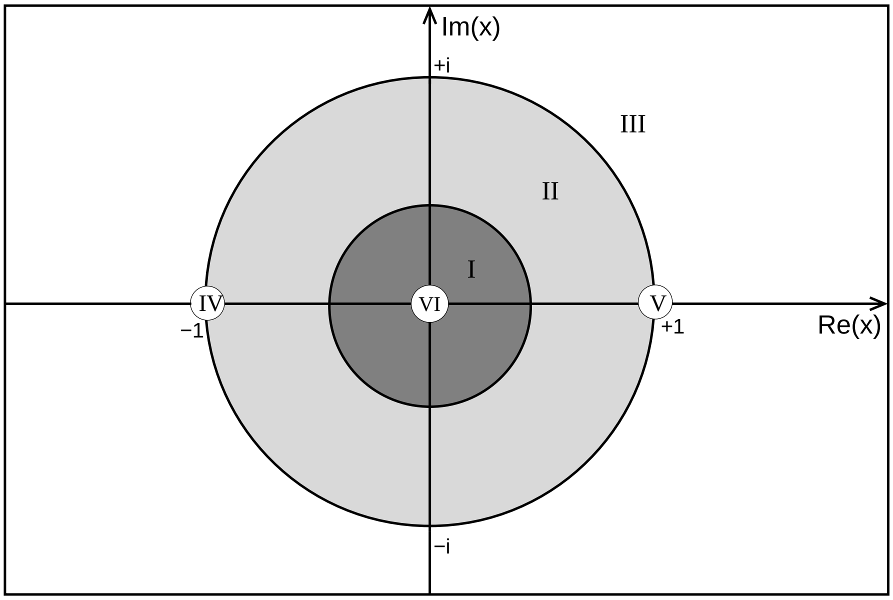

Figure 4.1.: The different regions of the complex plane in the CHAPLIN library.

4.3. The CHAPLIN library

The results from the previous section, i.e. the reduction of the 120 HPLs through weight 4 to basis functions, the inversion relations for all basis functions and their respective series expansions in $\log(1-x)$ and $\log(x)$, respectively, were all implemented in the `Fortran` code CHAPLIN.

The whole code is written in double-precision variables, i.e. the *maximal* accuracy we can achieve is 16 relative digits. Checking against arbitrary-precision codes like the GiNaC implementation for HPLs [126] or the MATHEMATICA package HPL [124,125], we were able to verify that the evaluation of any HPL up to weight four is correct to at least 13 relative digits for any complex argument. The lost digits are due to finite-precision rounding errors in the reduction to basis functions.

In order to preserve this precision also near the points $x = 0, \pm 1$ where some basis functions develop spurious singularities (i.e. even though the HPL of interest is finite in these points, some basis functions in its reduction are separately divergent) and big numerical cancellation flawing the final precision would occur, we implemented dedicated Taylor expansion for every HPL around these points, essentially by just using the nested sum relation eq. (4.16). For $x = 0$, eq. (4.16) is directly applicable, for $x = \pm 1$ the HPL had to be expressed as a superposition of HPLs with argument $x \mp 1$ via symbol calculus, each of which was then expressed through its series representation.

The strategy for the numerical evaluation is summarised in figure 4.1:

- Region I: inside an annulus $0.025 < |x| \leq 0.3$, the basis functions are evaluated by using the expansions in $\log(1-x)$.
- Region II: inside an annulus $0.3 \leq |x| \leq 1$, the basis functions are evaluated by using the expansions in $\log(x)$.
- Region III: points outside the unit disc, $|x| > 1$, are mapped back to the interior of the unit disc via inversion relations.
- Regions IV, V & VI: For points closer than $|x - x_0| = 0.025$ to $x_0 \in \{0, \pm 1\}$, Taylor expansions to evaluate the individual HPLs without proceeding to a decomposition into basis functions are used.

If the user attempts to call a HPL at a divergent point, for example $\mathrm{H}(0;0)$, an exception is thrown and the evaluation is aborted. For more information about CHAPLIN such as installation or usage guidelines, we kindly refer to the original publication [135] and the website

$$\text{http://projects.hepforge.org/chaplin/} \tag{4.46}$$

4.4. Conclusions

After a historical introduction, we have defined the class of harmonic polylogarithms via a recursive integration over the three weight functions given in eq. (4.2). It is straightforward to understand that these functions will naturally arise in perturbative QFT, as phase-space integrations of particle propagators will produce exactly this kind of iterated integrals.

A feature of functions that can be defined as nested integrations in general is the shuffle algebra which we present in section 4.1.1. This structure provides us with a large number of identities among HPLs and is useful to extract logarithmic singularities from the functions.

Alternatively, HPLs can be represented as nested sums for arguments within the unit disc. While in physical calculations, this form is less common, it provides a easy way of obtaining the values for HPLs when their argument is at ± 1 in the non-divergent cases. These values are found to be alternating multiple zeta values.

In section 4.2, we explain how the library CHAPLIN works. A general HPL is reduced to a set of basis functions which we need 32 of to cover all HPLs up to weight four, using the full set of identities among them which is found using Symbol calculus. The basis functions are found to consist of only six different functions, most of which are classical polylogarithms with various arguments. In a second step, the argument of the basis functions is mapped inside the unit disc of the complex plane if necessary, via inversion relations.

Finally, for the six remaining functions, there are two different series expansions, in the variables $\log(x)$ and $\log(1-x)$, respectively. They converge fast enough in their respective regimes depicted in fig. 4.1 such that a truncation of the series after at most 50 terms ensures the best possible precision achievable with a fixed-precision code. To avoid numerical instabilities, the points $x \in \{0, \pm 1\}$ are treated with dedicated Taylor expansions for every HPL individually. This three-step programme allows for the fast and reliable evaluation of any HPL up to weight four for arbitrary complex arguments.

Since its creation, the library Chaplin has been used in various numerical codes [64, 83, 136–138] with great success.

5. Phenomenology of Higgs production

Having established, in the form of the program `iHixs`, a tool to describe Higgs production in gluon fusion with the best possible precision available at fixed order in perturbation theory, we proceed by giving a phenomenological profile of the Higgs boson at hadron colliders.

As the better part of the work contained in this thesis has been completed before the Higgs mass was determined, we will present some observables with variable Higgs mass, especially in cases where clearly different behaviour emerges when $m_H \neq 125\,\text{GeV}$.

Unless mentioned otherwise, all results in this chapter were obtained for a Higgs mass of 125 GeV. The default PDF set we have used is the MSTW08 set, for the perturbative order under consideration. The value for the strong coupling at the Z-mass is always chosen accordingly to the PDF set in use, which for the MSTW08 set means $\alpha_s(m_Z) = 0.139$ (LO set), $\alpha_s(m_Z) = 0.120$ (NLO set) and $\alpha_s(m_Z) = 0.117$ (NNLO set). From the scale m_Z, the coupling was run to the scale μ_r using the respective order of eq. (2.36).

The heavy quark masses were in general treated using the $\overline{\text{MS}}$ scheme and set to $\overline{m}_t(\overline{m}_t) = 163.7\,\text{GeV}$ and $\overline{m}_b(10\,\text{GeV}) = 3.63\,\text{GeV}$, and run to the scale μ_r using the corresponding order of eq. (2.47). The Higgs width was, except for the dedicated study on the Higgs propagator, treated in the zero-width approximation, as the difference to other schemes is below the per cent level for $m_H = 125\,\text{GeV}$, but the program runs much faster (one dimension less in the Monte-Carlo integration).

Electroweak effects were always included except in the section investigating their numerical impact. The same holds for the exact NLO QCD corrections, which were preferred over the HQET NLO cross section in all plots unless stated otherwise.

5.1. Perturbative convergence and scale uncertainty

In figure 5.1, we show the three lowest orders of the gluon fusion cross section as a function of the Higgs mass, for values between 100 and 400 GeV, as it used to be practice before the TeVatron and LHC first started excluding certain mass ranges and finally found the Higgs signal at a mass of 125 GeV. We still decided to show this plot

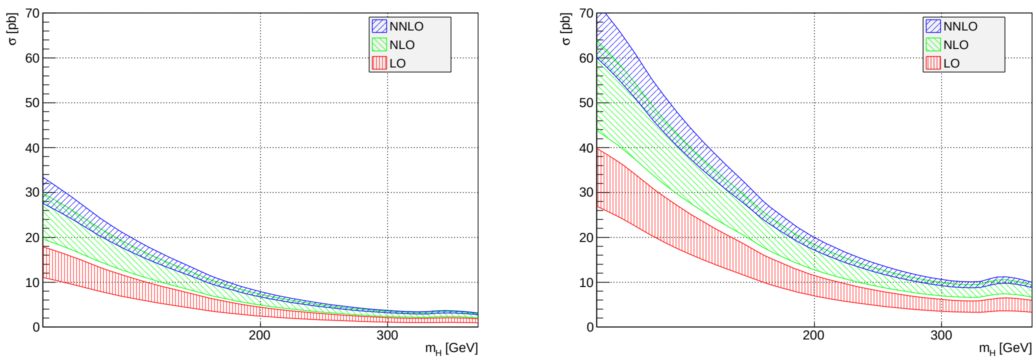

(a) 8 TeV (b) 13 TeV

Figure 5.1.: The first three orders of the gluon fusion cross section as a function of the Higgs mass for the 8 (left) and 13 (right) TeV LHC. The bands represent the scale-uncertainty.

to give the reader an idea of the dependence of the production rate on the Higgs mass. Obviously, the cross section decreases as the hypothetical Higgs mass becomes larger, which is due to luminosity suppression (i.e. it becomes increasingly harder to find two gluons that are energetic enough to produce a Higgs boson). The exception to this behaviour is the region around 350 GeV where there is an intermediate enhancement due to the $t\bar{t}$-threshold.

The increase in cross section when going from 8 to 13 TeV centre-of-mass energy is a tad more than a factor of two for light Higgs masses such as 125 GeV and would have been even more significant for a heavier Higgs boson. Again, this increase is purely luminosity-related. The left panel of figure 5.2 shows the gluon fusion cross section for $m_H = 125\,\text{GeV}$ as a function of the centre-of-mass energy of a hypothetical future pp-collider. While the slope of the curve flattens out a bit towards the high-energy end, for the intermediate region from 10 to 50 TeV we find that doubling the centre-of-mass energy enhances the production cross section by about a factor of three.

The perturbative convergence of the cross section is obviously quite slow, as the NLO curve is about 70% higher than the LO curve, and the NNLO corrections add another 20% on top of that. The prescription of estimating the uncertainty due to missing higher-order terms by varying the unphysical scales μ_r and μ_f by a factor of two up and down around the central scale choice underestimates the uncertainty of the LO cross section, as the LO and NLO bands do not overlap. The situation becomes better when comparing the NLO and NNLO bands, which clearly overlap. Still, the NNLO central value is *just* within the NLO uncertainty band.

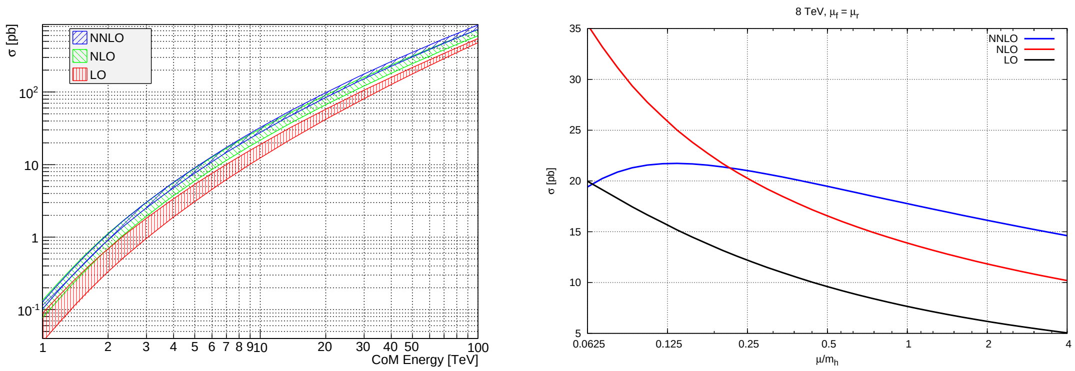

Figure 5.2.: Left: The gluon fusion cross section as a function of the centre-of-mass energy of the pp-collider. Right: Scale uncertainty of the first three orders of the gluon fusion cross section with μ_r and μ_f varied simultaneously.

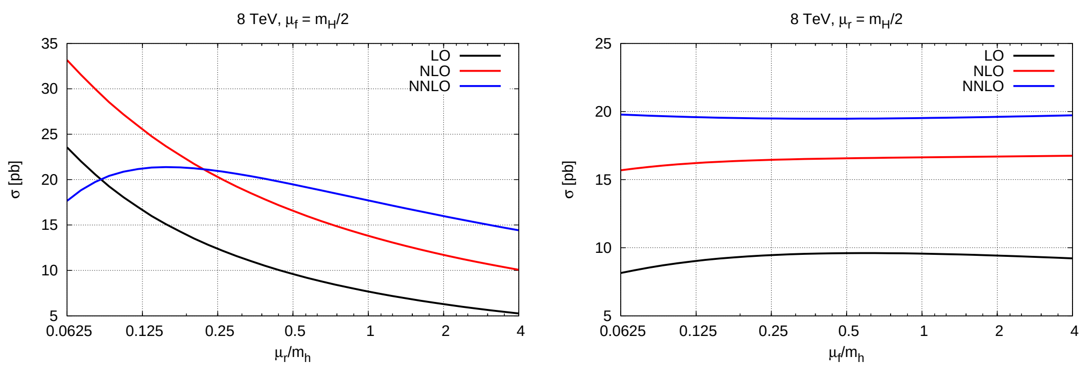

Figure 5.3.: Separate dependence on μ_r (left) and μ_f (right) of the gluon fusion cross section for the 8 TeV LHC.

Let us investigate the scale dependence a bit further. In the right panel figure 5.2, we show the three lowest orders of the gluon fusion cross section at the 8 TeV LHC and a Higgs mass of 125 GeV as a function of the renormalisation scale μ_r and the factorisation scale μ_f which are set equal and varied in the interval $[m_H/16, 4m_H]$. We observe that the LO and NLO curves are monotonously decreasing with increasing scale and exhibit a steep slope, i.e. a strong dependence on the scales. The NNLO curve is significantly flatter and sports a more complex behaviour, with a maximum at $\mu \sim m_H/10$.

The choice of scale for the gluon fusion cross section has been an issue of debate. While traditionally, it was always chosen equal to the Higgs mass, there have been arguments based on differential calculations that the natural scale appearing in observables such as the average transverse momentum of the Higgs is actually lower [139]. Thus, there

Energy [TeV]	σ_{LO} [pb]	σ_{NLO} [pb]	σ_{NNLO} [pb]
8	$10.11\,^{+26.8\,\%}_{-20.1\,\%}$	$17.40\,^{+21.9\,\%}_{-15.9\,\%}$	$20.43\,^{+7.6\,\%}_{-8.5\,\%}$
13	$24.11\,^{+21.7\,,\%}_{-17.4\,\%}$	$39.52^{+19.9\,\%}_{-14.4\,\%}$	$46.59\,^{+7.7\,\%}_{-7.9\,\%}$
40	$142.8\,^{+12.0\,,\%}_{-11.4\,\%}$	$204.9^{+15.2\,\%}_{-11.2\,\%}$	$243.4\,^{+7.9\,\%}_{-6.7\,\%}$
100	$514.7\,^{+5.7\,,\%}_{-6.9\,\%}$	$652.7^{+11.3\,\%}_{-8.7\,\%}$	$775.2\,^{+8.1\,\%}_{-6.0\,\%}$

Table 5.1.: Values for the three orders of the cross section and their scale uncertainties for pp-colliders at different centre-of-mass energies.

has been a paradigm shift in the last couple of years to use $m_H/2$ as the preferred scale. Looking at figure 5.2, we note that at lower scales, the perturbative convergence seems to be faster, i.e. the NNLO curve is closer to the NLO one. This might suggest that indeed, the correct[1] scale choice is rather $m_H/2$. We have adopted this choice for all plots in this chapter. To find the uncertainty associated with the scale dependence, we vary the scales by a factor of two up and down around the central scale $\mu_0 = m_H/2$, i.e. in the interval $[m_H/4, m_H]$. The bands in figure 5.1 have been obtained with this prescription.

Figure 5.3 shows the separate dependence of the cross section on μ_r (left panel) and μ_f (right panel), with the other scale set to $m_H/2$ in both cases. We observe that the dependence on μ_f is actually insignificant and below the per cent level for the NNLO cross section, with μ_r accounting for almost all of the variation in fig. 5.2. It has to be noted, though, that the dependence of a single initial-state channel such as the gg channel or the qg channel on the factorisation scale can be significantly larger. In the sum of all channels, this dependence is almost fully cancelled, resulting in the flat curves of fig. 5.3. The relative scale dependence of the cross sections is almost identical at 8 and 13 TeV, which is why we did not include the plots of figures 5.2 and 5.3 for the 13 TeV case.

We conclude the section by giving the central value and the scale uncertainty for the physical case of $m_H = 125\,\text{GeV}$ for the LHC centre-of-mass energies 8 and 13 TeV, as well as for some hypothetical higher-energy pp-colliders whose construction is currently being discussed, in table 5.1. The massive decrease in uncertainty for the LO and to a lesser extent the NLO cross section is due to a strong sensitivity to the scale which the LO and

[1] "Correct" in the sense that by choosing the scale accordingly, the bulk of the (inclusive) higher-order corrections is included.

NLO PDFs acquire when invoked for such high energies. The scale dependence of the PDF is opposite to the one of the strong coupling, which is why the two differences nearly cancel out in the 100 TeV case. For the current LHC energies, the scale dependence of the PDFs is much milder. This is most likely an artefact of the LO and NLO PDFs and the resulting scale dependence is artificially small. The NNLO cross section exhibits a much more robust behaviour when changing the centre-of-mass energy.

5.2. PDF comparisons

Apart from the scale dependence studied in the previous section, the second main source of theoretical uncertainty for the gluon fusion cross section are the parton distribution functions. To estimate PDF uncertainties, the collaborations distribute a whole collection of PDFs (up to 100 for the NNPDF collaboration), each of which uses a different parametrisation. To obtain the PDF uncertainty, one has to evaluate the cross section of interest using each of these member sets and combine the obtained results using a provider-dependent prescription. The dominant gluon distributions are less constrained by direct measurements of DIS observables because the gluon does not interact with the electron directly, contrarily to the quarks inside the proton. Thus, gluon PDFs are only influenced by these types of experiments via sum-rules which constrain the whole set of PDFs for all partons. Global PDF fits which include jet data from hadron colliders can constrain the gluon density further, decreasing its uncertainty.

On top of the uncertainty of the gluon density itself, there is the additional uncertainty associated with the value of the strong coupling each PDF collaboration chooses to use. There are two paradigms for this choice. Either, the strong coupling[2] α_s is chosen as an input parameter to the PDF fit and fixed to a certain value, or it is treated as a free variable like all other variables that are fitted to the dataset. In the PDFs we are considering in this section, the former philosophy is adopted by the CT10 and NNPDF2.3 collaborations, while the latter is performed by the MSTW08, ABM11 and JR09 groups. Actually, the CT10 and NNPDF2.3 sets are available for a whole range of $\alpha_s(m_Z)$ values ranging from 0.114 to 0.124, but each collaboration also chooses a preferred value.

In figure 5.4, we have plotted the NNLO gluon fusion cross section at the 8 TeV LHC using five different PDF sets. Notice that in the case of the MSTW08 set, we provide the result both using the usual 68%CL fit, as well as the 90%CL one. The errorbars on the points represent the PDF error obtained using the respective prescription for every

[2]Notice that by "strong coupling" and α_s, we always mean $\alpha_s(m_Z)$ in this context, i.e. the input value at the Z-mass which the coupling then is run from.

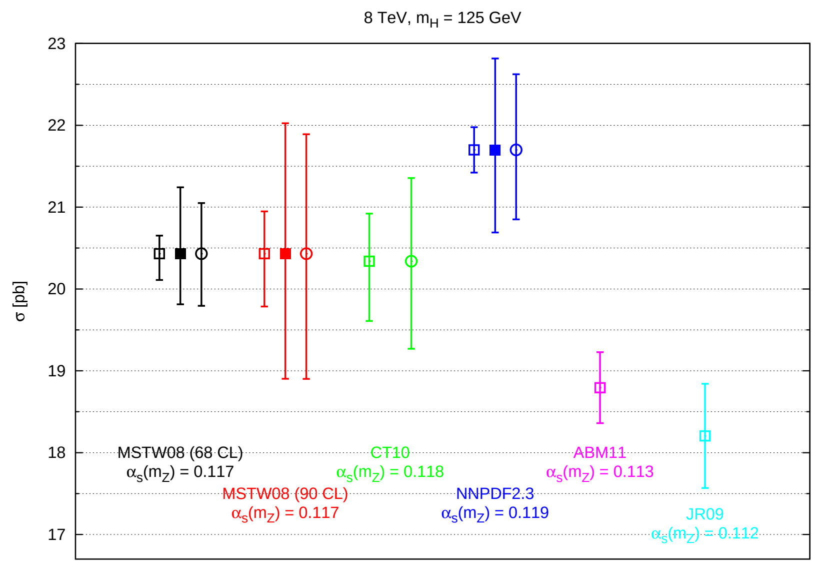

Figure 5.4.: Comparison of the NNLO cross section for different PDF providers at 8 TeV. See text for explanations about the various points.

collaboration, which is the antisymmetric Hessian technique for the MSTW08 and CT10 fits, the symmetric Hessian approach for the JR09 set and the Monte-Carlo approach for the NNPDF2.3 and ABM11 fits[3].

In the case of the ABM11 and JR09 sets, the uncertainty obtained this way is already the combined PDF+α_s uncertainty, as every member set used in the determination of the uncertainty uses a different value of the strong coupling. For remaining three sets, we provide three different types of errorbars. The leftmost entry with the empty box for a point is the PDF uncertainty only, for a fixed value of α_s. The two other entries are the combined PDF+α_s uncertainties obtained in two different ways. In the case of the filled box point, the "envelope" prescription was used, i.e. the for each value of α_s (the higher and lower one w.r.t the central choice), the PDF-only uncertainty was calculated, and the combined uncertainty then is given by the two "outermost" points one obtains, hence the name of the prescription. The errorbars for the rightmost entry with the empty circular point is calculated by combining the uncertainty obtained by varying α_s and the PDF-only uncertainty in quadrature. The former prescription, which will always result in a larger combined uncertainty, is advised by the MSTW collaboration, while the latter is suggested by the CT and NNPDF groups. Figure 5.5 shows the same plot

[3]see for example ref. [106] for details on the Hessian approach, and ref. [112] for the Monte-Carlo approach.

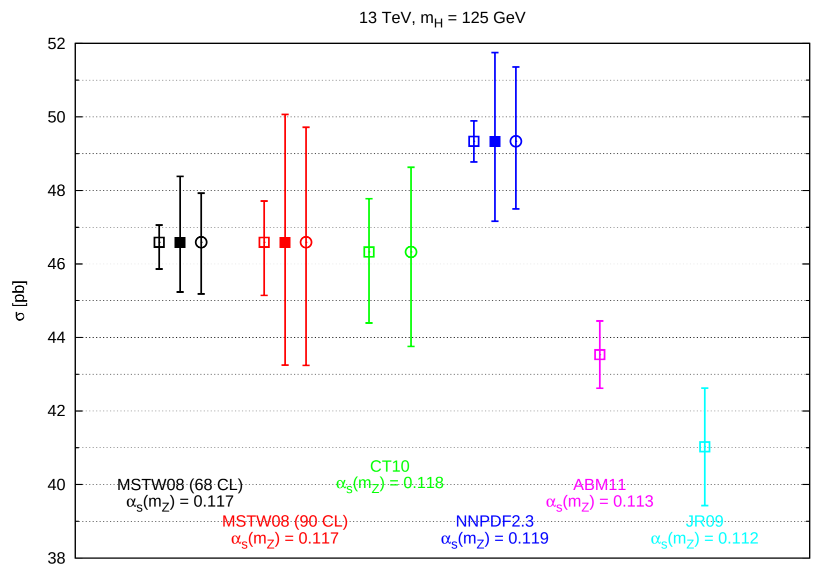

Figure 5.5.: Comparison of the NNLO cross section for different PDF providers at 13 TeV. See text for explanations about the various points.

for the 13 TeV LHC.

The first feature we notice are the vast differences among the various PDF collaborations. While the MSTW08 and CT10 fits agree very well, the NNPDF collaboration predicts a cross section which is a bit more than 6% higher. The ABM11 and JR09 fits, on the other hand, suggest cross sections which lie below the MSTW08 and CT10 central values by 8% and 11%, respectively. At 13 TeV centre-of-mass energy, the ABM11 point moves slightly upwards to 6.5% less than the MSTW08 value, while all other points hardly move from their relative places. The better part of these discrepancies may be stemming from the choice of $\alpha_s(m_Z)$ of the respective collaboration which is provided below each PDF name. The higher the chosen value, the larger the prediction for the cross section. Yet, there are non-negligible residual effects which seem to have their origin in the actual PDF parametrisations, as for example the MSTW08 and CT10 points are very close to each other even though their choices for the strong coupling are as far apart as CT10 and NNPDF2.3, which clearly are in tension with one another. The movement of the ABM11 point as we increase the energy must have a different origin, as well.

Regarding the errorbars, we notice that in general, even the combined PDF+α_s uncertainties are apparently underestimating the actual uncertainties, as most central values lie beyond the reach of the errorbars of other PDFs. Only the much wider errorband of

PDF provider	$\sigma_{\text{NNLO}}\Big\vert_{8\,\text{TeV}}$ [pb]	$\sigma_{\text{NNLO}}\Big\vert_{13\,\text{TeV}}$ [pb]
MSTW08 68%CL	$20.43\,^{+4.0\,\%}_{-3.0\,\%}$	$46.59\,^{+3.8\,\%}_{-2.9\,\%}$
MSTW08 90%CL	$20.43\,^{+7.8\,\%}_{-7.5\,\%}$	$46.59\,^{+7.5\,\%}_{-7.2\,\%}$
CT10	$20.34\,^{+5.0\,\%}_{-5.3\,\%}$	$46.33\,^{+5.0\,\%}_{-5.6\,\%}$
NNPDF2.3	$21.70\,^{+4.3\,\%}_{-3.9\,\%}$	$49.33\,^{+4.1\,\%}_{-3.7\,\%}$
ABM11	$18.79\,^{+2.3\,\%}_{-2.3\,\%}$	$43.53\,^{+2.1\,\%}_{-2.1\,\%}$
JR09	$18.20\,^{+3.5\,\%}_{-3.5\,\%}$	$41.03\,^{+3.9\,\%}_{-3.9\,\%}$

Table 5.2.: NNLO gluon fusion predictions using different PDF sets and their associated uncertainties for the LHC at 8 and 13 TeV.

the MSTW08 90%CL set engulfs all other predictions (with the exception of the JR09 point, and barely the 8 TeV ABM11 value). The choice of how to combine the PDF and α_s uncertainty does not result in very different uncertainties. In the CT10 case, the envelope method could not be performed because the PDF sets with $\alpha_s(m_Z) \neq 0.118$ consist of one member set only, i.e. they do not allow for a separate PDF-only error calculation.

The conclusion of figures 5.4 and 5.5 is that we should not use just one single PDF set and trust its predictions and associated uncertainties, even if one disregards the ABM11 and JR09 sets due to their choices for the strong coupling which are many standard deviations below the current world average, and also because they fit to a very selective set of data. The prescription made by the PDF4LHC working group [140] to resolve this issue is to just take the envelope of all predictions and their respective uncertainties and the corresponding midpoint as the best prediction, which is a very conservative approach. A recent publication [141] suggests to rather combine predictions statistically, since the envelope prescription is an *ad-hoc* way of combining different values and tends to overestimate the uncertainty.

We hope that the inclusion of LHC data and further progress in PDF fitting resolves these tensions and that the various predictions converge further towards one another in the future. In table 5.2 we provide the values for the NNLO gluon fusion cross section for all PDF sets under consideration in this section, for both the 8 and 13 TeV LHC, together with their respective PDF+α_s uncertainty. The combined uncertainty was

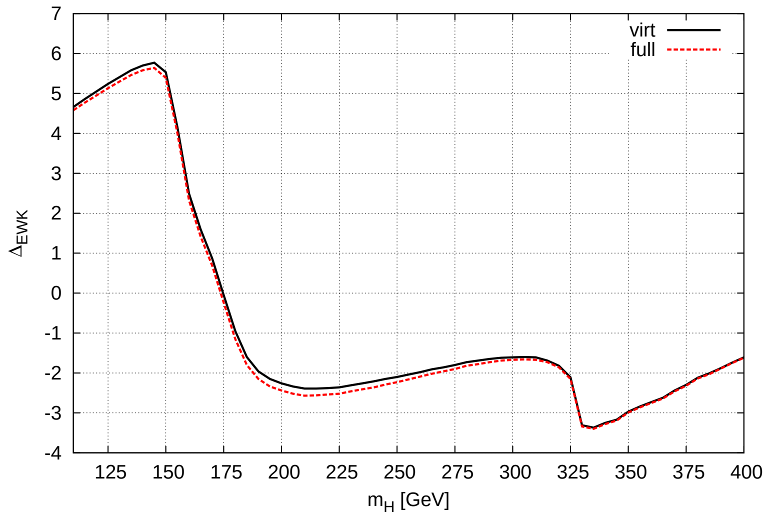

Figure 5.6.: Numerical impact of the electroweak corrections as a function of the Higgs mass. Solid line: virtual corrections only, dashed line: virtual plus real corrections.

evaluated according to the respective prescription by the PDF provider.

5.3. Electroweak contributions

To gauge the numerical impact of electroweak corrections discussed in section 3.3, we evaluate the NNLO gluon fusion cross section once using QCD contributions only and once with the electroweak contributions added. Furthermore, we separately switch on and off the electroweak contributions to the real-radiation processes $qg \to Hq$ and $q\bar{q} \to Hg$, to study the relative importance of the different electroweak corrections.

Figure 5.6 shows the quantities

$$\Delta_{\text{EWK}}^{\text{virt}} = \frac{\sigma_{\text{QCD+EWK-virtual}}}{\sigma_{\text{QCD}}} \times 100\,\%\,, \quad \text{and} \quad \Delta_{\text{EWK}}^{\text{full}} = \frac{\sigma_{\text{QCD+EWK-full}}}{\sigma_{\text{QCD}}} \times 100\,\%\,, \quad (5.1)$$

as a function of the Higgs mass. We chose to vary the Higgs mass to illustrate the strong dependence of the electroweak contributions on it. The corrections are positive and as big as $\sim 6\%$ for Higgs masses below the WW-threshold, and then change sign and remain at the $\sim 3\%$-level for masses above 200 GeV, with another threshold-enhancement at the $t\bar{t}$-resonance. Furthermore, we can observe that the real-radiation contributions are numerically insignificant over the whole range of Higgs masses under consideration. Their (negative) impact is at most at the per mille level. Due to this domination of virtual effects, the situation is exactly the same at 13 TeV centre-of-mass energy, which is why we do not provide the plot for this energy.

For the physical case of $m_H = 125\,\text{GeV}$, we see that the effect of the electroweak corrections is an enhancement of the cross section prediction of about 5%, which is of the order of the residual scale uncertainty found in section 5.1 and thus certainly not negligible. Interestingly, when considering figure 23 of ref. [58] where the full virtual electroweak corrections are compared to the contributions coming from light quark-loops only, one observes that for a Higgs mass of about 125 GeV, the two lines intersect, i.e. the numerical impact of the diagrams containing massive quarks vanishes. This coincidental fact means that we could obtain a very good estimate for the electroweak corrections to gluon fusion by just implementing the analytic formulae for the light quark contributions from ref. [69].

5.4. Higgs propagator treatment

Next, we consider the effects of the various schemes we implemented in `iHixs` to treat the Higgs width. The numerical impact of the four different schemes zero-width approximation (ZWA), naive Breit-Wigner (BW), Running width Breit-Wigner (RUN) and the Seymour-scheme (SEY) is summarised in figure 5.7. Again, we scan over a wide range of Higgs masses since the differences among the schemes only become important for higher Higgs masses. The total width of the Higgs boson for each mass was obtained with the code `Hdecay` [89].

We observe that below the $t\bar{t}$-threshold, the BW- and RUN-schemes start deviating upwards w.r.t the ZWA. The enhancement is about 0.6% at $m_H = 125$ GeV, hits 5% at about 300 GeV and peaks at about 7% at the $t\bar{t}$-threshold. Except for a slightly less pronounced enhancement at the $t\bar{t}$-threshold, the RUN-scheme and the BW-scheme exhibit very similar behaviour, and only in the very high-mass regime above 650 GeV they start to deviate from one another. The SEY-scheme, on the other hand, stays very close to the ZWA below the $t\bar{t}$-threshold, then predicts a lower cross section (closer to the two Breit-Wigner schemes) up to $m_H \sim 500$ GeV, only to then blow up in a spectacular way until the enhancement over the ZWA is at the level of a factor of three at $m_H = 800$ GeV.

These vast differences are not all that surprising, as the Higgs width grows enormously as more and more decay channels become available for higher masses. While the total width of the SM Higgs boson is as small as about 3×10^{-5} times the mass at 125 GeV, it becomes 1 % at about 218 GeV, 10 % at 440 GeV and reaches almost 40 % at $m_H = 800$

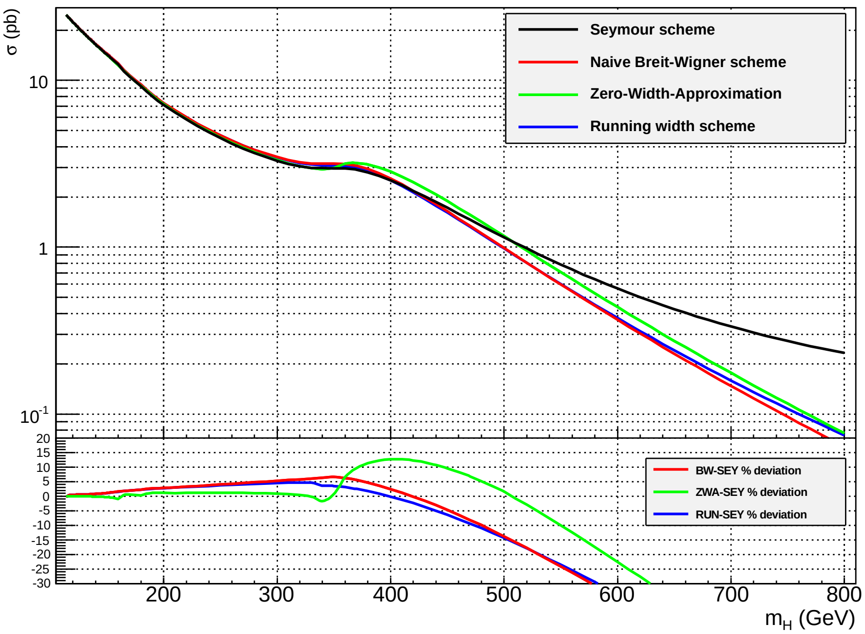

Figure 5.7.: Numerical impact of the four different schemes for the treatment of the Higgs propagator as a function of the Higgs mass, for the 8 TeV LHC. Top panel: absolute cross section, bottom panel: relative differences.

GeV, where the notion of a particle may even be inappropriate to describe such a broad resonance. So width effects are actually expected to be important for high Higgs masses. Furthermore, it makes sense that the cross section in the Seymour-scheme becomes larger than in the other schemes, as it is designed to take the signal-background interference effects into account which are no longer suppressed for a broad resonance.

In addition to the total cross section, `iHixs` also provides histograms for the invariant mass distribution of the final-state Higgs boson which may be off-shell if a scheme other than the ZWA is used. In figure 5.8 we show this distribution for the default (BW) and the Seymour scheme, normalised with the total cross section. As expected, in the case of $m_H = 200$ GeV, the bulk of the cross section is in the central bin at the nominal Higgs mass, as the width is still fairly narrow in this scenario. The higher the mass, the wider the distributions become, which again is to be expected. What is less obvious, though, are the differences in shape between the two schemes in consideration. Starting already at $m_H = 600$ GeV and very much so for $m_H = 800$ GeV, the bigger part of the signal is at invariant masses well below the nominal Higgs mass. There could have been

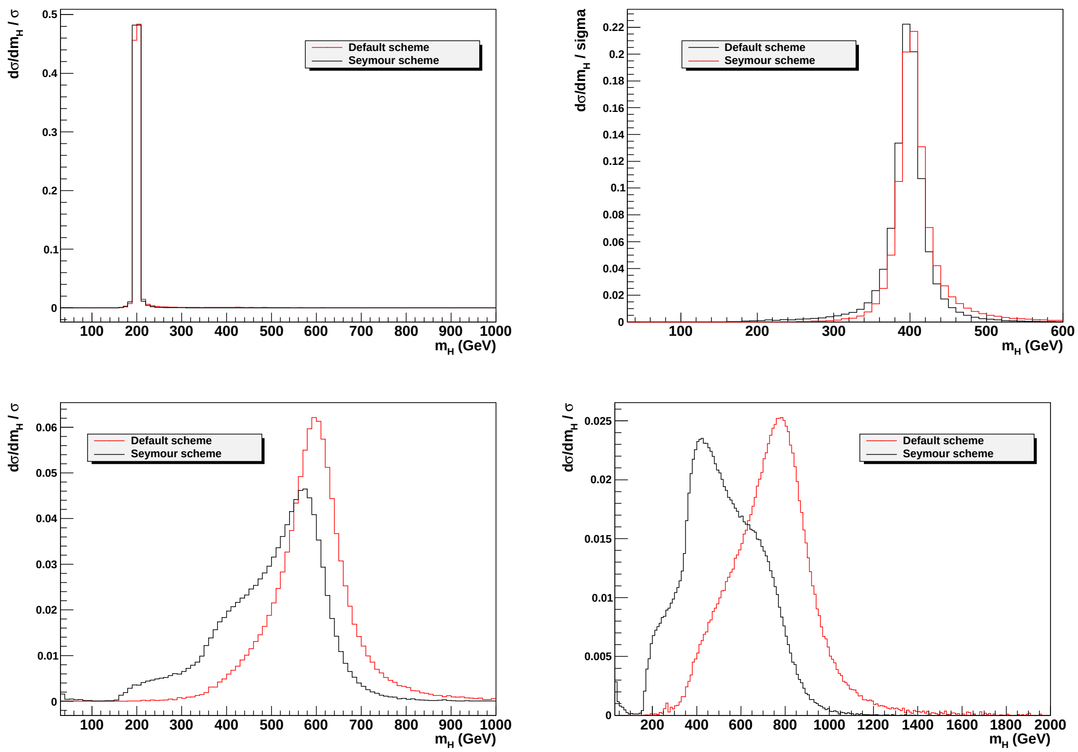

Figure 5.8.: The normalised invariant mass distribution of the Higgs boson with $m_H =$ 200, 400, 600, 800 GeV, in the default and the Seymour scheme.

profound implications for experimental searches if one were to believe that the Seymour scheme described the heavy Higgs best, like the danger of finding a completely wrong value for the Higgs mass in the WW and ZZ channels. In our original publication [64], we investigated these issues a bit further by studying which portion of the cross section is missed out when applying cuts on the invariant mass. We kindly refer the interested reader to ref. [64] for these considerations.

However, since we now know that the Higgs mass is about 125 GeV, most of the investigations of this section are obsolete, at least in the SM. In BSM models with more than one Higgs boson, the case of a heavy and broad Higgs resonance may become an issue again. For the time being, though, we have refrained from further investigations on this topic and have employed the zero-width approximation in all other studies in this chapter.

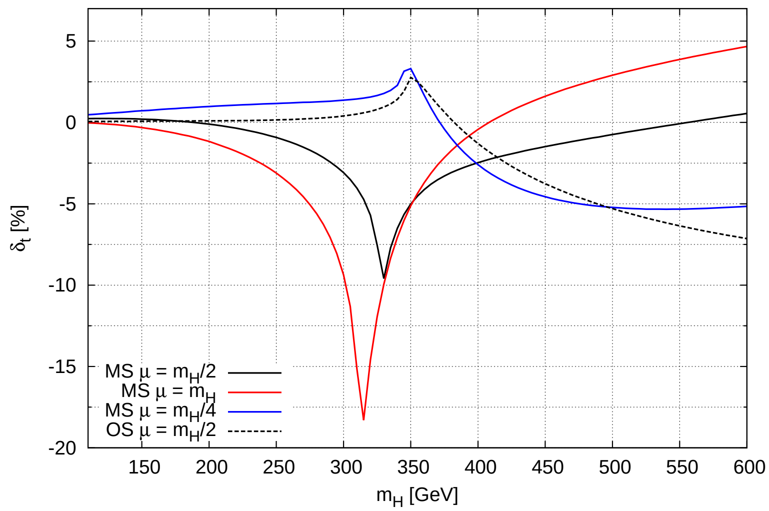

Figure 5.9.: The relative difference of the exact and effective NLO cross sections as defined in eq. (5.2), in the $\overline{\text{MS}}$ and OS renormalisation schemes.

5.5. Heavy quark effects

In what follows we will study the sensitivity of the gluon fusion cross section on various parameters which all have to do with heavy quarks. We start by studying the impact of treating the two heaviest quarks of the SM, the top and the bottom quark, in an exact way, comparing it to the effective theory approach and investigating whether the choice of renormalisation scheme and non-zero quark width effects play a significant role. Towards the end of the chapter we will venture into more exotic territories beyond the SM which affect either the amount of heavy quarks or their coupling to the Higgs boson.

5.5.1. Effective vs. exact NLO top-only

In section 3.4 we have claimed that the HQET with the top quark integrated out (rescaled to the exact LO cross section) is an excellent approximation even well beyond the nominal range of validity $m_H \ll m_t$, and used this fact to justify the use of the effective theory approach at NNLO. Here, we want to assess how well this approximation really is at NLO. Figure 5.9 shows the relative differences

$$\delta_t = \frac{\sigma_{\text{NLO}}^{\text{exact}} - \sigma_{\text{NLO}}^{\text{HQET}}}{\sigma_{\text{NLO}}^{\text{HQET}}} \times 100\%\,, \tag{5.2}$$

where we consider the top quark only, and plot the curves for for the two different renormalisation schemes for the top mass, the $\overline{\text{MS}}$ (solid lines) and the on-shell (OS) (dashed lines) scheme. For the $\overline{\text{MS}}$ scheme, we furthermore plot the three curves corresponding to the three different scale choices $\mu \in \{m_H/4, m_H/2, m_H\}$. The input mass in the OS case was taken to be $M_t = 173.5\,\text{GeV}$ [38].

As one can observe, the rescaled effective theory indeed does a very good job in approximating the full result for light Higgs masses, as until a Higgs mass of about 200 GeV, the difference between the two curves is below the per cent level in both schemes and all scale choices. In the OS scheme, the approximation is especially good and the per cent difference is only reached at a Higgs mass close to 330 GeV.

The biggest differences obviously occur at the $t\bar{t}$-threshold. First, note that the location of the threshold depends strongly on the scale choice in the $\overline{\text{MS}}$ scheme, as the top mass is run from its input value

$$\overline{m}_t\left(\overline{m}_t\right) = 163.7\,\text{GeV}\,, \tag{5.3}$$

to the renormalisation scale μ_r. At the location of the threshold in the OS scheme, which is at a Higgs mass of $m_H = 347\,\text{GeV}$, the $\overline{\text{MS}}$ mass for the three scale choices is,

$$\overline{m}_t(\mu_r) = \begin{cases} 172.3\,\text{GeV}\,, & \mu_r = \frac{m_H}{4} \\ 163.0\,\text{GeV}\,, & \mu_r = \frac{m_H}{2} \\ 155.0\,\text{GeV}\,, & \mu_r = m_H \end{cases}\,. \tag{5.4}$$

There is further difference among the curves apart from the different locations of the threshold, which is of course shared by the effective cross section entering each curve and uses the same mass. This difference is due to the finite part of the OS renormalisation constant which leads to the difference in the virtual two-loop amplitude as given in eq. (3.18),

$$\mathcal{G}_{1/2}^{(2l),\text{OS}}(x) - \mathcal{G}_{1/2}^{(2l),\overline{\text{MS}}}(x) \propto \left(\frac{4}{3} + \log\left(\frac{\mu_r^2}{m_t^2}\right)\right)\mathcal{F}_{1/2}^{(2l,b)}(x)\,, \tag{5.5}$$

In figure 5.10 we have plotted the two-loop amplitude $\mathcal{G}^{(2l)}$ in the OS scheme, where the solid black line denotes its real part and the dashed black line the imaginary part. Along the x-axis we vary the variable

$$\frac{1}{\tau_q} = \frac{m_H^2}{4m_t^2}\,, \tag{5.6}$$

from zero (corresponding to the light Higgs or equivalently the heavy top limit) to two

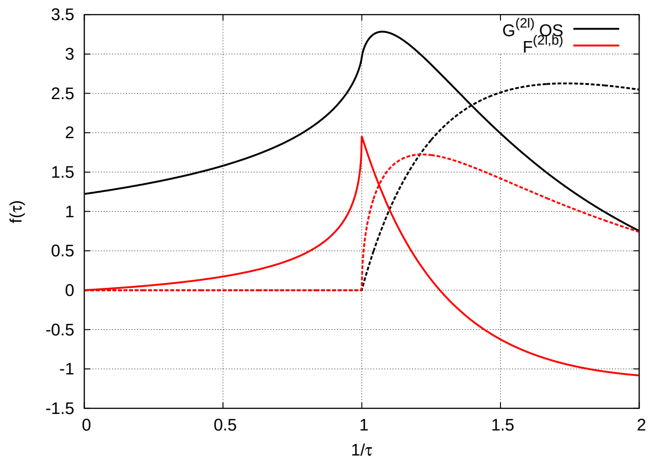

Figure 5.10.: The real (solid) and imaginary (dashed) part of the two-loop amplitude $\mathcal{G}^{(2l)}$ in the OS scheme and the scheme dependent piece $\mathcal{F}^{(2l,b)}$.

(where the Higgs is much heavier than the top quark). The $t\bar{t}$-threshold is found at one. In this scheme choice, the amplitude is a peaked but smooth function of τ_q.

The red lines represent the scheme dependent part of the amplitude, $\mathcal{F}^{(2l,b)}$, which is the derivative of the Born amplitude w.r.t. the top mass. Again, the solid line denotes the real and the dashed line the imaginary part. We observe that the function peaks sharply at threshold, while it vanishes in the heavy top limit. Thus, the scale dependent scheme-conversion factor given in eq. (5.5) is given a big weight at threshold (and to a lesser extent above), while the schemes converge in the heavy top limit. This is exactly what happens in figure 5.9. Notice that in the case of the lower-edge scheme choice $\mu = m_H/4$, the logarithm

$$\log\left(\frac{\mu_r^2}{m_t^2}\right) = \log\left(\left(\frac{347}{4\times 172.3}\right)^2\right) \approx -1.37\,, \quad \text{as opposed to} \quad \frac{4}{3} \approx 1.33\,, \tag{5.7}$$

i.e. the two terms almost cancel each other out. This is why the $\overline{\text{MS}}$ curve for this scale choice mimics the OS curve so closely.

In figure 5.11 we plot the exact and effective NLO cross section in absolute numbers for Higgs masses around threshold, to see what the actual numerical impact of the scheme and scale choice is. The left panel shows the exact (solid) and effective (dashed) NLO cross section in the $\overline{\text{MS}}$ scheme, the right panel displays the same quantities in the OS scheme. In the OS case, the relative difference between exact and effective theory are the same for all three scale choices, and the scale uncertainty which enters through the PDF and α_s is much larger than the error of the effective approximation. In the $\overline{\text{MS}}$ case,

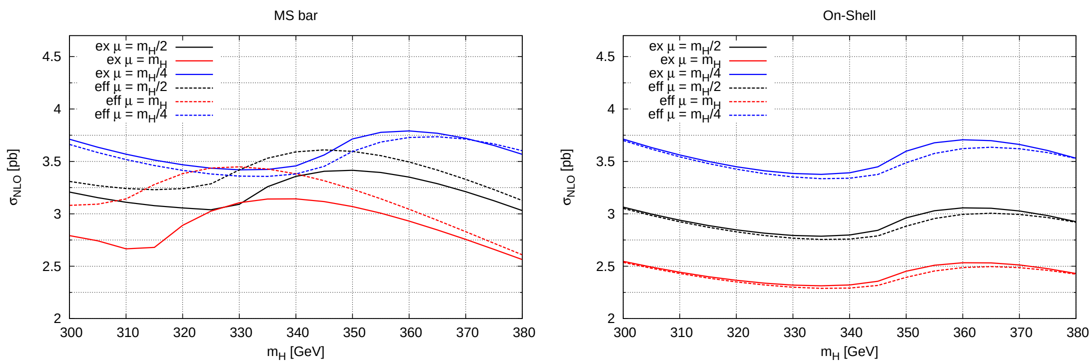

Figure 5.11.: The exact and effective NLO cross sections for Higgs masses around the $t\bar{t}$-threshold for three different scale choices. Left panel: $\overline{\text{MS}}$ scheme, right panel: OS scheme.

the various curves indeed vary wildly around the respective thresholds, especially the red curve that represents the scale choice $\mu_r = m_H$. Curiously, the overall combined uncertainty due to scales and effective approximation somehow conspires to a smaller value than in the OS case, i.e. for all points on the left plot the envelope of all curves is at most as wide as in the right plot. This observation, whether it is accidental or not, alleviates the worries that figure 5.9 has given us, which suggested that we have to account for a huge theoretical uncertainty due to the scheme choice.

Finally, figure 5.12 shows the exact NLO cross section in the OS and $\overline{\text{MS}}$ scheme across the whole range of Higgs masses from 110 GeV to 600 GeV, for the three usual scale choices. We observe that the scale uncertainty in the $\overline{\text{MS}}$ scheme captures the combined scheme and scale uncertainty over the whole mass range, except for the region around threshold. For this reason, we have chosen the $\overline{\text{MS}}$ scheme as our default scheme, as it looks to be the more conservative estimate.

In most plots in this chapter, and most importantly in the physical case of a 125 GeV Higgs, the scheme choice luckily is completely negligible.

5.5.2. SM bottom quark contributions

We proceed by investigating the numerical importance of retaining bottom quark effects in the SM Higgs production cross section estimates, which are summarised in figure 5.13. Even though `iHixs` also allows for the bottom mass to be treated in either renormalisation scheme, we have only considered the $\overline{\text{MS}}$ scheme in this case, since to us it seems the appropriate scheme to treat a quark which is much lighter than the scales considered. However, we have checked the impact of treating the bottom mass in the OS scheme

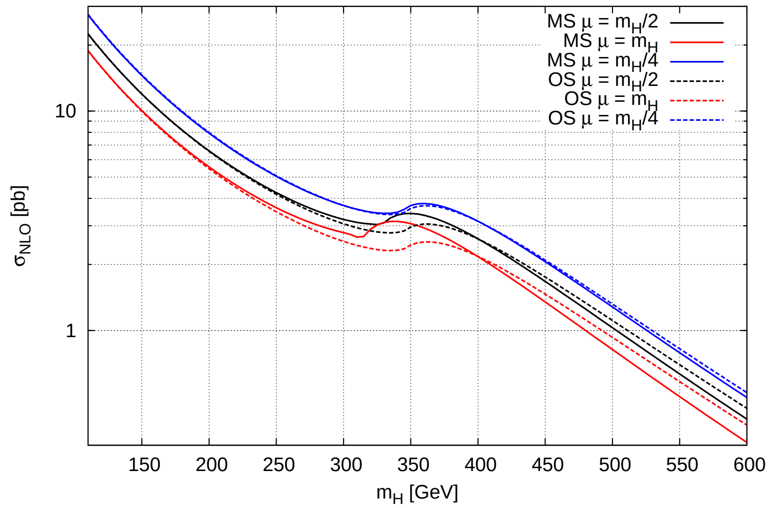

Figure 5.12.: The exact NLO cross sections in all combinations of scheme and scale choice for the whole Higgs mass range.

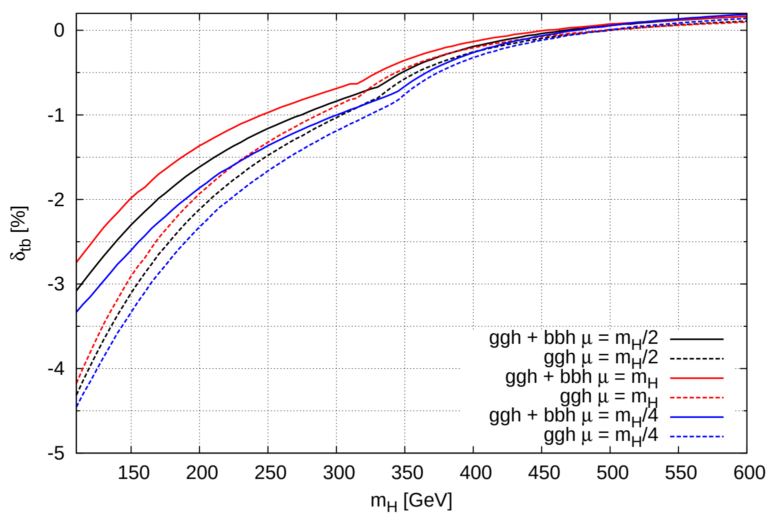

Figure 5.13.: Impact of bottom quarks on the NNLO Higgs production cross section. Dashed lines: gluon fusion only, solid lines: gluon fusion plus bottom quark fusion.

and found that it is negligible. This can be understood by the fact that the function $\mathcal{F}^{(2l,b)}$ as depicted in figure 5.10 also vanishes on the far right of the threshold, albeit more slowly than on the left. The scheme dependent part of the amplitude is therefore given very little weight in the bottom case, as $\mu_r \gg m_b$ in all of our applications.

Again, we scan over the Higgs mass range, in the same interval as in the previous section. The quantity plotted is

$$\delta_{tb} = \frac{\sigma^{\text{exact}}_{\text{t+b}} - \sigma^{\text{exact}}_{\text{t-only}}}{\sigma^{\text{exact}}_{\text{t-only}}} \times 100\% \,, \tag{5.8}$$

which measures the relative difference of the NNLO cross section with and without bottom quarks. The dashed lines represent this quantity for the three common scale choices, when just considering gluon fusion. We observe that the effect is a negative contribution, arising from the negative sign of the top-bottom interference diagrams (the squared bottom contribution is suppressed by another power of the bottom Yukawa and thus of negligible numerical significance). At the physical value of $m_H = 125$ GeV, the effect is a decrease in the gluon fusion cross section of about 3.8%. For Higgs masses above 300 GeV, the bottom effects drop below the per cent level and become insignificant.

But when we include the bottom quark in the gluon fusion process, we have to consequently also add the cross section from direct bottom quark fusion to the prediction since, as we have argued, the final state is indistinguishable in both cases when employing the five-flavour scheme. The cross section prediction when adding the NNLO bottom fusion contributions is given by the solid curves, which remove some of the gap between the top-only and the top+bottom gluon fusion curve, rendering the net effect at $m_H = 125$ GeV a decrease of about 2.8%. At higher Higgs masses the direct bottom fusion contributions grow very small.

Conclusively, we can state that the inclusion of exact bottom mass effects is more or less negligible, even in the (physical) case of a light Higgs boson, as the net effect on the cross section is well below the scale and PDF uncertainties we have established in the previous sections. Nevertheless, we advise to include them and have done so in all other plots in this chapter[4].

5.5.3. Top width effects

The inclusion of non-zero width effects for the top quark through the complex-mass scheme as in eq. (3.4) is another feature of `iHixs`. As mentioned in section 3.1, the

[4] We have actually only included the bottom effects in gluon fusion in the other plots, as the bottom fusion contributions are even more suppressed but require a separate run of `iHixs` every time.

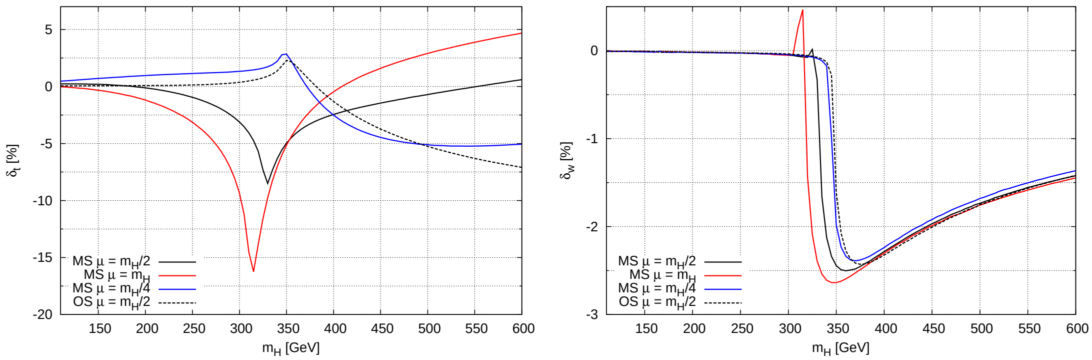

Figure 5.14.: Top width effects. Left panel: same plot as in fig. 5.9, but with a $\Gamma_t = 2\,\text{GeV}$. Right panel: Relative difference of the NNLO cross section with $\Gamma_t = 0$ and $\Gamma_t = 2\,\text{GeV}$.

consequence is the departure of the complex variable x_t from the unit circle (below the $t\bar{t}$-threshold) or the real axis (above), which poses no problem for us since we are able to evaluate the polylogarithmic expressions which depend on x_t for any complex argument using Chaplin.

We compare the numerical impact of the top width in figure 5.14. In the left panel, we plot again the same quantity as in figure 5.9, i.e. the relative difference between exact and effective theory as a function of the Higgs mass. Only this time, we have used a top width of $\Gamma_t = 2\,\text{GeV}$ which is equal to the current best measurement [38]. We see that the main feature of the curves, i.e. the strong scheme and scale dependence around threshold, persists. The width does smoothen out the choppy behaviour a bit, though. The right panel shows the relative difference of the NNLO cross section with and without the top width, again using $\Gamma_t = 2\,\text{GeV}$, parametrised as usual as

$$\delta_{\text{nw}} = \frac{\sigma_{\text{NNLO}}(\Gamma_t = 2\,\text{GeV}) - \sigma_{\text{NNLO}}(\Gamma_t = 0)}{\sigma_{\text{NNLO}}(\Gamma_t = 0)} \times 100\%\,. \tag{5.9}$$

We observe that the width effects are clearly most important at the $t\bar{t}$-threshold and to some extent above it, with a maximum impact of about -2.6% in the strongest case. The scheme and scale dependence is negligible. For light Higgs masses, the effect vanishes completely, which is directly explained with the decreased sensitivity of the variable x_q on the imaginary part of τ_q (see eq. (3.4)) in this region.

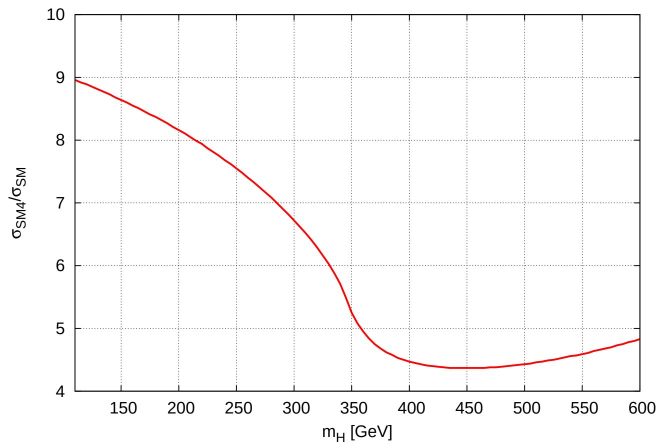

Figure 5.15.: Ratio of the NNLO QCD gluon fusion cross section in the SM4 and and the SM as a function of the Higgs mass.

5.5.4. Standard model with a fourth generation

As we have pointed out throughout chapter 3, `iHixs` allows for an arbitrary number of heavy quarks to propagate in the Higgs-producing loops in all implemented QCD contributions. It is thus straightforward to study the Higgs production cross section in the scenario of a Standard Model with a fourth family of fermions (SM4), which from a field-theoretical point of view is just as likely as the three-generation case, as the number of generations is not predicted by the gauge theory.

The SM4 model became fashionable in 2010, when the TeVatron and later the LHC started to become sensitive to Higgs observables. Since the amount of heavy quarks in the SM4 scenario is three times the amount of the SM, the gluon fusion cross section and thus essentially the total Higgs production rate is enhanced by a factor of $3 \times 3 = 9$ in a rough approximation, which allowed the experiments to set much tighter limits on the Higgs mass in the SM4 scenario. We will determine below how much the enhancement really is, using the exact NLO QCD results and the Wilson coefficient for arbitrarily many heavy quarks introduced in sections 3.2 and 3.4, respectively.

In our original publication on the Higgs production cross section in the SM4 scenario [142], we considered heavy quark masses between 300 and 450 GeV, which were not excluded by direct searches at the time. The most recent limits nowadays[5] exclude these masses, and we instead set the masses of the fourth generation quarks in depen-

[5]The latest ATLAS exclusions we were able to find exclude any heavy quark below 350 GeV [143] and top-like heavy quarks below 400 GeV [144], while CMS quotes the much higher limits of up to 675 GeV [145–147] which assume a certain decay chain, though.

dence of the Higgs mass to

$$m_{d_4} = 600\,\mathrm{GeV}\,, \quad m_{u_4} = m_{d_4} + \left(50 + 10 \times \log\left(\frac{m_H}{115\,\mathrm{GeV}}\right)\right)\,\mathrm{GeV}\,. \tag{5.10}$$

This setup has also been used in the most recent experimental exclusion study for an SM4 Higgs boson [148], which actually used `iHixs` to predict the gluon fusion cross section. The peculiar dependence of the fourth-generation down-type mass on the u_4- and the Higgs mass is chosen to evade constraints from electroweak precision parameters, as suggested by ref. [149].

Figure 5.15 shows the NNLO QCD cross section in this scenario, divided by the cross section using only the three known SM generations, at the 8 TeV LHC. One observes that, indeed, for very light Higgs masses the SM4 rate is enhanced by a factor of about nine. The ratio quickly drops lower, though, down to about 4.5 just below the $t\bar{t}$-threshold, before it slowly starts rising again. Simply approximating the SM4 cross section by multiplying the SM one with a factor of nine is thus a very crude approximation and would result in overly optimistic exclusion limits. But even with the correct enhancement factors provided by `iHixs`, reference [148] excludes the Higgs boson in the SM4 scenario given by eq. (5.10) in the mass range of 110 - 600 GeV at the 99% confidence level[6].

We would also like to point out ref. [150] where the leading electroweak corrections of the SM4 were computed. For the scenario (5.10) the authors find an increase of the cross section of about 11% for very light Higgs masses, which drops to about 4% at the $t\bar{t}$-threshold. For higher Higgs masses, the correction changes sign and reaches -12% at $m_H = 600$ GeV. The qualitative behaviour of the ratio depicted in fig. 5.15 does not change significantly, except for a flattening of the high-mass tail due to the large negative corrections (see fig. 2 of ref. [150]).

5.5.5. Enhanced bottom Yukawa coupling

To illustrate the capability of `iHixs` to compute the Higgs production cross sections if gluon fusion and bottom quark fusion for Yukawa couplings different from the SM ones, we consider the scenario where the bottom quark Yukawa coupling is larger than in the SM, i.e. the rescaling factor introduced in chapter 3 is much bigger than 1, $Y_b \gg 1$. At the same time, the top quark Yukawa coupling is kept at its SM value, $Y_t = 1$.

Such a flavour-dependent enhancement is actually a common feature of many BSM

[6] The exclusion relies heavily on the assumption that the fourth generation neutrino is not light enough for the Higgs to decay into. Otherwise, there would be a large invisible width and the exclusion limits would be significantly weaker.

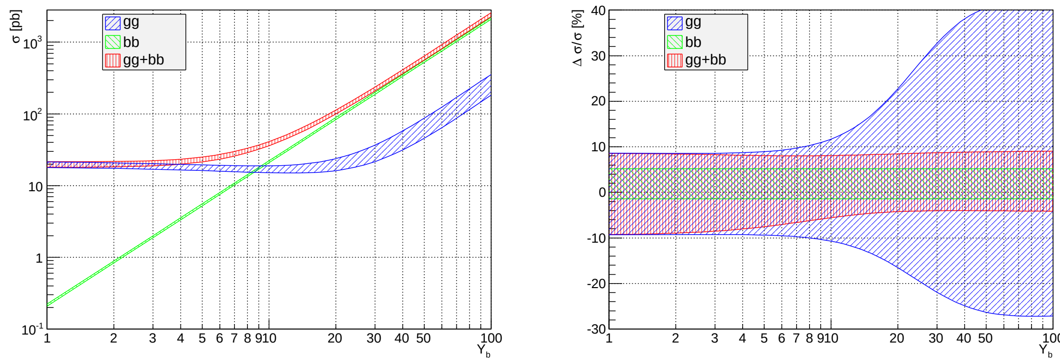

Figure 5.16.: Higgs production cross section for $m_H = 125$ GeV at the 8 TeV LHC as a function of a variable bottom Yukawa coupling. Left panel: absolute cross sections, right panel: Scale uncertainties

scenarios, especially all models involving a non-minimal Higgs sector with a second Higgs doublet such as the two-Higgs-doublet model [151] (2HDM) or supersymmetric models. Actually, the Minimal supersymmetric Standard model (MSSM) with a large value for the parameter $\tan\beta$ which features this enhancement property was one of the main motivations [101] to compute bottom quark fusion at higher orders in QCD, once it was realised that the MSSM could only evade Higgs mass bounds by a large value for $\tan\beta$.

In this scenario, the bottom quark contributions to Higgs production become more important, of course, as they are no longer suppressed by a factor of $m_t/m_b \sim 40$. The left panel of Figure 5.16 shows the gluon fusion and the bottom quark fusion Higgs production cross section as well as their sum for a Higgs mass of 125 GeV at the 8 TeV LHC for bottom Yukawa couplings varied all the way to the extreme scenario of 100 times its SM value. The bands are determined by the scale-uncertainty found by varying renormalisation and factorisation scale with a factor of two around the central scale. The scale-uncertainty of the sum is found by adding the individual uncertainties linearly. Although it is not very well visible, the gluon fusion curve actually decreases until $Y_b \sim 10$, as the negative top-bottom interference effects become more important with increasing values of Y_b. Only for Yukawa couplings strengths well above 20 times the SM one, the squared bottom quark diagrams start to dominate the cross section and increase the rate by about of 12 at $Y_b = 100$.

The bottom fusion cross section, on the other hand, exhibits a more straightforward behaviour, as it simply scales as Y_b^2. The cross section becomes as large as the gluon fusion one at $Y_b \sim 9$ and completely dominates the total Higgs production rate (depicted by the red curve) for large values of Y_b.

The right panel of figure 5.16 shows the same quantities, but normalised to the cross section for central scale choice. This allows us to study the uncertainty due to scale variation of the individual cross sections in dependence of Y_b. The plot points out a feature of the gluon fusion cross section which may not be obvious at first sight, namely the sudden growth of the scale uncertainty for high values of Y_b. This growth is explained by the fact that in gluon fusion, we can only account for bottom quark effects through NLO QCD, as the NNLO corrections are only known in the HQET approximation. In other words, we fall back to NLO accuracy for strongly enhanced bottom Yukawa couplings, because the dominant contributions in this scenario are only known to NLO QCD.

Such effects have to be taken into account when extrapolating SM predictions to BSM scenarios. In the present case, though, the increased uncertainty in the gluon fusion cross section only starts playing a role when the bottom quark fusion cross section is already dominating the total Higgs production rate. The scale-uncertainty of the total cross section given by the red curve in figure 5.16 thus remains below 10% throughout the plot.

While all fits of the Higgs couplings to data so far assume a uniform scaling of all fermionic couplings[7] and thus constraints on the H-b-$\bar{b}$ coupling are not available yet, the scenario outlined above seems to be ruled out at least for the Higgs particle observed at a mass of 125 GeV as all observed final states are consistent with the SM hypothesis and a strong enhancement of the bottom Yukawa coupling would suppress the branching ratios of all final states except the bottom pair decay channel[8].

5.6. Conclusions

The overall assessment after what we have found in this chapter is that we understand inclusive Higgs production reasonably well. The QCD corrections are found to be large, both in the NLO and NNLO case. The main source of uncertainty is the dependence on the renormalisation scale μ_r due to the truncation of the perturbative expansion. When we choose our central scale at values smaller than m_H, such as $m_H/2$ in our case, we find that the perturbative convergence of the inclusive cross section accelerates, i.e. the NNLO cross section and its scale uncertainty are almost entirely engulfed by the NLO

[7]See for example ref. [152] or [26] for such fits.

[8]Bottom quark effects in loop-induced decays such as the diphoton final state can also be large, but to a first approximation the $H \to \gamma\gamma$ amplitude behaves like the gluon fusion production cross section for variable Yukawa couplings, i.e. the enhancement is of much smaller nature than the enhancement in the direct bottom pair decay. The diphoton branching ratio would thus also be strongly suppressed.

band. The dependence of the cross section on the factorisation scale μ_f is very mild. The scale uncertainty of the NNLO cross section using our central scale and varying it by a factor of two up and down is about $\pm 8\%$.

The second main source of uncertainty comes from parton distribution functions. The uncertainties one obtains when using the prescriptions provided by the individual PDF providers to estimate the combined PDF+α_s uncertainty are below the 5% level for all five providers we have considered. Their respective central values differ by larger amounts, though, i.e. there seems to be an underestimation of the PDF uncertainty. The better part of the discrepancy among the various PDFs can be attributed to the different values for $\alpha_s(m_Z)$ they prescribe, some of which are many standard deviations from the current world average. When discarding the PDF sets that do not rely on a global fit including hadronic data, we rather find a PDF uncertainty of about $\pm 8\%$, which is of the same size as the scale uncertainty.

Electroweak contributions are sizable and have a variable impact depending on the Higgs mass, both in size and sign. For the physical 125 GeV Higgs, the corrections amount to an increase of the cross section of about 5%.

The numerical impact of the Higgs propagator treatment increases with its mass, as the total width of the Higgs grows very rapidly as a function of the Higgs mass. Below the $t\bar{t}$ threshold, the deviations among the four schemes we consider remain in the region of a few per cent, whereas above, especially the Seymour scheme which is supposed to mimic signal-background interference predicts a much larger cross section. In addition to the difference for the total inclusive cross section, we found a vastly different invariant mass distribution when comparing the Seymour and the naive Breit-Wigner scheme at high Higgs masses. Since neither of all the schemes to treat the Higgs propagator rely on completely solid grounds, theoretically, and because the effect is negligible for light Higgs masses, we have therefore decided to keep using the zero-width approximation.

The effective theory approximation, rescaled with the exact LO, does an excellent job of estimating the full cross section at NLO. Indeed, the relative difference stays below the five per cent level all the way up to a Higgs mass of about 450 GeV, except for the region around the $t\bar{t}$-threshold. For the 125 GeV Higgs, the difference is even smaller than one per cent.

The exact NLO QCD corrections exhibit a strong dependence regarding the choice of renormalisation scheme for the top mass around the $t\bar{t}$ threshold. A logarithm $\log(\mu_r^2/m_t^2)$ whose value obviously depends crucially on the choice of the renormalisation scale is given a big impact on threshold by a sharply peaked function which multiplies it in the two-loop amplitude. The scale uncertainty in the $\overline{\text{MS}}$ scheme does not grow bigger at threshold, though, but rather narrows down as scheme and scale effects cancel each other out. Across the rest of the Higgs mass range, the $\overline{\text{MS}}$ scheme seems to be the more conservative choice. At light Higgs masses, the scheme dependence is negligible.

The inclusion of bottom quarks lower the NNLO gluon fusion cross section by about 4%, due to the negative top-bottom interference. When the cross section of Higgs production through bottom quark fusion is added, the net effect is a decrease of 2.8%, i.e. much less than the remaining uncertainties due to scales and PDFs. The impact of both bottom quark effects diminishes further for higher Higgs masses. Top width effects exhibit the opposite behaviour, i.e. they are completely negligible for light Higgs masses, but reach the level of a few per cent once the $t\bar{t}$-threshold is crossed.

When considering the inclusive cross section for Higgs production in the Standard Model with four fermion generations, we observe that simply multiplying the SM cross section with a factor of nine is a bad approximation except for very light Higgs bosons. The enhancement is only five-fold anymore towards the high end of the mass interval we have considered. However, the SM4 scenario has been discarded by the LHC experiments at a very high level of confidence.

The final section of the chapter dealt with the generic BSM scenario of an enhanced coupling of bottom quarks to the Higgs and its implications on the Higgs production rate. We find that for enhancements larger than a factor of nine, the total Higgs production cross section is dominated by the direct bottom quark fusion which scales like Y_b^2. The gluon fusion cross section intermediately even decreases significantly due to strong top-bottom interference. A surprising feature is seen when studying the scale uncertainty of the respective cross sections in this scenario, which blows up by a factor of three for gluon fusion. This can readily be explained by the fact that we describe bottom quarks only to NLO accuracy, since the NNLO QCD corrections are only known in the effective theory approach. However, bottom Yukawa enhancements of this size are also highly incompatible with the Higgs production and decay rates observed until now.

We conclude that inclusive Higgs production in gluon and bottom quark fusion is described very well by the available contributions, all of which are assembled in `iHixs`. Effects which are understood less well like the Higgs propagator treatment or the scheme dependence of the top mass do not play a role for the Higgs mass that has been observed. Nevertheless, the two main sources of uncertainty, which are the sensitivity to renormalisation and factorisation scale and the PDFs, still account for a large theory error of the best estimate we can deliver. The latter uncertainty may become lower in the future with improved parton distributions. The former can only be decreased by going to higher orders in perturbation theory, which is what we will investigate in the next chapter.

6. QCD Contributions beyond NNLO to gluon fusion

As the remaining uncertainty on the gluon fusion cross section remains sizable even for the best predictions established in the previous chapters, the need to go even higher in perturbation theory becomes apparent. The future programme of the LHC experiments includes a precise measurement of all couplings of the Higgs boson to SM particles as well as its self-couplings. As statistical uncertainties have already shrunk to sizes comparable to the theoretical uncertainty, a complete N^{3}LO QCD description of the gluon fusion cross section in HQET seems mandatory.

Let us write out the formula governing the finite partonic cross section, to get an idea of the ingredients needed for the full N^{3}LO corrections. We denote the finite cross section by σ_{ij} and the bare (i.e. before renormalisation and mass factorisation) cross section by $\hat{\sigma}_{ij}$. Combining equations (2.44), (3.44) and (2.67), we find

$$\begin{aligned}
\sigma_{ij}^{(3)} =& \hat{\sigma}_{ij}^{(3)}\bar{\mu}^{6\epsilon} + \left(Z_\alpha^{(1)} + 2Z_1^{(1)}\right)\hat{\sigma}_{ij}^{(2)}\bar{\mu}^{4\epsilon} + \left(Z_\alpha^{(2)} + 2Z_1^{(2)} + \left(Z_1^{(1)}\right)^2\right)\hat{\sigma}_{ij}^{(1)}\bar{\mu}^{2\epsilon} \\
&+ \left(Z_\alpha^{(3)} + 2Z_1^{(3)} + 2Z_1^{(1)}Z_1^{(2)}\right)\hat{\sigma}_{ij}^{(0)} \\
&- \Gamma_{ik}^{(1)} \otimes \sigma_{kj}^{(2)} - \Gamma_{jk}^{(1)} \otimes \sigma_{ik}^{(2)} - \Gamma_{ik}^{(2)} \otimes \sigma_{kj}^{(1)} - \Gamma_{jk}^{(2)} \otimes \sigma_{ik}^{(1)} \\
&- \Gamma_{ik}^{(1)} \otimes \Gamma_{jl}^{(1)} \otimes \sigma_{kl}^{(1)} - \Gamma_{ik}^{(3)} \otimes \sigma_{kj}^{(0)} - \Gamma_{jk}^{(3)} \otimes \sigma_{ik}^{(0)} \\
&- \left(\Gamma_{ik}^{(2)} \otimes \Gamma_{jl}^{(1)} + \Gamma_{ik}^{(1)} \otimes \Gamma_{jl}^{(2)}\right) \otimes \sigma_{kl}^{(0)}
\end{aligned} \tag{6.1}$$

The very first term on the RHS contains the “pure” N^{3}LO contributions, i.e. diagrams with three loops (triple-virtual or VVV), two loops and the emission of an additional parton (real-double-virtual or RVV), one loop and the emission of two additional partons (double-real-virtual or RRV) and the diagrams describing the emission of three additional partons (triple-real or RRR). We will not consider any of these pure N^{3}LO contributions in this work. Some of them have already been computed, though. The triple-virtual diagrams are nothing else than the three-loop correction to the gluon form-factor. Its poles have been computed already some time ago [153], and for four years, the result up to $\mathcal{O}(\epsilon^0)$ has been available [154–156].

Furthermore, this year a computation of all master integrals needed for the triple-real corrections has been completed in the kinematic limit where the Higgs boson is created almost at rest (i.e. the threshold limit) [157]. The remaining real-double-virtual and double-real-virtual pieces are currently being computed in the same limit, such that soon, a full description of the bare N^{3}LO cross section will be available in the threshold limit.

All other terms on the RHS of eq. (6.1) do not require the calculation of any new Feynman diagrams, as they only depend on lower order partonic cross sections and the renormalisation constants Z_α and Z_1, as well as on the collinear factorisation kernels Γ_{ij}.

Still, they do not come for free, as due to the explicit ϵ-poles in Z_α, Z_1 and Γ_{ij}, higher orders in ϵ than previously needed are "pulled down" from the lower-order partonic cross sections to contribute to the finite part of $\sigma_{ij}^{(3)}$. This requires the calculation of master integrals to higher orders in ϵ, which is a non-trivial feat at NNLO. Furthermore, the convolutions of collinear factorisation kernels and partonic cross sections are challenging to compute, as well.

The calculation of the whole RHS of eq. (6.1) except for the pure N^{3}LO pieces is the content of this chapter. We notice that, besides the fact that these terms are needed in any case for the full N^{3}LO cross section, their poles provide an excellent check during the computation of the pure N^{3}LO contributions since these poles are required to cancel exactly among all terms on the RHS ($\sigma_{ij}^{(3)}$ is a finite quantity).

We will first consider the calculation of the higher orders in ϵ of the lower-order partonic cross sections in section 6.1, then turn to the computation of all convolutions of collinear factorisation kernels and partonic cross sections in section 6.2. Finally, in section 6.3, some numerical results involving the newly found terms will be presented.

6.1. Higher terms in ϵ of lower-order cross sections

In this section, we will report on the computation of the higher-order terms in the ϵ-expansion of lower-order gluon fusion cross sections. Note that most of these results have been published in [158].

6.1.1. Leading and next-to-leading order

The leading order cross section is multiplied with at most cubic poles in ϵ in the expression (6.1). Thus, knowledge of its expansion up to $\mathcal{O}(\epsilon^3)$ is required. The ϵ-expansion of the LO cross section $\hat{\sigma}_{gg}^{(0)}$ is straightforward, as the matrix element squared does not have any dependence on the dimensional regularisation parameter. The only dependence of the cross section on it comes from averaging over the polarisations of the incoming gluons. In dimensional regularisation, there are $D-2$ gluon polarisations, such that this averaging factor becomes (one factor of $D-2$ cancels out with a $D-2$ coming from summing over the gluon polarisation vectors)

$$\frac{1}{D-2} = \frac{1}{4-2\epsilon-2} = \frac{1}{2(1-\epsilon)} = \frac{1}{2}\left(1+\epsilon+\epsilon^2+\epsilon^3+\dots\right) . \tag{6.2}$$

So all ϵ-orders of the LO partonic cross section are the same,

$$\hat{\sigma}^{(0)}_{gg}(z) = \sigma^{(0)}_{gg}(z) = \sigma_0\,\delta(1-z)\left(1+\epsilon+\epsilon^2+\epsilon^3+\dots\right) , \tag{6.3}$$

where σ_0 is the term in front of the sum in eq. (3.53), rescaled with the exact LO amplitude squared. The NLO cross section, which is needed up to $\mathcal{O}(\epsilon^2)$ does not sport such a trivial expansion. There are two master integrals appearing in the matrix elements after reduction. The massless bubble,

$$= \mathrm{Bub}(s) = \int \frac{\mathrm{d}^D k}{i\pi^{D/2}} \frac{1}{k^2(k+p)^2} , \quad \text{where} \quad p^2 = s = m_H^2 , \tag{6.4}$$

which contributes to the virtual corrections in the process $gg \to H$, as well as the cut bubble integral with one internal mass,

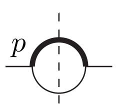

$$= \mathrm{cBub}(s) = \int \frac{\mathrm{d}^D k}{i\pi^{D/2}}\,\delta\left(k^2 - m_H^2\right)\delta\,(k+p)^2 = \int \mathrm{d}\Phi_2 , \ \text{where } p^2 = s , \tag{6.5}$$

which appears in the real emission contributions $gg \to gH$, $qg \to qH$, $q\bar{q} \to gH$. The cut bubble, as denoted in the equation above is actually a phase-space integral, not a loop integral. Using the technique of reverse unitarity, the two notions can be linked, and methods to solve loop integrals can be applied to phase-space integrals. We will introduce reverse unitarity in the following section.

It is straightforward to obtain expressions for these master integrals at all orders in ϵ. We will quickly work through the calculation of the massless bubble. Feynman parametrisation [2] yields

$$\begin{aligned}
\mathrm{Bub}(s) &= \int \frac{\mathrm{d}^D k}{i\pi^{D/2}} \int_0^1 \mathrm{d}y \,\left[k^2 y + (k+p)^2(1-y)\right]^{-2} \\
&= \int \frac{\mathrm{d}^D k}{i\pi^{D/2}} \int_0^1 \mathrm{d}y \,\left[(k+(1-y)p)^2 + sy(1-y)\right]^{-2}
\end{aligned}$$

$$= \int \frac{\mathrm{d}^D k}{i\pi^{D/2}} \int_0^1 \mathrm{d}y \, \left[k^2 + sy(1-y)\right]^{-2} \,, \tag{6.6}$$

where we have shifted to loop momentum $k \to k - (1-y)p$ in the last step. We can now integrate out the loop momentum, using the formula [2]

$$\int \frac{\mathrm{d}^D k}{i\pi^{D/2}} \frac{1}{(k^2-\Delta)^2} = \frac{(-1)^n \Gamma\left(n - \frac{d}{2}\right)}{\Gamma(n)} \Delta^{\frac{d}{2}-n} \,, \tag{6.7}$$

and find

$$\mathrm{Bub}(s) = \frac{\Gamma(\epsilon)}{(-s)^\epsilon} \int_0^1 \mathrm{d}y \, [y(1-y)]^{-\epsilon} \,. \tag{6.8}$$

The remaining integral over y yields a Beta function,

$$\int_0^1 \mathrm{d}y \, y^{-\epsilon}(1-y)^{-\epsilon} = B(1-\epsilon, 1-\epsilon) = \frac{\Gamma(1-\epsilon)^2}{\Gamma(2-2\epsilon)}, \tag{6.9}$$

such that the whole massless bubble becomes

$$\mathrm{Bub}(s) = \frac{\Gamma(\epsilon)\Gamma(1-\epsilon)^2}{\Gamma(2-2\epsilon)(-s)^\epsilon} \,. \tag{6.10}$$

For the cut bubble with one internal mass, we directly evaluate the phase-space integral, using the parametrisation for the d-dimensional phase-space of a massive and a massless particle given in eq. (A.5),

$$\begin{aligned} \mathrm{cBub}(s) = \int \mathrm{d}\Phi_2 &= \frac{s^{-\epsilon}(1-z)^{1-2\epsilon}}{2^{3-2\epsilon}\pi^{1-\epsilon}\Gamma(1-\epsilon)} \int_0^1 \mathrm{d}y_{13} \, [y_{13}(1-y_{13})]^{-\epsilon} \\ &= \frac{s^{-\epsilon}(1-z)^{1-2\epsilon}}{2^{3-2\epsilon}\pi^{1-\epsilon}} \frac{\Gamma(1-\epsilon)}{\Gamma(2-2\epsilon)} \,, \end{aligned} \tag{6.11}$$

where we have again absorbed the integral into a Beta function, and $z = m_H^2/s$.

The squared matrix elements depend on the master integrals linearly, with coefficients which in general are rational functions in ϵ and z. Except for the averaging over gluon polarisations, there is no other dependence on ϵ. Thus, with the all-order solutions for the master integrals at hand, it is trivial to obtain the partonic cross sections $\hat{\sigma}^{(1)}_{gg}, \hat{\sigma}^{(1)}_{qg}, \hat{\sigma}^{(1)}_{q\bar{q}}$ up to any order in ϵ, particularly up to $\mathcal{O}(\epsilon^2)$ which is required for the N^{3}LO cross section.

Notice that for the expansions of the finite NLO cross sections $\sigma^{(1)}_{gg}, \sigma^{(1)}_{qg}, \sigma^{(1)}_{q\bar{q}}$, we also need the convolutions of collinear factorisation kernel and LO cross section to higher orders in ϵ (to $\mathcal{O}(\epsilon^3)$ actually, since these convolutions come with an explicit ϵ^{-1}). These convolutions are trivial to obtain, though, since all ϵ-orders of the LO cross section are simply the delta-function $\delta(1-x)$, and a convolution with a delta-function is trivial, as we will see in section 6.2.

6.1.2. Integration-by-parts identities

Before we proceed to the computation of the NNLO cross section, we have to introduce a bit of technology. We start with a brief introduction of integration-by-parts (IBP) identities which relate different scalar loop-diagrams within a topology. We do not elaborate on how to turn the general tensor integrals that appear in loop diagrams into scalar integrals, see e.g. chapter 3 of ref. [159] for further information. Also, note that a scalar integral containing scalar products of loop momenta and external momenta in the numerator can always be rewritten as a combination of scalar integrals with trivial numerators by enhancing the denominator with a suitable auxiliary propagator.

A general scalar two-loop diagram with n propagators can be written as

$$\int \frac{\mathrm{d}^D k}{2\pi^D} \frac{\mathrm{d}^D l}{2\pi^D} \frac{1}{D_1^{\nu_1} D_2^{\nu_2} \cdots D_n^{\nu_n}}\,, \tag{6.12}$$

where the denominator factors D_i denote the (massive or massless) propagators. For example, consider the following two-loop diagram which appears in the real-virtual and double-real contributions to gluon fusion,

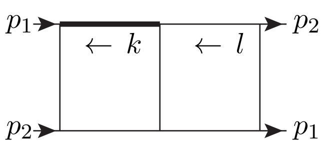

$$= \int \frac{\mathrm{d}^D k}{2\pi^D} \frac{\mathrm{d}^D l}{2\pi^D} \frac{1}{D_1 D_2 D_3 D_4 D_5 D_6 D_7}\,, \tag{6.13}$$

with

$$\begin{aligned}
&D_1 = k^2 - m_H^2\,, \quad D_2 = (k+p_1)^2\,, \quad D_3 = (k+p_{12})^2\,, \quad D_4 = (l+p_{12})^2\,, \\
&D_5 = (l+p_2)^2\,, \quad D_6 = l^2\,, \quad D_7 = (k-l)^2\,, \quad p_{12} \equiv p_1 + p_2\,.
\end{aligned} \tag{6.14}$$

The thick line denotes the massive propagator D_1, while thin lines are massless.

A collection of propagators $\{D_i\}$ defines a so-called topology, and a general integral within a given topology $\mathcal{I}$ is then specified uniquely by the propagator powers $\{\nu_i\}$,

$$\mathcal{I}(\nu_1, \nu_2, \ldots, \nu_n) \equiv \int \frac{\mathrm{d}^D k}{2\pi^D} \frac{\mathrm{d}^D l}{2\pi^D} \frac{1}{D_1^{\nu_1} D_2^{\nu_2} \cdots D_n^{\nu_n}}\,. \tag{6.15}$$

Note that the exponents $\{\nu_i\}$ can also be zero, or even negative (corresponding to numerator factors).

The IBP identities rely on the fact that, in dimensional regularisation,

$$\int \frac{\mathrm{d}^D k}{2\pi^D} \frac{\partial}{\partial k_\mu} f(k) = 0\,, \tag{6.16}$$

which is basically Gauss' theorem. We can then generate a whole set of identities for a given two-loop topology by considering all combinations

$$\int \frac{\mathrm{d}^D k}{2\pi^D} \frac{\mathrm{d}^D l}{2\pi^D} \frac{\partial}{\partial p_\mu} \frac{v^\mu}{D_1^{\nu_1} D_2^{\nu_2} \cdots D_n^{\nu_n}} = 0\,, \tag{6.17}$$

where $p_\mu \in \{k_\mu, l_\mu\}$ and v^μ denotes any four-vector appearing in the integral, i.e. any internal or external momentum. In the example above, $v^\mu \in \{k^\mu, l^\mu, p_1^\mu, p_2^\mu\}$. The scalar product that are generated in the numerator can always be replaced by a sum of propagators or external invariants. Let us consider an example using the topology defined in (6.14),

$$\begin{aligned}
0 &= \int \frac{\mathrm{d}^D k}{2\pi^D} \frac{\mathrm{d}^D l}{2\pi^D} \frac{\partial}{\partial k_\mu} \frac{p_1^\mu}{D_1^{\nu_1} D_2^{\nu_2} D_3^{\nu_3} D_4^{\nu_4} D_5^{\nu_5} D_6^{\nu_6} D_7^{\nu_7}} \\
&= \int \frac{\mathrm{d}^D k}{2\pi^D} \frac{\mathrm{d}^D l}{2\pi^D} \frac{(-2)\left(\frac{\nu_1 k p_1}{D_1} + \frac{\nu_2 k p_1}{D_2} + \frac{\nu_3 (k p_1 + p_1 p_2)}{D_3} + \frac{\nu_7 (k p_1 - l p_1)}{D_7}\right)}{D_1^{\nu_1} D_2^{\nu_2} D_3^{\nu_3} D_4^{\nu_4} D_5^{\nu_5} D_6^{\nu_6} D_7^{\nu_7}}\,.
\end{aligned} \tag{6.18}$$

Using (with $p_1^2 = p_2^2 = 0$ and $(p_1 + p_2)^2 = s$),

$$2kp_1 = D_2 - D_1 - m_H^2\,, \quad 2p_1 p_2 = s\,, \quad 2lp_1 = D_4 - D_5 - s\,, \tag{6.19}$$

we find the IBP identity

$$\begin{aligned}
0 =&(\nu_1 - \nu_2)\mathcal{I}(\nu_1, \nu_2, \nu_3, \nu_4, \nu_5, \nu_6, \nu_7) - \nu_1 \mathcal{I}(\nu_1 + 1, \nu_2 - 1, \nu_3, \nu_4 - 1, \nu_5, \nu_6, \nu_7 + 1) \\
&+ m_H^2 \nu_1 \mathcal{I}(\nu_1 + 1, \nu_2, \nu_3, \nu_4, \nu_5, \nu_6, \nu_7) + \nu_2 \mathcal{I}(\nu_1 - 1, \nu_2 + 1, \nu_3, \nu_4, \nu_5, \nu_6, \nu_7) \\
&+ m_H^2 \nu_2 \mathcal{I}(\nu_1, \nu_2 + 1, \nu_3, \nu_4, \nu_5, \nu_6, \nu_7) - \nu_3 \mathcal{I}(\nu_1, \nu_2 - 1, \nu_3 + 1, \nu_4, \nu_5, \nu_6, \nu_7) \\
&+ \nu_3 \mathcal{I}(\nu_1 - 1, \nu_2, \nu_3 + 1, \nu_4, \nu_5, \nu_6, \nu_7) + (m_H^2 - s)\nu_3 \mathcal{I}(\nu_1, \nu_2, \nu_3 + 1, \nu_4, \nu_5, \nu_6, \nu_7) \\
&- \nu_7 \mathcal{I}(\nu_1, \nu_2 - 1, \nu_3, \nu_4, \nu_5, \nu_6, \nu_7 + 1) + \nu_7 \mathcal{I}(\nu_1 + 1, \nu_2, \nu_3, \nu_4, \nu_5, \nu_6, \nu_7 + 1) \\
&+ \nu_7 \mathcal{I}(\nu_1, \nu_2, \nu_3, \nu_4 - 1, \nu_5, \nu_6, \nu_7 + 1) - \nu_7 \mathcal{I}(\nu_1, \nu_2, \nu_3, \nu_4, \nu_5 - 1, \nu_6, \nu_7 + 1) \\
&+ (m_H^2 - s)\nu_7 \mathcal{I}(\nu_1, \nu_2, \nu_3, \nu_4, \nu_5, \nu_6, \nu_7 + 1)\,.
\end{aligned} \tag{6.20}$$

On top of the IBP identities, there are additional identities among loop integrals based on Lorentz-invariance [160] (LI). In fact, there are enough identities to reduce all loop integrals of a given topology to a small number of master integrals, which are the only ones that actually need to be computed. Furthermore, Laporta [161] devised an algorithm that, given a topology and all IBP/LI identities, automatically identifies a set of master integrals. The Laporta algorithm makes use of a measure for the complexity of a loop integral, and always solves the identities to reduce complicated integrals to simpler ones. Nevertheless, the choice of master integrals one uses is not unique and may be chosen to fit other constraints, as we will see when introducing the method of differential equations.

There are by now many publicly available computer codes that perform the task of reducing a topology to its master integrals, for any number of loops and propagators (in principle), such as the Maple code AIR [162], the Mathematica code FIRE [163] or the `C++` implementation Reduze [164, 165].

6.1.3. The method of reverse unitarity

Next, we describe the method of reverse unitarity which is a very useful technique to treat contributions coming from real emission diagrams on the same footing as loop diagrams.

Traditionally, unitarity methods have been used to facilitate the calculation of loop diagrams by relating them to tree-level diagrams integrated over their respective final states' phase-space. Cutkosky's rules [166] provide a prescription of how to turn a multiloop integral into a phase-space integral, by "cutting" internal propagators of the diagram, which corresponds to putting the virtual particle on-shell, i.e. replacing a propagator

$$\frac{1}{k^2 - m^2 + i\varepsilon} \;\to\; -2\pi i\delta(k^2 - m^2)\,. \tag{6.21}$$

Unitarity ideas re-appeared in the 1980s and 1990s [167, 168] and were applied with great success to NLO QCD corrections for processes with many legs in the later 2000s [169, 170], such as $W + 5\,$jets production [171] earlier this year. The main advantage of these purely numerical approach is the automated and efficient generation of tree-level amplitudes [172, 173], which are then "fused" into the one-loop amplitude.

Reverse unitarity [56, 157, 158, 174–178], on the other hand, uses Cutkosky's rules in the other direction, and comes in handy when analytic calculations of inclusive quantities are performed.

Let us consider a general phase-space integral for the process $q_1+q_2 \to q_H+q_3+\ldots+q_N$. We will take H to be the only massive particle among the $N-1$ final-state particles, with all other momenta light-like,

$$q_H^2 = M^2\,, \quad q_i^2 = 0\,,\, i \in \{1, \dots, N\}\,. \tag{6.22}$$

This of course anticipates the application to real radiation contributions in Higgs production. But let us stress that the method of reverse unitarity also works for processes with more masses involved.

The integral in question is the integration of the squared matrix element $|\mathcal{M}|^2$ over the $(N-1)$-particle final-state phase-space,

$$I = \int \mathrm{d}\Phi_{N-1}(q_H, q_3, \dots, q_N; M^2; s; D)|\mathcal{M}|^2(\{q_j\}, q_1, q_2; D)\,, \tag{6.23}$$

where the phase-space measure reads

$$\begin{aligned}&\mathrm{d}\Phi_{N-1}(q_H, q_3, \dots, q_N; M^2; s; D) = \\ &(2\pi)^D \delta^{(D)}(q_{12} - q_H - q_{3\dots N}) \frac{\mathrm{d}^D q_H}{(2\pi)^{D-1}} \delta_+(q_H^2 - M^2) \prod_{j=3}^{N} \frac{\mathrm{d}^D q_j}{(2\pi)^{D-1}} \delta_+ q_j^2\,.\end{aligned} \tag{6.24}$$

After using the D-dimensional delta-function to integrate out the Higgs momentum, we are left with the integral

$$I = 2\pi \int \prod_{j=3}^{N} \frac{\mathrm{d}^D q_j}{(2\pi)^{D-1}} \delta_+(q_j^2)\, \delta_+\left([q_{3\dots N} - q_{12}]^2 - M^2\right) |\mathcal{M}|^2(\{q_j\}, q_1, q_2; D)\,. \tag{6.25}$$

Now, we can rewrite the integral via the replacement of the final-state particles' on-shell constraints with a cut propagator,

$$\delta_+(p^2 - m^2) \;\to\; \left(\frac{1}{p^2 - m^2}\right)_c \equiv \frac{1}{2\pi i}\left(\frac{1}{p^2 - m^2 + i\varepsilon} - \frac{1}{p^2 - m^2 - i\varepsilon}\right)\,. \tag{6.26}$$

Doing so, we arrive at

$$I = 2\pi \int \prod_{j=3}^{N} \frac{\mathrm{d}^D q_j}{(2\pi)^{D-1}} \left(\frac{1}{q_j^2}\right)_c \left(\frac{1}{[q_{3\dots N} - q_{12}]^2 - M^2}\right)_c |\mathcal{M}|^2(\{q_j\}, q_1, q_2; D)\,, \tag{6.27}$$

which indeed describes $(N+L-2)$-loop Feynman integral with $N-1$ cut propagators, if the squared matrix element $|\mathcal{M}|^2$ contains additional L loop integrations. For pure real-emission contributions, $|\mathcal{M}|^2$ is a tree-level diagram and $L = 0$.

A cut propagator behaves like a normal propagator under differentiation w.r.t its momentum,

$$\frac{\partial}{\partial p_\mu}\left[\left(\frac{1}{p^2-m^2}\right)_c\right]^\nu = -2\nu p^\mu \left[\left(\frac{1}{p^2-m^2}\right)_c\right]^{\nu+1} . \tag{6.28}$$

Thus, the IBP-identities among loop diagrams with cut propagators are the same as the ones for the normal loop diagrams, and one may use the Laporta-algorithm to reduce the system of cut loop diagrams to a number of master integrals. The algorithm may be sped up by noting that integrals where one of the cut propagators is missing or has a positive power cannot contribute to a phase-space integral since there would be a final-state particle missing (i.e. the replacement in eq. (6.26) could not be undone when re-interpreting the cut loop integral as a phase-space integral). These integrals can thus immediately be set to zero,

$$\left[\left(\frac{1}{p^2}\right)_c\right]^\nu = 0 \quad \text{for} \quad \nu = 0, -1, -2, \ldots . \tag{6.29}$$

The clear advantage is the algorithmic fashion one obtains to solve the system of all real emission diagrams of a given number of final-state particles. If it were not for reverse unitarity, one would have to treat each phase-space integral on its own, by parametrising the final state momenta, or rather all invariants appearing in propagators, in a suitable parametrisation for the $(N-1)$-particle phase-space.

In addition, there are benefits when one actually has to find the expressions for the master integrals, because the method of differential equations can be applied to the cut loop integrals. This method to solve integrals efficiently will be presented in the next section.

6.1.4. The method of differential equations

Using the reverse unitarity method presented in the previous section, we are basically ready to compute all contributions to the NNLO partonic cross section through $\mathcal{O}(\epsilon)$ in the same way, namely as two-loop four-point integrals with three, two or just one cut propagators, which depend on a small set of master integrals.

The calculation of these master integrals is a delicate task, though. While the result for the one-loop massless bubble example in section 6.1.1 was fairly easy to obtain, solving a two-loop integral with up to seven propagators via Feynman parametrisation becomes very cumbersome.

A simpler technique to compute a system of multiloop integrals is the method of differential equations [160, 179, 180]. The idea is to differentiate each integral w.r.t. an external kinematic invariant (either a particles mass or a non-vanishing Lorentz-invariant made up from momenta of external particles). In our case, this invariant will be the Higgs mass m^2. The differentiated integrals will be Feynman integrals of the same topology, since no scalar products are generated when differentiating w.r.t. the mass m^2. Once again, we can then use the IBP identities to express the differentiated integrals in the basis of master integrals, and obtain a closed system of (generally coupled) differential equations.

Formally, if we denote the set of master integrals as a vector $\mathbf{MI}(s, m^2)$ depending on our two external scales, the system of differential equations can be written in matrix form,

$$\frac{\partial}{\partial m^2}\mathbf{MI}(s, m^2) = \mathbf{A}(s, m^2) \cdot \ \mathbf{MI}(s, m^2)\,. \tag{6.30}$$

The coefficient matrix $\mathbf{A}$ is a rational function in s, m^2 and the spacetime dimension D. Its entries are determined by the differentiation w.r.t. m^2 and the IBP identities used in reducing the differentiated integral to master integrals.

Actually, since every master integral has a fixed mass dimension, we may factorise an appropriate factor of s from every one of them, rendering the remaining function depending on the dimensionless variable $z \equiv m^2/s$, only. Thus, the system of differential equations consists of ordinary differential equations, which is significantly simpler to solve than a system of partial differential equations,

$$\frac{\mathrm{d}}{\mathrm{d}z}\mathbf{MI}(z) = \mathbf{A}(z) \cdot \ \mathbf{MI}(z)\,. \tag{6.31}$$

Notice that this only holds true for the case of exactly two mass scales which the master integrals depend on.

Ideally, one would like to have the matrix $\mathbf{A}$ diagonal, such that there are no coupled differential equations. This may lead to a new choice of master integrals, and it has recently even been conjectured that there is always a basis of master integrals that trivialises the system of differential equations [181]. But even in the case of coupled equations, there is often a decoupling occurring when one expands each differential equation in ϵ.

For example, in our case of interest, the NNLO gluon-fusion master integrals, there are coupled differential equations in the double-real master integrals, one of which reads

$$\begin{aligned}\frac{\mathrm{d}}{\mathrm{d}z}\mathbf{X}_1 =& \frac{(1-z-\epsilon(1-2z))}{z(1-z)}\mathbf{X}_1(z) - \frac{3(1-\epsilon)}{(1-z)}\mathbf{X}_{11a}(z) \\ \frac{\mathrm{d}}{\mathrm{d}z}\mathbf{X}_{11a} =& -\frac{3(1-\epsilon)}{(1-z)}\mathbf{X}_{11a}(z) + \frac{\epsilon}{(1-z)}\mathbf{X}_1(z)\,,\end{aligned} \tag{6.32}$$

where we refer to the next section for the definition of the master integrals. We furthermore know from the boundary condition at the soft limit of the master integrals that both of them start at the zeroth order in ϵ, i.e. we can insert the ansatz

$$\mathbf{X}_1(z) = \sum_{k=0}^{\infty} \mathbf{X}_1^{(k)}(z)\,\epsilon^k\,, \quad \mathbf{X}_{11a}(z) = \sum_{k=0}^{\infty} \mathbf{X}_{11a}^{(k)}(z)\,\epsilon^k \tag{6.33}$$

into equation (6.32) and consider the $\mathcal{O}(\epsilon^0)$ coefficient,

$$\begin{aligned}\frac{\mathrm{d}}{\mathrm{d}z}\mathbf{X}_1^{(0)} &= \frac{1}{z}\mathbf{X}_1^{(0)}(z) - \frac{3}{(1-z)}\mathbf{X}_{11a}^{(0)}(z)\\ \frac{\mathrm{d}}{\mathrm{d}z}\mathbf{X}_{11a}^{(0)} &= -\frac{3}{(1-z)}\mathbf{X}_{11a}^{(0)}(z)\,.\end{aligned} \tag{6.34}$$

The second equation has indeed decoupled, and we find that $\mathbf{X}_{11a}^{(0)}(z) \propto (1-z)^3$ immediately. This result can subsequently be inserted into the first equation, and the solution for $\mathbf{X}_1^{(0)}(z)$ can be found. At every higher order in ϵ, the equation for $\mathbf{X}_{11a}$ will only depend on the lower orders of $\mathbf{X}_1$ and $\mathbf{X}_{11a}$ which will have been determined by then. The system has become *triangular*, order by order in ϵ. This holds true for all differential equations we encounter for the NNLO gluon-fusion master integrals when we choose the basis of master integrals appropriately.

For the solution of inhomogeneous ordinary differential equations, we employ the usual textbook method of the variation of the constant [182]. Specifically, if $\omega(z)$ is a homogeneous solution of the inhomogeneous equation

$$\frac{\mathrm{d}}{\mathrm{d}z}y(z) = A(z)y(z) + B(z)\,, \tag{6.35}$$

then the solution of the inhomogeneous equation is given by

$$y(z) = \alpha\,\omega(z) + \omega(z)\int \mathrm{d}z'\,\frac{B(z')}{\omega(z')}\,, \tag{6.36}$$

where $\alpha \in \mathbb{R}$ is an integration constant. The zeroes of the homogeneous solution become poles in the integral in eq. (6.36). They are determined by the poles in the coefficient function $A(z)$, as one can see in the above example where the homogeneous solution for $\mathbf{X}_{11a}^{(0)}(z)$ is proportional to a power of $(1-z)$ because the coefficient function in eq. (6.34) is proportional to $(1-z)^{-1}$.

Thus, by examining the structures appearing in the homogeneous parts of the system of differential equations, we can anticipate the different poles we will encounter in the integrals we have to solve. In our case, we find that there are just three types of pole structures, namely poles in $z = 0$ and/or $z = \pm 1$. Repeated integrals over integrands with poles in $\{0, \pm 1\}$ are just the definition of HPLs, so we can already anticipate that all our results will be expressible in HPLs only.

As usual for a first-order differential equation, there is also the need for a boundary condition to fix integration constants. We therefore need to know the expression for each master integral for a specific value of z. Since $0 < z < 1$, there are two obvious candidates, $z = 0$ and $z = 1$. The point $z = 0$ corresponds to the limit where the produced Higgs boson is massless. This limit, though, may not be smooth, as massless particles potentially are associated with more singularities that arise in the matrix element.

Thus, we choose the opposite limit, $z = 1$ for our boundary conditions. This corresponds to the *soft limit* (or threshold limit), where the Higgs boson is created at rest, and all extra radiation is infinitely soft, i.e. the momenta of additionally radiated partons vanish.

We define the soft limit of a general master integral $\mathbf{X}(z, \epsilon)$ multiplicatively, i.e. it is the unique function

$$\mathbf{X}^S(z, \epsilon) = \sum_{n \in \mathbf{Z}^\times} \mathbf{X}_n(\epsilon)\,(1 - z)^{\alpha + n\epsilon}\,, \quad \alpha \in \mathbb{Z}_{\geq -1}\,, \tag{6.37}$$

such that

$$\lim_{z \to 1} \frac{\mathbf{X}(z, \epsilon)}{\mathbf{X}^S(z, \epsilon)} = 1\,. \tag{6.38}$$

In the first equation, $\mathbb{Z}^\times$ denotes integers excluding zero and α is the integrals leading power in the Laurent-expansion in $(1 - z)$ (i.e. for integrals that have a divergence at the soft limit, α will be -1. Lower powers of α do not occur, the divergences are at most simple poles).

The difference between the full master integral and its soft limit then defines the hard part $\mathbf{X}^H$, i.e.

$$\mathbf{X}(z, \epsilon) = \mathbf{X}^S(z, \epsilon) + \mathbf{X}^H(z, \epsilon)\,. \tag{6.39}$$

Notice that the soft limit of the master integrals deserves special attention independent of its role as a boundary condition for differential equations. When we fabricate the partonic cross section from the master integrals, and expand in ϵ, we need to isolate divergences that cancel among the different parts of the finite cross section, such as real and virtual contributions. Specifically, there are divergences in the soft limit which we isolate by using the plus-expansion

$$(1-z)^{-1+n\epsilon} = \frac{\delta(1-z)}{n\epsilon} + \sum_{k=0}^{\infty} \frac{(n\epsilon)^k}{k!} \mathcal{D}_k(1-z)\,. \tag{6.40}$$

The first term in this expansion sets z to 1, and comes with an extra pole in ϵ. Thus, we need to know the soft limit of our cross section and therefore also of the master integrals to *one order higher* in ϵ than the hard parts. A dedicated study of the soft limit of all master integrals is thus inevitable, and the fact that we may use it as a boundary condition for the differential equations essentially comes for free.

6.1.5. NNLO master integrals to $\mathcal{O}(\epsilon)$

Having acquired the necessary technology, we are now ready to tackle the computation of the NNLO partonic cross sections for gluon fusion through $\mathcal{O}(\epsilon)$, which boils down to the computation of the 29 master integrals that remain after reduction. Note that we will not comment on the reduction itself, which has been carried out in ref. [56] using the Laporta algorithm [161]. We divide up the discussion into three subsections, separately covering the double-real, real-virtual and double-virtual master integrals.

6.1.6. Double-real master integrals

In [56], a basis of 18 master integrals was found for all integrals appearing in the production of one massive and two massless particles. We proceed by first listing all integrals in terms of diagrams and fixing our conventions, proceed to derive their soft limits and then comment on the full result obtained via the method of differential equations.

Definitions and conventions

We give the 18 master integrals in graphic form as two-loop diagrams with three cut propagators, as well as their definition in terms of the integral over the three-particle phase-space. Thick lines denote the massive particle, and short-dashed lines represent numerator factors. The long-dashed line represents the reverse unitarity cut. In the definition, the overall mass-dimension is factorised, such that the remaining objects $\mathbf{X}_i$ are a function of the dimensionless variable z, as discussed in section 6.1.4.

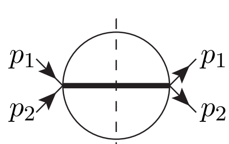

$$= \int d\Phi_3 = s^{1-2\epsilon}\,\mathcal{P}(\epsilon)\,\mathbf{X}_1(z,\epsilon)\,, \tag{6.41}$$

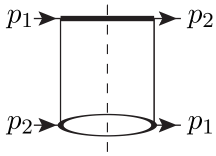

$$= \int \frac{d\Phi_3}{s_{234}s_{134}} = s^{-1-2\epsilon}\,\mathcal{P}(\epsilon)\,\mathbf{X}_2(z,\epsilon)\,, \tag{6.42}$$

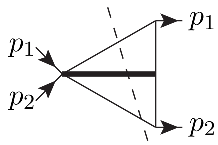

$$= \int \frac{d\Phi_3}{s_{14}s_{23}} = s^{-1-2\epsilon}\,\mathcal{P}(\epsilon)\,\mathbf{X}_3(z,\epsilon)\,, \tag{6.43}$$

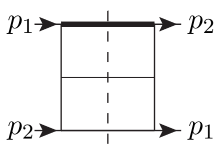

$$= \int \frac{d\Phi_3}{s_{234}s_{23}s_{13}s_{134}} = s^{-3-2\epsilon}\,\mathcal{P}(\epsilon)\,\mathbf{X}_4(z,\epsilon)\,, \tag{6.44}$$

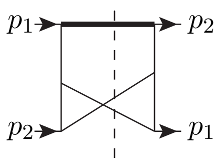

$$= \int \frac{d\Phi_3}{s_{234}s_{24}s_{13}s_{134}} = s^{-3-2\epsilon}\,\mathcal{P}(\epsilon)\,\mathbf{X}_5(z,\epsilon)\,, \tag{6.45}$$

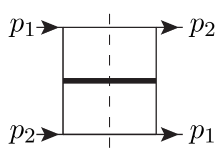

$$= \int \frac{d\Phi_3}{s_{13}s_{23}s_{14}s_{24}} = s^{-3-2\epsilon}\,\mathcal{P}(\epsilon)\,\mathbf{X}_6(z,\epsilon)\,, \tag{6.46}$$

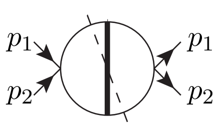

$$= \int \frac{d\Phi_3}{s_{123}s_{124}} = s^{-1-2\epsilon}\,\mathcal{P}(\epsilon)\,\mathbf{X}_7(z,\epsilon)\,, \tag{6.47}$$

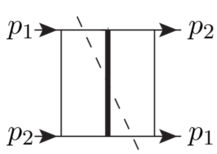

$$= \int \frac{d\Phi_3}{s_{123}s_{124}s_{14}s_{13}} = s^{-3-2\epsilon}\,\mathcal{P}(\epsilon)\,\mathbf{X}_8(z,\epsilon)\,, \tag{6.48}$$

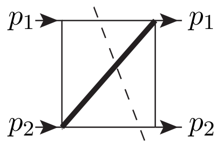

$$= \int \frac{d\Phi_3}{s_{14}s_{23}} = s^{-1-2\epsilon}\,\mathcal{P}(\epsilon)\,\mathbf{X}_9(z,\epsilon)\,, \tag{6.49}$$

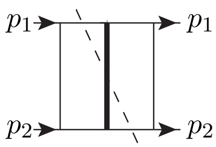

$$= \int \frac{d\Phi_3}{s_{123}s_{124}s_{14}s_{23}} = s^{-3-2\epsilon}\,\mathcal{P}(\epsilon)\,\mathbf{X}_{10}(z,\epsilon)\,, \tag{6.50}$$

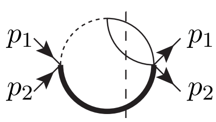

$$= \int d\Phi_3 s_{34} = s^{2-2\epsilon}\,\mathcal{P}(\epsilon)\,\mathbf{X}_{11}(z,\epsilon)\,, \tag{6.51}$$

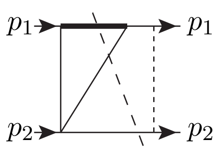

$$= \int \frac{d\Phi_3 s_{23}}{s_{234}s_{123}} = s^{-2\epsilon}\,\mathcal{P}(\epsilon)\,\mathbf{X}_{12}(z,\epsilon)\,, \tag{6.52}$$

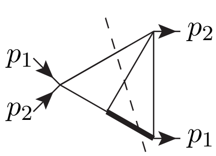

$$= \int \frac{d\Phi_3}{s_{234}s_{123}} = s^{-1-2\epsilon}\,\mathcal{P}(\epsilon)\,\mathbf{X}_{13}(z,\epsilon)\,, \tag{6.53}$$

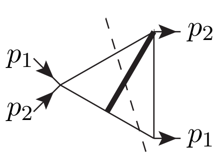

$$= \int \frac{d\Phi_3}{s_{13}s_{124}} = s^{-1-2\epsilon}\,\mathcal{P}(\epsilon)\,\mathbf{X}_{14}(z,\epsilon)\,, \tag{6.54}$$

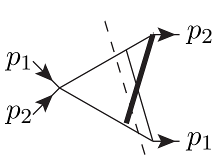

$$= \int \frac{d\Phi_3}{s_{13}s_{124}s_{134}} = s^{-2-2\epsilon}\,\mathcal{P}(\epsilon)\,\mathbf{X}_{15}(z,\epsilon)\,, \tag{6.55}$$

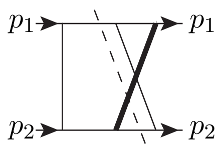

$$= \int \frac{d\Phi_3}{s_{14}s_{23}s_{234}s_{124}} = s^{-3-2\epsilon}\,\mathcal{P}(\epsilon)\,\mathbf{X}_{16}(z,\epsilon)\,, \tag{6.56}$$

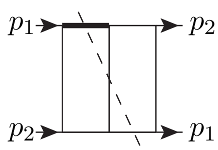

$$= \int \frac{d\Phi_3}{s_{34}s_{13}s_{234}s_{123}} = s^{-3-2\epsilon}\,\mathcal{P}(\epsilon)\,\mathbf{X}_{17}(z,\epsilon)\,, \tag{6.57}$$

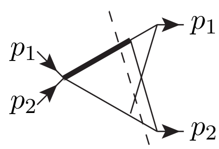

$$= \int \frac{d\Phi_3}{s_{34}s_{13}s_{24}} = s^{-2-2\epsilon}\,\mathcal{P}(\epsilon)\,\mathbf{X}_{18}(z,\epsilon)\,. \tag{6.58}$$

The common normalisation factor $\mathcal{P}(\epsilon)$ is given by

$$\mathcal{P}(\epsilon) = \frac{1}{2}\,\frac{1}{(4\pi)}^{3-2\epsilon}\,\frac{\Gamma(1-\epsilon)^2}{\Gamma(2-2\epsilon)^2}\,. \tag{6.59}$$

The system of differential equations for the basis above is triangular order by order in ϵ, as discussed in section 6.1.4 except for the two integrals $\mathbf{X}_1$ and $\mathbf{X}_{11}$. In order to decouple them, we rotate the basis, i.e. we define the linear combination

$$\mathbf{X}_{11a}(z,\epsilon) = \frac{1}{2}\left[(1+z)\mathbf{X}_1(z,\epsilon) - \mathbf{X}_{11}(z,\epsilon)\right]\,, \tag{6.60}$$

and replace $\mathbf{X}_{11}$ with $\mathbf{X}_{11a}$.

Soft Limit

For the calculation of the full result for each master integral, we will use reverse unitarity to relate the phase-space integrals to loop diagrams and apply the method of differential equations to them. The calculation of the soft limits, on the other hand, is performed rather straightforwardly. We insert a suitable phase-space parametrisation for the three-particle phase-space that factorises the propagators that appear in the integrals when the soft limit is considered, such that the remaining integrals can easily be solved.

We start with the simplest case $\mathbf{X}_1$, which is just the empty phase-space integral, i.e. we have to calculate the soft phase-space volume. We use the "Energies and angles" parametrisation of the 3-particle phase-space measure as given in eq. (A.7),

$$\int \mathrm{d}\Phi_3 = \frac{(2\pi)^{-3+2\epsilon}}{16\Gamma(1-2\epsilon)} \int_0^1 \prod_{i=1}^{4} \mathrm{d}x_i \left(\frac{s\bar{z}^3\kappa^4 x_1\bar{x}_1}{2-\kappa}\right) \left(s^2\bar{z}^4\kappa^4 x_1^2\bar{x}_1^2 x_3\bar{x}_3 x_4\bar{x}_4 \sin^2(\pi x_2)\right)^{-\epsilon}, \tag{6.61}$$

where $\bar{z} = 1-z$ and $\bar{x}_i = 1-x_i$. In the soft limit $z \to 1$, the measure simplifies due to the limit $\kappa \to 1$ and we obtain the soft measure $\mathrm{d}\Phi_3^S$,

$$\int \mathrm{d}\Phi_3^S = \frac{(2\pi)^{-3+2\epsilon}}{16\Gamma(1-2\epsilon)} \int_0^1 \prod_{i=1}^{4} \mathrm{d}x_i \left(s\bar{z}^3 x_1\bar{x}_1\right) \left(s^2\bar{z}^4 x_1^2\bar{x}_1^2 x_3\bar{x}_3 x_4\bar{x}_4 \sin^2(\pi x_2)\right)^{-\epsilon}. \tag{6.62}$$

Carrying out the integrations over x_1, x_3 and x_4 is now straightforward, as we can directly absorb them into a Beta-function,

$$\int_0^1 \mathrm{d}t\, t^{x-1}\,(1-t)^{y-1} = B(x,y) = \frac{\Gamma(x)\Gamma(y)}{\Gamma(x+y)}. \tag{6.63}$$

Thus,

$$\int \mathrm{d}\Phi_3^S = \frac{(2\pi)^{-3+2\epsilon} s^{1-2\epsilon}\bar{z}^{3-4\epsilon}}{16\Gamma(1-2\epsilon)} \frac{\Gamma(1-\epsilon)^4}{\Gamma(4-4\epsilon)} \int_0^1 \mathrm{d}x_2 \sin^{-2\epsilon}(\pi x_2). \tag{6.64}$$

The remaining integral over x_2 may be solved with the substitution $u = \sin^2(\pi x_2)$, which enables us to find yet another Beta-function,

$$\int_0^1 \mathrm{d}x_2 \sin^{-2\epsilon}(\pi x_2) = \frac{1}{\pi}\int_0^1 \mathrm{d}u\, u^{-\frac{1}{2}-\epsilon}\bar{u}^{-\frac{1}{2}} = \frac{B\left(\frac{1}{2},\frac{1}{2}-\epsilon\right)}{\pi} = \frac{\Gamma\left(\frac{1}{2}-\epsilon\right)}{\sqrt{\pi}\Gamma(1-\epsilon)}, \tag{6.65}$$

where we have evaluated $\Gamma(1/2) = \sqrt{\pi}$. Finally, we use the Gamma-functions "duplication formula" [182]

$$\Gamma(z)\Gamma\left(z+\frac{1}{2}\right) = 2^{1-2z}\sqrt{\pi}\Gamma(2z), \tag{6.66}$$

to replace

$$\Gamma\left(\frac{1}{2}-\epsilon\right) = 2^{1+2\epsilon}\sqrt{\pi}\frac{\Gamma(-2\epsilon)}{\Gamma(-\epsilon)} = 2^{2\epsilon}\sqrt{\pi}\frac{\Gamma(1-2\epsilon)}{\Gamma(1-\epsilon)}. \tag{6.67}$$

Thus, we finally find

$$\int \mathrm{d}\Phi_3^S = \frac{1}{2}\frac{s^{1-2\epsilon}\bar{z}^{3-4\epsilon}}{(4\pi)^{3-2\epsilon}}\frac{\Gamma(1-\epsilon)^2}{\Gamma(4-4\epsilon)}, \tag{6.68}$$

which means that

$$\mathbf{X}_1^S(z,\epsilon) = (1-z)^{3-4\epsilon}\frac{\Gamma(2-2\epsilon)^2}{\Gamma(4-4\epsilon)}\,. \tag{6.69}$$

For most of the other soft integrals, it is convenient to use the following parametrisation for the $2 \to 3$ phase space,

$$\begin{aligned}\int d\Phi_3 =& \frac{(2\pi)^{-3+2\epsilon}}{16\Gamma(1-2\epsilon)}\int_0^1 dx_2 \left(\prod_{i=1}^4 dy_i\right)\delta\left(\sum_{i=1}^4 y_i - 1\right) \\ &\times \left(\frac{s\bar{z}^3\kappa^4}{2-\kappa}\right)\left(s^2\bar{z}^4\kappa^4\sin^2(\pi x_2)\prod_{i=1}^4 y_i\right)^{-\epsilon}\,,\end{aligned} \tag{6.70}$$

which may be derived from the "Energies and angles" parametrisation via the following transformation

$$y_1 = x_1 x_3, \qquad y_2 = x_1\bar{x}_3, \qquad y_3 = \bar{x}_1 x_4, \qquad y_4 = \bar{x}_1\bar{x}_4\,. \tag{6.71}$$

In this parametrisation the propagators of the massless partons we encounter in the master integrals read [183]

$$\begin{aligned} s_{13} =& -s\bar{z}\kappa y_1, \qquad s_{23} = -s\bar{z}\kappa y_2, \\ s_{14} =& -s\bar{z}\kappa y_3, \qquad s_{24} = -s\bar{z}\kappa y_4, \\ s_{34} =& s\bar{z}\kappa^2\xi\,, \end{aligned} \tag{6.72}$$

where

$$\xi = \bar{z}\left(y_1y_4 + y_2y_3 + 2\cos(x_2\pi)\sqrt{y_1y_4y_2y}\right)\,, \tag{6.73}$$

and

$$\kappa = \frac{1-\sqrt{1-4\xi}}{2\xi}\,. \tag{6.74}$$

There are also three-parton invariants appearing in the propagators, namely

$$\begin{aligned} s_{134} &= s_{13} + s_{14} + s_{34}\,, \qquad s_{234} = s_{23} + s_{24} + s_{34}\,, \\ s_{123} &= s_{12} + s_{23} + s_{13}\,, \qquad s_{124} = s_{12} + s_{24} + s_{14}\,. \end{aligned} \tag{6.75}$$

If we now consider the soft limit $z \to 1$, these three-parton invariants simplify significantly, as we only have to keep the terms with the lowest power of $\bar{z}$ in their sum-definition. In other words, since $s_{12} \propto \bar{z}^0$, $s_{34} \propto \bar{z}^2$ and all other invariants $s_{ij} \propto \bar{z}^1$, we find that in the soft limit,

$$\begin{aligned}
&\lim_{z\to 1} s_{123} = \lim_{z\to 1} s_{124} = s_{12}\,, \qquad && \lim_{z\to 1} \kappa = 1\,, \\
&\lim_{z\to 1} s_{134} = s_{13} + s_{14}\,, && \lim_{z\to 1} s_{234} = s_{23} + s_{24}\,.
\end{aligned} \tag{6.76}$$

If we now perform the change of variables

$$y_1 = t_1 t_3, \qquad y_2 = \bar{t}_1 t_4, \qquad y_3 = t_1 \bar{t}_3, \qquad y_4 = \bar{t}_1 \bar{t}_4\,, \tag{6.77}$$

with the Jacobian $|J| = t_1 \bar{t}_1$, it is easy to see from eqs. (6.72) and (6.77) that in the soft limit all the invariants, except for s_{34}, take a fully factorized form. In particular the terms $s_{13}+s_{14}$ and $s_{23}+s_{24}$ effectively reduce to t_1 and $\bar{t}_1$ respectively. This construction therefore allows one to derive all the soft limits of almost all master integrals, with the exception of $\mathbf{X}_{17}$ and $\mathbf{X}_{18}$, in terms of simple Beta-functions.

As an example, we calculate $\mathbf{X}_{13}^S$. In the soft limit the denominator $s_{234}s_{123}$ becomes

$$s_{234}^S s_{123}^S = s_{12}(s_{23} + s_{24}) = -s_{12}^2 \bar{z}(y_2 + y_4) = -s^2 \bar{z}\bar{t}_1\,, \tag{6.78}$$

and thus,

$$\begin{aligned}
s^{-1-2\epsilon}\mathcal{P}(\epsilon)\mathbf{X}_{13}^S(z,\epsilon) &= \int \frac{\mathrm{d}\Phi_3^S}{s_{234}s_{123}} = -\frac{s^{-1-2\epsilon}\bar{z}^{2-4\epsilon}}{(2\pi)^{3-2\epsilon}16\Gamma(1-2\epsilon)} \\
&\quad \times \int_0^1 \mathrm{d}x_2 \mathrm{d}t_1 \mathrm{d}t_3 \mathrm{d}t_4\, t_1 \left(t_1^2 \bar{t}_1^2 t_3 \bar{t}_3 t_4 \bar{t}_4 \sin^2(\pi x_2)\right)^{-\epsilon} \\
&= -\frac{1}{2}\frac{s^{-1-2\epsilon}\bar{z}^{2-4\epsilon}}{(4\pi)^{3-2\epsilon}} \frac{\Gamma(1-2\epsilon)\Gamma(1-\epsilon)^2}{\Gamma(3-4\epsilon)\Gamma(2-2\epsilon)}\,,
\end{aligned} \tag{6.79}$$

which, after rewriting ($\Gamma(z+1) = z\Gamma(z)$)

$$\frac{\Gamma(1-2\epsilon)}{\Gamma(3-4\epsilon)\Gamma(2-2\epsilon)} = \frac{3-4\epsilon}{1-2\epsilon}\frac{1}{\Gamma(4-4\epsilon)}\,, \tag{6.80}$$

leads to

$$\mathbf{X}_{13}^S(z,\epsilon) = -\frac{(3-4\epsilon)}{\bar{z}(1-2\epsilon)}\,\mathbf{X}_1(z,\epsilon)\,. \tag{6.81}$$

For the soft limit of the master integral $\mathbf{X}_{17}$, we choose the "hierarchical" phase-space parametrisation from eq. (A.10),

$$\int \mathrm{d}\Phi_3 = \frac{(2\pi)^{-3+2\epsilon}}{16\Gamma(1-2\epsilon)} \int_0^1 \prod_{i=1}^4 \mathrm{d}x_i \left(\frac{s\bar{z}^3 x_1 \bar{x}_1}{z + x_1\bar{z}}\right) \left(\frac{s^2 \bar{z}^4 x_1^2 \bar{x}_1^2 x_2 \bar{x}_2 x_3 \bar{x}_3 \sin^2(\pi x_4)}{z + x_1 \bar{z}}\right)^{-\epsilon} . \tag{6.82}$$

After exchanging p_1 and p_2 which we are free to do, the propagator invariants in the denominator of $\mathbf{X}_{17}$ are

$$s_{34} = \frac{s\bar{z}x_1\bar{x}_1 x_2}{z + x_1\bar{z}}\,, \quad s_{23} = -s\bar{z}\bar{x}_1 x_3\,, \quad s_{134} = -s\bar{z}x_1\,, \tag{6.83}$$

and s_{123} which simplifies to s in the soft limit. The recurring denominator $z + x_1\bar{z}$ becomes just 1 in the soft limit and we obtain the fully factorised expression

$$\begin{aligned}
\int \frac{\mathrm{d}\Phi_3^S}{s_{34}s_{23}s_{134}s_{123}} = {} & \frac{s^{-3-2\epsilon}\bar{z}^{-1-4\epsilon}}{(2\pi)^{3-2\epsilon}16\Gamma(1-2\epsilon)} \int_0^1 \prod_{i=1}^4 \mathrm{d}x_i \\
& \times \; x_1^{-1-2\epsilon}\bar{x}_1^{-1-2\epsilon} x_2^{-1-\epsilon}\bar{x}_2^{-\epsilon} x_3^{-1-\epsilon}\bar{x}_3^{-\epsilon} \sin^{-2\epsilon}(\pi x_4) \\
& = \frac{s^{-3-2\epsilon}\bar{z}^{-1-4\epsilon}}{2(4\pi)^{3-2\epsilon}\Gamma(1-2\epsilon)} B(-2\epsilon,-2\epsilon)B(-\epsilon,1-\epsilon)^2 \frac{\Gamma(1-2\epsilon)}{\Gamma(1-\epsilon)^2} \\
& = \frac{s^{-3-2\epsilon}\bar{z}^{-1-4\epsilon}}{2(4\pi)^{3-2\epsilon}} \frac{\Gamma(-2\epsilon)^2\Gamma(-\epsilon)^2}{\Gamma(-4\epsilon)\Gamma(1-2\epsilon)^2} \,.
\end{aligned} \tag{6.84}$$

If we again use the defining property of the Gamma-function extensively to rewrite

$$\frac{\Gamma(-2\epsilon)^2\Gamma(-\epsilon)^2}{\Gamma(-4\epsilon)\Gamma(1-2\epsilon)^2} = -\frac{(1-4\epsilon)(2-4\epsilon)(3-4\epsilon)}{\epsilon^3} \frac{\Gamma(1-\epsilon)^2}{\Gamma(4-4\epsilon)}\,, \tag{6.85}$$

we finally find

$$\mathbf{X}_{17}^S(z,\epsilon) = -\frac{2(1-4\epsilon)(1-2\epsilon)(3-4\epsilon)}{\bar{z}^4\epsilon^3}\mathbf{X}_1^S(z,\epsilon)\,. \tag{6.86}$$

Unfortunately, we are not aware of any parametrisation which allows one to factorise all denominators of $\mathbf{X}_{18}$ simultaneously. We proceed by expressing the integral in terms of energies and angles, i.e., by writing $p_i = E_i(1, \vec{n}_i)$, where $\vec{n}_i$ is a unit vector in the direction of the spatial component of p_i. The integral over the energies of p_3 and p_4 yields a Beta-function, and we arrive at

$$\mathcal{P}(\epsilon)\mathbf{X}_{18}^S = 4(4\pi)^{-5+4\epsilon} \frac{B(-2\epsilon,-2\epsilon)}{(1-z)^{1+4\epsilon}} \int \frac{\mathrm{d}\Omega_3^{(d-1)}\mathrm{d}\Omega_4^{(d-1)}}{(1+\cos\theta_{13})(1-\cos\theta_{14})(1-\cos\theta_{34})}\,, \tag{6.87}$$

where $\mathrm{d}\Omega_i^{(d-1)}$ is differential volume element of the $(d-1)$ dimensional solid angle of p_i

and the angles are defined as $\cos\theta_{ij} = \vec{n}_i.\vec{n}_j$. We then use the result [167]

$$\begin{aligned}
\Omega_{11} =& \int \frac{\mathrm{d}\Omega_4^{(d-1)}}{(1-\cos\theta_{14})(1-\cos\theta_{34})} \\
=&\Omega^{(d-3)} \int_0^\pi \frac{\mathrm{d}\theta_{13}(\sin\theta_{13})^{d-3}\mathrm{d}\phi_{34}(\sin\phi_{34})^{d-4}}{(1-\cos\theta_{14})(1-\cos\theta_{14}\cos\theta_{13}-\cos\phi_{34}\sin\theta_{14}\sin\theta_{13})} \\
=&-\frac{1}{4}(4\pi)^{1-\epsilon}\frac{\Gamma(-\epsilon)}{\epsilon\Gamma(-2\epsilon)}\,{}_2F_1\left(1,1;1-\epsilon;\frac{1+\cos\theta_{13}}{2}\right),
\end{aligned} \tag{6.88}$$

where ${}_2F_1$ is the hypergeometric function which can be defined via its integral representation

$$ {}_2F_1(a,b;c;z) = \frac{\Gamma(c)}{\Gamma(b)\Gamma(c-b)}\int_0^1 \mathrm{d}t\, t^{b-1}(1-t)^{c-b-1}(1-zt)^{-a}\,. \tag{6.89}$$

The integral then becomes

$$\begin{aligned}
\mathcal{P}(\epsilon)\mathbf{X}_{18}^S = -&\frac{(4\pi)^{-4+3\epsilon}}{(1-z)^{1+4\epsilon}}\frac{\Gamma(-\epsilon)\Gamma(-2\epsilon)}{\epsilon\Gamma(-4\epsilon)}\Omega^{(d-2)} \\
&\times\int_0^\pi \frac{\mathrm{d}\theta_{13}(\sin\theta_{13})^{d-3}}{1+\cos\theta_{13}}{}_2F_1\left(1,1;1-\epsilon;\frac{1+\cos\theta_{13}}{2}\right).
\end{aligned} \tag{6.90}$$

Changing variables to $y = \frac{1+\cos\theta_{13}}{2}$, eq. (6.90) may be written as

$$\begin{aligned}
\mathcal{P}(\epsilon)\mathbf{X}_{18}^S =&\frac{(4\pi)^{-3+2\epsilon}}{(1-z)^{1+4\epsilon}}\frac{\Gamma(-2\epsilon)}{\epsilon^2\Gamma(-4\epsilon)}\int_0^1 \mathrm{d}y y^{-1-\epsilon}(1-y)^{-\epsilon}{}_2F_1\left(1,1;1-\epsilon;y\right) \\
=&\frac{1}{2}\frac{(4\pi)^{-3+2\epsilon}}{(1-z)^{1+4\epsilon}}\frac{\Gamma(-\epsilon)^2}{\epsilon^2\Gamma(-4\epsilon)}\,{}_3F_2\left(1,1,-\epsilon;1-\epsilon,1-2\epsilon;1\right),
\end{aligned} \tag{6.91}$$

where we used the recursive definition of the ${}_pF_q$ function [182],

$$\begin{aligned}
&{}_{p+1}F_{q+1}(a_1,\ldots,a_p,c;b_1,\ldots,b_q,d;z) = \\
&\frac{\Gamma(d)}{\Gamma(c)\Gamma(d-c)}\int_0^1 \mathrm{d}t\, t^{c-1}(1-t)^{d-c-1}{}_pF_q(a_1,\ldots,a_p;b_1,\ldots,b_q;tz)\,.
\end{aligned} \tag{6.92}$$

Hence we have arrived at expressions valid to all orders in ϵ for the soft limits of all the double-real master integrals. We observe that in all cases, except for $\mathbf{X}_{18}^S$, the results are proportional to the soft limit of the phase space volume,

$$\mathbf{X}_1^S(z,\epsilon) = (1-z)^{3-4\epsilon}\frac{\Gamma(2-2\epsilon)^2}{\Gamma(4-4\epsilon)}\,, \tag{6.93}$$

the constant of proportionality being a rational function of z and ϵ. We therefore define

$$\mathbf{X}_i^S(z,\epsilon) = \mathbf{S}_i(z,\epsilon)\,\mathbf{X}_1^S(z,\epsilon)\,. \tag{6.94}$$

In this normalisation the results for the soft limits of the master integrals read

$$\mathbf{S}_1(z,\epsilon) = \mathbf{S}_7(z,\epsilon) = \mathbf{S}_{11a}(z,\epsilon) = 1\,, \tag{6.95}$$

$$\mathbf{S}_2(z,\epsilon) = \frac{2(3-4\epsilon)}{(1-2\epsilon)\,(1-z)^2}\,, \tag{6.96}$$

$$\mathbf{S}_3(z,\epsilon) = \mathbf{S}_8(z,\epsilon) = \mathbf{S}_9(z,\epsilon) = \mathbf{S}_{10}(z,\epsilon) = 2\frac{(1-2\epsilon)(3-4\epsilon)}{\epsilon^2(1-z)^2}\,, \tag{6.97}$$

$$\mathbf{S}_4(z,\epsilon) = \mathbf{S}_5(z,\epsilon) = -2\,\frac{(1-2\epsilon)\,(3-4\epsilon)\,(1-4\epsilon)}{\epsilon^3(1-z)^4}\,, \tag{6.98}$$

$$\mathbf{S}_6(z,\epsilon) = -8\,\frac{(1-2\epsilon)\,(3-4\epsilon)\,(1-4\epsilon)}{\epsilon^3(1-z)^4}\,, \tag{6.99}$$

$$\mathbf{S}_{12}(z,\epsilon) = \frac{1}{2}\,, \tag{6.100}$$

$$\mathbf{S}_{13}(z,\epsilon) = -\frac{3-4\epsilon}{(1-2\epsilon)\,(1-z)}\,, \tag{6.101}$$

$$\mathbf{S}_{14}(z,\epsilon) = \frac{3-4\epsilon}{\epsilon\,(1-z)}\,, \tag{6.102}$$

$$\mathbf{S}_{15}(z,\epsilon) = \frac{(1-2\epsilon)(3-4\epsilon)}{\epsilon^2(1-z)^2}\,, \tag{6.103}$$

$$\mathbf{S}_{16}(z,\epsilon) = \frac{(1-2\epsilon)\,(3-4\epsilon)\,(1-4\epsilon)}{\epsilon^3(1-z)^3}\,, \tag{6.104}$$

$$\mathbf{S}_{17}(z,\epsilon) = -2\,\frac{(1-2\epsilon)\,(3-4\epsilon)\,(1-4\epsilon)}{\epsilon^3(1-z)^4}\,, \tag{6.105}$$

$$
\begin{aligned}
\mathbf{S}_{18}(z,\epsilon) =& -4\frac{(1-2\epsilon)(3-4\epsilon)(1-4\epsilon)}{\epsilon^3(1-z)^4}\,{}_3F_2\left(1,1,-\epsilon;1-\epsilon,1-2\epsilon;1\right) \\
=& \frac{1}{(1-z)^4}\Bigg[-\frac{18}{\epsilon^3}+\frac{132}{\epsilon^2}+\frac{1}{\epsilon}\left(12\zeta_2-288\right)-88\zeta_2+60\zeta_3+192 \\
&+\left(\frac{372}{5}\zeta_2^2+192\zeta_2-440\zeta_3\right)\epsilon \\
&+\left(-\frac{2728}{5}\zeta_2^2+24\zeta_3\zeta_2-128\zeta_2+444\zeta_5+960\zeta_3\right)\epsilon^2 \\
&+\mathcal{O}(\epsilon^3)\Bigg].
\end{aligned}
\tag{6.106}
$$

In [158], there is a semi-numerical proof that the generalised hypergeometric function ${}_3F_2\left(1,1,-\epsilon;1-\epsilon,1-2\epsilon;1\right)$ can not be reduced to a product of Gamma-functions, thus proving that the soft master integral $\mathbf{X}_{18}^S$ can not be reduced to $\mathbf{X}_1^S$ times a rational factor. By now, this fact is understood better due to the work on triple-real master integrals published in ref. [157].

The authors of ref. [157] realised that the technique of IBP-identities can be extended to the notion of soft integrals, i.e. the expansion coefficients in $\bar{z}$ of a given phase-space integral. Via the Laporta algorithm, soft master integrals for each order in $\bar{z}$ can then be identified. When applying this method to all topologies in the double-real corrections to Higgs production in gluon fusion, the authors find that there are exactly two soft master integrals for the lowest order in $\bar{z}$, $\mathbf{X}_1^S$ and $\mathbf{X}_{18}^S$, which is in accordance with the result above. Furthermore, for $2 \leq i \leq 17$, the IBP relation among the soft integrals $\mathbf{X}_i^S$ and $\mathbf{X}_1^S$ are just the $\mathbf{S}_i$ factors above, which we have derived by shifting the arguments of Gamma-functions.

In [157], the method of soft master integrals is applied to the triple-real corrections to Higgs production in gluon fusion, and a basis of ten soft master integrals is identified. Also, the ϵ-expansion up to orders sufficient for N^{3}LO computations of all soft master integrals is calculated by choosing a suitable soft phase-space parametrisation and disentangling integration variables by introducing Mellin-Barnes integrals, whose ϵ-expansion is calculable.

Full results

Having the soft limit of all master integrals at our disposal, we can now tackle the problem of solving the 18 differential equations. We first list the equations, suppressing the dependence of the $\mathbf{X}_i$ on z and ϵ,

$$\frac{\mathrm{d}}{\mathrm{d}z}\mathbf{X}_1 = \frac{((1-\epsilon)(1-z)+\epsilon z)\,\mathbf{X}_1}{(1-z)\,z} - 3\,\frac{(1-\epsilon)\,\mathbf{X}_{11a}}{(1-z)\,z} \tag{6.107}$$

$$\begin{aligned}\frac{\mathrm{d}}{\mathrm{d}z}\mathbf{X}_2 =& -\frac{\mathbf{X}_2\,(1-3\,z)\,\epsilon}{(1-z)\,z} - 3\,\frac{(z+1)\,(1-\epsilon)\,\mathbf{X}_{11a}}{z^2\,(1-z)^3}\\ &+ \frac{((1-\epsilon)(1-z)^2+2\epsilon z)\,\mathbf{X}_1}{z^2\,(1-z)^3}\end{aligned} \tag{6.108}$$

$$\begin{aligned}\frac{\mathrm{d}}{\mathrm{d}z}\mathbf{X}_3 =& -2\,\frac{\epsilon\,\mathbf{X}_3}{z} - 3\,\frac{(1-\epsilon)\,(1-2\,\epsilon)\,(2-\epsilon\,z-7\,\epsilon)\,\mathbf{X}_{11a}}{(1-z)^3\,\epsilon^2 z}\\ &+ \frac{(1-2\,\epsilon)\,\left(\epsilon\,z^2-7\,\epsilon\,z-z^2-2\,\epsilon+3\,z\right)\mathbf{X}_1}{\epsilon\,(1-z)^3\,z}\end{aligned} \tag{6.109}$$

$$\begin{aligned}\frac{\mathrm{d}}{\mathrm{d}z}\mathbf{X}_4 =& \frac{(1+2\,\epsilon)\,\mathbf{X}_4}{1-z} + 6\,\frac{(1-\epsilon)\,(1-2\,\epsilon)\,(\epsilon\,z+7\,\epsilon-2)\,\mathbf{X}_{11a}}{z\epsilon^2\,(1-z)^5}\\ &+ 2\,\frac{(1-2\,\epsilon)\,\left(\epsilon\,z^2-7\,\epsilon\,z-z^2-2\,\epsilon+3\,z\right)\mathbf{X}_1}{\epsilon\,z\,(1-z)^5} + 2\,\frac{(1-2\,\epsilon)\,\mathbf{X}_2}{z\,(1-z)^2}\end{aligned} \tag{6.110}$$

$$\begin{aligned}\frac{\mathrm{d}}{\mathrm{d}z}\mathbf{X}_5 =& -\frac{(1-2\,z)\,(1+2\,\epsilon)\,\mathbf{X}_5}{(1-z)\,z} - 3\,\frac{(1-2\,\epsilon)\,(z+1)\,(1-\epsilon)\,(\epsilon\,z-9\,\epsilon+2)\,\mathbf{X}_{11a}}{z^2\epsilon^2\,(1-z)^5}\\ &- \frac{(1-2\,\epsilon)\,\left(\epsilon\,z^3-4\,\epsilon\,z^2-z^3+19\,\epsilon\,z+4\,z^2-9\,z+2\right)\mathbf{X}_1}{\epsilon\,z^2\,(1-z)^5}\\ &- 2\,\frac{(1-2\,\epsilon)\,\mathbf{X}_2}{z\,(1-z)^2} - 2\,\frac{\mathbf{X}_3\,\epsilon}{z^2\,(1-z)}\end{aligned} \tag{6.111}$$

$$\begin{aligned}\frac{\mathrm{d}}{\mathrm{d}z}\mathbf{X}_6 =& \frac{(1+2\,\epsilon)\,\mathbf{X}_6}{1-z} + 6\,\frac{(1-2\,\epsilon)\,(1-\epsilon)\,\left(\epsilon\,z^2+22\,\epsilon\,z+9\,\epsilon-6\,z-2\right)\mathbf{X}_{11a}}{z\epsilon^2\,(1-z)^5}\\ &+ 2\,\frac{(1-2\,\epsilon)\,\left(\epsilon\,z^3-10\,\epsilon\,z^2-z^3-23\,\epsilon\,z+2\,z^2+9\,z-2\right)\mathbf{X}_1}{\epsilon\,z\,(1-z)^5}\\ &- 4\,\frac{\mathbf{X}_3\,\epsilon}{(1-z)\,z}\end{aligned} \tag{6.112}$$

$$\begin{aligned}\frac{\mathrm{d}}{\mathrm{d}z}\mathbf{X}_7 = &- \frac{\mathbf{X}_7\,\epsilon\,(1+2\,z)}{(1+z)\,z} - 6\,\frac{(1-\epsilon)\,\mathbf{X}_{11a}}{z^2\,(1-z)} \\ &- 2\,\frac{\left(\epsilon\,z^2 - 4\,\epsilon\,z - z^2 + \epsilon + 2\,z - 1\right)\mathbf{X}_1}{z^2\,(1+z)\,(1-z)}\end{aligned} \tag{6.113}$$

$$\begin{aligned}\frac{\mathrm{d}}{\mathrm{d}z}\mathbf{X}_8 = &- \frac{(1+2\,\epsilon)\,\mathbf{X}_8}{1+z} + 2\,\frac{(1-2\,\epsilon)\,\mathbf{X}_7}{z\,(1+z)} + 8\,\frac{\mathbf{X}_3\,\epsilon}{z\,(1+z)} \\ &+ 12\,\frac{(1-2\,\epsilon)\,(1-\epsilon)\left(2\,\epsilon\,z^2 + 7\,\epsilon\,z - \epsilon - 2\,z\right)\mathbf{X}_{11a}}{(1-z)^3\,\epsilon^2 z^2\,(z+1)} \\ &+ 4\,\frac{(1-2\,\epsilon)\left((1-\epsilon)(1-3z+6z^2-2z^3) - 6\epsilon z^2\right)\mathbf{X}_1}{z^2\epsilon\,(1-z)^3\,(1+z)}\end{aligned} \tag{6.114}$$

$$\begin{aligned}\frac{\mathrm{d}}{\mathrm{d}z}\mathbf{X}_9 = &- 2\,\frac{\epsilon\,\mathbf{X}_9}{z} + 3\,\frac{(1-\epsilon)\,(1-2\,\epsilon)\,(\epsilon\,z + 7\,\epsilon - 2)\,\mathbf{X}_{11a}}{(1-z)^3\,\epsilon^2 z} \\ &+ \frac{(1-2\,\epsilon)\left(\epsilon\,z^2 - 7\,\epsilon\,z - z^2 - 2\,\epsilon + 3\,z\right)\mathbf{X}_1}{\epsilon\,(1-z)^3\,z}\end{aligned} \tag{6.115}$$

$$\begin{aligned}\frac{\mathrm{d}}{\mathrm{d}z}\mathbf{X}_{10} = &- \frac{(1+2\,\epsilon)\,\mathbf{X}_{10}}{z} - 2\,\frac{(1-2\,\epsilon)\,\mathbf{X}_7}{(1+z)\,z} - 4\,\frac{\epsilon\,\mathbf{X}_3}{z^2} \\ &- 2\,\frac{(1-2\,\epsilon)\left(3\,\epsilon\,z^3 - 14\,\epsilon\,z^2 - 3\,z^3 + 29\,\epsilon\,z + 10\,z^2 - 2\,\epsilon - 15\,z + 4\right)\mathbf{X}_1}{z^2\epsilon\,(1-z)^3\,(1+z)} \\ &- 6\,\frac{(1-2\,\epsilon)\,(1-\epsilon)\,(3\,\epsilon\,z - 11\,\epsilon + 2)\,\mathbf{X}_{11a}}{z^2\,(1-z)^3\,\epsilon^2}\end{aligned} \tag{6.116}$$

$$\frac{\mathrm{d}}{\mathrm{d}z}\mathbf{X}_{11a} = - 3\,\frac{(1-\epsilon)\,\mathbf{X}_{11a}}{1-z} + \frac{\epsilon\,\mathbf{X}_1}{1-z} \tag{6.117}$$

$$\frac{\mathrm{d}}{\mathrm{d}z}\mathbf{X}_{12} = - \frac{(z(1-3\epsilon)+\epsilon)\,\mathbf{X}_{12}}{(1-z)\,z} - 3\,\frac{(1-\epsilon)\,\mathbf{X}_{11a}}{z^2\,(1-z)} + \frac{\mathbf{X}_1\,(1-\epsilon)\,(1+z)}{z^2\,(1-z)} \tag{6.118}$$

$$\begin{aligned}\frac{\mathrm{d}}{\mathrm{d}z}\mathbf{X}_{13} = &- 2\,\frac{\epsilon\,\mathbf{X}_{13}}{z} + 6\,\frac{(1-\epsilon)\,\mathbf{X}_{11a}}{z^2\,(1-z)^2} + \frac{\mathbf{X}_{12}\,(1-2\,\epsilon)}{(1-z)\,z} \\ &- 2\,\frac{((1-\epsilon)(1-z)+\epsilon z)\,\mathbf{X}_1}{z^2\,(1-z)^2}\end{aligned} \tag{6.119}$$

$$\frac{\mathrm{d}}{\mathrm{d}z}\mathbf{X}_{14} = -2\,\frac{\epsilon\,\mathbf{X}_{14}}{z} - 3\,\frac{(1+z)\,(1-\epsilon)\,(1-2\,\epsilon)\,\mathbf{X}_{11a}}{(1-z)^2\,\epsilon\,z^2} + \frac{(1-2\,\epsilon)\,\big((1-\epsilon)(1-z)^2+2\epsilon z\big)\,\mathbf{X}_1}{(1-z)^2\,\epsilon\,z^2} \tag{6.120}$$

$$\begin{aligned}\frac{\mathrm{d}}{\mathrm{d}z}\mathbf{X}_{15} = &-\frac{(1+4\,\epsilon)\,\mathbf{X}_{15}}{1+z} + 3\,\frac{\left(2\,\epsilon^2z^2-18\,\epsilon^2z-\epsilon\,z^2+11\,\epsilon\,z+2\,\epsilon-2\,z\right)(1-\epsilon)\,\mathbf{X}_{11a}}{(1-z)^3\,\epsilon^2z^2\,(1+z)}\\ &+\frac{\left(2\epsilon^2z^3+2\epsilon^2z^2-3\epsilon z^3+12\epsilon^2z+5\epsilon z^2+z^3-16\epsilon z-3z^2+2\epsilon+6z-2\right)\mathbf{X}_1}{z^2\epsilon\,(1-z)^3\,(1+z)}\\ &+2\,\frac{(1-2\,\epsilon)\,\mathbf{X}_{12}}{z\,(1-z)\,(1+z)} + 2\,\frac{\epsilon\,\mathbf{X}_{14}}{z\,(1+z)}\end{aligned} \tag{6.121}$$

$$\begin{aligned}\frac{\mathrm{d}}{\mathrm{d}z}\mathbf{X}_{16} = &-\frac{(1+2\,\epsilon)\,\mathbf{X}_{16}}{z} - 4\,\frac{(1-2\,\epsilon)\,\mathbf{X}_{12}}{z\,(1+z)\,(1-z)^2} + 2\,\frac{\epsilon\,\mathbf{X}_{14}}{z^2\,(1+z)} - \frac{(1+4\,\epsilon)\,\mathbf{X}_{15}}{z\,(1+z)}\\ &+3\,\Big(2\,\epsilon^2z^3+56\,\epsilon^2z^2-\epsilon\,z^3+10\,\epsilon^2z-36\,\epsilon\,z^2-4\,\epsilon^2-13\,\epsilon\,z+6\,z^2+2\,\epsilon+2\,z\Big)\\ &\times\frac{(1-\epsilon)\,\mathbf{X}_{11a}}{(1+z)\,z^3\,(1-z)^4\,\epsilon^2}\\ &+\Big(2\,\epsilon^2z^4-32\,\epsilon^2z^3-3\,\epsilon\,z^4-42\,\epsilon^2z^2+16\,\epsilon\,z^3+z^4+12\,\epsilon^2z+47\,\epsilon\,z^2-\\ &-4\,\epsilon^2-18\,\epsilon\,z-15\,z^2+6\,\epsilon+8\,z-2\Big)\times\frac{\mathbf{X}_1}{\epsilon\,(1+z)\,z^3\,(1-z)^4}\end{aligned} \tag{6.122}$$

$$\begin{aligned}\frac{\mathrm{d}}{\mathrm{d}z}\mathbf{X}_{17} = &\frac{(1+2\,\epsilon)\,\mathbf{X}_{17}}{1-z} - 6\,\frac{(1-\epsilon)\left(2\,\epsilon^2z^2+16\,\epsilon^2z-\epsilon\,z^2-2\,\epsilon^2-11\,\epsilon\,z+2\,z\right)\mathbf{X}_{11a}}{z^2\epsilon^2\,(1-z)^5}\\ &-2\,\frac{\left(2\,\epsilon^2z^3-18\,\epsilon^2z^2-3\,\epsilon\,z^3+2\,\epsilon^2z+15\,\epsilon\,z^2+z^3-2\,\epsilon^2-2\,\epsilon\,z-3\,z^2+2\,\epsilon\right)\mathbf{X}_1}{\epsilon\,z^2\,(1-z)^5}\\ &+2\,\frac{\mathbf{X}_{12}\,(1-2\,\epsilon)}{z\,(1-z)^3}\end{aligned} \tag{6.123}$$

$$\begin{aligned}\frac{\mathrm{d}}{\mathrm{d}z}\mathbf{X}_{18} = &\frac{(1+4\,\epsilon)\,\mathbf{X}_{18}}{1-z} + 3\,\frac{(1-\epsilon)\,(1-2\,\epsilon)\,(\epsilon\,z+7\,\epsilon-2)\,\mathbf{X}_{11a}}{\epsilon^2\,(1-z)^4\,z}\\ &+\frac{(1-2\,\epsilon)\left(\epsilon\,z^2-7\,\epsilon\,z-z^2-2\,\epsilon+3\,z\right)\mathbf{X}_1}{\epsilon\,(1-z)^4\,z} - 2\,\frac{\epsilon\,\mathbf{X}_3}{(1-z)\,z}\end{aligned} \tag{6.124}$$

Solving the equations above order by order in ϵ is straightforwardly achieved using the method of variation of constants, as presented in section 6.1.4. We note that the inhomogeneities occurring most are proportional to $\mathbf{X}_1$ and $\mathbf{X}_{11a}$. Once they have been found, many differential equations decouple. But in any case, the equations are triangular order by order in ϵ, as can be verified by expanding each equation in ϵ, where the leading ϵ-order of each $\mathbf{X}_i$ can be obtained from the soft limits in the previous subsection.

For illustrative purposes, we calculate the lowest ϵ-order of $\mathbf{X}_{11a}$ and $\mathbf{X}_1$. As already seen in section 6.1.4, we obtain

$$\mathbf{X}_{11a}^{(0)}(z) = \alpha\,(1-z)^3\,, \tag{6.125}$$

for the lowest order of $\mathbf{X}_{11a}$. There is no inhomogeneity to integrate over, so this is the full solution at this order. We fix the integration constant by requiring equality with the leading order of the soft limit,

$$\mathbf{X}_{11a}^{S}(z,\epsilon) = (1-z)^{3-4\epsilon}\frac{\Gamma(2-2\epsilon)^2}{\Gamma(4-4\epsilon)} = \frac{(1-z)^3}{6} + \mathcal{O}(\epsilon)\,, \tag{6.126}$$

fixing α to 1/6. This also means that $\mathbf{X}_{11a}^{H,(0)} = 0$. We proceed to the calculation of the lowest order of $\mathbf{X}_1$. The equation reads

$$\frac{\mathrm{d}}{\mathrm{d}z}\mathbf{X}_1^{(0)} = \frac{1}{z}\mathbf{X}_1^{(0)} - \frac{3}{z(1-z)}\mathbf{X}_{11a}^{(0)} = \frac{1}{z}\mathbf{X}_1^{(0)} - \frac{(1-z)^2}{2z}\,. \tag{6.127}$$

The general homogeneous solution is easily found to be $\mathbf{X}_1^{\mathrm{hom},(0)} = \alpha\,z$. According to eq. (6.36), the solution to the full equation thus is

$$\mathbf{X}_1^{(0)}(z,\epsilon) = \alpha\,z - \frac{z}{2}\int \mathrm{d}z'\,\frac{(1-z')^2}{z'^2} = \alpha\,z - \frac{z^2}{2} + \frac{1}{2} + z\log(z)\,. \tag{6.128}$$

After expanding

$$\log(z) = -\sum_{k=1}^{\infty}\frac{(1-z)^k}{k}\,, \tag{6.129}$$

we equate this to $\mathbf{X}_1^{S,(0)} = (1-z)^3/6$ and find $\alpha = 0$, i.e.

$$\mathbf{X}_1^{(0)}(z) = z\log(z) - \frac{z^2}{2} + \frac{1}{2} \;\Rightarrow\; \mathbf{X}_1^{H,(0)}(z) = z\log(z) + \frac{1}{6}(1-z)\left(2+5z-z^2\right)\,. \tag{6.130}$$

The integrals in this example have been easy to solve. In general, we encounter polylogarithmic integrals of the type

$$\int \mathrm{d}x\frac{x^n\mathrm{H}(a_1,\ldots,a_k;x)}{x^{d_1}(1-x)^{d_2}(1+x)^{d_3}}\,,\quad n,\,d_i \geq 0\,,\quad a_i \in \{-1,0,1\} \tag{6.131}$$

The first step is always to use partial fractioning, such that we only have do deal with one type of denominator at a time. Also, numerator powers of the integration variable x can be expanded in terms of the remaining denominator (e.g. $x = -(1-x) - 1$ if the denominator in question is $(1-x)^{n-1}$), such that we have to deal only with either a denominator or a numerator factor. Subsequently, we integrate by parts repeatedly, taking the derivative of the HPL (which is trivial to obtain, see eq. (4.5)) and integrating the rational part of the integrand. If the integration by parts produces a mixed denominator, another partial fractioning has to be performed. These steps are repeated until either of the two termination conditions apply:

- The HPL has been lowered all the way to weight 0 and is thus just one of the three functions
$$f_1(x) = \frac{1}{1-x}\,, \quad f_0(x) = \frac{1}{x}\,, \quad f_{-1}(x) = \frac{1}{1+x}\,, \tag{6.132}$$
in which case the whole integrand becomes a rational function and is easily solved.

- The denominators power becomes 1, at which point the recursive definition of the HPLs eq. (4.2) may be applied.

To clarify, we give a simple example,

$$\begin{aligned}\int \mathrm{d}x \frac{\mathrm{H}(0,1;x)}{(1-x)^2} =& \frac{\mathrm{H}(0,1;x)}{1-x} - \int \mathrm{d}x \frac{\mathrm{H}(1;x)}{x(1-x)} \\ =& \frac{\mathrm{H}(0,1;x)}{1-x} - \int \mathrm{d}x \frac{\mathrm{H}(1;x)}{x} - \int \mathrm{d}x \frac{\mathrm{H}(1;x)}{1-x} \\ =& \frac{\mathrm{H}(0,1;x)}{1-x} - \mathrm{H}(0,1;x) - \mathrm{H}(1,1;x)\,,\end{aligned} \tag{6.133}$$

where in the second step, a partial fractioning of the denominator was performed.

The important point here is that the integrals appearing in the inhomogeneous parts of the differential equations are straightforwardly and algorithmically solvable. We can thus easily cope with the large number of integrals we need to solve by implementing the algorithm outlined above in a computer-algebra-system (CAS) such as Maple or Mathematica. In the present case, we used the in-house Mathematica package `PolyLogTools` [184] for this task.

The full results for all hard parts of the master integrals are too lengthy to be presented here, but they are all given in appendix A.3. of ref. [158] and also in machine-readable form in the ancillary files of the same publication.

6.1.7. Real-virtual master integrals

For the real-virtual master integrals, we follow the same steps as in the previous section for the double-real masters.

Definitions and conventions

In [56], six master integrals for the real-virtual contributions to an inclusive $2 \to 1$ partonic cross section were identified.

We define the common prefactor

$$\mathcal{Q}(\epsilon) = \frac{1}{2}\frac{(4\pi)^\epsilon}{4\pi}\frac{\Gamma(1+\epsilon)\Gamma(1-\epsilon)}{\Gamma(2-2\epsilon)}, \tag{6.134}$$

as well as the one-loop integrals

$$\begin{aligned}
\mathbf{Bub}(p^2) &= \int \frac{d^D k}{i\pi^{D/2}} \frac{1}{k^2(k+p)^2}, \\
\mathbf{Tri}(s_{23}, s_{123}) &= \int \frac{d^D k}{i\pi^{D/2}} \frac{1}{k^2(k+p_1)^2(k+p_{123})^2}, \\
\mathbf{Box}(s_{12}, s_{23}, s_{123}) &= \int \frac{d^D k}{i\pi^{D/2}} \frac{1}{k^2(k+p_1)^2(k+p_{12})^2(k+p_{123})^2}.
\end{aligned} \tag{6.135}$$

The master integrals can then be defined as the following integrals over the two-particle phase-space,

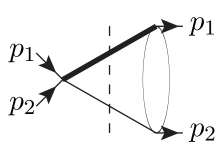

$$= \int d\Phi_2 \mathbf{Bub}(s_{13}) = s^{-2\epsilon}\mathcal{Q}(\epsilon)\mathbf{Y}_1(z,\epsilon), \tag{6.136}$$

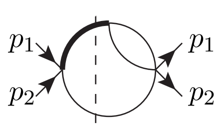

$$= \int d\Phi_2 \mathbf{Bub}(m_X^2) = s^{-2\epsilon}\mathcal{Q}(\epsilon)\mathbf{Y}_2(z,\epsilon), \tag{6.137}$$

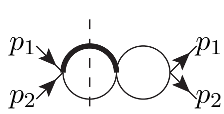

$$= \int d\Phi_2 \mathbf{Bub}(s_{12}) = s^{-2\epsilon}\mathcal{Q}(\epsilon)\mathbf{Y}_5(z,\epsilon), \tag{6.138}$$

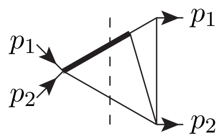

$$= \int d\Phi_2 \mathbf{Tri}(s_{13}, m_X^2) = s^{-1-2\epsilon} \mathcal{Q}(\epsilon) \mathbf{Y}_3(z, \epsilon), \tag{6.139}$$

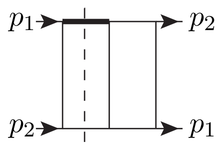

$$= \int d\Phi_2 \frac{\mathbf{Box}(s_{13}, s_{12}, m_X^2)}{s_{23}} = s^{-3-2\epsilon} \mathcal{Q}(\epsilon) \mathbf{Y}_4(z, \epsilon), \tag{6.140}$$

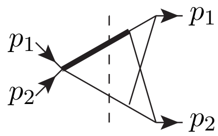

$$= \int d\Phi_2 \mathbf{Box}(s_{13}, s_{23}, m_X^2) = s^{-2-2\epsilon} \mathcal{Q}(\epsilon) \mathbf{Y}_6(z, \epsilon). \tag{6.141}$$

Soft limit

The computation of the soft limits of the real-virtual master integrals is done in a similar fashion to the double-real case. The phase-space integration simplifies significantly since there are just two instead of three final-state particles, and we can again use the parametrisation

$$\int \mathrm{d}\Phi_2 = \frac{(4\pi)^{-1+\epsilon} s^{-\epsilon} \bar{z}^{1-2\epsilon}}{2\Gamma(1-\epsilon)} \int_0^1 \mathrm{d}x_1 \, (x_1 \bar{x}_1)^{-\epsilon} \,, \tag{6.142}$$

with the invariants s_{13} and s_{23} given by

$$s_{13} = -s\bar{z}x_1 \,, \quad s_{23} = -s\bar{z}\bar{x}_1 \,. \tag{6.143}$$

On the other hand, there are the massless one-loop integrals inside the phase-space integration which complicate the calculation. There are results for the Bubble, the Triangle and the Box valid to all orders in ϵ,

$$\mathbf{Bub}(s) = \frac{\Gamma(1+\epsilon)\Gamma(1-\epsilon)^2}{\epsilon\Gamma(2-2\epsilon)} (-s)^{-\epsilon} \,, \tag{6.144}$$

which we have derived in section 6.1.1,

$$\mathbf{Tri}(s,t) = -2 \, \frac{\Gamma(1+\epsilon)\Gamma(1-\epsilon)^2}{\epsilon^2 \Gamma(1-2\epsilon)} \, \frac{(-s)^{-\epsilon} - (-t)^{-\epsilon}}{s-t} \,, \tag{6.145}$$

and [136, 183]

$$\begin{aligned}\mathbf{Box}(s,t,m^2) =& \frac{2\Gamma(1+\epsilon)\Gamma(1-\epsilon)^2}{\epsilon\Gamma(1-2\epsilon)}\frac{1}{st}\Bigg[-(-m^2)^{-\epsilon}{}_2F_1\left(1,-\epsilon,1-\epsilon;-\frac{um^2}{st}\right)\\ &+(-t)^{-\epsilon}{}_2F_1\left(1,-\epsilon;1-\epsilon;-\frac{u}{s}\right)+(-s)^{-\epsilon}{}_2F_1\left(1,-\epsilon,1-\epsilon;-\frac{u}{s}\right)\Bigg],\end{aligned} \tag{6.146}$$

where $u \equiv m^2 - s - t$. In the case of the bubble and triangle insertions, the integrands directly factorise and we are able to carry out the integral over x_1, producing yet another Beta-function. For $\mathbf{Y}_4$ and $\mathbf{Y}_6$, the argument of the hypergeometric function has to vanish in the soft limit, i.e. we need it to be proportional to $\bar{z}$. If that is not the case, the argument has to be remapped using one of the identities [138]

$${}_2F_1(a,b;c;z) = (1-z)^{-b}{}_2F_1\left(c-a,b;c;\frac{z}{z-1}\right), \tag{6.147}$$

or

$$\begin{aligned}{}_2F_1(a,b;c;z) =& \frac{\Gamma(b-a)\Gamma(c)}{\Gamma(b)\Gamma(c-a)}(-z)^{-a}{}_2F_1\left(a,a-c+1;a-b+1;\frac{1}{z}\right)\\ &+\frac{\Gamma(a-b)\Gamma(c)}{\Gamma(a)\Gamma(c-b)}(-z)^{-b}{}_2F_1\left(b,b-c+1;b-a+1;\frac{1}{z}\right).\end{aligned} \tag{6.148}$$

The hypergeometric function is just 1 for vanishing argument, and the integration over the soft phase-space becomes trivial.

We thus find the following soft limits for the six real-virtual master integrals,

$$\mathbf{Y}_1^S(z,\epsilon) = (1-z)^{1-3\epsilon}\frac{\Gamma(1-\epsilon)\Gamma(1-2\epsilon)}{\epsilon\,\Gamma(2-3\epsilon)}, \tag{6.149}$$

$$\mathbf{Y}_2^S(z,\epsilon) = (1-z)^{1-2\epsilon}\cos(\pi\epsilon)\frac{\Gamma(1-\epsilon)^2}{\epsilon\,\Gamma(2-2\epsilon)}, \tag{6.150}$$

$$\mathbf{Y}_5^S(z,\epsilon) = \mathbf{Y}_2^S(z,\epsilon), \tag{6.151}$$

$$\mathbf{Y}_3^S(z,\epsilon) = 0, \tag{6.152}$$

$$\mathbf{Y}_4^S(z,\epsilon) = -3(1-z)^{-1-3\epsilon}\frac{\Gamma(2-2\epsilon)\Gamma(1-\epsilon)}{\epsilon^3\,\Gamma(1-3\epsilon)}\,, \tag{6.153}$$

$$\mathbf{Y}_6^S(z,\epsilon) = -2(1-z)^{-1-4\epsilon}\,\cos(\pi\epsilon)\,\frac{\Gamma(1-2\epsilon)\Gamma(2-2\epsilon)\Gamma(1-\epsilon)\Gamma(1+\epsilon)}{\epsilon^3\,\Gamma(1-4\epsilon)}\,. \tag{6.154}$$

Note that only the real part of the master integrals is shown, as the imaginary part never enters the computation of a physical observable. The factors of $\cos(\pi\epsilon)$ come from taking the real part of the term $(-1)^\epsilon$.

Full results

The full results for the real-virtual master integrals are derived in the exact same way as the double-real ones, by solving the differential equations order by order in ϵ.

We again list all equations,

$$\frac{\mathrm{d}}{\mathrm{d}z}\mathbf{Y}_1 = -\frac{(1-3\epsilon)}{1-z}\mathbf{Y}_1\,, \tag{6.155}$$

$$\frac{\mathrm{d}}{\mathrm{d}z}\mathbf{Y}_2 = -\frac{(z+\epsilon-3\epsilon z)}{z(1-z)}\mathbf{Y}_2\,, \tag{6.156}$$

$$\frac{\mathrm{d}}{\mathrm{d}z}\mathbf{Y}_3 = -\frac{2\epsilon}{z}\mathbf{Y}_3 - 2\,\frac{(1-3\epsilon)(1-2\epsilon)}{\epsilon\,z(1-z)^2}\mathbf{Y}_1 - \frac{(1-2\epsilon)^2}{\epsilon\,z(1-z)}\mathbf{Y}_2\,, \tag{6.157}$$

$$\begin{aligned}\frac{\mathrm{d}}{\mathrm{d}z}\mathbf{Y}_4 =& \frac{(1+2\epsilon)}{1-z}\mathbf{Y}_4 - \frac{(1-3\epsilon)(1-2\epsilon)(1+2z)}{\epsilon\,z(1-z)^3}\mathbf{Y}_1\\ &- 2\,\frac{(1-2\epsilon)^2}{\epsilon\,z(1-z)^2}\mathbf{Y}_2 + 2\frac{\epsilon}{z(1-z)}\mathbf{Y}_3\,,\end{aligned} \tag{6.158}$$

$$\frac{\mathrm{d}}{\mathrm{d}z}\mathbf{Y}_5 = -\frac{(1-2\epsilon)}{1-z}\mathbf{Y}_5\,, \tag{6.159}$$

$$\frac{\mathrm{d}}{\mathrm{d}z}\mathbf{Y}_6 = \frac{(1+4\epsilon)}{1-z}\mathbf{Y}_6 - 2\,\frac{(1-3\epsilon)(1-2\epsilon)}{\epsilon\,z(1-z)^2}\mathbf{Y}_1 + 4\,\frac{\epsilon}{z(1-z)}\mathbf{Y}_3\,. \tag{6.160}$$

The integrations over inhomogeneities produces the same types of terms, and we again end up with results given by HPLs. Again, we refer to appendix A.2. or the ancillary files of ref. [158] for the full analytic results of the master integrals.

Thanks to the relatively simple structure of the phase-space and the known all-order results for all massless one-loop integrals, we were able to numerically verify the new, higher-order in ϵ, results that had not been published in [56]. The strategy was as follows:

1. Substitute known expressions for the one-loop master integrals which are valid to all-orders in ϵ.

2. Apply analytic continuation formulae (eqs. (6.147) and (6.148)) to the hypergeometric functions which express the box integrals, if required. The criterion is that in the limits $x_1 \to 0$ and $x_1 \to 1$, the hypergeometric function is well-defined and finite, i.e. all divergences associated with the limits above have to be extracted via remappings.

3. Expand the hypergeometric function in terms of polylogarithmic functions, using the MATHEMATICA package `HypExp` [185, 186].

4. Expand the real emission singularities (these are factorised here) in terms of delta- and plus-distributions.

5. Evaluate the coefficients numerically.

Using this approach, we were able to verify all terms in the ϵ-expansion of the real-virtual master integrals.

6.1.8. Double-virtual master integrals

The double-virtual master integrals which contribute to the two-loop corrections to the Born process $gg \to H$ have a trivial dependence on phase-space, since $\mathrm{d}\Phi_1 \propto \delta(1-z)$. The task is equivalent to calculating the two-loop corrections to the QCD form factor, which is another way of denoting the ggH-vertex in an effective theory. Parts of the two-loop QCD form factor have been calculated many years ago [187, 188], and as of the year 2000, the full $\mathcal{O}(\epsilon^0)$ result had been found [189]. Since 2005, the result is known to all orders in ϵ [190]. The most difficult master integral (the crossed triangle) was found to be a sum of generalised hypergeometric functions with unit argument, which can be expanded to any desired order in ϵ using `HypExp` [185, 186].

For completeness, we list the results obtained from [190] in our diagrammatic notation and normalisation. Note that we again only provide the real part of the master integrals.

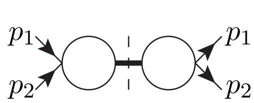

$$= \delta(1-z)\, \frac{\Gamma(1+\epsilon)^2\, \Gamma(1-\epsilon)^4}{\epsilon^2\, \Gamma(2-2\epsilon)^2}\,, \tag{6.161}$$

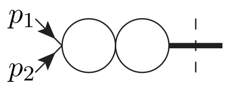

$$= \delta(1-z)\,\cos(2\pi\epsilon)\,\frac{\Gamma(1+\epsilon)^2\,\Gamma(1-\epsilon)^4}{\epsilon^2\,\Gamma(2-2\epsilon)^2}\,. \tag{6.162}$$

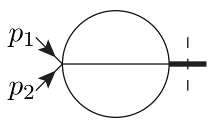

$$= -\delta(1-z)\,\cos(2\pi\epsilon)\,\frac{\Gamma(1-\epsilon)^3\Gamma(1+2\epsilon)}{2(1-2\epsilon)\,\epsilon\,\Gamma(3-3\epsilon)}\,, \tag{6.163}$$

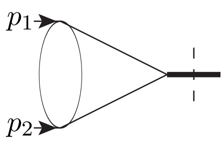

$$= \delta(1-z)\,\cos(2\pi\epsilon)\,\frac{\Gamma(1-2\epsilon)\Gamma(1-\epsilon)^2\Gamma(1+\epsilon)\Gamma(1+2\epsilon)}{2(1-2\epsilon)\epsilon^2\Gamma(2-3\epsilon)}\,, \tag{6.164}$$

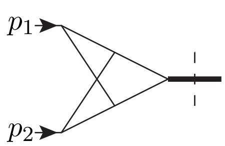

$$\begin{aligned} &= \delta(1-z)\,\cos(2\pi\epsilon)\,\Gamma(1+\epsilon)^2\left\{\frac{1}{\epsilon^4} - \frac{7}{\epsilon^2}\zeta_2 - \frac{27}{\epsilon}\zeta_3 - \frac{57}{5}\zeta_2^2\right. \\ &\quad \left. + \Big[102\zeta_2\zeta_3 - 117\zeta_5\Big]\epsilon + \mathcal{O}(\epsilon^2)\right\}, \end{aligned} \tag{6.165}$$

6.2. Convolutions of collinear factorisation kernels and lower-order cross sections

With the prerequisites at hand, we can now turn to the task of computing all terms save the first of the RHS of eq. (6.1).

The renormalisation terms in the first two lines are trivial to obtain, once the bare cross sections are known to sufficiently high order, as they involve only multiplications.

We do not comment on them further.

The terms originating in mass factorisation, on the other hand, require some effort, since they consist of (multiple) convolutions of splitting kernels and cross sections. Both these objects consist of three types of terms, delta-, plus- and regular terms,

$$\sigma_{ij}^{(n,m)}(x) = a_{ij}^{(n,m)}\,\delta(1-x) + \sum_k b_{ij}^{(n,m),k}\,\mathcal{D}_k(1-x) + c_{ij}^{(n,m)}(x)\,, \tag{6.166}$$

$$P_{ij}^{(n)}(x) = A_{ij}^{(n)}\,\delta(1-x) + \sum_k B_{ij}^{(n),k}\,\mathcal{D}_k(1-x) + C_{ij}^{(n)}(x)\,, \tag{6.167}$$

where we have expanded the partonic cross section in ϵ,

$$\sigma_{ij}(z) = C_1^2\sigma_0 \sum_{n,m=0}^{\infty} \sigma_{ij}^{(n,m)}(z) a_s^n \epsilon^m\,, \tag{6.168}$$

i.e. the $\sigma^{(n,0)}$ correspond to the $\Delta^{(n)}$ as defined in eq. (3.53). The regular pieces $c_{ij}^{(n,m)}(x)$ and $C_{ij}^{(n)}(x)$ consist of HPLs times polynomials in x and/or factors of $1/x$ and $1/(1-x)$, respectively. The convolution operation is linear,

$$\begin{aligned}
\left(f\otimes(\alpha g_1+\beta g_2)\right)(z) &= \int_0^1 \mathrm{d}x\,\mathrm{d}y\, f(x)(\alpha g_1(y)+\beta g_2(y))\delta(xy-z)\\
&= \alpha\int_0^1 \mathrm{d}x\,\mathrm{d}y\, f(x)g_1(y)\delta(xy-z) + \beta\int_0^1 \mathrm{d}x\,\mathrm{d}y\, f(x)g_2(y)\delta(xy-z)\\
&= \alpha\left(f\otimes g_1\right)(z) + \beta\left(f\otimes g_2\right)(z)\,,
\end{aligned} \tag{6.169}$$

symmetric,

$$\left(f\otimes g\right)(z) = \int_0^1 \mathrm{d}x\,\mathrm{d}y\, f(x)g(y)\delta(xy-z) = \left(g\otimes f\right)(z)\,, \tag{6.170}$$

and associative,

$$\begin{aligned}
\left(f\otimes(g\otimes h)\right)(z) &= \int_0^1 \mathrm{d}x\,\mathrm{d}y\, f(x)\left(g\otimes h\right)(y)\delta(xy-z)\\
&= \int_0^1 \mathrm{d}x\,\mathrm{d}y\,\mathrm{d}v\,\mathrm{d}w\, f(x)g(v)h(w)\delta(xy-z)\delta(vw-y)\\
&= \int_0^1 \mathrm{d}x\,\mathrm{d}v\,\mathrm{d}w\, f(x)g(v)h(w)\delta(xvw-z)\\
&= \int_0^1 \mathrm{d}x\,\mathrm{d}y\,\mathrm{d}v\,\mathrm{d}w\, f(x)g(v)h(w)\delta(yw-z)\delta(xv-y)\\
&= \int_0^1 \mathrm{d}w\,\mathrm{d}y\, \left(f\otimes g\right)(y)h(w)\delta(yw-z)\\
&= \left((f\otimes g)\otimes h\right)(z)\,.
\end{aligned} \tag{6.171}$$

Furthermore, the convolution of two expressions consisting of delta-, plus- and regular polylogarithmic terms will itself have the same structure, i.e. we generate no new classes of functions with the convolution operation. Therefore, we only need to consider the case of a single convolution involving two convolutants, as the multiple convolutions can iteratively be reduced to a single one. In practice, when we have to deal with terms like

$$P_{ik}^{(0)} \otimes P_{kl}^{(0)} \otimes P_{lm}^{(0)} \otimes \sigma_{mj}^{(0)}\,, \tag{6.172}$$

we first calculate the triple convolution of the LO kernels among themselves, before we finally convolute with the partonic cross section. This is the preferred order for two reasons. First, the kernels do not have an ϵ-expansion, i.e. we do not have to keep track of different ϵ-orders in the intermediate expression. And second, the same double and triple convolutions of splitting kernels appear with different partonic cross sections. So computing (and storing) them first is a more efficient procedure.

Using the symmetry of the convolution and taking into account that certain channels only open up at NLO or NNLO, we find that we require 80 different convolutions for the N^{3}LO cross section. Let us now examine the different combinations of convolutants we can encounter.

6.2.1. Convolutions involving delta-terms

Whenever one of the convolutants is a delta-function, the convolution trivialises,

$$\left(\delta(1-x) \otimes f(y)\right)(z) = \int_0^1 \mathrm{d}x\,\mathrm{d}y\,\delta(1-x) f(y) \delta(xy-z) = f(z)\,, \tag{6.173}$$

regardless whether f is a regular function, a plus-distribution or a delta-function itself. This immediately solves all 30 convolutions involving the LO cross section

$$\sigma_{ij}^{(0,m)}(z) = \delta_{ig}\delta_{jg}\,\delta(1-z)\,, \quad m = 0,1,2,3\,, \tag{6.174}$$

although we may still have to compute intermediate double or triple convolutions as mentioned above.

6.2.2. Convolutions of two plus-distributions

Convolutions where both convolutants are plus-distributions,

$$(\mathcal{D}_n(1-x)\otimes\mathcal{D}_m(1-y))\,(z)=\int_0^1 dx\,dy\left[\frac{\log(1-x)^n}{1-x}\right]_+\left[\frac{\log(1-y)^m}{1-y}\right]_+\delta(xy-z) \tag{6.175}$$

are a more delicate endeavour. We can not simply use the delta-function to get rid of one integration variable, as we do when there are regular functions involved, since a plus-distribution with a rational argument is no object we can make sense of. Let us instead consider the following convolution integral,

$$I_{ab}(z)=\int_0^1 dx\,dy\,(1-x)^{-1+a\epsilon}(1-y)^{-1+b\epsilon}\delta(xy-z)\,. \tag{6.176}$$

We use the delta-function to get rid of x and then remap the integral onto the unit interval:

$$\begin{aligned}
I_{ab}(z)&=\int_z^1 dy\,\frac{1}{y}\left(1-\frac{z}{y}\right)^{-1+a\epsilon}(1-y)^{-1+b\epsilon}=\int_z^1 dy\,y^{-a\epsilon}(y-z)^{-1+a\epsilon}(1-y)^{-1+b\epsilon}\\
&=\int_0^1 d\lambda\,(1-z)[z+(1-z)\lambda]^{-a\epsilon}[\lambda(1-z)]^{-1+a\epsilon}[(1-z)(1-\lambda)]^{-1+b\epsilon}\\
&=(1-z)^{-1+(a+b)\epsilon}\int_0^1 d\lambda\,[z+(1-z)\lambda]^{-a\epsilon}\lambda^{-1+a\epsilon}(1-\lambda)^{-1+b\epsilon}\\
&=(1-z)^{-1+(a+b)\epsilon}\int_0^1 d\lambda\,[(1-\lambda)+z\lambda]^{-a\epsilon}\lambda^{-1+b\epsilon}(1-\lambda)^{-1+a\epsilon}\\
&=(1-z)^{-1+(a+b)\epsilon}\,B(a\epsilon,b\epsilon)\,{}_2F_1(a\epsilon,b\epsilon,(a+b)\epsilon;1-z)\,.
\end{aligned} \tag{6.177}$$

In the second to last step, we mapped $\lambda\mapsto 1-\lambda$ and in the last step, the Euler definition of the hypergeometric function was used,

$$B(b,c-b)\,{}_2F_1(a,b,c;z)=\int_0^1 dx\,x^{b-1}(1-x)^{c-b-1}\underbrace{(1-zx)}_{(1-x)+(1-z)x}{}^{-a}\,. \tag{6.178}$$

On the other hand, we may also directly expand the integrands in I_{ab} in terms of a delta-function and a tower of plus-distributions,

$$I_{ab}(z)=\int_0^1 dx\,dy\left(\frac{\delta(1-x)}{a\epsilon}+\sum_{n\geq 0}\frac{(a\epsilon)^n}{n!}\mathcal{D}_n(1-x)\right)\times$$

$$
\begin{aligned}
&\times\left(\frac{\delta(1-y)}{b\epsilon}+\sum_{m\geq 0}\frac{(b\epsilon)^m}{m!}\mathcal{D}_m(1-y)\right)\delta(xy-z)\\
&=\frac{\delta(1-z)}{ab\epsilon^2}+\frac{1}{a\epsilon}\sum_{n\geq 0}\frac{(b\epsilon)^n}{n!}\mathcal{D}_n(1-z)\frac{1}{b\epsilon}\sum_{n\geq 0}\frac{(a\epsilon)^n}{n!}\mathcal{D}_n(1-z)+\\
&+\sum_{n,m\geq 0}\frac{(a\epsilon)^n\,(b\epsilon)^m}{n!\,m!}\left(\mathcal{D}_n(1-x)\otimes\mathcal{D}_m(1-y)\right)(z)\,. \qquad (6.179)
\end{aligned}
$$

When we now expand the first term of eq 6.177 in the same way,

$$
(1-z)^{-1+(a+b)\epsilon}=\frac{\delta(1-z)}{(a+b)\epsilon}+\sum_{n\geq 0}\frac{((a+b)\epsilon)^n}{n!}\mathcal{D}_n(1-z)\,, \qquad (6.180)
$$

and expand the Beta-function and the ${}_2F_1$ (using `HypExp` [185, 186]) in ϵ as well, we can equate the two sides order by order in ϵ.
The double and single poles cancel and for $\mathcal{O}(\epsilon^0)$ we find the equation

$$
\left(\mathcal{D}_0(1-x)\otimes\mathcal{D}_0(1-y)\right)(z)=-\frac{\pi^2}{6}\delta(1-z)+2\mathcal{D}_1(1-z)-\frac{\log(z)}{1-z}\,. \qquad (6.181)
$$

Higher orders in ϵ of the equation contain more than one plus-plus-convolutions, but they can be isolated by extracting the corresponding coefficient of a and b. To find the expression for the convolution $\left(\mathcal{D}_n(1-x)\otimes\mathcal{D}_m(1-y)\right)(z)$, one has to take the $\mathcal{O}(\epsilon^{n+m}a^n b^m)$ coefficient of the equation, or equivalently the $\mathcal{O}(\epsilon^{n+m}a^m b^n)$ coefficient since the expressions are symmetric in a and b.

In this way, any plus-plus convolution appearing in the mass factorisation for the N^{3}LO gluon fusion cross section can be obtained, without actually solving any integrals. We list all convolutions we need, for completeness.

$$
\left(\mathcal{D}_0\otimes\mathcal{D}_0\right)(z)=-\frac{\pi^2}{6}\delta(1-z)+2\mathcal{D}_1(1-z)-\frac{\log(z)}{1-z} \qquad (6.182)
$$

$$
\left(\mathcal{D}_0\otimes\mathcal{D}_1\right)(z)=\zeta_3\,\delta(1-z)-\frac{\pi^2}{6}\mathcal{D}_0(1-z)+\frac{3}{2}\mathcal{D}_2(1-z)-\frac{\log(z)\log(1-z)}{1-z} \qquad (6.183)
$$

$$
\begin{aligned}
\left(\mathcal{D}_0\otimes\mathcal{D}_2\right)(z)=&\frac{\pi^4}{45}\delta(1-z)+\frac{4}{3}\mathcal{D}_3(1-z)-\frac{\pi^2}{3}\mathcal{D}_1(1-z)+2\zeta_3\,\mathcal{D}_0(1-z)\\
&-\frac{\log(z)\log^2(1-z)}{1-z} \qquad (6.184)
\end{aligned}
$$

$$(\mathcal{D}_1 \otimes \mathcal{D}_1)(z) = -\frac{\pi^4}{360}\delta(1-z) + \mathcal{D}_3(1-z) - \frac{\pi^2}{3}\mathcal{D}_1(1-z) + 2\zeta_3\,\mathcal{D}_0(1-z) - \frac{\log(z)\log^2(1-z)}{1-z} - \frac{\log(z)\mathrm{Li}_2(z)}{1-z} + 2\frac{\mathrm{Li}_3(z)-\zeta_3}{1-z} \tag{6.185}$$

$$(\mathcal{D}_0 \otimes \mathcal{D}_3)(z) = 6\zeta_5\,\delta(1-z) + \frac{5}{4}\mathcal{D}_4(1-z) - \frac{\pi^2}{2}\mathcal{D}_2(1-z) + 6\zeta_3\,\mathcal{D}_1(1-z) - \frac{\pi^4}{15}\mathcal{D}_0(1-z) - \frac{\log(z)\log^3(1-z)}{1-z} \tag{6.186}$$

$$\begin{aligned}(\mathcal{D}_1 \otimes \mathcal{D}_2)(z) = &\left(4\zeta_5 - \frac{\pi^2\zeta_3}{3}\right)\delta(1-z) + \frac{5}{6}\mathcal{D}_4(1-z) - \frac{\pi^2}{2}\mathcal{D}_2(1-z)\\ &+ 6\zeta_3\,\mathcal{D}_1(1-z) - \frac{\pi^4}{36}\mathcal{D}_0(1-z) + \frac{\mathrm{Li}_2^2(1-z)}{1-z}\\ &+ 4\frac{\log(1-z)(\mathrm{Li}_3(z)-\zeta_3)}{1-z} + \frac{\log(z)}{1-z}\Big[2\log(z)\log^2(1-z)\\ &- \log^3(1-z) - \frac{\pi^2}{3}\log(1-z) + 2\log(1-z)\mathrm{Li}_2(1-z)\\ &+ 2\mathrm{Li}_3(1-z) - 2\zeta_3\Big]\end{aligned} \tag{6.187}$$

$$(\mathcal{D}_0 \otimes \mathcal{D}_4)(z) = -\frac{8\pi^6}{315}\delta(1-z) + \frac{6}{5}\mathcal{D}_5(1-z) - \frac{2\pi^2}{3}\mathcal{D}_3(1-z) + 12\zeta_3\,\mathcal{D}_2(1-z) - \frac{4\pi^4}{15}\mathcal{D}_1(1-z) + 24\zeta_5\,\mathcal{D}_0(1-z) - \frac{\log(z)\log^4(1-z)}{1-z} \tag{6.188}$$

$$\begin{aligned}(\mathcal{D}_1 \otimes \mathcal{D}_3)(z) = &\left(3\zeta_3^2 - \frac{\pi^6}{210}\right)\delta(1-z) + \frac{3}{4}\mathcal{D}_5(1-z) - \frac{2\pi^2}{3}\mathcal{D}_3(1-z)\\ &+ 12\zeta_3\,\mathcal{D}_2(1-z) - \frac{3\pi^4}{20}\mathcal{D}_1(1-z)\left(18\zeta_5 - \pi^2\zeta_3\right)\mathcal{D}_0(1-z)\\ &+ \frac{1}{1-z}\Bigg[3\log^3(1-z)\log^2(z) + \log(z)\Bigg(\frac{\pi^4}{15} - \frac{\pi^2\log^2(1-z)}{2}\\ &- \log^4(1-z) + 3\log^2(1-z)\mathrm{Li}_2(1-z) + 6\log(1-z)\mathrm{Li}_3(1-z)\\ &- 6\mathrm{Li}_4(1-z) - 6\zeta_3\log(1-z)\Bigg) + 12\,\mathrm{H}_{3,2}(1-z)\end{aligned}$$

$$+ 24\,\mathrm{H}_{4,1}(1-z) + 6\log^2(1-z)(\mathrm{Li}_3(z) - \zeta_3)$$
$$+ 3\log(1-z)\mathrm{Li}_2^2(1-z) - 6\mathrm{Li}_2(1-z)\mathrm{Li}_3(1-z)\Bigg] \tag{6.189}$$

6.2.3. Regular convolutions

The remaining two combinations are regular-regular and plus-regular, which we will treat on the same footing. We write the convolution as a single integration, using the delta-function to get rid of the other one,

$$(f \otimes g)(z) = \int_0^1 \mathrm{d}x\,\mathrm{d}y\, f(x)g(y)\delta(xy-z) = \int_z^1 \mathrm{d}x\, f(x) g\left(\frac{z}{x}\right)\frac{1}{x}\,, \tag{6.190}$$

$$\begin{aligned}(\mathcal{D}_n \otimes f)(z) = &\int_0^1 \mathrm{d}x\,\mathrm{d}y\,\mathcal{D}_n(1-x)f(y)\delta(xy-z) = \int_z^1 \mathrm{d}x\,\mathcal{D}_n(1-x)\frac{f\left(\frac{z}{x}\right)}{x}\\ =&\frac{\log^{n+1}(1-z)}{n+1}f(z) + \int_z^1 \mathrm{d}x\,\frac{\log^n(1-x)}{1-x}\left(\frac{f\left(\frac{z}{x}\right)}{x} - f(z)\right)\,,\end{aligned} \tag{6.191}$$

where we have picked up a boundary term when evaluating the plus-distribution in an interval different from $(0,1)$.

Even though we know, from the denominator-structures appearing in the integrals, that our final result can only consist of HPLs (times polynomials in z and factors of $\frac{1}{z}$ or $\frac{1}{1-z}$), we have to step into the realm of multiple polylogarithms (MPLs) in intermediate steps of the calculation. MPLs are defined analogously to HPLs, but allow for any complex number in the index vector instead of only $\{-1,0,1\}$ in the HPL case. Recursively,

$$G(x_1,x_2,\ldots,x_n;z) = \int_0^z \mathrm{d}t\frac{G(x_2,\ldots,x_n;t)}{t-x_1}\,,\ \{x_i\}\in\mathbb{C} \quad \text{and} \quad G(\,;z) = 1\,. \tag{6.192}$$

Specifically, a MPL may be a function of multiple variables that appear anywhere in the index vector $(x_1,\ldots,x_n)$. The relation to HPLs reads

$$\mathrm{H}(a_1,\ldots,a_n;x) = (-1)^k G(a_1,\ldots,a_n;x)\,, \quad \{a_i\}\in\{-1,0,1\}\,, \tag{6.193}$$

where k is the number of $+1$ indices in $(a_1,\ldots,a_n)$. This sign difference is due to the fact that HPLs use $\frac{1}{1-t}$ as the weight function when adding a $+1$ to the index vector.

For more detailed information on multiple polylogarithms, see references [121,122,130] and references therein. Note that the order of the MPLs indices is often reversed. We

follow the convention of [130].
The subsequent steps to solve the integrals are as follows:

1. We first remap the integral by $x \mapsto 1-x$, such that the integration region becomes $(0, 1-z)$.

2. HPLs with argument $1-x$ and $\frac{z}{1-x}$ have to be written as a combination of MPLs with the integration variable x as their argument, or no x-dependence at all. For example,

$$\begin{aligned} \mathrm{H}\left(1; \frac{z}{1-x}\right) &= -\log\left(1-\frac{z}{1-x}\right) = -\log\left(\frac{1-x-z}{1-x}\right) \\ &= \log(1-x) - \log\left((1-z)\left(1-\frac{x}{1-z}\right)\right) \\ &= G(1;x) - G(1;z) - G(1-z;x)\,, \end{aligned} \tag{6.194}$$

   where we've used that $G(a;b) = \log\left(1-\frac{b}{a}\right)$ for $a \neq 0$. For MPLs of higher weights, one can find these translations by using the recursive definition of MPLs and changing variables in the integration. This becomes very tedious, though, so it proved to be more practical to use the symbol calculus formalism we have described in chapter 4.

   We generated the symbol for a MPL expression using an in-house MATHEMATICA package [184]. Matching the symbol to MPLs with x as the argument is straightforward, and the equality of the two expressions was additionally ensured numerically for some random test values of x and z, using `Ginsh`, the interactive front end of the computer algebra system GiNaC [126].

3. Once all MPLs are of the form $G(\ldots, x)$, we get rid of products of MPLs via the shuffle algebra,

$$G(\vec{x}_1;x)G(\vec{x}_2;x) = \sum_{\vec{x}_{12}\in\vec{x}_1\Delta\vec{x}_2} G(\vec{x}_{12};x)\,, \tag{6.195}$$

   where we remind the reader that $\vec{x}_1 \,\Delta\, \vec{x}_2$ denotes all permutations of the entries of the index vectors that leave the order of the individual vectors invariant.

4. We are left with integrals of a single MPL with argument x times factors of x^k ($k \geq -1$) or $\frac{1}{1-x}$, which can all immediately be solved via the MPLs recursive definition and integration by parts. The easiest cases are the ones with a denominator, where

the recursive definition of the MPLs can directly be applied,

$$\int_0^{1-z} \mathrm{d}x \, \frac{G(x_1,\ldots,x_n;x)}{x} = G(0,x_1,\ldots,x_n;1-z)\,, \tag{6.196}$$

$$\int_0^{1-z} \mathrm{d}x \, \frac{G(x_1,\ldots,x_n;x)}{1-x} = -\,G(1,x_1,\ldots,x_n;1-z)\,. \tag{6.197}$$

For the integrals with positive powers of x, one has to integrate by parts recursively. For example,

$$\begin{aligned}
\int_0^{1-z} \mathrm{d}x\, x\, G(0,1;x) &= \left[\frac{x^2}{2} G(0,1;x)\right]_0^{1-z} - \int_0^{1-z} \mathrm{d}x\, \frac{x^2}{2}\frac{G(1;x)}{x} \\
&= \left[\frac{x^2}{2} G(0,1;x) - \frac{x^2}{4} G(1;x)\right]_0^{1-z} + \int_0^{1-z} \mathrm{d}x\, \frac{x^2}{4(x-1)} \\
&= \left[\frac{x^2}{2} G(0,1;x) - \frac{x^2}{4} G(1;x)\right]_0^{1-z} \\
&\quad + \frac{1}{4}\int_0^{1-z} \mathrm{d}x\, \left(1 + x + \frac{1}{x-1}\right) \\
&= \left[\frac{x^2}{2} G(0,1;x) - \frac{x^2}{4} G(1;x) + \frac{x}{4} + \frac{x^2}{8} + \frac{G(1;x)}{4}\right]_0^{1-z} \\
&= \frac{(1-z)^2}{2}\left(G(0,1;1-z) - \frac{G(1;1-z)}{2} + \frac{1}{4}\right) + \frac{1-z}{4} \\
&\quad + \frac{G(1;1-z)}{4}\,,
\end{aligned} \tag{6.198}$$

where in the third step we performed a partial fractioning of the rational integrand. This procedure can be automated straightforwardly in Mathematica, since the derivative of a MPL is easy to obtain.

5. At this stage, all integrations have been performed. The result still contains MPLs where the variable z appears multiple times in the index vector. Since we know that these expressions can be written as combinations of HPLs, we can, for each power of z and each degree of transcendentality n, take the most general combination of HPLs as an ansatz,

$$\sum_{a_1\ldots a_n} C_{a_1,\ldots,a_n} \mathrm{H}(a_1,\ldots,a_n;z) + (\text{lower-weight comb.})\,, \quad \{a_i\} \in \{-1,0,1\}\,, \tag{6.199}$$

and find the coefficients by equating the symbol, or, more generally, all iterations of the coproduct [130] of the two expressions. Lower-weight combinations denote terms like

$$\pi^2 \mathrm{H}(a_1, \ldots, a_{n-2}; z) \quad \text{or} \quad \log(2)\mathrm{H}(a_1, \ldots, a_{n-1}; z)\,, \tag{6.200}$$

which have the same degree of transcendentality as a weight-n HPL. The coproduct fixes all these terms unambiguously.

6. The final numerical check on the result consists of the comparison of the original integral using the numerical integration of MATHEMATICA(with the package `HPL` [124, 125] to evaluate the HPLs numerically) and our final expression, using `Ginsh`, the interactive front end of the computer algebra system GiNaC [126], for a random value of z.

For more details on the method used to calculate the convolutions (called symbolic integration), we refer the reader to appendix D of [157].

The results we find are very lengthy, too lengthy even to be put into an appendix. We simply give one of the shortest results as an illustration,

$$\begin{aligned}
\left(P_{qg}^{(0)} \otimes \sigma_{qQ}^{(2)}\right)(x) = & \left(\left(\frac{8}{81x} - \frac{5x}{27}\right)\pi^2 + \frac{136}{27} - \frac{943}{243x} - \frac{353x}{54} + \frac{32x^2}{243}\right)\mathrm{H}_0(x) \\
& + \left(\frac{1156}{81} - \frac{1742}{243x} - \frac{586x}{81} + \frac{32x^2}{243}\right)\mathrm{H}_1(x) \\
& + \left(\left(\frac{2x}{27} - \frac{4}{27}\right)\pi^2 + \frac{34}{9} + \frac{16x^2}{27} - \frac{124}{81x} - \frac{7x}{3}\right)\mathrm{H}_{0,0}(x) \\
& + \left(\frac{52}{9} - \frac{248}{81x} - 4x + \frac{64x^2}{81}\right)\mathrm{H}_2(x) + \left(10 - \frac{124}{27x} - 6x + \frac{16x^2}{27}\right)\mathrm{H}_{1,0}(x) \\
& + \left(\frac{40}{3} - \frac{496}{81x} - 8x + \frac{64x^2}{81}\right)\mathrm{H}_{1,1}(x) + \left(-\frac{8}{9} - \frac{16}{27x} + \frac{2x}{3}\right)\mathrm{H}_{0,0,0}(x) \\
& + \left(\frac{16x}{9} - \frac{32}{27x}\right)\mathrm{H}_3(x) + \left(2x - \frac{16}{9x}\right)\mathrm{H}_{2,0}(x) + \left(\frac{8x}{3} - \frac{64}{27x}\right)\mathrm{H}_{2,1}(x) \\
& + \left(\frac{8}{9} - \frac{4x}{9}\right)\mathrm{H}_{0,0,0,0}(x) + \left(\frac{16}{9} - \frac{8x}{9}\right)\mathrm{H}_4(x) + \left(\frac{8}{3} - \frac{4x}{3}\right)\mathrm{H}_{3,0}(x) \\
& + \left(\frac{32}{9} - \frac{16x}{9}\right)\mathrm{H}_{3,1}(x) + \left(\frac{8}{135} - \frac{4x}{135}\right)\pi^4 \\
& + \left(-\frac{11}{27} + \frac{62}{243x} + \frac{x}{3} - \frac{8x^2}{81}\right)\pi^2 - \frac{4x}{9}\zeta_3 + \frac{214x^2}{729} - \frac{3203x}{972} \\
& + \frac{2711}{243} - \frac{23779}{2916x} + \mathcal{O}(\epsilon)\,,
\end{aligned} \tag{6.201}$$

where we have set $\mu_f = m_h$ and have only displayed the ϵ^0-component which contributes to the $1/\epsilon$ pole at N^{3}LO, but not the much longer ϵ-component which contributes to the finite N^{3}LO piece.

The full set of convolutions can be found in machine-readable form (both Maple and Mathematica) in the ancillary files accompanying the arXiv publication of [83].

6.2.4. Soft expansion of the convolutions

While the full N^{3}LO corrections to the gluon fusion cross section may still be out of reach for the time being, a description in the soft limit could be feasible already in the close future. This was the succession at NNLO, as well, where the expansion of the cross section up to $\mathcal{O}((1-z)^{16})$ [54, 55] was published before the full computation [56, 57]. The numerical agreement between the two computations proved to be excellent, so, anticipating the same behaviour at N^{3}LO, the soft expansion of the N^{3}LO corrections would be a very important result to obtain. The first pure N^{3}LO piece of the third order soft expansion, the soft triple-real emission contribution, has been published in [157].

In the limit $z \to 1$, the partonic cross section (and all convolutions contributing to it) can be cast in the following form (suppressing partonic indices)

$$\sigma^{(n,m)}(z) = a^{(n,m)}\delta(1-z) + \sum_{k=0}^{2n-1} b^{(n,m),k}\mathcal{D}_k(1-z) + \sum_{k=0}^{2n-1}\sum_{l=0}^{\infty} c_{kl}^{(n,m)} \log(1-z)^k \,(1-z)^l \,. \tag{6.202}$$

We thus need to expand the regular part as a polynomial in $(1-z)$, times $\log(1-z)$ terms. We proceed as follows:

1. We define $z' \equiv 1-z$. Thus, our expressions now consist of HPLs with argument $1-z'$ times powers of z'. The desired limit is $z' \to 0$.

2. We want to rewrite the HPLs with argument $1-z'$ as MPLs with argument z', which results in changing the array of indices from $\{-1, 0, 1\}$ to $\{0, 1, 2\}$, as can be easily seen by taking the integral definition eq. (6.192) for $x_1 \in \{-1, 0, 1\}$ and changing variables $t \mapsto 1-t$. The rewriting is achieved with the same techniques as in the previous section, i.e. we take the symbol of our HPLs and match it to MPLs with argument z'.

3. The expansion of any MPL in its argument is straightforward, since the connection between polylogarithms and multiple nested sums provided in section 4.1.2,

$$\mathrm{Li}_{m_1,\ldots,m_k}(x_1,\ldots,x_k) = \sum_{n_k=1}^{\infty} \frac{x_k^{n_k}}{n_k^{m_k}} \sum_{n_{k-1}=1}^{n_k-1} \cdots \sum_{n_1=1}^{n_2-1} \frac{x_1^{n_1}}{n_1^{m_1}} \tag{6.203}$$

also holds for multiple polylogarithms. The translation from MPLs to nested sums is given by

$$\begin{aligned} &G\Big(\underbrace{0,\ldots,0}_{m_k-1},1,\underbrace{0,\ldots,0}_{m_{k-1}-1},a_{k-1},\ldots,\underbrace{0,\ldots,0}_{m_1-1},a_1;x_k\Big) \\ &= (-1)^k \operatorname{Li}_{m_1,\ldots,m_k}\left(\frac{a_2}{a_1},\frac{a_3}{a_2},\ldots,\frac{a_{k-1}}{a_{k-2}},\frac{1}{a_{k-1}},x_k\right). \end{aligned} \tag{6.204}$$

The specific form of the MPL on the left-hand side of the equation above can be obtained via the scaling property, $G(x_1,\ldots,x_n;z) = G(\lambda x_1,\ldots,\lambda x_n,\lambda z)$, where $\lambda \neq 0 \neq x_n$. MPLs with a rightmost index of 0 must be rewritten using the shuffle product, e.g.

$$G(a,0;x) = G(0;x)G(a;x) - G(0,a;x) = \log(x)G(a;x) - G(0,a;x)\,, \tag{6.205}$$

until all rightmost zeroes have been turned into explicit logarithms. The remaining MPLs can then be safely translated to nested sums.

The crucial point is that the variable x_k only appears in the outermost sum in eq. (6.203), while the inner nested sums only depend on the $x_{i<k}$, which in our case are the indices $a_i \in \{0,1,2\}$. We thus easily obtain the desired expansion when we just truncate the sum over n_k in eq. (6.203) at the highest power of z' we are interested in.

4. The validity of the soft expansions of the convolutions was checked numerically for some small values of z'.

We again refer to the ancillary files accompanying the arXiv publication of [83], where all soft expansions of the convolutions up to $\mathcal{O}\left((1-z)^{12}\right)$ can be found in machine-readable form.

6.3. Numerical results

The results of the previous enable us to perform two calculations. First, we are able to predict the poles of the N^{3}LO cross section. Once the bare cross section $\hat{\sigma}_{ij}^{(3)}$ is added, all these poles should cancel at the analytical level. To test our prediction for the N^{3}LO poles, we performed a numerical check, where we obtained the mass-factorisation poles in a different way, namely by creating bare PDFs. We will describe this procedure in the next section.

The second calculation we are able to do is determining all scale-dependent pieces of the N^{3}LO gluon fusion cross section since they are all proportional to the computed convolutions. This enables us, with some reasonable assumptions about the missing finite contributions, to estimate the scale-uncertainty of the N^{3}LO hadronic gluon fusion cross section. We will present these estimates in section 6.3.2.

6.3.1. Poles of the N^{3}LO gluon fusion cross section

To test our prediction for the cubic, quadratic and single poles of the bare N^{3}LO partonic cross sections, we implemented two different numerical implementations to calculate them.

First, we took the analytic results for the convolutions from the previous section and combined them according to eqs. (6.1) and (2.63). The expressions for each pole in ϵ and each initial-state channel were translated into `C++` code and convoluted with the parton distribution functions according to eq. (2.67). Notice that in the ϵ-orders contributing to the finite N^{3}LO corrections, we encounter HPLs of weight 5. But in the pole coefficient functions, the maximal weight is 4 and thus, we were able to evaluate them using Chaplin.

The second implementation only took the bare lower-order cross sections $\hat{\sigma}_{ij}^{(n)}$ $(n \leq 2)$ as an input, without any renormalisation or mass factorisation terms. Obtaining the renormalisation terms of eq. (6.1) from this is trivial, of course, simply by multiplying with the appropriate expansion coefficient of the Beta-function. To obtain the mass factorisation terms directly from the bare cross sections, we have to invert the relation between $\hat{\sigma}$ and σ in eq. (2.67), i.e. we look for the correct kernel $\Gamma_{ij}^{-1} \equiv \Delta_{ij}$ such that

$$\sigma_{ij}(x) = \left(\Delta_{ki} \otimes \Delta_{lj} \otimes \hat{\sigma}_{kl}\right)(x)\,. \tag{6.206}$$

Equivalently, we can say that this kernel Δ_{ij} extracts the bare PDF from the renormalised one,

$$f_i^0(x) = \left(\Delta_{ij} \otimes f_j\right)(x)\,, \tag{6.207}$$

which is the inverse of eq. (2.62).

The perturbative expansion of Δ_{ij} is easy to obtain via its defining condition of being the inverse of Γ_{ij},

$$\left(\Gamma_{ik} \otimes \Delta_{kj}\right)(x) \stackrel{!}{=} \delta_{ij}\delta(1-x)\,, \tag{6.208}$$

and we find,

$$
\begin{aligned}
\Delta_{ij}(\mu,x) = & \, \delta_{ij}\delta(1-x) + a_s(\mu)\frac{P_{ij}^{(0)}(x)}{\epsilon} \\
& + a_s^2(\mu)\left\{\frac{1}{2\epsilon}P_{ij}^{(1)}(x) + \frac{1}{2\epsilon^2}\left[\left(P_{ik}^{(0)}\otimes P_{kj}^{(0)}\right)(x) - \beta_0 P_{ij}^{(0)}(x)\right]\right\} \\
& + a_s^3(\mu)\left\{\frac{1}{6\epsilon^3}\left[\left(P_{ik}^{(0)}\otimes P_{kl}^{(0)}\otimes P_{lj}^{(0)}\right)(x) - 3\beta_0\left(P_{ik}^{(0)}\otimes P_{kj}^{(0)}\right)(x)\right.\right. \\
& \left. + 2\beta_0^2 P_{ij}^{(0)}(x)\right] + \frac{1}{12\epsilon^2}\left[3\left(P_{ik}^{(0)}\otimes P_{kj}^{(1)}\right)(x) + 3\left(P_{ik}^{(1)}\otimes P_{kj}^{(0)}\right)(x)\right. \\
& \left.\left. - 4\beta_1 P_{ij}^{(0)}(x) - 4\beta_0 P_{ij}^{(1)}(x)\right] + \frac{1}{3\epsilon}P_{ij}^{(2)}(x)\right\} + \mathcal{O}(a_s^4)\,. \qquad (6.209)
\end{aligned}
$$

The hadronic cross section was then evaluated in the spirit of eq. (2.64), as a convolution of the bare PDFs and bare partonic cross section. The bare PDF was obtained numerically according to eq. (6.207), where we simply added two dimensions of integration to the Monte-Carlo integration routine,

$$
\int \mathrm{d}x_1\,\mathrm{d}z \;\mapsto\; \int \mathrm{d}x_1\,\mathrm{d}z\,\mathrm{d}y_1\,\mathrm{d}y_2\,, \qquad (6.210)
$$

where the y_i parametrise the convolutions to extract the bare PDF f_i^0 from f_i. Notice that this numerical approach to obtain the poles from mass factorisation from bare PDFs also works at the differential level. We will comment on this in the next chapter.

The two different ways of obtaining the poles of the N^{3}LO fully agreed within the error associated with the Monte-Carlo integrations. Even if the numbers themselves are meaningless, we give them here for completeness. They are multiplied with the appropriate factors of α_s, but not rescaled with the exact LO cross section,

$$
\eta_{ij}^{(3)}(\tau) \equiv \left(\frac{\sigma^{(0)}_{gg,m_t=\infty}}{\sigma^{(0)}_{gg,\mathrm{exact}}}\right)\left(f_i\otimes f_j\otimes\hat{\sigma}_{ij}^{(3)}\right)(\tau)\,, \qquad (6.211)
$$

without summation over i,j.

We find, using the MSTW08 NNLO PDF set,

$$
\begin{aligned}
\eta_{gg}^{(3)} = & \frac{0.408(4)}{\epsilon^3} + \frac{10.75(6)}{\epsilon^2} + \frac{66.0(5)}{\epsilon} + \mathcal{O}(\epsilon^0)\,, \\
\eta_{qg}^{(3)} = & -\frac{0.4695(5)}{\epsilon^3} - \frac{5.857(2)}{\epsilon^2} - \frac{25.68(2)}{\epsilon} + \mathcal{O}(\epsilon^0)\,,
\end{aligned}
$$

$$\begin{aligned}
\eta^{(3)}_{q\bar{q}} =& \frac{0.00806(5)}{\epsilon^3} + \frac{0.0649(8)}{\epsilon^2} + \frac{0.2020(2)}{\epsilon} + \mathcal{O}(\epsilon^0)\,, \\
\eta^{(3)}_{qq} =& \frac{0.01240(2)}{\epsilon^3} + \frac{0.0704(1)}{\epsilon^2} + \frac{0.2621(5)}{\epsilon} + \mathcal{O}(\epsilon^0)\,, \\
\eta^{(3)}_{qQ} =& \frac{0.04928(8)}{\epsilon^3} + \frac{0.3121(4)}{\epsilon^2} + \frac{1.146(1)}{\epsilon} + \mathcal{O}(\epsilon^0)\,.
\end{aligned} \tag{6.212}$$

Notice that this check could be performed with dummy PDFs instead of the actual parton distribution functions, since the poles of the bare cross section are no physical result anyways. The important point is find the same numbers for the two different implementations, as a check on the analytic prediction for the poles. We still opted to use real PDF sets, since the computer code for these had already been at hand. Also, the order of magnitude of the poles we found was compared to the established lower orders, and the pattern was found to be similar, providing another loose check on the results.

6.3.2. Scale dependence of the N^{3}LO gluon fusion cross section

To understand that all scale-dependent pieces of the N^{3}LO cross section are proportional to convolutions of splitting kernels and lower-order cross sections, we again consider eq. (6.1). The bare cross sections $\hat{\sigma}^{(n)}_{ij}$ all come with a factor of $\mu^{2n\epsilon}/s^{n\epsilon}$, where the $\mu^{2\epsilon}$-powers stem from the renormalisation replacement eq. (2.44) and the s^{ϵ}-powers can be factorised from the cross section, and essentially originate in the phase-spaces and loop integrations carried out[1]. Now, when we expand these terms in ϵ,

$$\left(\frac{\mu^2}{s}\right)^n = 1 + n\epsilon \log\left(\frac{\mu^2}{s}\right) + \frac{n\epsilon^2}{2}\log^2\left(\frac{\mu^2}{s}\right) + \mathcal{O}(\epsilon^3)\,, \tag{6.213}$$

we see that the poles of the bare cross section are multiplied with powers of the logarithm $\log(\mu^2/s)$, which generates contributions to the finite $\mathcal{O}(\epsilon^0)$ part. But since these poles are required to cancel exactly against the poles of the collinear counterterms which are proportional to our convolutions, we find that indeed, all scale-dependent parts of the cross section can be obtained from lower-order information.

Usually, the scale at which eq. (6.1) is put together and the poles are cancelled is chosen to be μ_f. To set the scale at which a_s is evaluated different from μ_f, we can introduce the second scale μ_r and separate the two scales using the scale translation formula for the strong coupling constant which we derive from the RGE for α_s in appendix C. The

[1]For example, one can see that the phase-space measures given in appendix A scale like $\Phi_n \propto s^{(n-1)\epsilon}$, and the 1-loop integrals in section 6.1.7 all are proportional to some mass scale to the power of 2ϵ.

scale translation formula relates the coupling at μ_f to the coupling at μ_r and reads, to third order,

$$\begin{aligned} a_s(\mu_f) =& a_s(\mu_r) + a_s^2(\mu_r)\beta_0 L + a_s^3(\mu_r)\left[\beta_1 L + \beta_0^2 L^2\right] + \\ &+ a_s^4(\mu_r)\left[\beta_2 L + \frac{5}{2}\beta_1\beta_0 L^2 + \beta_0^3 L^3\right] + \mathcal{O}(a_s^5)\,, \end{aligned} \tag{6.214}$$

with $L \equiv \log(\mu_r^2/\mu_f^2)$.

The explicit logarithm L essentially counters the running of the coupling constant up to the order considered, such that the effect of varying the unphysical scale is weakened for higher orders in perturbation theory, i.e. the perturbative series is converging to its all-order value, as can be seen by taking the total derivative of the partonic cross section w.r.t μ_r,

$$\frac{\mathrm{d}\sigma_{ij}}{\mathrm{d}\log(\mu_r^2)} = \frac{\partial\sigma_{ij}}{\partial\log(\mu_r^2)} + \frac{\partial\sigma_{ij}}{\partial a(\mu_r)}\underbrace{\frac{\partial a(\mu_r)}{\partial\log(\mu_r^2)}}_{\beta(\mu_r)} = \mathcal{O}(a^5)\,, \tag{6.215}$$

and the same holds true for the $\log(\mu_f^2/s)$ terms, which counter the DGLAP evolution of the PDFs.

We have therefore extended our numerical code `iHixs` to N^{3}LO order in HQET, implementing all the known contributions up to now. Besides the $\log(\mu_f^2/m_H^2)$- and $\log(\mu_r^2/\mu_f^2)$-terms, this also includes the pure N^{3}LO 'plus'-terms which were determined in [191] using mass factorisation arguments[2]. The Wilson coefficient C_1 is implemented to four-loop order according to eq. (3.49), and a_s is run using three-loop running (i.e. including β_3) although the numerical difference w.r.t 2-loop running is negligible. In principle N^{3}LO parton distribution functions should be used, but there are no such fits available. The numerical difference to NNLO PDFs is expected to be small, though.

Simply adding all scale-dependent parts but nothing else does not result in a reasonable estimate of the N^{3}LO cross section and its overall scale-dependence, though. As we mentioned above, the explicit logarithms $\log(\mu_f^2/m_H^2)$ and $\log(\mu_r^2/\mu_f^2)$ are meant to cancel against the same logarithms absorbed into the running PDF and coupling constant, respectively. With the pure N^{3}LO pieces multiplying these implicit logarithms missing, terms like

$$\sigma_{gg}^{(3)}(\mu) \quad \ni \quad 4\beta_0 \log\left(\frac{\mu^2}{m_H^2}\right)\sigma_{gg}^{(2)}(m_H)\,, \tag{6.216}$$

[2]Basically, the authors used the knowledge of all poles from purely virtual contributions to infer the poles from real-radiation diagrams by demanding pole cancellation. This fixes the coefficients of all plus-distributions unambiguously.

which becomes large and negative for $\mu \ll m_H$ "overcompensate" and produce an unnaturally strong scale-dependence. For this reason, we chose to introduce artificial pure N^{3}LO contributions, by simply multiplying the corresponding NNLO contributions with a "scaling factor" K,

$$a_{ij}^{(3,0)} = K\, a_{ij}^{(2,0)}\,, \qquad f_i \otimes f_j \otimes c_{ij}^{(3,0)} = K\left(f_i \otimes f_j \otimes c_{ij}^{(2,0)}\right)\,. \tag{6.217}$$

There is no *a priori* reason why the scaling factor for the delta and the regular terms should be the same. However, it turns out that the numerical impact of the delta coefficient $a_{ij}^{(3,0)}$ is negligible (for scaling coefficients that do not break the pattern observed from lower orders by orders of magnitudes), in contrast with the coefficient of the regular part, so we adopt here a common scaling factor to keep the parametrisation simple. For the same reason we use the same K scaling coefficient for all initial state channels.

A loose argument about the size of K can be derived if one assumes a good perturbative behaviour at $\mu_r = \mu_f = m_H$ where all other terms of order a_s^5 vanish. Since $a_s(m_H) \sim 1/30$ one expects K not to be much larger than 30. For comparison, the corresponding rescaling factors between NNLO and NLO are

$$\frac{f_g \otimes f_g \otimes c_{gg}^{(2,0)}}{f_g \otimes f_g \otimes c_{gg}^{(1,0)}} \sim 30\,, \quad \frac{a_{gg}^{(2,0)}}{a_{gg}^{(1,0)}} \sim 1.5\,, \tag{6.218}$$

for $m_H = 125$ GeV and $\mu_f = \mu_r = m_H$.

In what follows we study the inclusive cross section as a function of the scales, in the HQET approach rescaled with the exact leading order cross section. For the parton distributions, the MSTW08 NNLO set was used with its associated value for $\alpha_s(m_Z)$. Furthermore, to cross-check our results, a second implementation was programmed in `C++`, where the convolutions of splitting kernels and partonic cross sections were performed numerically, analogously to the extraction of the bare PDFs described in the previous section. For both codes, the numerical evaluation of HPLs was performed using the library Chaplin [135]. The results from the two implementations fully agreed.

In figure 6.1, the different orders of the hadronic gluon fusion cross section for the 8 TeV LHC and a Higgs mass of 125 GeV, along with several N^{3}LO approximants for various numerical values of K are plotted as a function of the renormalisation scale μ_r, while the factorisation scale is fixed to $\mu_f = m_H$. Note that the convolutions of splitting kernels and partonic cross sections do not enter in this plot, since they are proportional to $\log(\mu_f^2/m_h^2)$. The μ_r scale variation for LHC with 14 TeV centre-of-mass energy is shown in fig. 6.3. The μ_f scale dependence, shown in figure 6.5 for 8 TeV centre-of-mass

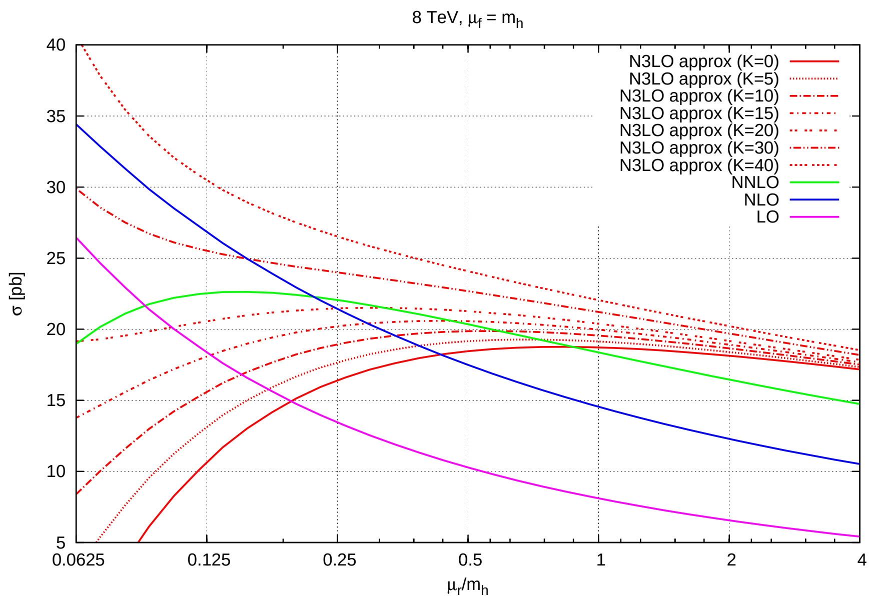

Figure 6.1.: Scale variation of the different orders of the gluon fusion cross section at 8 TeV. μ_f is fixed to m_H and only μ_r is varied. The scaling coefficient K is varied from 0 to 40 to estimate the impact of the unknown N^{3}LO contributions.

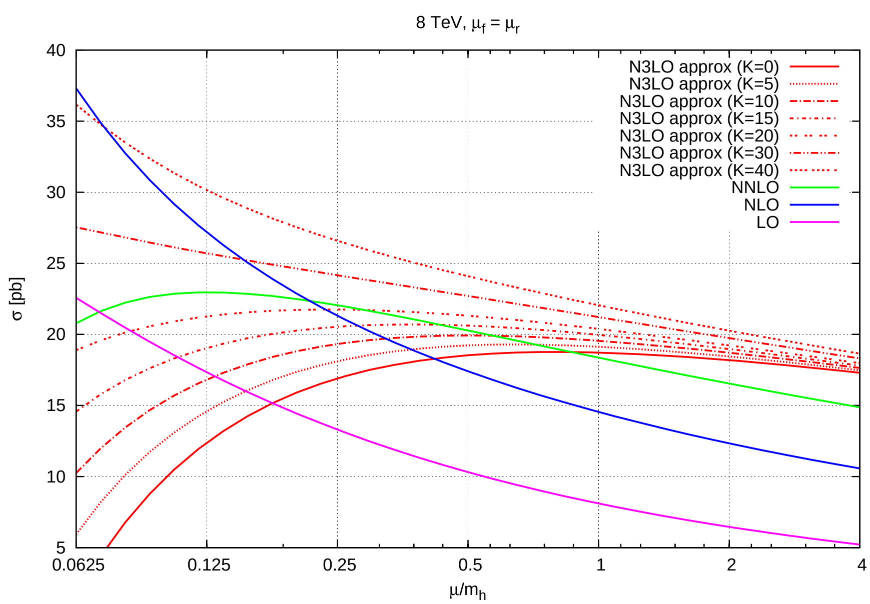

Figure 6.2.: Scale variation of the different orders of the gluon fusion cross section at 8 TeV. μ_f and μ_r are varied simultaneously. The scaling coefficient K is varied from 0 to 40.

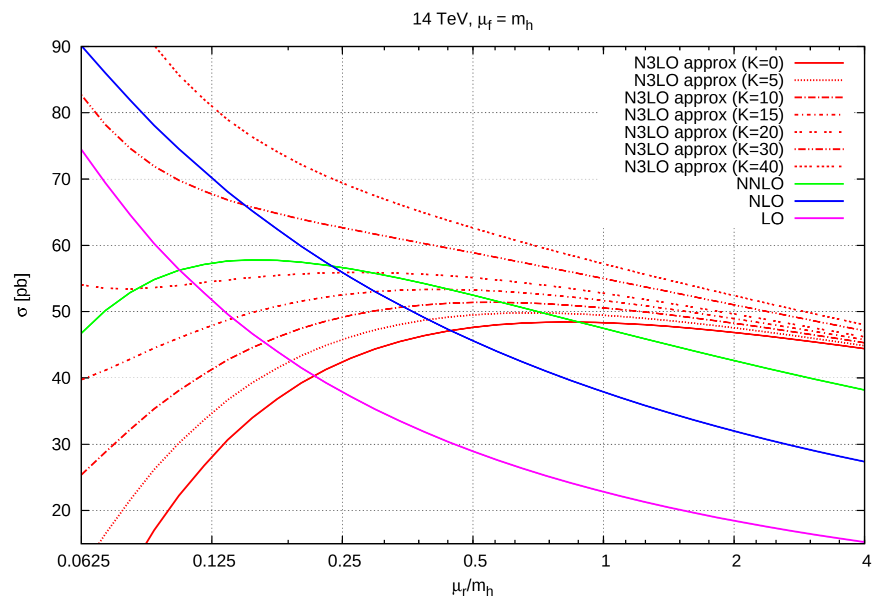

Figure 6.3.: Scale variation of the different orders of the gluon fusion cross section at 14 TeV. μ_f is fixed to m_H and only μ_r is varied. The scaling coefficient K is varied from 0 to 40.

energy, is, as expected, extremely mild, in accordance with what is observed at NNLO.

Figures 6.2 and 6.4 display the overall scale dependence with both scales set to be equal and varied simultaneously, as is practice when estimating the theoretical uncertainty. We note that the curves for the approximate N^{3}LO cross section with various Ks spread widely in the low scale region, i.e. for $\mu < 30$ GeV. This is not unreasonable, though, as in this regime, the unknown N^{3}LO contributions that are neglected become much more important due to the running of α_s. Indeed, at the lowest renormalisation scale considered, $\mu = m_H/16 \approx 7$ GeV, the coupling becomes as big as $\alpha_s \approx 0.2$, i.e. we are barely in the perturbative regime.

It can hardly be overemphasised that the above prescription does not represent a proper calculation of the N^{3}LO matrix elements, but just a way of parametrising their unknown numerical importance. Once the height of the N^{3}LO curve at $(\mu_r, \mu_f) = (1,1)$ is set, the shape of the full curve only depends on lower order cross sections (which we know exactly), the running of a_s and the parton distribution functions, respectively.

The unknown, numerically important coefficient functions $c_{gg}^{(3,0)}(z)$ contain logarithmic contributions that are singular at threshold, $\log(1-z)$, contributions that are regular and contributions that are singular at the opposite, high energy limit $\log(z)$. The leading and

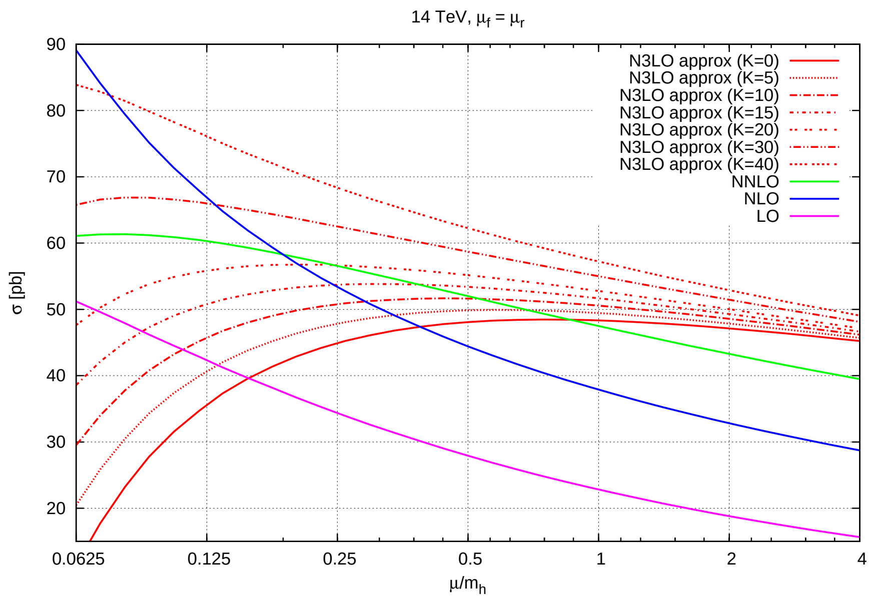

Figure 6.4.: Scale variation of the different orders of the gluon fusion cross section at 14 TeV. μ_f and μ_r are varied simultaneously. The scaling coefficient K is varied from 0 to 40.

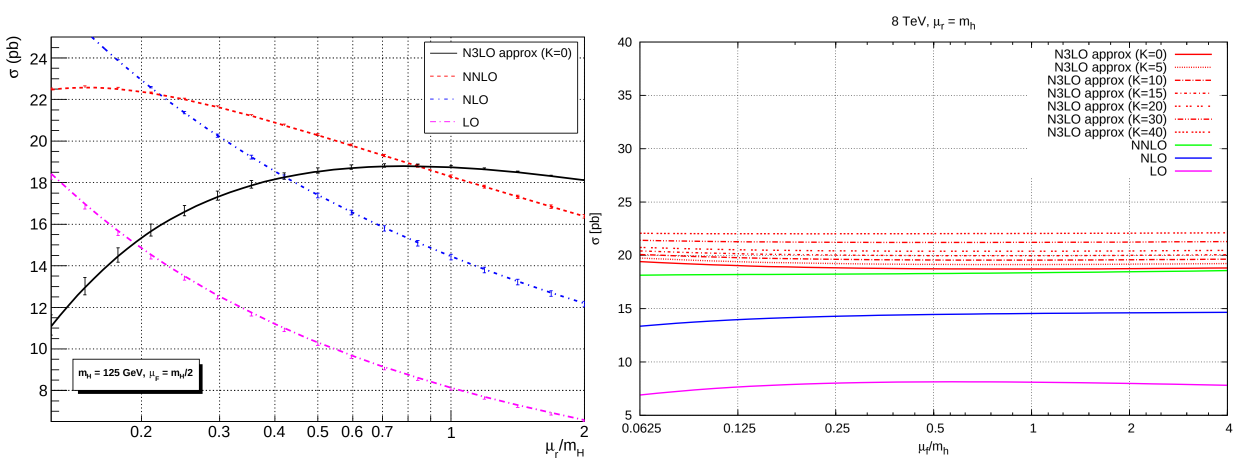

(a)

(b)

Figure 6.5.: Scale variation of the different orders of the gluon fusion cross section at 8 TeV. In (a) μ_r is varied along the x-axis, while the bars represent variation of μ_f around the central value $m_H/2$. In (b) μ_r is fixed to m_H and only μ_f is varied. The scaling coefficient K is varied from 0 to 40.

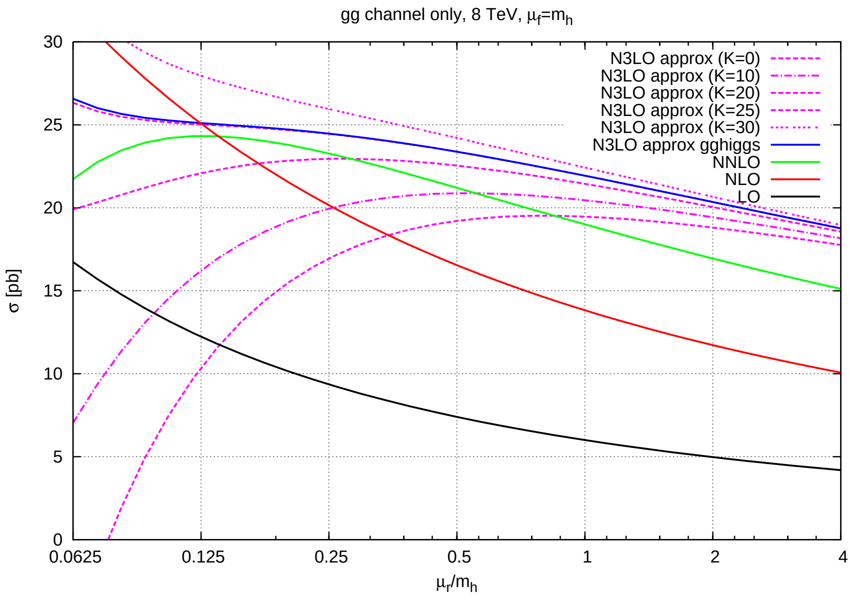

Figure 6.6.: Scale variation of the different orders of the gluon fusion cross section at 8 TeV. μ_f is fixed to m_H and only μ_r is varied. K is varied from 0 to 30. Only the gg channel is plotted, and compared to the results obtained with the program **gghiggs** [192].

several, but not all, subleading threshold contributions are associated with multiple soft emissions and can be recovered by resummation techniques. The authors of [191] have used the expressions for $b_{ij}^{(3,0),k}$ that they have derived to perform a soft approximation in Mellin space, resulting in a N^{3}LO approximant with a scale uncertainty of $\approx$ 4%. Recently, the authors of [192] estimate $c_{gg}^{(3,0)}(z)$ by interpolating in Mellin space, between the soft approximation (that captures threshold logarithms) and the BFKL limit (that captures high energy $\log(z)$ terms). This approach matches the NNLO cross section neatly, and results in an approximant for the N^{3}LO with a scale uncertainty of 7% if the scale is varied in the interval $[m_H/2, 2m_H]$ (or smaller, if the interval chosen is $[m_H/4, m_H]$).

When comparing our results for the μ_r-dependence of the N^{3}LO cross section for the gluon-gluon initial state with the numbers obtained with the numerical program **gghiggs** [192], we find agreement between the two curves when setting K to 25, as is displayed in figure 6.6.

While it is plausible that the leading logarithmic contributions, being threshold enhanced, capture the bulk of the cross section, it is unclear whether the unknown subleading contributions, as well as the non-logarithmic terms, are really negligible. Their

Order	Cross section [pb]	$\sigma/\sigma_{\text{NNLO}}$	$\sigma/\sigma_{\text{LO}}$
LO	$10.31\,^{+29.1\%}_{-21.3\%}$	0.51	1.00
NLO	$17.41\,^{+22.6\%}_{-16.4\%}$	0.86	1.69
NNLO	$20.27\,^{+8.8\%}_{-9.4\%}$	1.00	1.97
N^{3}LO (K=0)	$18.53\,^{+1.2\%}_{-8.9\%}$	0.91	1.80
N^{3}LO (K=5)	$19.23\,^{+0.3\%}_{-5.9\%}$	0.95	1.87
N^{3}LO (K=10)	$19.92\,^{+0.0\%}_{-3.1\%}$	0.98	1.93
N^{3}LO (K=15)	$20.62\,^{+0.4\%}_{-3.1\%}$	1.02	2.00
N^{3}LO (K=20)	$21.31\,^{+2.0\%}_{-4.3\%}$	1.05	2.07
N^{3}LO (K=30)	$22.70\,^{+6.5\%}_{-6.5\%}$	1.12	2.20
N^{3}LO (K=40)	$24.09\,^{+10.4\%}_{-8.4\%}$	1.19	2.34

Table 6.1.: Cross sections and scale uncertainties for the 8 TeV LHC. The central scale choice is $\mu_r = \mu_f = m_H/2$, and uncertainties are found by varying the two scales simultaneously by a factor of two.

importance certainly rises for the LHC at 14 TeV, as the luminosity function suppresses the region away from threshold less, resulting in more phase space for real-radiation. One might, therefore, want to be conservative about their magnitude, and hence on the size of the scale uncertainty to be anticipated before the full N^{3}LO result is available. Table 6.1 shows the estimates for various values of the rescaling factor K, covering the range from relatively mild to extremely strong N^{3}LO corrections, resulting in scale uncertainties varying from 2% to as large as 8% or more. The scale uncertainties cited here are evaluated by varying the scales in the interval $[m_H/4, m_H]$.

As previously mentioned in section 5.1, the choice of the central scale around which the variation is performed has been an issue of debate, since the two most common choices $\mu = m_H$ and $\mu = m_H/2$ result in slightly different scale uncertainty estimates but also in different central values for the cross section. As we have mentioned, improved perturbative convergence and differential information such as as the average transverse momentum of the Higgs boson led us to choose $\mu = m_H/2$ as a central scale. An alternative indication comes from the considerations of [193], where it is argued, looking at examples from jet physics, that a reasonable indication would be the position of the saddle point in a contour plot of the cross section as a function of μ_r and μ_f. In figs. 6.7 and 6.8 we show such contour plots for Higgs production at LO, NLO, NNLO and N^{3}LO

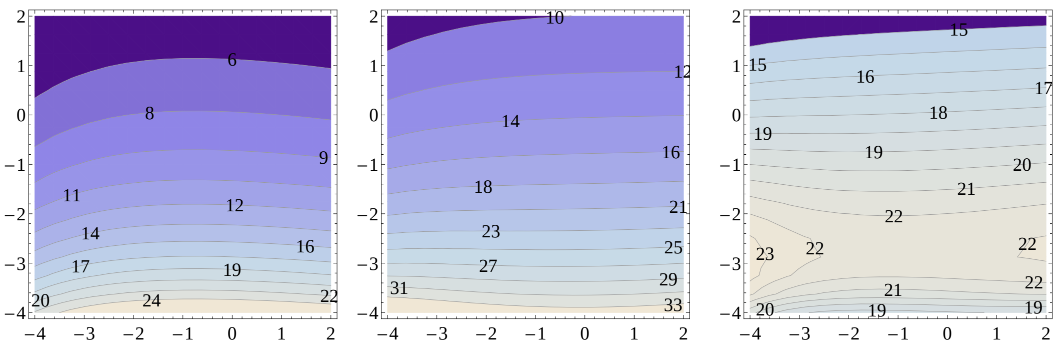

(a) LO (b) NLO (c) NNLO

Figure 6.7.: 2-D contour plots of the LO, NLO and NNLO cross section at the 8 TeV LHC. The value on the contours is the cross section in picobarns. The x-axis is $\log_2(\mu_f)$, the y-axis $\log_2(\mu_r)$. Our preferred central scale choice is located at (-1,-1).

(for three values of the parameter K). In the cases where a saddle point exists, its position points indeed to lower scale choices, and in the cases without a saddle point the plateau region is also located in lower scales. Given the extremely mild factorisation scale dependence, the saddle point or plateau region is largely determined by the μ_r plateau in all previous figures.

6.4. Conclusions

The motivation to calculate the N^{3}LO QCD corrections to the gluon fusion cross section in heavy quark effective theory comes from the fact that the scale uncertainty of the NNLO cross section is still fairly large. Since the full N^{3}LO calculation is a huge task, we focused all parts which can be obtained from lower-order cross sections.

This first required the calculation of the LO, NLO and NNLO partonic cross sections to one order higher in the dimensional regulator ϵ, which is only non-trivial in the NNLO case, where 29 master integrals have to be computed to the next order in ϵ. The notion of master integrals to treat all types of NNLO corrections (double virtual, real-virtual and double-real) relies on the techniques of IBP identities and reverse unitarity which are presented in sections 6.1.2 and 6.1.3, respectively.

In the actual computation of the master integrals we use the method of differential equations from section 6.1.4 which can be implemented straightforwardly to solve for the master integrals algorithmically. The main difficulty was the computation of the soft limit as a boundary condition for every master integral, for which we give some

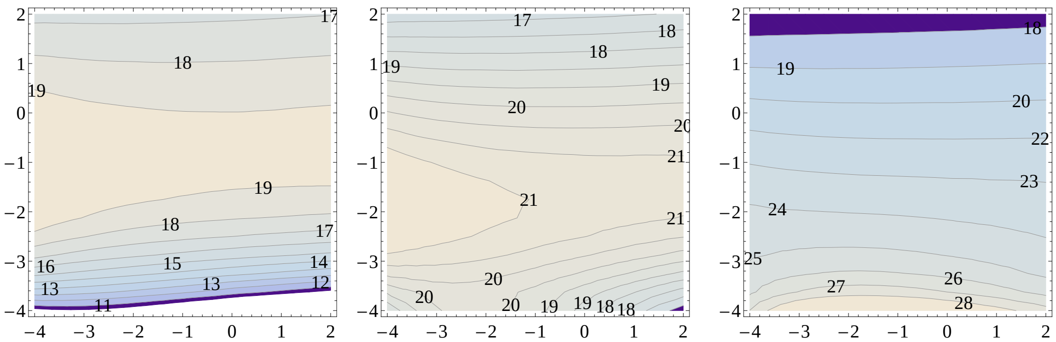

(a) N^{3}LO ($K = 10$) (b) N^{3}LO ($K = 20$) (c) N^{3}LO ($K = 30$)

Figure 6.8.: 2-D contour plots of the approximated N^{3}LO cross section at the 8 TeV LHC. The value on the contours is the cross section in picobarns. The x-axis is $\log_2(\mu_f)$, the y-axis $\log_2(\mu_r)$. Our preferred central scale choice is located at (-1,-1).

calculatory details. The soft limits for all master integrals are found to all orders in ϵ, while the full results are expanded up to the required order and in general consist of harmonic polylogarithms of up to weight four.

In section 6.2 we perform the convolutions of splitting kernels and partonic cross sections which appear in the collinear subtraction terms at N^{3}LO, of which there are 80 different ones. Both functions taking part in the convolution in general consist of delta-, plus- and regular terms. While plus-plus convolutions and any convolution involving a delta-function are straightforward, the remaining regular convolution need actual integrations to be performed. These integrals are again solved algorithmically, employing properties of HPLs and Symbol calculus. The results for the convolutions agree with previously published results obtained with a different method.

We also compute the convolutions as expansions around the threshold limit $z = 1$, anticipating the completion of the full N^{3}LO cross section in this limit first.

Finally in section 6.3, we use the results of the previous sections to numerically predict the poles of the N^{3}LO cross section remaining after renormalisation and mass-factorisation and to estimate the scale uncertainty of the N^{3}LO result.

While we are able to fully determine all explicitly scale-dependent terms of the N^{3}LO partonic cross section, determining the final scale uncertainty of the N^{3}LO gluon fusion is not possible because of the implicit scale-dependence hidden in the running of the strong coupling $\alpha_s(\mu)$. To find some numerical estimates, we approximate the missing pure N^{3}LO corrections with a scaling factor K times the NNLO corrections, which at the inclusive level is an entirely legitimate thing to do. The range of scaling factors considered is chosen very broad, yet for all values, the resulting scale uncertainty is found to be smaller than 8% for the prescription we use.

Comparing our results with other approximations for the N^3LO corrections which are based on expansions of threshold-resummed cross sections, we find agreement for values of K in the range of 20 to 25. We still choose to remain agnostic about the size of the N^3LO corrections until the proper fixed-order computation is available. Our estimates suggest that this venture will be worth the effort.

7. Differential Higgs production in bottom quark fusion

In section 6.3.1 we introduced a way retrieving the bare parton distribution functions from the renormalised PDFs that various collaborations provide. While for that particular case, it only served as a numerical check on the analytic result, we employed the very same technique in an actual physical application, namely in the development of a computer code for Higgs production in bottom quark fusion at the fully differential level, the result of which were published in [138].

As we have already discussed in chapter 5, the inclusive rate of Higgs boson production through the bottom quark fusion process in the SM is more or less negligible, amounting to about 5% of the inclusive rate of the gluon fusion process. Furthermore, compared to other subleading production channels like associated production or vector boson fusion, bottom fusion exhibits the exact same final state as gluon fusion, a Higgs and nothing else[1], so it is not distinguishable from the latter by demanding the presence of certain additional final-state particles.

However, the importance of the bottom fusion process may be enhanced in the presence of final-state cuts, or in distinct regions of a distribution of kinematic observables. These hypotheses can only be tested when the fully differential cross section is computed, i.e. the production cross section of a Higgs boson (and potential additional radiation) with full knowledge of the final-state momenta. Precise knowledge of where (i.e. in which differential distribution) to look for a $b\bar{b} \to H$ signal would then also allow to constrain the H-b-b Yukawa coupling, which in turn may constrain BSM models where an enhancement of this coupling is a common feature.

Further motivation to perform the differential bottom fusion computation came from a more technical point of view. Since the LO process is very simple due to its tree-level and $2 \to 1$ nature, it is a nice "laboratory" for new techniques in NNLO calculations. The publication [138] was the first hadronic production process where the technique of non-linear mappings [183, 194] to deal with overlapping singularities in double-real-

[1]This is not true if we treat bottom fusion in the four-flavour scheme as we have discussed in section 3.6. But then the total cross section is again smaller.

radiation corrections was applied, after a first successful application in the related decay process $H \to b\bar{b}$ [136].

7.1. Differential Calculations

Since, up to this point, all observables we dealt with in this thesis were inclusive cross sections, we give a brief introduction into differential calculations, pointing out the differences and challenges compared to the inclusive case.

Differential computations by definition retain full knowledge of all four-momenta of the final-state particles, as opposed to inclusive calculations where these momenta are integrated over. Fully differential partonic cross sections are therefore functions of all phase-space variables, i.e. in the case of NNLO corrections to a $2 \to 1$ process which contains up to three final-state particles, the differential cross section is a function of the four variables $x_i\,,\ i \in \{1,2,3,4\}$ on top of the variable z as defined e.g. in the parametrisation of eq. (A.7).

One of the main merits of differential calculations is the possibility to arrive at theoretical predictions for cross sections in the presence of final-state phase-space cuts, like those used in experimental analyses. The second advantage over the inclusive cross section is the possibility to define a wealth of different observables by marginalising over a certain set of variables while remaining differential in the others. This allows one to characterise the process in much more detail, and possibly find an optimal observable in which signal and background behave differently.

One may ask why we even bother to calculate inclusive cross sections, since experiments by construction always feature selection cuts because the detectors can never hermetically cover the collision points which results in angular cuts, and the detectors have sensitivity thresholds in e.g. the calorimeters which corresponds to a cut on the energy of final-state particles). But inclusive calculations are in general easier to perform at higher orders in perturbation theory. Thus, an approximation to a differential cross section at a higher order is usually obtained by taking the highest known differential result rescaled with the inclusive K-factor. This practice is widely used in experimental searches, but of course relies on the assumption that the shapes of differential distributions do not change strongly from one order to the other in perturbation theory.

The dependence on arbitrary phase-space constraints (cuts) can be contained in the so-called jet function, or measurement function, $\mathcal{J}(\{p\}_f)$, where $\{p\}_f$ denotes the set of final-state momenta in the laboratory frame. Using this notion, we can cast the fully differential partonic cross section schematically as

$$\sigma_{ij}[\mathcal{J}] = \sum_f \int \mathrm{d}\Phi_f \, \sigma_{ij\to f}\left(\{p\}_f\right) \, \mathcal{J}\left(\{p\}_f\right) \, , \tag{7.1}$$

where the sum is over all final states f.

The role of the jet function $\mathcal{J}$ is two-fold. On the one hand, it applies arbitrary final-state phase-space cuts while ensuring infrared safety. This means it is basically a combination of Heaviside theta-functions, i.e. it is either equal to 0 or 1, depending on whether the set $\{p\}_f$ passes the selection cuts. The infrared safety property demands that the jet function does not separate IR-divergent contributions which are supposed to cancel each other by letting only parts of them pass. In other words, the jet function has to be 1 in all soft and collinear regions of the final-state phase-space.

The second task of the jet function is keeping track of the bin-integrated cross section for any given differential observable (with or without applying phase-space cuts). This is achieved at the level of Monte-Carlo integration by passing to $\mathcal{J}$ not only the set of final-state momenta but also the weight of the given event. The jet function thus represents the observable under consideration.

The effect of the presence of the jet function on the partonic cross section (7.1) is profound: it no longer depends on just the single variable $z = m_H^2/\hat{s}$, but rather on all phase-space variables of the final state. Whereas in the inclusive case, we were able to fully integrate out all variables that parametrise the final-state phase-space into some Beta- or hypergeometric functions, all the integrations over phase-space variables have to be performed numerically in the differential case, because the jet function cuts out some regions of phase-space.

Actually, since the $2 \to 1$ phase-space is just proportional to $\delta(1-z)$, the statements above do not apply to bottom quark fusion with LO kinematics, as there is no difference between the inclusive and differential cross section at this level. Starting from the real corrections at NLO, where the $2 \to 2$ phase-space depends on the additional variable y (see eq. (A.5)), and especially in the double-real corrections where the $2 \to 3$ phase-space depends on four additional variables (eq. (A.7)), the differential partonic cross section depends on multiple variables, though.

There exist several approaches on how to perform differential NLO and NNLO computations, which we will not give a comprehensive review about. Roughly, one can divide the approaches into two families. The first family regulates divergences by subtracting a counterterm which mimics the behaviour of the full amplitude in a singular limit from the real emission contributions. The same subtraction term integrated over the additional parton is added to the virtual piece, where it cancels ϵ-poles analytically. Examples of this approach are the Catani-Seymour dipole subtraction [195] which is the most popular choice for NLO computations, or the Antenna-subtraction method [196] for NNLO computations, which has only recently been completed for applications to hadron collider processes. Notice that it took a long time to adapt this approach to NNLO calculations, due to the manifold ways particles can become soft and collinear to one another, and the problem of overlapping divergences.

The second family regulates singularities in real emission contributions by choosing an appropriate phase-space parametrisation which factorises the singular variable, say x, from the rest of the respective term in the amplitude and extracting the singularity using the plus-expansion

$$x^{-1+n\epsilon} = \frac{\delta(x)}{n\epsilon} + \sum_{k=0}^{\infty} \frac{(n\epsilon)^k}{k!} \mathcal{D}_k(x)\,. \tag{7.2}$$

Again, this technique is rather straightforward to apply at NLO, where the factorisation of singular variables is easily achieved. At NNLO, where singularity structure are much more involved due to the wealth of phase-space variables, one has to resort to techniques like sector decomposition [197], where the phase-space integral containing an overlapping singularity is split into two separate integrals with factorised singularities, or the younger technique of non-linear mappings [194] which manages to factorise singular variables with, as the name suggests, non-linear mappings of the integration variables[2]. It is the latter approach which was used in the present case of bottom quark fusion at NNLO QCD.

The plus-distributions generated by the expansion (7.2) also act on the jet-function, or rather on the variable x the jet-function depends on (through the parametrisation of the final-state momenta). The real emission contributions thus contain terms that, schematically, look like

$$\frac{1}{\epsilon}\sigma\left[\mathcal{J}\right]\Big|_{x=0} + \sum_{k=0}^{\infty} \frac{(n\epsilon)^k}{k!} \int_0^1 \mathrm{d}x\, \frac{\log^k(x)}{x} \left[\sigma\left[\mathcal{J}\right] - \sigma\left[\mathcal{J}\right]\Big|_{x=0}\right]. \tag{7.3}$$

The cancellation of poles is performed numerically in this approach. For each order in ϵ, one has to bin the contributions in the distribution of interest, and find that all distributions for the poles in ϵ vanish when real and virtual contributions are added together. When the pole-cancellation for a given observable has been observed once, the computation of the poles can be omitted thereafter.

[2] Although some divisions of integrals like in sector decomposition still have to be carried out to deal with line singularities.

Care has to be taken in the choice of the bin-size for the observable under consideration. The first and the second term in the square bracket in eq. (7.3) are evaluated at different x-values, and thus different kinematics. They may thus be put in different bins of a differential distribution, which is perfectly reasonable. But when the bin-size is taken to be too small, large contributions that arise from approaching the divergence at $x = 0$ and are inclusively regulated by the vanishing term in the square bracket are still put in different bins, destabilising the numerical integration. When the bin-size is chosen appropriately, the numerical regularisation using (in general nested) plus-prescriptions is very well-behaved. One just has to make sure that quantities which are supposed to cancel actually do end up in the same bin of the differential distribution one is considering, following the slogan "Thou shalt not separate what the plus has joined".

When we consider the hadronic cross section in differential computations, it is not desirable anymore to analytically carry out the convolutions of collinear splitting kernels and bare cross sections like we did in section 6.2. While it would technically still be possible to perform the convolution over z while keeping all other final-state integration variables resolved, this would create integrands of unevaluable size and complexity, since the variable z is hidden in every Lorentz-invariant s_{ij}.

The logical way out is to evaluate the differential hadronic cross section in the spirit of eq. (2.64), i.e. integrating the product of bare PDFs and bare cross section instead of their mass-factorised counterparts,

$$\sigma\left[\mathcal{J}\right] = \int_0^1 dx_1 dx_2\, \theta(x_1 x_2 - \tau) f_i^0(x_1) f_j^0(x_2)\, \hat{\sigma}_{ij}[\mathcal{J}]\,. \tag{7.4}$$

7.1.1. Bare parton distribution functions

We thus have to obtain the bare PDF, i.e. the parton distribution function with uncancelled soft and collinear divergences which manifest themselves as poles in ϵ. The extraction of the bare PDFs from the finite ones the PDF collaborations provide us with was performed according to eq. (6.207), which we repeat for convenience,

$$f_i^0(x) = \left(\Delta_{ij} \otimes f_j\right)(x)\,, \tag{7.5}$$

where Δ_{ij} is given in eq. (6.209). It consists of Altarelli-Parisi splitting kernels, or more generally of products thereof, and has explicit poles in ϵ. The bare PDF f^0 is therefore given by an expansion both in a_s and in ϵ. As we have seen before, the splitting kernels generally consist of delta-, plus- and regular parts, which means that the convolution

(7.5) has the general form

$$(f \otimes \Delta)(x) = \int_x^1 \frac{\mathrm{d}y}{y} f\left(\frac{x}{y}\right) \left\{ a\delta(1-x) + \sum_n b_n \mathcal{D}_n + C(x) \right\}. \tag{7.6}$$

with

$$\left(\mathcal{D}_m \otimes f\right)(x) = \frac{\log(1-x)^{m+1}}{m+1} f(x) + \int_x^1 \mathrm{d}y\, \log(1-y)^m \frac{\frac{1}{y} f\left(\frac{x}{y}\right) - f(x)}{1-y}. \tag{7.7}$$

As the finite PDF f_i is a purely numerical function, the integrals above have to be carried out numerically, too. In the case of the poles of the N^{3}LO gluon fusion cross section in section 6.3.1, we simply added two more dimensions to the Monte-Carlo integration of the inclusive cross section.

For the differential bottom fusion calculation, we were more reluctant to add more dimensions to the integration routine, since it is already of rather high dimensionality due to the full resolution of the final-state momenta. Instead, we opted for the option of pre-computing the integral (7.6) for 3000 fixed values of x and storing the values in a grid. During the actual Monte-Carlo run, no convolution integral has to be calculated anymore, just a quadratic interpolation using the closest stored points to give a value for the bare PDF at the requested x-value. The precision of this interpolation procedure is well (at least two orders of magnitude) below the usual Monte-Carlo error associated with differential observables.

While there are differences among gluons and the different quark flavours, all parton distribution functions share the feature that they slope sharply downward as a function of x, i.e. their value at small x is far larger than the one for x close to 1, as can be seen in figure 7.1.

For this reason, we parametrise both the distribution of the interpolation grid and the integration variable y in eq. (7.6) quadratically,

$$y = x + (1-x)z^2\,, \tag{7.8}$$

with z uniformly distributed in $(0,1)$. Thus, the steeply sloping small-x region is covered by more points than the flatter $x \sim 1$ region.

Since we are dealing with a one-dimensional integral consisting of well-behaved functions, we find that the easiest option to carry out the integral (7.6) for each of the 3000 x-grid points is a simple deterministic algorithm which is significantly faster than a Monte-Carlo algorithm. We use the trapezoidal rule after dividing the unit interval

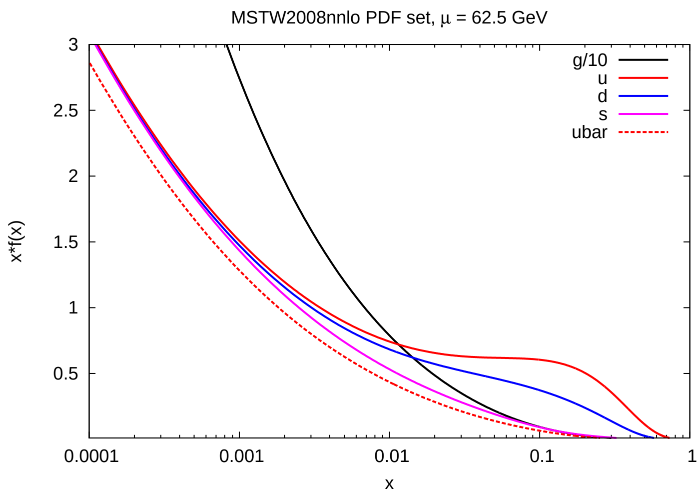

Figure 7.1.: Parton distributions for some selected partons, evaluated at a scale typical for the processes described in this thesis.

containing z into about 50’000 equispaced intervals.

In the most complicated case needed for NNLO bottom fusion, the $\mathcal{O}(a_s^2/\epsilon)$-piece of the bare (anti)bottom PDF, the pre-computation of the x-grid takes about 90 seconds. $\mathcal{O}(a_s/\epsilon)$-grids take about 10 seconds to finish.

Having obtained the bare PDF order by order in the dimensional regulator ϵ, we can substitute them directly into eq. (7.4). The singularities appearing as poles in the ϵ-expansion, cancel the initial state collinear singularities of the partonic cross section. This cancellation can be observed bin by bin in e.g. the rapidity distribution of the Higgs boson, or any other differential observable. One can achieve this cancellation in each initial state channel separately, at the cost of separating the convolution integrals depending on the initial state parton in the convolution, i.e. by not performing the implicit j-summation in eq. (7.5).

7.2. Results

When adding all perturbative corrections and integrating the resulting (renormalised but not mass factorised) cross section over the bare PDFs, we indeed find cancellation of poles in every differential distribution we considered, well within the Monte-Carlo precision. Notice that while at NLO, the only distribution where pole-cancellation is spread across all bins is the Higgs rapidity, this is no longer true in the NNLO case, where the cancellation between real-virtual and double-real takes place at arbitrary kinematics

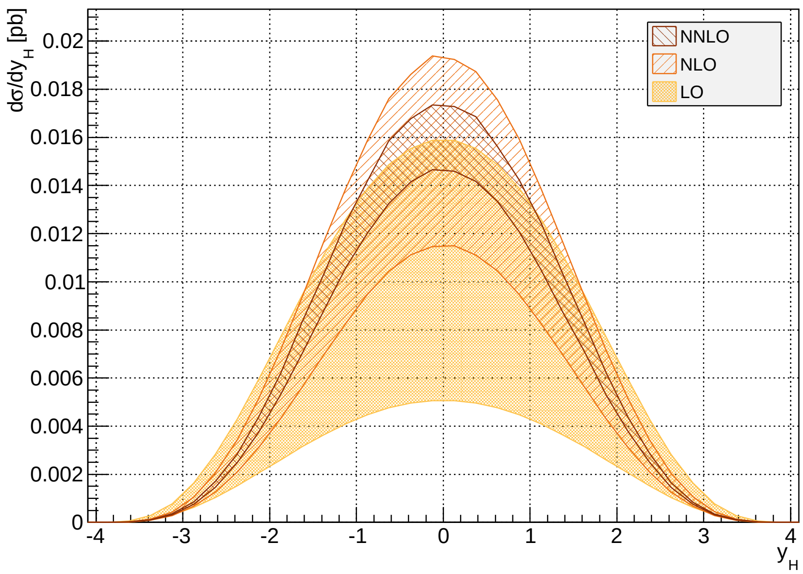

Figure 7.2.: The Higgs rapidity distribution. The bands describe the uncertainty due to the factorisation scale

for the Higgs.

We proceed by presenting a handful of plots of differential bottom fusion observables we obtained with our computer codes, for the LHC at 8 TeV centre-of-mass energy. We fix the mass of the Higgs boson to 125 GeV and use the MSTW08 (the 68%CL set) PDFs for all results. The value of α_s at m_Z that we use is the best-fit value of the PDF set at the corresponding order. We use $\mu_r = m_H$ as the central renormalisation scale. The value of α_s used is run from m_Z to μ_r through NNLO in QCD. The mass of the bottom quarks is set to zero in all matrix elements, consistently with the 5FS choice, except for the bottom Yukawa coupling. The Yukawa coupling, treated in the $\overline{\text{MS}}$ scheme, is run to μ_r from the Yukawa coupling at $\mu^* = 10$ GeV, using $m_b(\mu^*) = 3.63$ GeV.

We do not vary μ_r in what follows, since the μ_r scale dependence of the total cross section has been found to be very mild. We have also checked that the μ_r-dependence of differential distributions is very small.

Previous studies have shown that the inclusive cross section is very sensitive to the choice of factorisation scale. Arguments related to the validity of the 5FS approximation with respect to the collinearity of final state b-quarks, as well as to the matching to the 4FS calculation or to the need for a smoother perturbative expansion, point to factorisation scales that are much lower than the Higgs boson mass. We adopt the

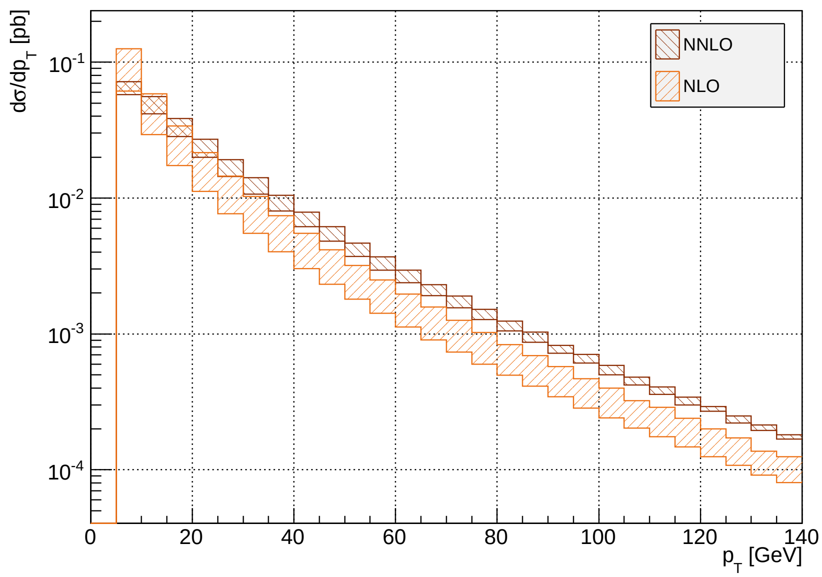

Figure 7.3.: The transverse momentum distribution of the Higgs.

choice $\mu_f = m_H/4$ as a central scale and vary it in the range $[m_H/8, m_H/2]$ to estimate the related uncertainty.

All Monte-Carlo integrations were performed with the `Cuba` [102] implementation of the Vegas algorithm.

The rapidity distribution of the Higgs boson is shown in fig. 7.2. As expected, the perturbative expansion is converging smoothly for this choice of central μ_f and the NNLO uncertainty band is entirely engulfed by the NLO one.

The transverse momentum distribution for the Higgs boson is shown in fig. 7.3. This observable starts at NLO in QCD and the fixed-order prediction fails, as usual, to describe the very low p_T spectrum due to the related large logarithms. At the large p_T range we see that the NNLO calculation leads to a harder spectrum than the NLO one and the NLO scale uncertainty fails to capture this feature. This implies that care should be taken when relying on NLO predictions for observables that are highly exclusive in the transverse momentum of the Higgs boson.

Furthermore, while for the Higgs-rapidity distribution the approximation of rescaling the NLO distribution with the inclusive K-factor would yield a good approximation, the same can not be said of the distribution of the transverse momentum of the Higgs since the slope of the NNLO result is clearly flatter than the NLO slope. The reason for this is the fact that, as mentioned, the transverse momentum only starts to be non-zero at

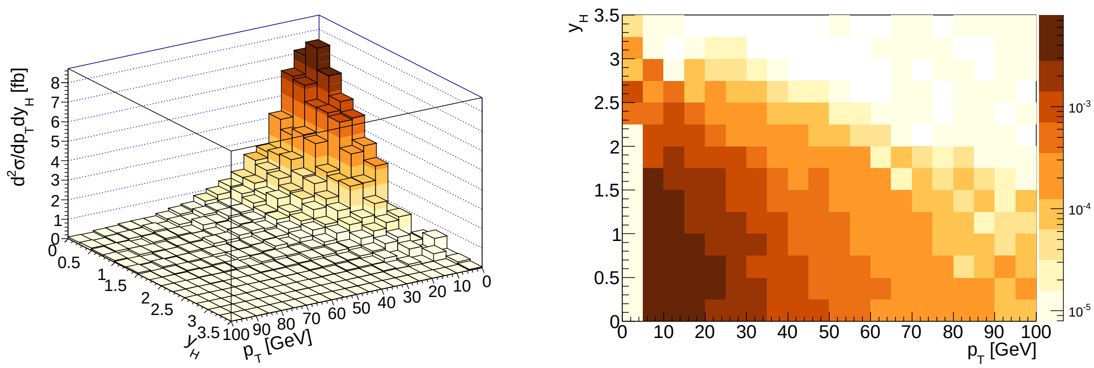

Figure 7.4.: Double-differential distribution in rapidity and transverse momentum of the Higgs boson.

NLO order, where it is essentially described by the LO cross section for the process $b\bar{b} \to H + \text{jet}$. Therefore, the NNLO curve is actually only the *first* order correction in QCD and we can not expect the shapes to be equal, as it is not the case among the LO and NLO curves of the rapidity distribution. This is a common phenomenon for any differential observable which starts to be non-zero at the NLO order, and we stress that only the full NNLO differential calculation provides a reasonable estimate for such observables.

The double-differential distribution in both the rapidity and the transverse momentum of the Higgs is shown in fig. 7.4, both in a three-dimensional Lego plot and in a density plot. We see that the bulk of the events are produced centrally (with $|y| < 2.5$) and at relatively low p_T ($35 - 50$GeV).

Finally, we show the cross section for zero, one and two jets, which always add up to the full cross section since we describe at most two emissions at NNLO QCD. We use the anti-k_T algorithm [198] for jet clustering[3] with a cone in the $y - \phi$ plane of radius $R = 0.4$. We show in fig. 7.5 the jet rates as a function of the jet p_T^{max} used to define them. Here we do not distinguish between b-jets and light jets. We find the jet rates for $p_T^{max} = 20$ GeV to be in agreement with those published in [199].

For more results which also include the more exclusive process of $b\bar{b} \to H \to \gamma\gamma$ with the typical diphoton selection cuts of the LHC experiments applied, we kindly refer to the original publication [138].

[3] At this order in perturbation theory, the anti-k_T, the k_T and the Cambridge-Aachen algorithms are actually completely equivalent.

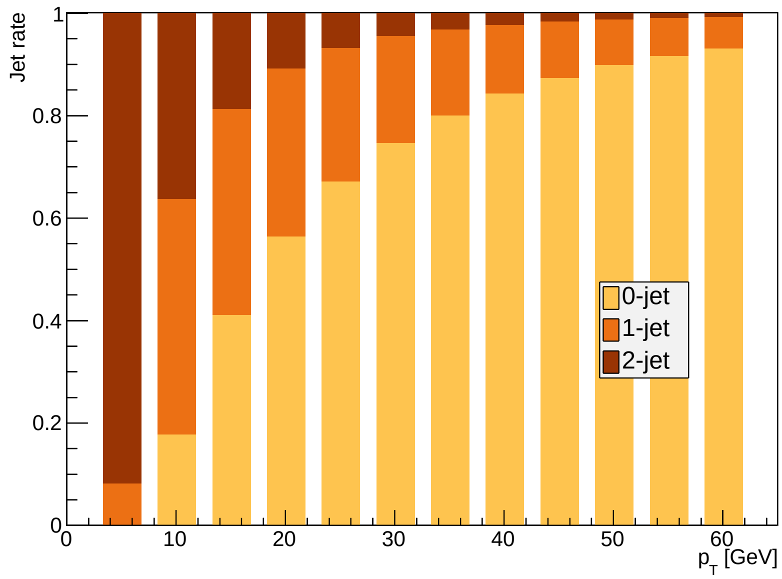

Figure 7.5.: The 0-, 1- and 2-jet rate as a function of the p_T used in the jet definition.

7.3. Conclusions

We have given a short introduction to differential computations, as opposed to the inclusive observables treated in the rest of the thesis. Differential computations retain full knowledge of final-state particle kinematics, which allows to apply selection cuts on the simulated events like in real experimental analyses. They furthermore allow for a much broader spectrum of observables to be defined, using all kinematic and quantum number information of the final state.

In section 7.1.1 we present our method to cancel initial-state collinear divergences in the computation of differential Higgs production in bottom quark fusion. The convolutions with the collinear counterterm, which in the inclusive application in chapter 6 were analytically carried out on the partonic cross sections, are now numerically performed on the parton distribution functions. We actually extract the bare PDF from the mass-factorised one. The poles obtained from integrating the bare PDFs over the renormalised partonic cross sections cancel out among all contributions, at the differential level (i.e. bin by bin in any differential observable we choose to calculate). Since we extract the bare PDFs prior to the actual Monte-Carlo run and store the obtained value in a grid used for interpolation, the method comes at zero additional cost during the phase-space Monte-Carlo integration.

In section 7.2 finally, we give selected results obtained with our differential code. The Higgs rapidity exhibits a nice perturbative convergence, while the Higgs transverse momentum curve at NNLO is not covered by the NLO band at high transverse momenta. The cross section values for such high-p_T events are tiny, though. Furthermore, we give the jet rates as a function of the jet definition p_T, which agree with the rates published in the literature.

8. Outlook

We live in exciting times. The Higgs boson has been discovered at LHC which confirms a conjecture which was put forward nearly 50 years ago. Where does particle physics move on from here, and how are the results of this thesis possibly used in the future?

The better part of the contents of this thesis focus on the inclusive Higgs production cross section in the gluon fusion process. The efforts put into the best possible description of this process by a large number of great physicists have paid off, as the production rate observed at the LHC so far is in agreement with the SM prediction which is, as we have said many times, mainly given by gluon fusion.

The light Higgs mass which is observed at the LHC renders the framework of heavy quark effective theory a very good approximation. Furthermore, it also spares us dealing with the strong scheme-dependence we found when treating heavy quark with masses close to $m_H/2$. The extension of the inclusive cross section to the next order in perturbative QCD which we have computed parts of and estimated the scale uncertainty in chapter 6 will certainly need to be completed in the years to come, if the theoretical uncertainty is supposed rival the experimental one, especially given the lack of any hints for new physics up to now. First steps towards N^3LO have already been taken, as we have mentioned, and we believe that the inclusive N^3LO cross section in the threshold limit will be available in the near future. To perform the computation in the full kinematics, some progress might need to be made in the way we have carried out such calculations up to now, considering the large number of master integrals (of the order of 300). Especially the case-by-case determination of the soft limits will become a major obstacle. Nevertheless we have strong faith in the theory community to find a solution for these calculatory challenges.

Since at the inclusive level, the step from one order to the next does not introduce special complications except for generally much longer expressions containing more difficult functions, the program `iHixs` can easily be modified to eventually include the N^3LO cross sections and possibly other newly-computed fixed-order contributions. It will remain a useful tool to study the impact of various contributions to Higgs production. Some features like the treatment of the Higgs-propagator may not appear necessary anymore due to the lightness of the Higgs mass, but could eventually become relevant again in case a second, heavy resonance is found by the LHC.

The library CHAPLIN has been used in numerical codes that need to evaluate harmonic polylogarithms with great success. Eventually, it will have to be extended to include HPLs of weight five, since we encounter these functions for example in the N^{3}LO QCD corrections to gluon fusion. The strategy of reduction to a set of basis functions and evaluation of the basis functions on the unit disc should be applicable without great complications, as the actual number of new functions that need to be series-expanded is not expected to be too large[1]. The reductions of individual HPLs to basis functions are expected to become very lengthy, though, such that an efficient structure avoiding unnecessary multiple calls to the same routine is imperative.

Since no significant enhancement of the bottom Yukawa coupling over its SM value has been observed at the LHC so far, the differential bottom quark fusion cross section will probably not play a major phenomenological role in the future. However, the techniques for differential NNLO computations that were applied successfully in said process can be applied to other processes, such as a new differential gluon fusion code which is under construction [200]. This holds especially true for the method of bare PDFs, as it is completely universal and does not rely on the partonic process under consideration at all.

Considering particle physics as a whole, there are mixed feelings of excitement and concern throughout the community. While the discovery of the Higgs can certainly be considered a great success, the preliminary agreement of its rates with the SM predictions and the complete lack of other signals of new particles have fuelled the fear of a “Higgs and nothing else” scenario. We think that it is certainly too early to be pessimistic. The measurement of the Higgs properties including all its couplings is an important task for the immediate future and holds new challenges for both experimental and theoretical collaborations. Furthermore, hints for BSM physics may as well come from a different frontier than the high-energy one, in particular from neutrino physics and/or dark matter searches.

To quote Nobel prize laureate David Gross from a lecture he recently gave in Zurich:

> *“The best is yet to come”.*

[1] there are 48 basis functions needed at weight five, 16 of which are given by classical polylogarithms of various arguments. The same arguments will also occur in the new functions needed to parametrise the remaining 32 basis functions, such that the whole basis could in principle be covered by two new functions that need to be series-expanded in addition to the classical pentalogarithm Li_5.

Appendices

A. D-dimensional phase-spaces for Higgs production

Here, we provide the phase-space parametrisations for the production of a single massive particle in addition with zero, one and two massless particles, that are used in real-radiation corrections to Higgs production throughout chapter 6. We provide the phase-space measures for these configurations here, without derivation which can be found in [183, 194]. The phase-spaces depend on the mass m of the massive final-state particle and $s = s_{12}$, the squared centre-of-mass energy. To have only one dimensionful quantity, we define the (dimensionless) variable

$$z \equiv \frac{m^2}{s} \,. \tag{A.1}$$

We remind the reader again about our definition of the Lorentz invariants $s_{i_1 \dots i_m}$,

$$s_{i_1 \dots i_m} = \left(p_{i_1 \dots i_m}\right)^2 \,, \tag{A.2}$$

where

$$p_{i_1 \dots i_m} = \tau_{i_1} p_{i_1} + \ldots + \tau_{i_m} p_{i_m} \,, \text{ with } \quad \tau_i = \begin{cases} +1 & \text{if } i = 1, 2 \,, \\ -1 & \text{if } i > 2 \,. \end{cases} \tag{A.3}$$

The single-particle phase-space $\mathrm{d}\Phi_1$ is trivial,

$$\mathrm{d}\Phi_1(s, z) = 2\pi s^{-1} \delta(1 - z) \,, \tag{A.4}$$

i.e. the centre-of-mass energy $\sqrt{s}$ has to correspond to the mass m.

The phase-space for the production of one massive and one massless particle is given by

$$\mathrm{d}\Phi_2(s, z) = \frac{s^{-\epsilon}(1-z)^{1-2\epsilon}}{2^{3-2\epsilon}\pi^{1-\epsilon}\Gamma(1-\epsilon)} \mathrm{d}y \left[y(1-y)\right]^{-\epsilon} \,, \tag{A.5}$$

where $y \in [0, 1]$ parametrises the angle between particles 1 and 3 (the massless final-state particle). The invariants s_{13} and s_{23} are given by

$$s_{13} = -s(1-z)y\,, \quad s_{23} = -s(1-z)(1-y)\,. \tag{A.6}$$

Finally, we give two different parametrisations for the $2 \to 3$ phase-space $\mathrm{d}\Phi_3$, where the massless final-state particles are labelled 3 and 4. First, the "Energies and angles" parametrisation, which as its name suggests is essentially obtained by parametrising all final-state momenta in their energies and the angles between them,

$$\mathrm{d}\Phi_3 = \frac{(2\pi)^{-3+2\epsilon}}{16\Gamma(1-2\epsilon)} \prod_{i=1}^{4} \mathrm{d}x_i \left(\frac{s\bar{z}^3\kappa^4 x_1\bar{x}_1}{2-\kappa}\right)\left(s^2\bar{z}^4\kappa^4 x_1^2\bar{x}_1^2 x_3\bar{x}_3 x_4\bar{x}_4 \sin^2(\pi x_2)\right)^{-\epsilon}\,, \tag{A.7}$$

where all variables $x_i \in [0,1]$, we have defined the shorthand notation $\bar{x}_i \equiv 1 - x_i$, $\bar{z} \equiv 1 - z$ and

$$\kappa = \frac{1-\sqrt{1-4\bar{z}x_1\bar{x}_1\tilde{x}_{34}}}{2\bar{z}x_1\bar{x}_1\tilde{x}_{34}}\,, \text{ with } \quad \tilde{x}_{34} = x_3\bar{x}_4 + x_4\bar{x}_3 - 2\cos(\pi x_2)\sqrt{x_3\bar{x}_3x_4\bar{x}_4}\,. \tag{A.8}$$

In this parametrisation the Lorentz invariants are given by

$$\begin{aligned}
&s_{13} = -s\bar{z}\kappa x_1 x_3\,, \qquad s_{23} = -s\bar{z}\kappa x_1\bar{x}_3\,,\\
&s_{14} = -s\bar{z}\kappa\bar{x}_1 x_4\,, \qquad s_{24} = -s\bar{z}\kappa\bar{x}_1\bar{x}_4\,,\\
&s_{34} = s\bar{z}^2\kappa^2 x_1\bar{x}_1\tilde{x}_{34}\,, \quad s_{134} = s\bar{z}\kappa\left[\bar{z}\kappa x_1\bar{x}_1\tilde{x}_{34} - x_1x_3 - \bar{x}_1x_4\right]\,,\\
&s_{234} = s\bar{z}\kappa\left[\bar{z}\kappa x_1\bar{x}_1\tilde{x}_{34} - x_1\bar{x}_3 - \bar{x}_1\bar{x}_4\right]\,.
\end{aligned} \tag{A.9}$$

Obviously, this parametrisation is useful mostly when none of the invariants s_{34}, s_{134}, s_{234} are present in the phase-space integral, as all other invariants are fairly simple and denominators including products of them fully factorise.

The second parametrisation is the "Hierarchical parametrisation", where the derivation makes use of the factorisation property of phase-spaces, i.e. the fact that the three-particle phase-space can be written as a (massive) two-particle phase-space where one of the final-state particles splits into two massless particles[1]. The phase-space measure reads

$$\mathrm{d}\Phi_3 = \frac{(2\pi)^{-3+2\epsilon}}{16\Gamma(1-2\epsilon)} \prod_{i=1}^{4} \mathrm{d}x_i \left(\frac{s\bar{z}^3 x_1\bar{x}_1}{z+x_1\bar{z}}\right)\left(\frac{s^2\bar{z}^4 x_1^2\bar{x}_1^2 x_2\bar{x}_2 x_3\bar{x}_3 \sin^2(\pi x_4)}{z+x_1\bar{z}}\right)^{-\epsilon}\,, \tag{A.10}$$

[1] See chapter 5 of [183]

where, again, all integration variables $x_i \in [0,1]$. The invariants $s_{i_1 \ldots i_m}$ read

$$
\begin{aligned}
& s_{23} = -s\bar{z}\bar{x}_1 x_3\,, \qquad s_{134} = -s\bar{z}x_1\,, \qquad s_{24} = -s\bar{z}\bar{x}_1\bar{x}_3\,, \\
& s_{234} = -s\bar{z}x_1 \left[\frac{z + 1_1\bar{x}_2\bar{z}}{z + x_1\bar{z}}\right], \qquad s_{34} = \frac{s\bar{z}^2 x_1\bar{x}_1 x_2}{z + x_1\bar{z}}\,, \\
& s_{13} = -s\bar{z}x_1 \left[x_3\bar{x}_2 + \frac{x_2\bar{x}_3}{z + x_1\bar{z}} - 2\cos(\pi x_4)\sqrt{\frac{x_2\bar{x}_2 x_3\bar{x}_3}{z + x_1\bar{z}}}\,\right], \\
& s_{14} = -s\bar{z}x_1 \left[\bar{x}_3\bar{x}_2 + \frac{x_2 x_3}{z + x_1\bar{z}} + 2\cos(\pi x_4)\sqrt{\frac{x_2\bar{x}_2 x_3\bar{x}_3}{z + x_1\bar{z}}}\,\right].
\end{aligned}
\tag{A.11}
$$

Clearly, this parametrisation is somewhat complementary to the “Energies and angles” parametrisation, as it yields a simpler expressions for s_{34}, s_{134} and s_{234}, while s_{13} and s_{14} become much more complicated and do not allow for straightforward factorisation of integration variables.

B. Splitting Kernels

Here, we list the Altarelli-Parisi splitting kernels used throughout the thesis, especially in section 6.2. We remind the reader that $P_{ij}(x)$ quantifies the amplitude for a parton j to split into a parton i and a third, implicit, parton, with i carrying the momentum fraction x of the initial parton j.

The kernels are expanded in the strong coupling,

$$P_{ij}(x) = \sum_{n=0}^{\infty} a_s^{n+1} P_{ij}^{(n)}(x)\,. \tag{B.1}$$

Please notice that there exist other conventions in the literature, such as labelling the kernels with the order of a_s they come with (i.e. the lowest-order kernels are denoted by $P_{ij}^{(1)}$ instead of $P_{ij}^{(0)}$). Also, the expansion parameter a_s is sometimes defined to be $\alpha_s/(2\pi)$ or $\alpha_s/(4\pi)$, which introduces factors of 2 and 4, respectively, in the splitting kernels to compensate.

Since we retrieved all the kernels from [201, 202], where notation and conventions are oriented towards PDF evolution rather than mass factorisation, we will give the relation between our kernels $P_{ij}^{(n)}$ and the expressions that are given in [201, 202] which we shall denote as $\mathcal{P}_{ij}^{(n)}$, as well as the explicit formulae for our kernels.

At the leading order, there are four kernels,

$$P_{gg}^{(0)}(x) = \beta_0\,\delta(1-x) + 3\left(\mathcal{D}_0(1-x) + x(1-x) - 2 + \frac{1}{x}\right)\,. \tag{B.2}$$

$$P_{gq}^{(0)}(x) = \frac{2}{3}\frac{1+(1-x)^2}{x}\,. \tag{B.3}$$

$$P_{qg}^{(0)}(x) = \frac{1}{4}\left(x^2 + (1-x)^2\right)\,. \tag{B.4}$$

$$P_{qq}^{(0)}(x) = \delta(1-x) + \frac{2}{3}\left(2\mathcal{D}_0(1-x) - 1 - x\right)\,, \tag{B.5}$$

where the relation to the $\mathcal{P}_{ij}$ is given by

$$P_{gg}^{(0)} = \frac{1}{4}\mathcal{P}_{gg}^{(0)}\,, \quad P_{gq}^{(0)} = \frac{1}{4}\mathcal{P}_{gq}^{(0)} \quad P_{qg}^{(0)} = \frac{1}{4}\frac{1}{2N_F}\mathcal{P}_{qg}^{(0)}\,, \quad P_{qq}^{(0)} = \frac{1}{4}\mathcal{P}_{ns}^{(0)}\,. \tag{B.6}$$

The factors of 4 originate from the different prescription for a_s mentioned above. The additional factor of $1/(2N_F)$ in P_{qg} stems from the fact that $\mathcal{P}_{qg}$ gives the amplitude for a gluon emitting *any* kind of quark, while our kernel parametrises the emission of a quark of a given flavour q_i.

At the two-loop order, there are six kernels, as there are now non-vanishing amplitudes for a quark emitting an antiquark of the same flavour, $P^{(1)}_{q\bar{q}}$, or a quark of a different flavour, $P^{(1)}_{qQ}$ (with $Q \neq q$ and $Q \neq \bar{q}$). The expressions are already a bit lengthier,

$$\begin{aligned}
P^{(1)}_{gg}(x) =& \delta\,(1-x)\left(6 - 2/3\,N_F + \frac{27}{4}\,\zeta\,(3)\right) + \left(\frac{67}{4} - 5/6\,N_F - 3/4\,\pi^2\right)\mathcal{D}_0(1-x) \\
&+ \left(N_F\,\left(-3/2 - \frac{13}{6}\,x\right) - \frac{75}{4} + \frac{33}{4}\,x - 33\,x^2\right)\mathrm{H}\,(0;x) \\
&+ 9\left(2 + x^{-1} + x + x^2 - (1+x)^{-1}\right)\mathrm{H}\,(-1,0;x) \\
&+ 9\left(-2 + (1-x)^{-1} + x^{-1} + x - x^2\right)\mathrm{H}\,(0,1;x) \\
&+ 9\left(-2 + (1-x)^{-1} + x^{-1} + x - x^2\right)\mathrm{H}\,(1,0;x) \\
&+ \left(-\frac{2N_F}{3}\,(1+x) + 9\,(2-2\,x)^{-1} + 18\,x - 9\,x^2 + 9\,(2+2\,x)^{-1}\right)\mathrm{H}\,(0,0;x) \\
&+ N_F\,\left(-1/4 - \frac{61}{36}\,x^{-1} - 1/4\,x + \frac{109}{36}\,x^2\right) \\
&- \frac{25}{8} + 3\,\pi^2 - \frac{109}{8}\,x + 3/2\,\pi^2 x^2 - 3\,\frac{\pi^2}{4+4\,x}\,,
\end{aligned} \tag{B.7}$$

$$\begin{aligned}
P^{(1)}_{gq}(x) =& \left(14/3 - 14/3\,x^{-1} - \frac{31}{9}\,x + N_F\,\left(-4/9 + 4/9\,x^{-1} + 2/9\,x\right)\right)\mathrm{H}\,(1;x) \\
&+ \left(\frac{28}{9} + \frac{22}{9}\,x\right)\mathrm{H}\,(0,0;x) + \left(-4 + 4\,x^{-1} + 2\,x\right)\mathrm{H}\,(0,1;x) \\
&+ \left(-\frac{20}{9} + \frac{20}{9}\,x^{-1} + \frac{10}{9}\,x\right)\mathrm{H}\,(1,1;x) + \left(4 + 4\,x^{-1} + 2\,x\right)\mathrm{H}\,(-1,0;x) \\
&+ \left(-4 + 4\,x^{-1} + 2\,x\right)\mathrm{H}\,(1,0;x) + \left(-\frac{100}{9} - \frac{31}{9}\,x - 8/3\,x^2\right)\mathrm{H}\,(0;x) \\
&+ 1 + 2/3\,\pi^2 + x^{-1} + \frac{23}{9}\,x + \frac{44}{9}\,x^2 + N_F\,\left(\frac{20}{27} - \frac{20}{27}\,x^{-1} - \frac{16}{27}\,x\right)\,,
\end{aligned} \tag{B.8}$$

$$\begin{aligned}
P^{(1)}_{qg}(x) =& \left(5/8 + 8/3\,x + \frac{37}{6}\,x^2\right)\mathrm{H}\,(0;x) + \left(5/6\,x - 5/6\,x^2\right)\mathrm{H}\,(1;x) \\
&+ \left(-3/4 - 3/2\,x - 3/2\,x^2\right)\mathrm{H}\,(-1,0;x) + \left(-\frac{7}{12} - \frac{11}{6}\,x + 2/3\,x^2\right)\mathrm{H}\,(0,0;x) \\
&+ \left(1/3 - 2/3\,x + 2/3\,x^2\right)\mathrm{H}\,(0,1;x) + \left(1/3 - 2/3\,x + 2/3\,x^2\right)\mathrm{H}\,(1,0;x)
\end{aligned}$$

$$+\left(-\frac{5}{12}+5/6\,x-5/6\,x^2\right)\mathrm{H}\,(1,1;x)$$
$$+\frac{5}{12}-1/18\,\pi^2+5/6\,x^{-1}+\frac{167}{24}\,x-\frac{5}{36}\,\pi^2x-\frac{89}{12}\,x^2-1/9\,\pi^2x^2\,, \tag{B.9}$$

$$\begin{aligned}P^{(1)}_{qq}(x)=&\delta\,(1-x)\left(\frac{7}{8}+\frac{7}{18}\,\pi^2+N_F\,\left(-1/36-1/27\,\pi^2\right)-1/3\,\zeta\,(3)\right)\\&+\left(\frac{67}{9}-\frac{10}{27}\,N_F-1/3\,\pi^2\right)\mathcal{D}_0(1-x)\\&+\left(\frac{N_F}{9}\,\left(1-2\,(1-x)^{-1}+x\right)-2/3+7\,(3-3\,x)^{-1}-\frac{8}{9}\,x+4/9\,x^2\right)\mathrm{H}\,(0;x)\\&+\frac{8}{9}\left(-1+2\,(1-x)^{-1}-\,x\right)\mathrm{H}\,(0,1;x)\\&+\frac{8}{9}\left(-1+2\,(1-x)^{-1}-\,x\right)\mathrm{H}\,(1,0;x)\\&+\left(-\frac{16}{9}+2\,(1-x)^{-1}-\frac{16}{9}\,x\right)\mathrm{H}\,(0,0;x)\\&+\frac{7}{18}+1/6\,\pi^2+\frac{10}{27}\,x^{-1}-\frac{43}{6}\,x+1/6\,\pi^2x-\frac{28}{27}\,x^2\\&+N_F\,\left(-1/27+\frac{11}{27}\,x\right)\,,\end{aligned} \tag{B.10}$$

$$\begin{aligned}P^{(1)}_{q\bar{q}}(x)=&\left(1/18+\frac{13}{18}\,x+4/9\,x^2\right)\mathrm{H}\,(0;x)+\frac{2}{9}\left(-1+x+2\,(1+x)^{-1}\right)\mathrm{H}\,(-1,0;x)\\&+\frac{2}{9}\left(-1-2\,x-(1+x)^{-1}\right)\mathrm{H}\,(0,0;x)\\&-5/9-\frac{1}{54}\,\pi^2+\frac{10}{27}\,x^{-1}+\frac{11}{9}\,x+\frac{1}{54}\,\pi^2x-\frac{28}{27}\,x^2+\frac{\pi^2}{27+27\,x}\,,\end{aligned} \tag{B.11}$$

$$\begin{aligned}P^{(1)}_{qQ}(x)=&\left(1/6+5/6\,x+4/9\,x^2\right)\mathrm{H}\,(0;x)-\frac{1}{3}\,(1+x)\,\mathrm{H}\,(0,0;x)\\&-1/3+\frac{10}{27}\,x^{-1}+x-\frac{28}{27}\,x^2\,.\end{aligned} \tag{B.12}$$

The relations to the $\mathcal{P}_{ij}$ are given by

$$\begin{aligned}P^{(1)}_{gg}&=\left(\frac{1}{4}\right)^2\mathcal{P}^{(1)}_{gg}\,,\quad P^{(1)}_{gq}=\left(\frac{1}{4}\right)^2\mathcal{P}^{(1)}_{gq}\quad P^{(1)}_{qg}=\left(\frac{1}{4}\right)^2\frac{1}{2N_F}\mathcal{P}^{(1)}_{qg}\,,\\P^{(1)}_{qq}&=\left(\frac{1}{4}\right)^2\left[\frac{1}{2}\left(\mathcal{P}^{(1)+}_{ns}+\mathcal{P}^{(1)-}_{ns}\right)+\frac{1}{2N_F}\mathcal{P}^{(1)}_{ps}\right]\,,\\P^{(1)}_{q\bar{q}}&=\left(\frac{1}{4}\right)^2\left[\frac{1}{2}\left(\mathcal{P}^{(1)+}_{ns}-\mathcal{P}^{(1)-}_{ns}\right)+\frac{1}{2N_F}\mathcal{P}^{(1)}_{ps}\right]\,,\end{aligned}$$

$$P_{qQ}^{(1)} = \left(\frac{1}{4}\right)^2 \frac{1}{2N_F}\mathcal{P}_{ps}^{(1)} \,. \tag{B.13}$$

At the three-loop order, the expressions for the kernels become very long. We only require the two kernels $P_{gg}^{(2)}$ and $P_{gq}^{(2)}$, whose relation to the expressions is simply

$$P_{gg}^{(2)} = \left(\frac{1}{4}\right)^3 \mathcal{P}_{gg}^{(2)} \,, \qquad P_{gq}^{(2)} = \left(\frac{1}{4}\right)^3 \mathcal{P}_{gq}^{(2)} \,, \tag{B.14}$$

i.e. no combination of different kernels as in the quark-case is required. Thus, we simply refer to eqs. (4.14) and (4.15) of [201] for these two kernels. The only subtlety one has to pay attention to is the implicit way that the plus-distribution appears. In the notation of [201], it is understood that any term proportional to $(1-x)^{-1}$ that diverges (i.e. is not regulated by a $\log(x)$ or a combination of terms going to zero as $x \to 1$ has to be treated as a plus-distribution.

The kernels in our conventions and notation can be found in machine-readable form (both Maple and Mathematica) in the ancillary files of the arXiv publication of ref. [83].

C. Re-installing scale dependence and separating scales

In chapter 6 we outlined how to obtain all scale-dependent pieces of an n^{th}-order QCD cross section by adding together all lower-order bare cross sections and the appropriate collinear counter-terms, and subsequently expanding the whole expression in ϵ, which generates the scale-dependent logarithms by expansion of terms like $\mu^{k\epsilon}$.

There is also a way to obtain all these logarithms from the finite (i.e. renormalised and mass-factorised) cross section, which is what we had to do to re-install the full scale-dependence of the NNLO QCD $b\bar{b} \to H$ cross section in the context of `iHixs` because the publication [101] only provides the finite partonic cross sections at the scale $\mu_f = \mu_r = m_H$ for which all explicit logarithms vanish.

In this situation one can employ the formulae for scale translations of coupling constants and parton distribution functions. They express a scale-dependent quantity living at a scale μ_0 as a combination of quantities that live at a different scale μ_1, times logarithms of the ratio of the two scales.

To be specific, the third-order expansion of $a_s(\mu_0)$ in terms of $a_s(\mu_1)$ reads

$$\begin{aligned} a_s(\mu_0) =& a_s(\mu_1) + a_s^2(\mu_1)\beta_0 L + a_s^3(\mu_1)\left[\beta_1 L + \beta_0^2 L^2\right] + \\ &+ a_s^4(\mu_1)\left[\beta_2 L + \frac{5}{2}\beta_1\beta_0 L^2 + \beta_0^3 L^3\right] + \mathcal{O}(a_s^5)\,, \end{aligned} \tag{C.1}$$

with $L \equiv \log(\mu_1^2/\mu_0^2)$. This result is obtained from the renormalisation group equation (RGE) for a_s,

$$\frac{\partial a_s(\mu)}{\partial \log(\mu^2)} = \beta(\mu)\, a_s(\mu) \quad \text{with} \quad \beta(\mu) = -\sum_{n=0} \beta_n a_s^{n+1}(\mu)\,, \tag{C.2}$$

in the following way. Integrating eq. (C.2) from μ_0 to μ_1 yields

$$a_s(\mu_1) = a_s(\mu_0) + \int_{\log(\mu_0^2)}^{\log(\mu_1^2)} \mathrm{d}\log(\mu^2)\beta(\mu)a_s(\mu)\,. \tag{C.3}$$

The $a_s(\mu)$ in the integral can now be replaced by the equation itself, i.e.

$$a_s(\mu_1) = a_s(\mu_0) + \int_{\log(\mu_0^2)}^{\log(\mu_1^2)} \mathrm{d}\log(\mu_2^2)\beta(\mu_2)\left[a_s(\mu_0) + \int_{\log(\mu_0^2)}^{\log(\mu_2^2)} \mathrm{d}\log(\mu^2)\beta(\mu)a_s(\mu)\right]. \tag{C.4}$$

Repeating these steps for all $a_s(\mu)$ inside the integrals until the desired order in a_s is reached and subsequently evaluating the integrals to obtain the logarithms of μ_1^2/μ_0^2 then yields eq. (C.1).

Analogously, we may integrate the RGE for the parton distribution function f_i, the DGLAP equation,

$$\frac{\partial f_i(\mu)}{\partial \log(\mu^2)} = P_{ij}(\mu) \otimes f_j(\mu) \quad \text{with} \quad P_{ij}(\mu) = \sum_{n=0} P_{ij}^{(n)} a_s^{n+1}(\mu)\,. \tag{C.5}$$

to obtain

$$f_i(\mu_1) = f_i(\mu_0) + \int_{\log(\mu_0^2)}^{\log(\mu_1^2)} \mathrm{d}\log(\mu^2) P_{ij}(\mu) \otimes f_j(\mu)\,, \tag{C.6}$$

and iterate (replacing $f_j(\mu)$ with the equation itself and the $a_s(\mu)$ in $P_{ij}(\mu)$ with eq. (C.1)) to arrive at the scale translation formula for the pdf,

$$\begin{aligned} f_i(\mu_0) =& f_i(\mu_1) - a_s(\mu_1) L P_{ij}^{(0)} \otimes f_j(\mu_1) \\ &+ a_s^2(\mu_1)\left[-L P_{ij}^{(1)} \otimes f_j(\mu_1) + \frac{L^2}{2}\left(P_{ik}^{(0)} \otimes P_{kj}^{(0)} - \beta_0 P_{ij}^{(0)}\right) \otimes f_j(\mu_1)\right] \\ &+ a_s^3(\mu_1)\Bigg[- L P_{ij}^{(2)} \otimes f_j(\mu_1) \\ &+ \frac{L^2}{2}\left(P_{ik}^{(1)} \otimes P_{kj}^{(0)} + P_{ik}^{(0)} \otimes P_{kj}^{(1)} - \beta_1 P_{ij}^{(0)} - 2\beta_0 P_{ij}^{(1)}\right) \otimes f_j(\mu_1) \\ &+ \frac{L^3}{6}\left(-P_{ik}^{(0)} \otimes P_{kl}^{(0)} \otimes P_{lj}^{(0)} + 3\beta_0 P_{ik}^{(0)} \otimes P_{kj}^{(0)} - 2\beta_0^2 P_{ij}^{(0)}\right) \otimes f_j(\mu_1)\Bigg]. \end{aligned} \tag{C.7}$$

Now, if one starts from the hadronic cross section at a given scale μ_0 (e.g. $\sqrt{s}$),

$$\sigma(\mu_0) = f_i(\mu_0) \otimes \sigma_{ij}(\mu_0) \otimes f_j(\mu_0)\,, \tag{C.8}$$

the factorisation scale can be changed by replacing $f_i(\mu_0)$ and $f_j(\mu_0)$ with their expansions at μ_f, according to eq. (C.7), as well as replacing all $a_s(\mu_0)$ in the expansion of $\hat{\sigma}_{ij}(\mu_0)$ according to eq. (C.1). Since the convolution is associative and commutative, the splitting kernels can be convoluted with the partonic cross section. This produces exactly the same convolutions and logarithms as the convolution of collinear subtraction terms and lower-order cross sections when cancelling IR poles.

To finally separate the scales μ_f and μ_r, one simply repeats the scale translation for the parameters one would like to live at the renormalisation scale, i.e. one replaces $a_s(\mu_f)$ (and possibly other parameters like masses) with its expansion in $a_s(\mu_r)$ by applying eq. (C.1) again.

D. Reduction of HPLs to Basis functions

In this appendix, we provide the reduction of all HPLs up to weight four to the basis functions defined in chapter 4, which consists only of the ordinary logarithm, the classical polylogs Li_2, Li_3 and Li_4 with various arguments, as well as the two "pure" HPLs $\mathrm{H}(0,1,0,-1,x)$ and $\mathrm{H}(0,1,1,-1,\pm x)$.

To save some space, we only provide a minimal set of reduction mappings. The reduction of a HPL which is not explicitly given can be obtained via shuffle-relations (eq. (4.13)). For example, the reduction for $\mathrm{H}(1,0;x)$ is not provided, but can be obtained by combining the reductions of the functions on the RHS of the shuffle-relation

$$\mathrm{H}(1,0;x) = \mathrm{H}(1;x)\mathrm{H}(0;x) - \mathrm{H}(0,1;x)\,, \tag{D.1}$$

which are all provided in the next section.

Please note that these identities have been derived and published by the authors of ref. [129] and are only repeated here for reasons of completeness.

D.1. Weight one and two

For weight one, the reduction is given by the definition of the HPLs,

$$\mathrm{H}(-1;x) = \log(1+x)\,, \quad \mathrm{H}(0;x) = \log(x)\,, \quad \mathrm{H}(1;x) = -\log(1-x)\,. \tag{D.2}$$

At weight two, we encounter the first non-trivial reductions,

$$\begin{aligned}
\mathrm{H}(-1,1;x) =& \log 2\log(1-x) - \log(1-x)\log(1+x) - \frac{1}{2}\log^2 2 - \mathrm{Li}_2\left(\frac{1-x}{2}\right) + \frac{\pi^2}{12}\,,\\
\mathrm{H}(0,-1;x) =& -\mathrm{Li}_2(-x)\,,\\
\mathrm{H}(0,1;x) =& \mathrm{Li}_2(x)\,.
\end{aligned} \tag{D.3}$$

D.2. Weight three

The reductions for weight three read

$$
\begin{aligned}
\mathrm{H}(-1,1,-1;x) =& -\mathrm{Li}_2\left(\frac{1-x}{2}\right)\log(1+x) - \frac{3}{2}\log^2 2\log(1+x) \\
&+ \log 2\log^2(1+x) - \log(1-x)\log^2(1+x) + \log 2\log(1-x)\log(1+x) \\
&+ \frac{1}{4}\pi^2\log(1+x) + \frac{1}{3}\log^3 2 - \frac{1}{6}\pi^2\log 2 - 2\mathrm{Li}_3\left(\frac{1+x}{2}\right) + \frac{7\zeta_3}{4}\,, \\
\mathrm{H}(-1,1,1;x) =& \mathrm{Li}_2\left(\frac{1-x}{2}\right)\log(1-x) - \frac{1}{2}\log 2\log^2(1-x) + \frac{1}{2}\log^2(1-x)\log(1+x) \\
&+ \frac{1}{6}\log^3 2 - \frac{1}{12}\pi^2\log 2 - \mathrm{Li}_3\left(\frac{1-x}{2}\right) + \frac{7\zeta_3}{8}\,, \\
\mathrm{H}(0,-1,-1;x) =& -\mathrm{Li}_2(-x)\log(1+x) + \frac{1}{6}\log^3(1+x) - \frac{1}{2}\log x\log^2(1+x) \\
&- \frac{\pi^2}{6}\log(1+x) - \mathrm{Li}_3\left(\frac{1}{1+x}\right) + \zeta_3\,, \\
\mathrm{H}(0,-1,1;x) =& \mathrm{Li}_2(-x)\log(1-x) - \frac{1}{6}\log^3(1-x) - \frac{1}{2}\log^2 2\log(1-x) \\
&+ \frac{1}{2}\log 2\log^2(1-x) + \frac{1}{2}\log^2(1-x)\log x - \frac{\pi^2}{12}\log(1-x) + \frac{1}{6}\log^3 2 \\
&- \frac{\pi^2}{12}\log 2 - \mathrm{Li}_3\left(\frac{1-x}{2}\right) + \mathrm{Li}_3(1-x) - \mathrm{Li}_3(-x) + \mathrm{Li}_3(x) \\
&+ \mathrm{Li}_3\left(\frac{2x}{x-1}\right) - \frac{1}{8}\zeta_3\,, \\
\mathrm{H}(0,0,-1;x) =& -\mathrm{Li}_3(-x)\,, \\
\mathrm{H}(0,0,1;x) =& \mathrm{Li}_3(x)\,, \\
\mathrm{H}(0,1,-1;x) =& \mathrm{Li}_2(x)\log(1+x) + \frac{1}{6}\log^3(1-x) - \frac{1}{2}\log^2 2\log(1+x) \\
&- \frac{1}{2}\log 2\log^2(1-x) - \frac{1}{2}\log(1-x)\log^2(1+x) - \frac{1}{2}\log^2(1-x)\log x \\
&+ \log 2\log(1-x)\log(1+x) + \frac{\pi^2}{6}\log(1-x) + \log(1-x)\log x\log(1+x) \\
&+ \frac{\pi^2}{12}\log(1+x) + \frac{1}{6}\log^3 2 - \frac{\pi^2}{12}\log 2 + \mathrm{Li}_3(-x) - \mathrm{Li}_3(x) - \mathrm{Li}_3\left(\frac{2x}{x-1}\right) \\
&+ \mathrm{Li}_3\left(\frac{1}{1+x}\right) - \mathrm{Li}_3\left(\frac{1-x}{1+x}\right) - \mathrm{Li}_3\left(\frac{1+x}{2}\right) + \frac{7}{8}\zeta_3\,, \\
\mathrm{H}(0,1,1;x) =& -\mathrm{Li}_2(x)\log(1-x) - \frac{1}{2}\log x\log^2(1-x) + \frac{\pi^2}{6}\log(1-x) \\
&- \mathrm{Li}_3(1-x) + \zeta_3\,.
\end{aligned} \tag{D.4}
$$

D.3. Weight four

For weight four, finally, some reductions become quite lengthy,

$$\begin{aligned}
\mathrm{H}(-1,1,-1,-1;x) =& -\frac{1}{2}\mathrm{Li}_2\left(\frac{1-x}{2}\right)\log^2(1+x) - 2\mathrm{Li}_3\left(\frac{1+x}{2}\right)\log(1+x) \\
& - \frac{7}{8}\zeta_3\log(1+x) - \frac{1}{6}\log^3 2\log(1+x) + \frac{1}{2}\log 2\log^3(1+x) \\
& - \frac{1}{2}\log(1-x)\log^3(1+x) - \frac{1}{2}\log^2 2\log^2(1+x) \\
& + \frac{1}{2}\log 2\log(1-x)\log^2(1+x) + \frac{\pi^2}{12}\log^2(1+x) + \frac{\pi^2}{12}\log 2\log(1+x) \\
& + 3\mathrm{Li}_4\left(\frac{1+x}{2}\right) - 3\mathrm{Li}_4\left(\frac{1}{2}\right), \\
\mathrm{H}(-1,1,-1,1;x) =& \frac{1}{2}\mathrm{Li}_2\left(\frac{1-x}{2}\right)\log^2 2 - \mathrm{Li}_2\left(\frac{1-x}{2}\right)\log 2\log(1-x) \\
& + \mathrm{Li}_2\left(\frac{1-x}{2}\right)\log(1-x)\log(1+x) + 2\mathrm{Li}_3\left(\frac{1+x}{2}\right)\log(1-x) \\
& - 2\zeta_3\log(1-x) + \frac{1}{4}\zeta_3\log(1+x) + \frac{1}{12}\log^4(1+x) \\
& + \frac{1}{3}\log^3 2\log(1+x) - \frac{1}{3}\log(1-x)\log^3(1+x) + \log^2 2\log^2(1-x) \\
& - \frac{1}{2}\log^2 2\log^2(1+x) + \frac{3}{2}\log^2 2\log(1-x)\log(1+x) \\
& - 2\log 2\log^2(1-x)\log(1+x) + \log^2(1-x)\log^2(1+x) \\
& + \frac{5}{12}\pi^2\log 2\log(1-x) - \frac{\pi^2}{6}\log 2\log(1+x) \\
& + \frac{1}{8}\log^4 2 - \frac{\pi^2}{24}\log^2 2 + \frac{1}{2}\mathrm{Li}_2\left(\frac{1-x}{2}\right)^2 - \frac{\pi^2}{12}\mathrm{Li}_2\left(\frac{1-x}{2}\right) \\
& + 2\mathrm{Li}_4\left(\frac{x-1}{x+1}\right) - 2\mathrm{Li}_4\left(\frac{1+x}{2}\right) + \frac{11}{480}\pi^4 - \frac{7}{6}\log^3 2\log(1-x) \\
& + \frac{\pi^2}{6}\log^2(1+x) - \frac{5}{12}\pi^2\log(1-x)\log(1+x) + 2\mathrm{Li}_4\left(\frac{1-x}{2}\right), \\
\mathrm{H}(0,-1,-1,-1;x) =& -\frac{1}{2}\mathrm{Li}_2(-x)\log^2(1+x) - \mathrm{Li}_3\left(\frac{1}{1+x}\right)\log(1+x) + \frac{1}{8}\log^4(1+x) \\
& - \frac{1}{3}\log x\log^3(1+x) - \frac{\pi^2}{12}\log^2(1+x) - \mathrm{Li}_4\left(\frac{1}{1+x}\right) + \frac{\pi^4}{90}, \\
\mathrm{H}(0,-1,-1,1;x) =& \mathrm{Li}_{2,2}(-1,x) + \mathrm{Li}_{2,2}\left(\frac{1}{2},\frac{2x}{x+1}\right) + \frac{1}{2}\mathrm{Li}_2\left(\frac{1-x}{2}\right)\log^2(1+x) \\
& - \frac{1}{2}\mathrm{Li}_2(-x)\log^2(1+x) + \frac{1}{2}\mathrm{Li}_2(x)\log^2(1+x) + \frac{1}{2}\mathrm{Li}_2(-x)\log^2 2 \\
& + \mathrm{Li}_2(-x)\log(1-x)\log(1+x) - 2\mathrm{Li}_3(x)\log(1+x)
\end{aligned}$$

$$
\begin{aligned}
&- 2\mathrm{Li}_3\left(\frac{2x}{x-1}\right)\log(1+x) - 2\mathrm{Li}_3\left(\frac{1-x}{1+x}\right)\log(1+x)\\
&- \mathrm{Li}_2(-x)\log 2\log(1-x) + \mathrm{Li}_3\left(\frac{1}{1+x}\right)\log(1-x) - \frac{5}{4}\zeta_3\log(1+x)\\
&- \frac{7}{8}\zeta_3\log(1-x) + \frac{5}{8}\log^4(1+x) - \frac{3}{2}\log 2\log^3(1+x)\\
&- \frac{2}{3}\log(1-x)\log^3(1+x) - \log x\log^3(1+x) - \frac{1}{2}\log^3 2\log(1+x)\\
&+ \frac{1}{3}\log^3(1-x)\log(1+x) + \log^2 2\log^2(1+x)\\
&+ 2\log(1-x)\log x\log^2(1+x) - \frac{5}{12}\pi^2\log^2(1+x)\\
&- \log 2\log^2(1-x)\log(1+x) - \log^2(1-x)\log x\log(1+x)\\
&+ \frac{\pi^2}{4}\log 2\log(1+x) + \frac{5}{12}\pi^2\log(1-x)\log(1+x) - \frac{1}{4}\mathrm{Li}_4\left(1-x^2\right)\\
&- \frac{1}{2}\mathrm{Li}_2(-x)^2 + \mathrm{Li}_2\left(\frac{1-x}{2}\right)\mathrm{Li}_2(-x) - \frac{\pi^2}{12}\mathrm{Li}_2(-x) + \mathrm{Li}_4(1-x)\\
&+ \mathrm{Li}_4(-x) + \mathrm{Li}_4(x) + \frac{1}{2}\mathrm{Li}_4\left(\frac{4x}{(x+1)^2}\right) - \frac{1}{2}\mathrm{Li}_4\left(\frac{1-x}{1+x}\right)\\
&+ 2\mathrm{Li}_4\left(\frac{x}{x+1}\right) - 2\mathrm{Li}_4\left(\frac{2x}{x+1}\right) + 3\mathrm{Li}_4\left(\frac{1+x}{2}\right) - 3\mathrm{Li}_4\left(\frac{1}{2}\right)\\
&+ \frac{\pi^4}{480} + \frac{3}{2}\log 2\log(1-x)\log^2(1+x) + \frac{1}{2}\mathrm{Li}_4\left(\frac{x-1}{x+1}\right),
\end{aligned}
$$

$$
\begin{aligned}
\mathrm{H}(0,-1,1,-1;x) = &- \mathrm{Li}_{2,2}(-1,x) - \mathrm{Li}_{2,2}\left(\frac{1}{2},\frac{2x}{x+1}\right) - \frac{1}{2}\mathrm{Li}_2\left(\frac{1-x}{2}\right)\log^2(1+x)\\
&+ \frac{1}{2}\mathrm{Li}_2(-x)\log^2(1+x) - \frac{1}{2}\mathrm{Li}_2(x)\log^2(1+x) - \frac{1}{2}\mathrm{Li}_2(-x)\log^2 2\\
&- \mathrm{Li}_3\left(\frac{1-x}{2}\right)\log(1+x) + \mathrm{Li}_3(1-x)\log(1+x)\\
&+ 3\mathrm{Li}_3(x)\log(1+x) + 3\mathrm{Li}_3\left(\frac{2x}{x-1}\right)\log(1+x)\\
&+ 2\mathrm{Li}_3\left(\frac{1-x}{1+x}\right)\log(1+x) + \mathrm{Li}_2(-x)\log 2\log(1-x)\\
&- \frac{19}{24}\log^4(1+x) + 2\log 2\log^3(1+x) + \frac{1}{2}\log(1-x)\log^3(1+x)\\
&+ \frac{7}{6}\log x\log^3(1+x) + \frac{7}{6}\log^3 2\log(1+x) - \frac{1}{2}\log^3(1-x)\log(1+x)\\
&- \frac{7}{4}\log^2 2\log^2(1+x) - \frac{3}{2}\log 2\log(1-x)\log^2(1+x)\\
&- 2\log(1-x)\log x\log^2(1+x) + \frac{17}{24}\pi^2\log^2(1+x)\\
&+ \frac{3}{2}\log 2\log^2(1-x)\log(1+x) - \frac{1}{2}\log^2 2\log(1-x)\log(1+x)
\end{aligned}
$$

$$
\begin{aligned}
&+\frac{3}{2}\log^2(1-x)\log x\log(1+x)-\frac{7}{12}\pi^2\log 2\log(1+x)\\
&-\frac{5}{12}\pi^2\log(1-x)\log(1+x)+\frac{1}{2}\mathrm{Li}_2(-x)^2-\mathrm{Li}_2\left(\frac{1-x}{2}\right)\mathrm{Li}_2(-x)\\
&+\frac{\pi^2}{12}\mathrm{Li}_2(-x)-\frac{1}{2}\mathrm{Li}_4(-x)-\frac{3}{2}\mathrm{Li}_4(x)-\frac{3}{4}\mathrm{Li}_4\left(\frac{4x}{(x+1)^2}\right)\\
&-\mathrm{Li}_4\left(\frac{1}{1+x}\right)-2\mathrm{Li}_4\left(\frac{x}{x+1}\right)+3\mathrm{Li}_4\left(\frac{2x}{x+1}\right)-6\mathrm{Li}_4\left(\frac{1+x}{2}\right)\\
&+6\mathrm{Li}_4\left(\frac{1}{2}\right)+\frac{\pi^4}{90}-\mathrm{Li}_3(-x)\log(1+x)+\frac{17}{8}\zeta_3\log(1+x)\,,
\end{aligned}
$$

$$
\begin{aligned}
\mathrm{H}(0,-1,1,1;x)=&-\frac{1}{2}\mathrm{Li}_2(-x)\log^2(1-x)+\mathrm{Li}_3\left(\frac{1-x}{2}\right)\log(1-x)\\
&+\mathrm{Li}_3(-x)\log(1-x)-\mathrm{Li}_3(x)\log(1-x)-\mathrm{Li}_3\left(\frac{2x}{x-1}\right)\log(1-x)\\
&+\frac{7}{4}\zeta_3\log(1-x)+\frac{19}{96}\log^4(1-x)+\frac{23}{96}\log^4(1+x)\\
&-\frac{7}{12}\log x\log^3(1-x)-\frac{1}{24}\log(1+x)\log^3(1-x)\\
&-\frac{1}{3}\log 2\log^3(1+x)-\frac{1}{4}\log x\log^3(1+x)-\frac{1}{3}\log^3 2\log(1+x)\\
&+\frac{1}{4}\log^2 2\log^2(1-x)-\frac{1}{16}\log^2(1+x)\log^2(1-x)\\
&+\frac{3}{16}\pi^2\log^2(1-x)+\frac{1}{4}\log x\log^2(1+x)\log(1-x)\\
&-\frac{13}{48}\pi^2\log^2(1+x)-\frac{\pi^2}{24}\log(1+x)\log(1-x)+\frac{\pi^2}{6}\log 2\log(1+x)\\
&+\frac{1}{4}\mathrm{Li}_4\left(1-x^2\right)-\frac{1}{4}\mathrm{Li}_4\left(\frac{x^2}{x^2-1}\right)-\mathrm{Li}_4\left(\frac{1-x}{2}\right)-\mathrm{Li}_4(1-x)\\
&-\frac{1}{2}\mathrm{Li}_4(-x)+\frac{1}{2}\mathrm{Li}_4(x)+2\mathrm{Li}_4\left(\frac{x}{x-1}\right)-\mathrm{Li}_4\left(\frac{2x}{x-1}\right)\\
&+2\mathrm{Li}_4\left(\frac{1}{1+x}\right)+2\mathrm{Li}_4\left(\frac{x}{x+1}\right)-2\mathrm{Li}_4\left(\frac{2x}{x+1}\right)+2\mathrm{Li}_4\left(\frac{1+x}{2}\right)\\
&-\mathrm{Li}_4\left(\frac{1}{2}\right)-\frac{\pi^4}{72}-\mathrm{Li}_3(1-x)\log(1-x)-\frac{1}{3}\log 2\log^3(1-x)\\
&-\frac{1}{24}\log^3(1+x)\log(1-x)+\frac{1}{4}\log x\log(1+x)\log^2(1-x)\\
&+\frac{1}{2}\log^2 2\log^2(1+x)+\frac{1}{4}\mathrm{Li}_4\left(\frac{4x}{(x+1)^2}\right)\,,
\end{aligned}
$$

$$
\begin{aligned}
\mathrm{H}(0,0,-1,-1;x)=&-\mathrm{Li}_3(-x)\log(1+x)+\zeta_3\log(1+x)+\frac{1}{12}\log^4(1+x)\\
&-\frac{\pi^2}{12}\log^2(1+x)+\mathrm{Li}_4(-x)+\mathrm{Li}_4\left(\frac{1}{1+x}\right)+\mathrm{Li}_4\left(\frac{x}{x+1}\right)-\frac{\pi^4}{90}
\end{aligned}
$$

$$
\begin{aligned}
&- \frac{1}{6}\log x \log^3(1+x)\,,\\
\mathrm{H}(0,0,-1,1;x) =&\mathrm{Li}_3(-x)\log(1-x) + \frac{3}{4}\zeta_3\log(1-x) + \frac{1}{32}\log^4(1-x) + \frac{23}{96}\log^4(1+x)\\
&- \frac{1}{12}\log x\log^3(1-x) - \frac{1}{24}\log(1+x)\log^3(1-x)\\
&- \frac{1}{3}\log 2\log^3(1+x) - \frac{1}{4}\log x\log^3(1+x) - \frac{1}{3}\log^3 2\log(1+x)\\
&- \frac{1}{16}\log^2(1+x)\log^2(1-x) + \frac{1}{4}\log x\log(1+x)\log^2(1-x)\\
&+ \frac{1}{4}\log x\log^2(1+x)\log(1-x) + \frac{1}{2}\log^2 2\log^2(1+x)\\
&- \frac{\pi^2}{24}\log(1+x)\log(1-x) + \frac{\pi^2}{6}\log 2\log(1+x) + \frac{1}{4}\mathrm{Li}_4\left(1-x^2\right)\\
&- \frac{1}{4}\mathrm{Li}_4\left(\frac{x^2}{x^2-1}\right) - \mathrm{Li}_4(1-x) - \frac{3}{2}\mathrm{Li}_4(-x) + \frac{1}{2}\mathrm{Li}_4(x) + \mathrm{Li}_4\left(\frac{x}{x-1}\right)\\
&+ \frac{1}{4}\mathrm{Li}_4\left(\frac{4x}{(x+1)^2}\right) + 2\mathrm{Li}_4\left(\frac{1}{1+x}\right) + 2\mathrm{Li}_4\left(\frac{x}{x+1}\right) - 2\mathrm{Li}_4\left(\frac{2x}{x+1}\right)\\
&+ 2\mathrm{Li}_4\left(\frac{1+x}{2}\right) - 2\mathrm{Li}_4\left(\frac{1}{2}\right) - \frac{\pi^4}{72} - \frac{1}{24}\log^3(1+x)\log(1-x)\\
&+ \frac{\pi^2}{16}\log^2(1-x) - \frac{13}{48}\pi^2\log^2(1+x)\,,\\
\mathrm{H}(0,0,0,-1;x) =& - \mathrm{Li}_4(-x)\,,\\
\mathrm{H}(0,0,0,1;x) =&\mathrm{Li}_4(x)\,,\\
\mathrm{H}(0,0,1,-1;x) =&\mathrm{Li}_3(x)\log(1+x) + \frac{3}{4}\zeta_3\log(1+x) - \frac{1}{6}\log^4(1+x) + \frac{1}{3}\log 2\log^3(1+x)\\
&+ \frac{1}{6}\log x\log^3(1+x) + \frac{1}{3}\log^3 2\log(1+x) - \frac{1}{2}\log^2 2\log^2(1+x)\\
&- \frac{\pi^2}{6}\log 2\log(1+x) + \frac{1}{2}\mathrm{Li}_4(-x) - \frac{3}{2}\mathrm{Li}_4(x) - \frac{1}{4}\mathrm{Li}_4\left(\frac{4x}{(x+1)^2}\right)\\
&- \mathrm{Li}_4\left(\frac{x}{x+1}\right) + 2\mathrm{Li}_4\left(\frac{2x}{x+1}\right) - 2\mathrm{Li}_4\left(\frac{1+x}{2}\right) + 2\mathrm{Li}_4\left(\frac{1}{2}\right) + \frac{\pi^4}{90}\\
&+ \frac{\pi^2}{6}\log^2(1+x) - \mathrm{Li}_4\left(\frac{1}{1+x}\right)\,,\\
\mathrm{H}(0,1,-1,-1;x) =&\frac{1}{2}\mathrm{Li}_2(x)\log^2(1+x) + \mathrm{Li}_3(-x)\log(1+x) - \mathrm{Li}_3(x)\log(1+x)\\
&- \mathrm{Li}_3\left(\frac{2x}{x-1}\right)\log(1+x) + \mathrm{Li}_3\left(\frac{1}{1+x}\right)\log(1+x)\\
&- \mathrm{Li}_3\left(\frac{1+x}{2}\right)\log(1+x) - \frac{3}{4}\zeta_3\log(1+x) + \frac{1}{6}\log^4(1+x)\\
&- \frac{1}{2}\log(1-x)\log^3(1+x) - \frac{1}{6}\log x\log^3(1+x) - \frac{1}{3}\log^3 2\log(1+x)
\end{aligned}
$$

$$
\begin{aligned}
&+\frac{1}{6}\log^3(1-x)\log(1+x)+\frac{1}{4}\log^2 2\log^2(1+x)\\
&+\log(1-x)\log x\log^2(1+x)-\frac{\pi^2}{8}\log^2(1+x)\\
&-\frac{1}{2}\log^2(1-x)\log x\log(1+x)+\frac{\pi^2}{6}\log 2\log(1+x)\\
&-\frac{1}{2}\mathrm{Li}_4(-x)+\frac{1}{2}\mathrm{Li}_4(x)+\frac{1}{4}\mathrm{Li}_4\left(\frac{4x}{(x+1)^2}\right)+\mathrm{Li}_4\left(\frac{1}{1+x}\right)\\
&+3\mathrm{Li}_4\left(\frac{1+x}{2}\right)-3\mathrm{Li}_4\left(\frac{1}{2}\right)-\frac{\pi^4}{90}-\mathrm{Li}_3\left(\frac{1-x}{1+x}\right)\log(1+x)\\
&-\frac{1}{2}\log 2\log^3(1+x)+\log 2\log(1-x)\log^2(1+x)\\
&-\frac{1}{2}\log 2\log^2(1-x)\log(1+x)+\frac{\pi^2}{6}\log(1-x)\log(1+x)\\
&-\mathrm{Li}_4\left(\frac{2x}{x+1}\right),
\end{aligned}
$$

$$
\begin{aligned}
\mathrm{H}(0,1,-1,1;x)=&-\frac{47}{96}\log^4(1-x)+\log 2\log^3(1-x)+\frac{11}{12}\log x\log^3(1-x)\\
&+\frac{1}{24}\log(1+x)\log^3(1-x)-\frac{1}{4}\log^2 2\log^2(1-x)\\
&-\log 2\log(1+x)\log^2(1-x)-\frac{5}{4}\log x\log(1+x)\log^2(1-x)\\
&-\frac{1}{2}\mathrm{Li}_2\left(\frac{1-x}{2}\right)\log^2(1-x)+\frac{1}{2}\mathrm{Li}_2(-x)\log^2(1-x)\\
&-\frac{17}{48}\pi^2\log^2(1-x)-\frac{1}{6}\log^3 2\log(1-x)+\frac{1}{24}\log^3(1+x)\log(1-x)\\
&-\frac{1}{4}\log x\log^2(1+x)\log(1-x)+\frac{\pi^2}{12}\log 2\log(1-x)\\
&+\frac{1}{2}\log^2 2\log(1+x)\log(1-x)-\frac{\pi^2}{24}\log(1+x)\log(1-x)\\
&+\log 2\,\mathrm{Li}_2(x)\log(1-x)-\log(1+x)\mathrm{Li}_2(x)\log(1-x)\\
&+\mathrm{Li}_3(x)\log(1-x)+3\mathrm{Li}_3\left(\frac{2x}{x-1}\right)\log(1-x)-\mathrm{Li}_3\left(\frac{1}{1+x}\right)\log(1-x)\\
&+\mathrm{Li}_3\left(\frac{1-x}{1+x}\right)\log(1-x)+\mathrm{Li}_3\left(\frac{1+x}{2}\right)\log(1-x)-\frac{29}{8}\zeta_3\log(1-x)\\
&-\frac{55}{96}\log^4(1+x)+\log 2\log^3(1+x)+\frac{7}{12}\log x\log^3(1+x)\\
&+\frac{29}{48}\pi^2\log^2(1+x)-\frac{\mathrm{Li}_2(x)^2}{2}-\mathrm{Li}_{2,2}(-1,x)+\mathrm{Li}_{2,2}\left(\frac{1}{2},\frac{2x}{x-1}\right)\\
&+\log^3 2\log(1+x)-\frac{\pi^2}{2}\log 2\log(1+x)-\frac{1}{2}\log^2 2\,\mathrm{Li}_2(x)\\
&+\mathrm{Li}_2(-x)\mathrm{Li}_2(x)+\frac{\pi^2}{12}\mathrm{Li}_2(x)+2\log(1+x)\mathrm{Li}_3(x)+3\mathrm{Li}_4(1-x)
\end{aligned}
$$

$$
\begin{aligned}
&-\frac{1}{2}\mathrm{Li}_4(-x)-\frac{3}{2}\mathrm{Li}_4(x)-2\mathrm{Li}_4\left(\frac{x}{x-1}\right)+3\mathrm{Li}_4\left(\frac{2x}{x-1}\right)\\
&-\frac{3}{4}\mathrm{Li}_4\left(\frac{4x}{(x+1)^2}\right)-4\mathrm{Li}_4\left(\frac{1}{1+x}\right)-4\mathrm{Li}_4\left(\frac{x}{x+1}\right)+6\mathrm{Li}_4\left(\frac{2x}{x+1}\right)\\
&-6\mathrm{Li}_4\left(\frac{1+x}{2}\right)-\frac{1}{4}\mathrm{Li}_4\left(1-x^2\right)+\frac{1}{4}\mathrm{Li}_4\left(\frac{x^2}{x^2-1}\right)+\frac{3}{2}\log(1+x)\zeta_3\\
&+6\mathrm{Li}_4\left(\frac{1}{2}\right)+\frac{\pi^4}{72}+\frac{9}{16}\log^2(1+x)\log^2(1-x)-\frac{1}{2}\mathrm{Li}_2(x)\log^2(1-x)\\
&-\mathrm{Li}_3(-x)\log(1-x)-\frac{3}{2}\log^2 2\log^2(1+x)-\mathrm{Li}_2\left(\frac{1-x}{2}\right)\mathrm{Li}_2(x)\,,
\end{aligned}
$$

$$
\mathrm{H}(0,1,0,-1;x)=-\mathrm{Li}_{2,2}(-1,x)\,,
$$

$$
\begin{aligned}
\mathrm{H}(0,1,0,1;x)=&2\mathrm{Li}_3(x)\log(1-x)-2\zeta_3\log(1-x)-\frac{1}{12}\log^4(1-x)\\
&-\frac{\pi^2}{6}\log^2(1-x)+\frac{\mathrm{Li}_2(x)^2}{2}+2\mathrm{Li}_4(1-x)-2\mathrm{Li}_4(x)\\
&+\frac{1}{3}\log x\log^3(1-x)-2\mathrm{Li}_4\left(\frac{x}{x-1}\right)-\frac{\pi^4}{45}\,,
\end{aligned}
$$

$$
\begin{aligned}
\mathrm{H}(0,1,1,-1;x)=&\mathrm{Li}_{2,2}(-1,x)-\mathrm{Li}_{2,2}\left(\frac{1}{2},\frac{2x}{x-1}\right)+\frac{1}{2}\mathrm{Li}_2\left(\frac{1-x}{2}\right)\log^2(1-x)\\
&-\frac{1}{2}\mathrm{Li}_2(-x)\log^2(1-x)+\frac{1}{2}\mathrm{Li}_2(x)\log^2(1-x)+\frac{1}{2}\mathrm{Li}_2(x)\log^2 2\\
&-\mathrm{Li}_2(x)\log 2\log(1-x)-2\mathrm{Li}_3\left(\frac{2x}{x-1}\right)\log(1-x)\\
&-2\mathrm{Li}_3(x)\log(1+x)+\frac{7}{4}\zeta_3\log(1-x)-\frac{5}{8}\zeta_3\log(1+x)\\
&+\frac{3}{8}\log^4(1+x)-\frac{2}{3}\log 2\log^3(1-x)-\frac{1}{3}\log x\log^3(1-x)\\
&-\frac{2}{3}\log 2\log^3(1+x)-\frac{1}{3}\log x\log^3(1+x)-\frac{2}{3}\log^3 2\log(1+x)\\
&+\frac{1}{2}\log^2 2\log^2(1-x)+\frac{\pi^2}{8}\log^2(1-x)+\log^2 2\log^2(1+x)\\
&+\frac{\pi^2}{12}\log 2\log(1-x)+\frac{\pi^2}{3}\log 2\log(1+x)+\frac{1}{4}\mathrm{Li}_4\left(1-x^2\right)+\frac{1}{2}\mathrm{Li}_2(x)^2\\
&+\mathrm{Li}_2\left(\frac{1-x}{2}\right)\mathrm{Li}_2(x)-\mathrm{Li}_2(-x)\mathrm{Li}_2(x)-\frac{\pi^2}{12}\mathrm{Li}_2(x)+\mathrm{Li}_4\left(\frac{1-x}{2}\right)\\
&-2\mathrm{Li}_4(1-x)+\mathrm{Li}_4(-x)+\mathrm{Li}_4(x)-2\mathrm{Li}_4\left(\frac{2x}{x-1}\right)+\frac{1}{2}\mathrm{Li}_4\left(\frac{4x}{(x+1)^2}\right)\\
&+3\mathrm{Li}_4\left(\frac{1}{1+x}\right)-\frac{1}{2}\mathrm{Li}_4\left(\frac{1-x}{1+x}\right)+\frac{1}{2}\mathrm{Li}_4\left(\frac{x-1}{x+1}\right)+2\mathrm{Li}_4\left(\frac{x}{x+1}\right)\\
&-4\mathrm{Li}_4\left(\frac{2x}{x+1}\right)+4\mathrm{Li}_4\left(\frac{1+x}{2}\right)-5\mathrm{Li}_4\left(\frac{1}{2}\right)-\frac{\pi^4}{288}
\end{aligned}
$$

$$
\begin{aligned}
& - \mathrm{Li}_3(1-x)\log(1+x) + \frac{7}{24}\log^4(1-x) - \frac{1}{6}\log^3 2\log(1-x) \\
& - \frac{3}{8}\pi^2\log^2(1+x)\,, \\
\mathrm{H}(0,1,1,1;x) = & \frac{1}{2}\mathrm{Li}_2(x)\log^2(1-x) + \mathrm{Li}_3(1-x)\log(1-x) + \frac{1}{3}\log x\log^3(1-x) \\
& - \frac{\pi^2}{12}\log^2(1-x) - \mathrm{Li}_4(1-x) + \frac{\pi^4}{90}\,. \qquad \text{(D.5)}
\end{aligned}
$$

Notice that we have actually used the function $\mathrm{Li}_{2,2}$ with three different arguments in the reductions, as these formulae were already available to us. To convert to the basis with $\mathrm{H}(0,1,0,-1;x)$ and $\mathrm{H}(0,1,1,-1;\pm x)$ as basis functions, one has to apply the identities

$$
\mathrm{Li}_{2,2}(-1,x) = -\mathrm{H}(0,1,0,-1;x)\,, \qquad \text{(D.6)}
$$

$$
\begin{aligned}
\mathrm{Li}_{2,2}\left(\frac{1}{2},\frac{2x}{x-1}\right) = & - \mathrm{H}(0,1,1,-1;x) - \mathrm{H}(0,1,0,-1;x) - \log 2\log(1-x)\,\mathrm{Li}_2(x) \\
& + 1/2\,(\log(1-x))^2\,\mathrm{Li}_2(1/2-1/2\,x) - 1/2\,(\log(1-x))^2\,\mathrm{Li}_2(-x) \\
& + 1/2\,(\log 2)^2\,\mathrm{Li}_2(x) - 2\,\log(1+x)\,\mathrm{Li}_3(x) \\
& - 2\,\log(1-x)\,\mathrm{Li}_3\left(\frac{2x}{-1+x}\right) + 1/2\,(\log(1-x))^2\,\mathrm{Li}_2(x) \\
& - \log(1+x)\,\mathrm{Li}_3(1-x) + \mathrm{Li}_2(1/2-1/2\,x)\,\mathrm{Li}_2(x) - \mathrm{Li}_2(-x)\,\mathrm{Li}_2(x) \\
& - 1/12\,\pi^2\mathrm{Li}_2(x) - 1/6\,(\log 2)^3\log(1-x) + 1/2\,(\log 2)^2\,(\log(1-x))^2 \\
& - 2/3\,\log 2\,(\log(1-x))^3 + 1/8\,\pi^2\,(\log(1-x))^2 + 7/4\,\log(1-x)\,\zeta_3 \\
& + 1/3\,\pi^2\log 2\log(1+x) + 1/12\,\pi^2\log 2\log(1-x) + \mathrm{Li}_4(-x) \\
& - 2\,\mathrm{Li}_4\left(\frac{2x}{-1+x}\right) + 1/2\,\mathrm{Li}_4\left(\frac{4x}{(1+x)^2}\right) + 2\,\mathrm{Li}_4\left(\frac{x}{1+x}\right) \\
& - 4\,\mathrm{Li}_4\left(\frac{2x}{1+x}\right) + 4\,\mathrm{Li}_4(1/2+1/2\,x) + 3\,\mathrm{Li}_4\left(\frac{1}{1+x}\right) \\
& - 1/2\,\mathrm{Li}_4\left(\frac{1-x}{1+x}\right) + 1/2\,\mathrm{Li}_4\left(\frac{x-1}{1+x}\right) + 1/4\,\mathrm{Li}_4\left(1-x^2\right) + \mathrm{Li}_4(x) \\
& - 5\,\mathrm{Li}_4(1/2) + \mathrm{Li}_4(1/2-1/2\,x) - 2\,\mathrm{Li}_4(1-x) + 1/2\,(\mathrm{Li}_2(x))^2 \\
& + 3/8\,(\log(1+x))^4 + \frac{7}{24}\,(\log(1-x))^4 - 2/3\,\log 2\,(\log(1+x))^3 \\
& - 1/3\,\log(x)\,(\log(1+x))^3 - 3/8\,\pi^2\,(\log(1+x))^2 - 5/8\,\log(1+x)\,\zeta_3 \\
& - 1/3\,(\log(1-x))^3\log(x) - 2/3\,(\log 2)^3\log(1+x) \\
& + (\log 2)^2\,(\log(1+x))^2 - \frac{1}{288}\,\pi^4\,, \qquad \text{(D.7)}
\end{aligned}
$$

$$
\begin{aligned}
\mathrm{Li}_{2,2}\left(\frac{1}{2},\frac{2x}{x+1}\right) =& -\mathrm{H}(0,1,1,-1,-x)+\mathrm{H}(0,1,0,-1,x)+\frac{7}{16}\,(\log(1+x))^4\\
&+\frac{7}{16}\,(\log(1-x))^4+3\,\mathrm{Li}_4\left(\frac{1}{1-x}\right)-1/2\,\mathrm{Li}_4\left(\frac{1+x}{1-x}\right)\\
&+1/2\,\mathrm{Li}_4\left(-\frac{1+x}{1-x}\right)-2\,\mathrm{Li}_4(1+x)-2\,\mathrm{Li}_4\left(\frac{2x}{1+x}\right)\\
&+1/2\,\mathrm{Li}_4\left(\frac{-4x}{(1-x)^2}\right)+2\,\mathrm{Li}_4\left(\frac{x}{x-1}\right)-4\,\mathrm{Li}_4\left(\frac{2x}{x-1}\right)\\
&+1/2\,(\mathrm{Li}_2(-x))^2-\mathrm{Li}_4(-x)+2\,\mathrm{Li}_4\left(\frac{x}{1+x}\right)+\mathrm{Li}_4(1/2+1/2\,x)\\
&-1/2\,\mathrm{Li}_4\left(\frac{x^2}{x^2-1}\right)+2\,\mathrm{Li}_4\left(\frac{1}{1+x}\right)+3/4\,\mathrm{Li}_4\left(1-x^2\right)-\mathrm{Li}_4(x)\\
&+2\,\mathrm{Li}_4\left(\frac{x}{-1+x}\right)-5\,\mathrm{Li}_4(1/2)+4\,\mathrm{Li}_4(1/2-1/2\,x)-2\,\mathrm{Li}_4(1-x)\\
&-1/2\,(\log(1+x))^2\,\mathrm{Li}_2(x)\\
&+\left(-1/3\,(\log(1-x))^3-1/3\,(\log(1+x))^3\right)\log(-x)\\
&+\left(-1/8\,(\log(1+x))^2-1/4\,\pi^2\right)(\log(1-x))^2\\
&+\left(-1/12\,\pi^2\log(1+x)+\frac{7}{8}\,\zeta_3-1/12\,(\log(1+x))^3\right)\log(1-x)\\
&+\Big(1/3\,\pi^2\log(1-x)+1/12\,\pi^2\log(1+x)-2/3\,(\log(1-x))^3\\
&-2/3\,(\log(1+x))^3\Big)\log 2+\Big(1/2\,\log(1-x)(\log(1+x))^2-1/6\,(\log(1+x))^3\\
&-1/6\,(\log(1-x))^3+1/2\,(\log(1-x))^2\log(1+x)\Big)\log(x)\\
&+(-2/3\,\log(1-x)-1/6\,\log(1+x))(\log 2)^3\\
&+\left(1/2\,(\log(1+x))^2+(\log(1-x))^2\right)(\log 2)^2\\
&-1/12\,(\log(1-x))^3\log(1+x)-1/12\,\pi^2(\log(1+x))^2\\
&+\frac{13}{4}\,\log(1+x)\,\zeta_3+\Big(-1/12\,\pi^2-\log 2\log(1+x)+\mathrm{Li}_2(1/2+1/2\,x)\\
&+1/2\,(\log(1+x))^2+1/2\,(\log 2)^2\Big)\mathrm{Li}_2(-x)\\
&+1/2\,(\log(1+x))^2\,\mathrm{Li}_2(1/2+1/2\,x)-2\,\log(1+x)\,\mathrm{Li}_3\left(\frac{2x}{1+x}\right)\\
&-\log(1-x)\,\mathrm{Li}_3(1+x)+2\,\log(1+x)\,\mathrm{Li}_3(x)-\frac{13}{1440}\,\pi^4\,.
\end{aligned}
\tag{D.8}
$$

Bibliography

[1] J. Verne, *Voyage au centre de la terre*. Hetzel, 1867.

[2] M. E. Peskin and D. V. Schroeder, *An Introduction to Quantum Field Theory*. Westview Press, 1995.

[3] S. Pokorski, *Gauge field theories*, vol. 136. Cambridge University Press, 2000.

[4] M. Srednicki, *Quantum field theory*. Cambridge University Press, 2007.

[5] S. Weinberg, *The quantum theory of fields: Foundations*, vol. 1. Cambridge university press, 1995.

[6] S. Weinberg, *The quantum theory of fields: Modern applications*, vol. 2. Cambridge university press, 1996.

[7] H. Georgi, "Weak interactions." http://www.people.fas.harvard.edu/~hgeorgi/weak.pdf.

[8] R. K. Ellis, W. J. Stirling, and B. R. Webber, *QCD and collider physics*, vol. 8. Cambridge University Press, 2003.

[9] F. Halzen and A. D. Martin, *Quarks and leptons: an introductory course in modern particle physics*. John Wiley and Sons, New York, NY, 1984.

[10] G. Dissertori, I. G. Knowles, and M. Schmelling, *Quantum chromodynamics: high energy experiments and theory*, vol. 70. Clarendon Press, 2003.

[11] A. G. Grozin, *Lectures on QED and QCD: Practical Calculations and Renormalization of One-and Multi-loop Feynman Diagrams*. World Scientific, 2007.

[12] A. Zee, *Quantum field theory in a nutshell*. Princeton University Press, 2003.

[13] Y. Nambu and G. Jona-Lasinio, *Dynamical Model of Elementary Particles Based on an Analogy with Superconductivity. 1.*, *Phys.Rev.* **122** (1961) 345–358.

[14] J. Goldstone, *Field Theories with Superconductor Solutions*, *Nuovo Cim.* **19** (1961) 154–164.

[15] F. Englert and R. Brout, *Broken Symmetry and the Mass of Gauge Vector Mesons*, *Phys.Rev.Lett.* **13** (1964) 321–323.

[16] P. W. Higgs, *Broken symmetries, massless particles and gauge fields*, *Phys.Lett.* **12** (1964) 132–133.

[17] P. W. Higgs, *Broken Symmetries and the Masses of Gauge Bosons*, *Phys.Rev.Lett.* **13** (1964) 508–509.

[18] G. Guralnik, C. Hagen, and T. Kibble, *Global Conservation Laws and Massless Particles*, *Phys.Rev.Lett.* **13** (1964) 585–587.

[19] P. W. Higgs, *Spontaneous Symmetry Breakdown without Massless Bosons*, *Phys.Rev.* **145** (1966) 1156–1163.

[20] T. Kibble, *Symmetry breaking in nonAbelian gauge theories*, *Phys.Rev.* **155** (1967) 1554–1561.

[21] S. Glashow, *Partial Symmetries of Weak Interactions*, *Nucl.Phys.* **22** (1961) 579–588.

[22] S. Weinberg, *A Model of Leptons*, *Phys.Rev.Lett.* **19** (1967) 1264–1266.

[23] A. Salam, *Weak and Electromagnetic Interactions*, *Conf.Proc.* **C680519** (1968) 367–377.

[24] **CMS Collaboration** Collaboration, S. Chatrchyan et al., *Observation of a new boson at a mass of 125 GeV with the CMS experiment at the LHC*, *Phys.Lett.* **B716** (2012) 30–61, [`arXiv:1207.7235`].

[25] **ATLAS Collaboration** Collaboration, G. Aad et al., *Observation of a new particle in the search for the Standard Model Higgs boson with the ATLAS detector at the LHC*, *Phys.Lett.* **B716** (2012) 1–29, [`arXiv:1207.7214`].

[26] **CMS Collaboration** Collaboration, S. Chatrchyan et al., *Observation of a new boson with mass near 125 GeV in pp collisions at sqrt(s) = 7 and 8 TeV*, `arXiv:1303.4571`.

[27] T. Kinoshita, *Mass singularities of Feynman amplitudes*, *J.Math.Phys.* **3** (1962) 650–677.

[28] T. Lee and M. Nauenberg, *Degenerate Systems and Mass Singularities*, *Phys.Rev.* **133** (1964) B1549–B1562.

[29] W. Pauli and F. Villars, *On the Invariant regularization in relativistic quantum theory*, *Rev.Mod.Phys.* **21** (1949) 434–444.

[30] G. 't Hooft and M. Veltman, *Regularization and Renormalization of Gauge Fields*, *Nucl.Phys.* **B44** (1972) 189–213.

[31] J. Smith and W. van Neerven, *The Difference between n-dimensional regularization and n-dimensional reduction in QCD*, *Eur.Phys.J.* **C40** (2005) 199–203, [hep-ph/0411357].

[32] J. C. Collins and J. J. C. Collins, *Renormalization.* Cambridge University Press, 1986.

[33] O. Tarasov, A. Vladimirov, and A. Y. Zharkov, *The Gell-Mann-Low Function of QCD in the Three Loop Approximation*, *Phys.Lett.* **B93** (1980) 429–432.

[34] S. Larin and J. Vermaseren, *The Three loop QCD Beta function and anomalous dimensions*, *Phys.Lett.* **B303** (1993) 334–336, [hep-ph/9302208].

[35] D. Gross and F. Wilczek, *Ultraviolet Behavior of Nonabelian Gauge Theories*, *Phys.Rev.Lett.* **30** (1973) 1343–1346.

[36] H. D. Politzer, *Reliable Perturbative Results for Strong Interactions?*, *Phys.Rev.Lett.* **30** (1973) 1346–1349.

[37] S. Bethke, *World Summary of α_s (2012)*, *Nucl.Phys.Proc.Suppl.* **234** (2013) 229–234, [arXiv:1210.0325].

[38] **Particle Data Group** Collaboration, J. Beringer et al., *Review of particle physics*, *Phys. Rev. D* **86** (Jul, 2012) 010001.

[39] H.-W. Lin, *Review of Baryon Spectroscopy in Lattice QCD*, *Chin.J.Phys.* **49** (2011) 827, [arXiv:1106.1608].

[40] J. C. Collins, D. E. Soper, and G. F. Sterman, *Factorization of Hard Processes in QCD*, *Adv.Ser.Direct.High Energy Phys.* **5** (1988) 1–91, [hep-ph/0409313].

[41] V. Gribov and L. Lipatov, *Deep inelastic e p scattering in perturbation theory*, *Sov.J.Nucl.Phys.* **15** (1972) 438–450.

[42] Y. L. Dokshitzer, *Calculation of the Structure Functions for Deep Inelastic Scattering and e+ e- Annihilation by Perturbation Theory in Quantum Chromodynamics.*, *Sov.Phys.JETP* **46** (1977) 641–653.

[43] G. Altarelli and G. Parisi, *Asymptotic Freedom in Parton Language*, *Nucl.Phys.* **B126** (1977) 298.

[44] **CMS Collaboration** Collaboration, S. Chatrchyan et al., *Search for the standard model Higgs boson produced in association with W and Z bosons in pp collisions at $\sqrt{s} = 7$ TeV*, *JHEP* **1211** (2012) 088, [`arXiv:1209.3937`].

[45] J. R. Ellis, M. K. Gaillard, and D. V. Nanopoulos, *A Phenomenological Profile of the Higgs Boson*, *Nucl.Phys.* **B106** (1976) 292.

[46] F. Wilczek, *Decays of Heavy Vector Mesons Into Higgs Particles*, *Phys.Rev.Lett.* **39** (1977) 1304.

[47] H. Georgi, S. Glashow, M. Machacek, and D. V. Nanopoulos, *Higgs Bosons from Two Gluon Annihilation in Proton Proton Collisions*, *Phys.Rev.Lett.* **40** (1978) 692.

[48] S. Dawson, *Radiative corrections to Higgs boson production*, *Nucl.Phys.* **B359** (1991) 283–300.

[49] A. Djouadi, M. Spira, and P. Zerwas, *Production of Higgs bosons in proton colliders: QCD corrections*, *Phys.Lett.* **B264** (1991) 440–446.

[50] M. Spira, A. Djouadi, D. Graudenz, and P. Zerwas, *Higgs boson production at the LHC*, *Nucl.Phys.* **B453** (1995) 17–82, [`hep-ph/9504378`].

[51] R. Harlander and P. Kant, *Higgs production and decay: Analytic results at next-to-leading order QCD*, *JHEP* **0512** (2005) 015, [`hep-ph/0509189`].

[52] U. Aglietti, R. Bonciani, G. Degrassi, and A. Vicini, *Analytic Results for Virtual QCD Corrections to Higgs Production and Decay*, *JHEP* **0701** (2007) 021, [`hep-ph/0611266`].

[53] C. Anastasiou, S. Beerli, S. Bucherer, A. Daleo, and Z. Kunszt, *Two-loop amplitudes and master integrals for the production of a Higgs boson via a massive quark and a scalar-quark loop*, *JHEP* **0701** (2007) 082, [`hep-ph/0611236`].

[54] S. Catani, D. de Florian, and M. Grazzini, *Higgs production in hadron collisions: Soft and virtual QCD corrections at NNLO*, *JHEP* **0105** (2001) 025, [hep-ph/0102227].

[55] R. V. Harlander and W. B. Kilgore, *Next-to-next-to-leading order Higgs production at hadron colliders*, *Phys.Rev.Lett.* **88** (2002) 201801, [hep-ph/0201206].

[56] C. Anastasiou and K. Melnikov, *Higgs boson production at hadron colliders in NNLO QCD*, *Nucl.Phys.* **B646** (2002) 220–256, [hep-ph/0207004].

[57] V. Ravindran, J. Smith, and W. L. van Neerven, *NNLO corrections to the total cross-section for Higgs boson production in hadron hadron collisions*, *Nucl.Phys.* **B665** (2003) 325–366, [hep-ph/0302135].

[58] S. Actis, G. Passarino, C. Sturm, and S. Uccirati, *NLO Electroweak Corrections to Higgs Boson Production at Hadron Colliders*, *Phys.Lett.* **B670** (2008) 12–17, [arXiv:0809.1301].

[59] C. Anastasiou, R. Boughezal, and F. Petriello, *Mixed QCD-electroweak corrections to Higgs boson production in gluon fusion*, *JHEP* **0904** (2009) 003, [arXiv:0811.3458].

[60] R. V. Harlander and K. J. Ozeren, *Finite top mass effects for hadronic Higgs production at next-to-next-to-leading order*, *JHEP* **0911** (2009) 088, [arXiv:0909.3420].

[61] A. Pak, M. Rogal, and M. Steinhauser, *Finite top quark mass effects in NNLO Higgs boson production at LHC*, *JHEP* **1002** (2010) 025, [arXiv:0911.4662].

[62] S. Catani, D. de Florian, M. Grazzini, and P. Nason, *Soft gluon resummation for Higgs boson production at hadron colliders*, *JHEP* **0307** (2003) 028, [hep-ph/0306211].

[63] V. Ahrens, T. Becher, M. Neubert, and L. L. Yang, *Renormalization-Group Improved Prediction for Higgs Production at Hadron Colliders*, *Eur.Phys.J.* **C62** (2009) 333–353, [arXiv:0809.4283].

[64] C. Anastasiou, S. Buehler, F. Herzog, and A. Lazopoulos, *Total cross-section for Higgs boson hadroproduction with anomalous Standard Model interactions*, *JHEP* **1112** (2011) 058, [arXiv:1107.0683].

[65] G. Giudice, C. Grojean, A. Pomarol, and R. Rattazzi, *The Strongly-Interacting Light Higgs*, *JHEP* **0706** (2007) 045, [hep-ph/0703164].

[66] A. Denner, S. Dittmaier, M. Roth, and D. Wackeroth, *Predictions for all processes e+ e- —> 4 fermions + gamma*, *Nucl.Phys.* **B560** (1999) 33–65, [hep-ph/9904472].

[67] A. Denner, S. Dittmaier, M. Roth, and L. Wieders, *Electroweak corrections to charged-current e+ e- —> 4 fermion processes: Technical details and further results*, *Nucl.Phys.* **B724** (2005) 247–294, [hep-ph/0505042].

[68] G. Passarino, C. Sturm, and S. Uccirati, *Higgs Pseudo-Observables, Second Riemann Sheet and All That*, *Nucl.Phys.* **B834** (2010) 77–115, [arXiv:1001.3360].

[69] U. Aglietti, R. Bonciani, G. Degrassi, and A. Vicini, *Two loop light fermion contribution to Higgs production and decays*, *Phys.Lett.* **B595** (2004) 432–441, [hep-ph/0404071].

[70] R. Bonciani, G. Degrassi, and A. Vicini, *On the Generalized Harmonic Polylogarithms of One Complex Variable*, *Comput.Phys.Commun.* **182** (2011) 1253–1264, [arXiv:1007.1891].

[71] G. Degrassi and F. Maltoni, *Two-loop electroweak corrections to Higgs production at hadron colliders*, *Phys.Lett.* **B600** (2004) 255–260, [hep-ph/0407249].

[72] S. Actis, G. Passarino, C. Sturm, and S. Uccirati, *NNLO Computational Techniques: The Cases H —> gamma gamma and H —> g g*, *Nucl.Phys.* **B811** (2009) 182–273, [arXiv:0809.3667].

[73] W.-Y. Keung and F. J. Petriello, *Electroweak and finite quark-mass effects on the Higgs boson transverse momentum distribution*, *Phys.Rev.* **D80** (2009) 013007, [arXiv:0905.2775].

[74] O. Brein, *Electroweak and Bottom Quark Contributions to Higgs Boson plus Jet Production*, *Phys.Rev.* **D81** (2010) 093006, [arXiv:1003.4438].

[75] M. A. Shifman, A. Vainshtein, M. Voloshin, and V. I. Zakharov, *Low-Energy Theorems for Higgs Boson Couplings to Photons*, *Sov.J.Nucl.Phys.* **30** (1979) 711–716.

[76] K. Chetyrkin, V. Spiridonov, and S. Gorishnii, *Wilson expansion for correlators of vector currents at the two loop level: Dimension four operators*, *Phys.Lett.* **B160** (1985) 149–153.

[77] K. Chetyrkin, B. A. Kniehl, and M. Steinhauser, *Decoupling relations to O (alpha-s**3) and their connection to low-energy theorems*, *Nucl.Phys.* **B510** (1998) 61–87, [`hep-ph/9708255`].

[78] Y. Schroder and M. Steinhauser, *Four-loop decoupling relations for the strong coupling*, *JHEP* **0601** (2006) 051, [`hep-ph/0512058`].

[79] A. Pak, M. Steinhauser, and N. Zerf, *Towards Higgs boson production in gluon fusion to NNLO in the MSSM*, *Eur.Phys.J.* **C71** (2011) 1602, [`arXiv:1012.0639`].

[80] C. Anastasiou, R. Boughezal, and E. Furlan, *The NNLO gluon fusion Higgs production cross-section with many heavy quarks*, *JHEP* **1006** (2010) 101, [`arXiv:1003.4677`].

[81] E. Furlan, *Gluon-fusion Higgs production at NNLO for a non-standard Higgs sector*, *JHEP* **1110** (2011) 115, [`arXiv:1106.4024`].

[82] M. Steinhauser, *Results and techniques of multiloop calculations*, *Phys.Rept.* **364** (2002) 247–357, [`hep-ph/0201075`].

[83] S. Buehler and A. Lazopoulos, *Scale dependence and collinear subtraction terms for Higgs production in gluon fusion at N3LO*, `arXiv:1306.2223`.

[84] T. T. N. Phenomina and D. C. Higgs Working Group), CDF Collaboration, *Combined CDF and D0 Upper Limits on Standard Model Higgs Boson Production with up to 8.6 fb-1 of Data*, `arXiv:1107.5518`.

[85] C. Collaboration, *SM Higgs Combination 2011*, .

[86] A. Collaboration, *Combination of the Searches for the Higgs Boson in 1 fb-1 of Data Taken with the ATLAS Detector at 7 TeV Center-of-Mass Energy*, .

[87] S. Goria, G. Passarino, and D. Rosco, *The Higgs Boson Lineshape*, *Nucl.Phys.* **B864** (2012) 530–579, [`arXiv:1112.5517`].

[88] S. Dittmaier, S. Dittmaier, C. Mariotti, G. Passarino, R. Tanaka, et al., *Handbook of LHC Higgs Cross Sections: 2. Differential Distributions*, `arXiv:1201.3084`.

[89] A. Djouadi, J. Kalinowski, and M. Spira, *HDECAY: A Program for Higgs boson decays in the standard model and its supersymmetric extension*, *Comput.Phys.Commun.* **108** (1998) 56–74, [hep-ph/9704448].

[90] M. H. Seymour, *The Higgs boson line shape and perturbative unitarity*, *Phys.Lett.* **B354** (1995) 409–414, [hep-ph/9505211].

[91] J. M. Campbell, R. K. Ellis, and C. Williams, *Gluon-Gluon Contributions to W+ W- Production and Higgs Interference Effects*, *JHEP* **1110** (2011) 005, [arXiv:1107.5569].

[92] T. Binoth, M. Ciccolini, N. Kauer, and M. Kramer, *Gluon-induced W-boson pair production at the LHC*, *JHEP* **0612** (2006) 046, [hep-ph/0611170].

[93] N. Kauer and G. Passarino, *Inadequacy of zero-width approximation for a light Higgs boson signal*, *JHEP* **1208** (2012) 116, [arXiv:1206.4803].

[94] E. N. Argyres, W. Beenakker, G. J. van Oldenborgh, A. Denner, S. Dittmaier, et al., *Stable calculations for unstable particles: Restoring gauge invariance*, *Phys.Lett.* **B358** (1995) 339–346, [hep-ph/9507216].

[95] S. P. Martin, *A Supersymmetry primer*, hep-ph/9709356.

[96] F. Maltoni, Z. Sullivan, and S. Willenbrock, *Higgs-boson production via bottom-quark fusion*, *Phys.Rev.* **D67** (2003) 093005, [hep-ph/0301033].

[97] E. Boos and T. Plehn, *Higgs boson production induced by bottom quarks*, *Phys.Rev.* **D69** (2004) 094005, [hep-ph/0304034].

[98] T. Plehn, *Charged Higgs boson production in bottom gluon fusion*, *Phys.Rev.* **D67** (2003) 014018, [hep-ph/0206121].

[99] R. Harlander, M. Kramer, and M. Schumacher, *Bottom-quark associated Higgs-boson production: reconciling the four- and five-flavour scheme approach*, arXiv:1112.3478.

[100] F. Maltoni, G. Ridolfi, and M. Ubiali, *b-initiated processes at the LHC: a reappraisal*, *JHEP* **1207** (2012) 022, [arXiv:1203.6393].

[101] R. V. Harlander and W. B. Kilgore, *Higgs boson production in bottom quark fusion at next-to-next-to leading order*, *Phys.Rev.* **D68** (2003) 013001, [hep-ph/0304035].

[102] T. Hahn, *CUBA: A Library for multidimensional numerical integration*, *Comput.Phys.Commun.* **168** (2005) 78–95, [hep-ph/0404043].

[103] A. van Hameren, *OneLOop: For the evaluation of one-loop scalar functions*, *Comput.Phys.Commun.* **182** (2011) 2427–2438, [arXiv:1007.4716].

[104] A. van Hameren, C. Papadopoulos, and R. Pittau, *Automated one-loop calculations: A Proof of concept*, *JHEP* **0909** (2009) 106, [arXiv:0903.4665].

[105] M. Whalley, D. Bourilkov, and R. Group, *The Les Houches accord PDFs (LHAPDF) and LHAGLUE*, hep-ph/0508110.

[106] A. Martin, W. Stirling, R. Thorne, and G. Watt, *Parton distributions for the LHC*, *Eur.Phys.J.* **C63** (2009) 189–285, [arXiv:0901.0002].

[107] S. Alekhin, J. Blumlein, S. Klein, and S. Moch, *The 3, 4, and 5-flavor NNLO Parton from Deep-Inelastic-Scattering Data and at Hadron Colliders*, *Phys.Rev.* **D81** (2010) 014032, [arXiv:0908.2766].

[108] P. Jimenez-Delgado and E. Reya, *Variable Flavor Number Parton Distributions and Weak Gauge and Higgs Boson Production at Hadron Colliders at NNLO of QCD*, *Phys.Rev.* **D80** (2009) 114011, [arXiv:0909.1711].

[109] S. Alekhin, J. Blumlein, and S. Moch, *Parton Distribution Functions and Benchmark Cross Sections at NNLO*, *Phys.Rev.* **D86** (2012) 054009, [arXiv:1202.2281].

[110] R. D. Ball et al., *Unbiased global determination of parton distributions and their uncertainties at NNLO and at LO*, *Nucl.Phys.* **B855** (2012) 153–221, [arXiv:1107.2652].

[111] J. Gao, M. Guzzi, J. Huston, H.-L. Lai, Z. Li, et al., *The CT10 NNLO Global Analysis of QCD*, arXiv:1302.6246.

[112] R. D. Ball, V. Bertone, S. Carrazza, C. S. Deans, L. Del Debbio, et al., *Parton distributions with LHC data*, *Nucl.Phys.* **B867** (2013) 244–289, [arXiv:1207.1303].

[113] L. C. Maximon, *The dilogarithm function for complex argument*, *Proceedings of the Royal Society of London. Series A: Mathematical, Physical and Engineering Sciences* **459** (2003), no. 2039 2807–2819.

[114] W. Spence, *Mathematical essays by the late william spence, esq*, *Edinburgh: Oliver and Boyd* (1820).

[115] N. Nielsen, *Der Eulersche Dilogarithmus und seine Verallgemeinerungen.* W. Engelmann in Leipzig in Komm., 1909.

[116] E. Remiddi and J. Vermaseren, *Harmonic polylogarithms*, *Int.J.Mod.Phys.* **A15** (2000) 725–754, [hep-ph/9905237].

[117] T. Gehrmann and E. Remiddi, *Two loop master integrals for gamma* –> 3 jets: The Nonplanar topologies*, *Nucl.Phys.* **B601** (2001) 287–317, [hep-ph/0101124].

[118] T. Gehrmann and E. Remiddi, *Numerical evaluation of two-dimensional harmonic polylogarithms*, *Comput.Phys.Commun.* **144** (2002) 200–223, [hep-ph/0111255].

[119] J. Ablinger, J. Blumlein, and C. Schneider, *Harmonic Sums and Polylogarithms Generated by Cyclotomic Polynomials*, *J.Math.Phys.* **52** (2011) 102301, [arXiv:1105.6063].

[120] A. Goncharov, *Multiple ζ-numbers, hyperlogarithms and mixed tate motives*, *Preprint MSRI* (1993) 058–93.

[121] A. B. Goncharov, *Multiple polylogarithms, cyclotomy and modular complexes*, *Math.Res.Lett.* **5** (1998) 497–516, [arXiv:1105.2076].

[122] A. B. Goncharov, *Multiple polylogarithms and mixed tate motives*, *arXiv preprint math/0103059* (2001).

[123] T. Gehrmann and E. Remiddi, *Numerical evaluation of harmonic polylogarithms*, *Comput.Phys.Commun.* **141** (2001) 296–312, [hep-ph/0107173].

[124] D. Maitre, *HPL, a mathematica implementation of the harmonic polylogarithms*, *Comput.Phys.Commun.* **174** (2006) 222–240, [hep-ph/0507152].

[125] D. Maitre, *Extension of HPL to complex arguments*, *Comput.Phys.Commun.* **183** (2012) 846, [hep-ph/0703052].

[126] J. Vollinga and S. Weinzierl, *Numerical evaluation of multiple polylogarithms*, *Comput.Phys.Commun.* **167** (2005) 177, [hep-ph/0410259].

[127] G. A.B., *A simple construction of Grassmannian polylogarithms*, arXiv:0908.2238.

[128] A. B. Goncharov, M. Spradlin, C. Vergu, and A. Volovich, *Classical Polylogarithms for Amplitudes and Wilson Loops*, *Phys.Rev.Lett.* **105** (2010) 151605, [arXiv:1006.5703].

[129] C. Duhr, H. Gangl, and J. R. Rhodes, *From polygons and symbols to polylogarithmic functions*, *JHEP* **1210** (2012) 075, [arXiv:1110.0458].

[130] C. Duhr, *Hopf algebras, coproducts and symbols: an application to Higgs boson amplitudes*, *JHEP* **1208** (2012) 043, [arXiv:1203.0454].

[131] A. Kotikov and L. Lipatov, *NLO corrections to the BFKL equation in QCD and in supersymmetric gauge theories*, *Nucl.Phys.* **B582** (2000) 19–43, [hep-ph/0004008].

[132] G. 't Hooft and M. Veltman, *Scalar one-loop integrals*, *Nuclear Physics B* **153** (1979), no. 0 365 – 401.

[133] L. Lewin, *Polylogarithms and associated functions.* North Holland Amsterdam, 1981.

[134] H. Cohen, L. Lewin, and D. Zagier, *A sixteenth-order polylogarithm ladder*, *Experimental Mathematics* **1** (1992), no. 1 25–34.

[135] S. Buehler and C. Duhr, *CHAPLIN - Complex Harmonic Polylogarithms in Fortran*, arXiv:1106.5739.

[136] C. Anastasiou, F. Herzog, and A. Lazopoulos, *The Fully differential decay rate of a Higgs boson to bottom-quarks at NNLO in QCD*, *JHEP* **1203** (2012) 035, [arXiv:1110.2368].

[137] A. Gehrmann-De Ridder, E. Glover, and J. Pires, *Real-Virtual corrections for gluon scattering at NNLO*, *JHEP* **1202** (2012) 141, [arXiv:1112.3613].

[138] S. Buehler, F. Herzog, A. Lazopoulos, and R. Mueller, *The Fully differential hadronic production of a Higgs boson via bottom quark fusion at NNLO*, *JHEP* **1207** (2012) 115, [arXiv:1204.4415].

[139] C. Anastasiou, K. Melnikov, and F. Petriello, *Fully differential Higgs boson production and the di-photon signal through next-to-next-to-leading order*, *Nucl.Phys.* **B724** (2005) 197–246, [hep-ph/0501130].

[140] M. Botje, J. Butterworth, A. Cooper-Sarkar, A. de Roeck, J. Feltesse, et al., *The PDF4LHC Working Group Interim Recommendations*, arXiv:1101.0538.

[141] S. Forte and G. Watt, *Progress in the Determination of the Partonic Structure of the Proton*, arXiv:1301.6754.

[142] C. Anastasiou, S. Buehler, E. Furlan, F. Herzog, and A. Lazopoulos, *Higgs production cross-section in a Standard Model with four generations at the LHC*, *Phys.Lett.* **B702** (2011) 224–227, [arXiv:1103.3645].

[143] **ATLAS Collaboration** Collaboration, G. Aad et al., *Search for pair-produced heavy quarks decaying to Wq in the two-lepton channel at $\sqrt{s} = 7$ TeV with the ATLAS detector*, *Phys.Rev.* **D86** (2012) 012007, [arXiv:1202.3389].

[144] **ATLAS Collaboration** Collaboration, G. Aad et al., *Search for pair production of a heavy up-type quark decaying to a W boson and a b quark in the lepton+jets channel with the ATLAS detector*, *Phys.Rev.Lett.* **108** (2012) 261802, [arXiv:1202.3076].

[145] **CMS Collaboration** Collaboration, S. Chatrchyan et al., *Search for heavy, top-like quark pair production in the dilepton final state in pp collisions at $\sqrt{s} = 7$ TeV*, *Phys.Lett.* **B716** (2012) 103–121, [arXiv:1203.5410].

[146] **CMS Collaboration** Collaboration, S. Chatrchyan et al., *Search for heavy bottom-like quarks in 4.9 inverse femtobarns of pp collisions at $\sqrt{s} = 7$ TeV*, *JHEP* **1205** (2012) 123, [arXiv:1204.1088].

[147] **CMS Collaboration** Collaboration, S. Chatrchyan et al., *Search for heavy quarks decaying into a top quark and a W or Z boson using lepton + jets events in pp collisions at $\sqrt{s} = 7$ TeV*, *JHEP* **1301** (2013) 154, [arXiv:1210.7471].

[148] **CMS Collaboration** Collaboration, S. Chatrchyan et al., *Searches for Higgs bosons in pp collisions at sqrt(s) = 7 and 8 TeV in the context of four-generation and fermiophobic models*, arXiv:1302.1764.

[149] G. D. Kribs, T. Plehn, M. Spannowsky, and T. M. Tait, *Four generations and Higgs physics*, *Phys.Rev.* **D76** (2007) 075016, [arXiv:0706.3718].

[150] A. Denner, S. Dittmaier, A. Muck, G. Passarino, M. Spira, et al., *Higgs Production and Decay with a Fourth Standard-Model-Like Fermion Generation*, *Eur.Phys.J.* **C72** (2012) 1992, [arXiv:1111.6395].

[151] T. Lee, *A Theory of Spontaneous T Violation*, *Phys.Rev.* **D8** (1973) 1226–1239.

[152] G. Belanger, B. Dumont, U. Ellwanger, J. Gunion, and S. Kraml, *Global fit to Higgs signal strengths and couplings and implications for extended Higgs sectors*, `arXiv:1306.2941`.

[153] S. Moch, J. Vermaseren, and A. Vogt, *Three-loop results for quark and gluon form-factors*, *Phys.Lett.* **B625** (2005) 245–252, [`hep-ph/0508055`].

[154] P. Baikov, K. Chetyrkin, A. Smirnov, V. Smirnov, and M. Steinhauser, *Quark and gluon form factors to three loops*, *Phys.Rev.Lett.* **102** (2009) 212002, [`arXiv:0902.3519`].

[155] R. Lee, A. Smirnov, and V. Smirnov, *Analytic Results for Massless Three-Loop Form Factors*, *JHEP* **1004** (2010) 020, [`arXiv:1001.2887`].

[156] T. Gehrmann, E. Glover, T. Huber, N. Ikizlerli, and C. Studerus, *Calculation of the quark and gluon form factors to three loops in QCD*, *JHEP* **1006** (2010) 094, [`arXiv:1004.3653`].

[157] C. Anastasiou, C. Duhr, F. Dulat, and B. Mistlberger, *Soft triple-real radiation for Higgs production at N3LO*, `arXiv:1302.4379`.

[158] C. Anastasiou, S. Buehler, C. Duhr, and F. Herzog, *NNLO phase space master integrals for two-to-one inclusive cross sections in dimensional regularization*, *JHEP* **1211** (2012) 062, [`arXiv:1208.3130`].

[159] S. Weinzierl, *The Art of computing loop integrals*, `hep-ph/0604068`.

[160] T. Gehrmann and E. Remiddi, *Differential equations for two loop four point functions*, *Nucl.Phys.* **B580** (2000) 485–518, [`hep-ph/9912329`].

[161] S. Laporta, *High precision calculation of multiloop Feynman integrals by difference equations*, *Int.J.Mod.Phys.* **A15** (2000) 5087–5159, [`hep-ph/0102033`].

[162] C. Anastasiou and A. Lazopoulos, *Automatic integral reduction for higher order perturbative calculations*, *JHEP* **0407** (2004) 046, [`hep-ph/0404258`].

[163] A. Smirnov, *Algorithm FIRE – Feynman Integral REduction*, *JHEP* **0810** (2008) 107, [`arXiv:0807.3243`].

[164] C. Studerus, *Reduze-Feynman Integral Reduction in C++*, *Comput.Phys.Commun.* **181** (2010) 1293–1300, [`arXiv:0912.2546`].

[165] A. von Manteuffel and C. Studerus, *Reduze 2 - Distributed Feynman Integral Reduction*, `arXiv:1201.4330`.

[166] R. Cutkosky, *Singularities and discontinuities of Feynman amplitudes*, *J.Math.Phys.* **1** (1960) 429–433.

[167] W. van Neerven, *Dimensional regularization of mass and infrared singularities in two loop on-shell vertex functions*, *Nucl.Phys.* **B268** (1986) 453.

[168] Z. Bern, L. J. Dixon, D. C. Dunbar, and D. A. Kosower, *Fusing gauge theory tree amplitudes into loop amplitudes*, *Nucl.Phys.* **B435** (1995) 59–101, [`hep-ph/9409265`].

[169] G. Ossola, C. G. Papadopoulos, and R. Pittau, *Reducing full one-loop amplitudes to scalar integrals at the integrand level*, *Nucl.Phys.* **B763** (2007) 147–169, [`hep-ph/0609007`].

[170] C. Anastasiou, R. Britto, B. Feng, Z. Kunszt, and P. Mastrolia, *D-dimensional unitarity cut method*, *Phys.Lett.* **B645** (2007) 213–216, [`hep-ph/0609191`].

[171] Z. Bern, L. Dixon, F. F. Cordero, S. Hoeche, H. Ita, et al., *Next-to-Leading Order W + 5-Jet Production at the LHC*, `arXiv:1304.1253`.

[172] F. A. Berends and W. Giele, *Recursive Calculations for Processes with n Gluons*, *Nucl.Phys.* **B306** (1988) 759.

[173] R. Britto, F. Cachazo, B. Feng, and E. Witten, *Direct proof of tree-level recursion relation in Yang-Mills theory*, *Phys.Rev.Lett.* **94** (2005) 181602, [`hep-th/0501052`].

[174] P. Baikov and V. A. Smirnov, *Equivalence of recurrence relations for Feynman integrals with the same total number of external and loop momenta*, *Phys.Lett.* **B477** (2000) 367–372, [`hep-ph/0001192`].

[175] C. Anastasiou, L. J. Dixon, and K. Melnikov, *NLO Higgs boson rapidity distributions at hadron colliders*, *Nucl.Phys.Proc.Suppl.* **116** (2003) 193–197, [`hep-ph/0211141`].

[176] C. Anastasiou and K. Melnikov, *Pseudoscalar Higgs boson production at hadron colliders in NNLO QCD*, *Phys.Rev.* **D67** (2003) 037501, [`hep-ph/0208115`].

[177] C. Anastasiou, L. J. Dixon, K. Melnikov, and F. Petriello, *Dilepton rapidity distribution in the Drell-Yan process at NNLO in QCD*, *Phys.Rev.Lett.* **91** (2003) 182002, [hep-ph/0306192].

[178] C. Anastasiou, L. J. Dixon, K. Melnikov, and F. Petriello, *High precision QCD at hadron colliders: Electroweak gauge boson rapidity distributions at NNLO*, *Phys.Rev.* **D69** (2004) 094008, [hep-ph/0312266].

[179] A. Kotikov, *Differential equations method: New technique for massive Feynman diagrams calculation*, *Phys.Lett.* **B254** (1991) 158–164.

[180] Z. Bern, L. J. Dixon, and D. A. Kosower, *Dimensionally regulated pentagon integrals*, *Nucl.Phys.* **B412** (1994) 751–816, [hep-ph/9306240].

[181] J. M. Henn, *Multiloop integrals in dimensional regularization made simple*, arXiv:1304.1806.

[182] I. N. Bronstein and K. A. Semendjajew, *Taschenbuch der Mathematik*. Harri Deutsch Verlag, 2008.

[183] F. Herzog, *QCD Corrections and Non-linear Mappings*. PhD thesis, ETH Zürich, 2012.

[184] C. Duhr, "Polylogtools." Private Communication, 2012.

[185] T. Huber and D. Maitre, *HypExp: A Mathematica package for expanding hypergeometric functions around integer-valued parameters*, *Comput.Phys.Commun.* **175** (2006) 122–144, [hep-ph/0507094].

[186] T. Huber and D. Maitre, *HypExp 2, Expanding Hypergeometric Functions about Half-Integer Parameters*, *Comput.Phys.Commun.* **178** (2008) 755–776, [arXiv:0708.2443].

[187] R. J. Gonsalves, *DIMENSIONALLY REGULARIZED TWO LOOP ON-SHELL QUARK FORM-FACTOR*, *Phys.Rev.* **D28** (1983) 1542.

[188] G. Kramer and B. Lampe, *INTEGRALS FOR TWO LOOP CALCULATIONS IN MASSLESS QCD*, *J.Math.Phys.* **28** (1987) 945.

[189] R. V. Harlander, *Virtual corrections to g g —> H to two loops in the heavy top limit*, *Phys.Lett.* **B492** (2000) 74–80, [hep-ph/0007289].

[190] T. Gehrmann, T. Huber, and D. Maitre, *Two-loop quark and gluon form-factors in dimensional regularisation*, *Phys.Lett.* **B622** (2005) 295–302, [hep-ph/0507061].

[191] S. Moch and A. Vogt, *Higher-order soft corrections to lepton pair and Higgs boson production*, *Phys.Lett.* **B631** (2005) 48–57, [hep-ph/0508265].

[192] R. D. Ball, M. Bonvini, S. Forte, S. Marzani, and G. Ridolfi, *Higgs production in gluon fusion beyond NNLO*, arXiv:1303.3590.

[193] F. I. Olness and D. E. Soper, *Correlated theoretical uncertainties for the one-jet inclusive cross section*, *Phys.Rev.* **D81** (2010) 035018, [arXiv:0907.5052].

[194] C. Anastasiou, F. Herzog, and A. Lazopoulos, *On the factorization of overlapping singularities at NNLO*, *JHEP* **1103** (2011) 038, [arXiv:1011.4867].

[195] S. Catani and M. Seymour, *A General algorithm for calculating jet cross-sections in NLO QCD*, *Nucl.Phys.* **B485** (1997) 291–419, [hep-ph/9605323].

[196] A. Gehrmann-De Ridder, T. Gehrmann, and E. N. Glover, *Antenna subtraction at NNLO*, *JHEP* **0509** (2005) 056, [hep-ph/0505111].

[197] T. Binoth and G. Heinrich, *An Automatized algorithm to compute infrared divergent multiloop integrals*, *Nucl.Phys.* **B585** (2000) 741–759, [hep-ph/0004013].

[198] M. Cacciari, G. P. Salam, and G. Soyez, *The Anti-k(t) jet clustering algorithm*, *JHEP* **0804** (2008) 063, [arXiv:0802.1189].

[199] R. Harlander and M. Wiesemann, *Jet-veto in bottom-quark induced Higgs production at next-to-next-to-leading order*, *JHEP* **1204** (2012) 066, [arXiv:1111.2182].

[200] F. Herzog and A. Lazopoulos, "ehixs." In preparation, 2013.

[201] A. Vogt, S. Moch, and J. Vermaseren, *The Three-loop splitting functions in QCD: The Singlet case*, *Nucl.Phys.* **B691** (2004) 129–181, [hep-ph/0404111].

[202] S. Moch, J. Vermaseren, and A. Vogt, *The Three loop splitting functions in QCD: The Nonsinglet case*, *Nucl.Phys.* **B688** (2004) 101–134, [hep-ph/0403192].

Acknowledgments

A lot of people have supported me a great deal throughout my time as a PhD student, all of whom I am very grateful to. First and foremost, I would like to thank my supervisor, Prof. Babis Anastasiou, for all that he has done for me. He sparked my interest for Quantum field theory in the lecture I took with him way back in 2008, later supervised my master's thesis and then accepted me as a PhD student. I am very grateful for this opportunity you gave me, Babis, and never regretted the decision to work in your group. Also, I would like to point out that I have hardly ever encountered anyone with a better physical intuition or stronger arm-wrestling skills.

Further thanks go to the whole particle theory group at the institute for theoretical physics. I thoroughly enjoyed all professional and private encounters with its members, and I think the great, uncomplicated atmosphere we have always had speaks for the ability of Babis and Aude Gehrmann-de Ridder to choose the right mixture of people for their groups.

Special thanks go to Achilleas for collaboration on many occasions, including extended sessions of "extreme programming" on the hunt for computer bugs, as well as to Franz and Claude who both very patiently answered any question I could think of, and came up with the answer every time. I would also like to thank all of my current and former office mates, Claude, Fede, Franz, Julian, Elisabetta, Ruben and Juan Carlos for bearing with me during the last four years. It has always been a lot of fun sharing office with you guys. Fede in particular made the office a lot cooler both figuratively and literally, with his vast knowledge of progressive music and the portable fan he brought to the office to make hot summer days bearable.

More thanks go to the secretaries of ITP, Beatrix, Denise, Irene, Sandra and Micheline who were always available for questions of administrative nature or a quick chat devoid of any physics topics. I am grateful to Fede, Gabriel, Julian and Romain for proof-reading parts of this thesis, as well. Also, I would like to acknowledge the support of Erich and Mathias with whom I shared the entire experience of studying physics at ETH and the subsequent venture of a PhD thesis in theoretical particle physics. You guys have become very close friends, and I wish you all the best for the future.

Furthermore, I would like to point out all the support and love I have received from my family and friends who were always there to cheer me up when my research was going through difficult times. I consider myself very lucky to have so many wonderful people around me. I am immensely grateful to my parents for their unconditional support over the last twenty-eight years both in emotional and financial matters. All this would never have been possible without you.

Finally, I want to express my gratitude to the person most important to me, my girlfriend Martina. You make me complete, and I certainly would not have stayed so upbeat during frustrating times if it had not been for the love you give me every single day. I love you with all my heart.

Curriculum Vitae

Personal data

Name:	Stephan Andreas Bühler
Date of birth:	May 11, 1985
Nationality:	Swiss, citizen of Uster ZH

Education

2009 - 2013	**ETH Zürich:** Doctoral Studies at the Institute for theoretical physics under the supervision of Prof. C. Anastasiou.
2007 - 2009	**ETH Zürich:** Master's studies of physics. Masters thesis: "Dynamically generated Yukawa couplings" under the supervision of Prof. C. Anastasiou.
2004 - 2007	**ETH Zürich:** Bachelor's studies of physics.
1997 - 2003	**Realgymnasium Rämibühl Zürich:** Matura (Latin & English).
1991 - 1997	Primary school.

Scientific publications

- **S. Buehler** and A. Lazopoulos,
  "Scale dependence and collinear subtraction terms for Higgs production
  in gluon fusion at N3LO"
  arXiv:1306.2223 [hep-ph], submitted to JHEP.

- C. Anastasiou, **S. Buehler**, C. Duhr and F. Herzog,
  "NNLO phase space master integrals for two-to-one inclusive cross sections
  in dimensional regularization,"
  JHEP **1211** (2012) 062, [arXiv:1208.3130 [hep-ph]].

- **S. Buehler**, F. Herzog, A. Lazopoulos and R. Mueller,
  "The Fully differential hadronic production of a Higgs boson via
  bottom quark fusion at NNLO,"
  JHEP **1207** (2012) 115, [arXiv:1204.4415 [hep-ph]].

- C. Anastasiou, **S. Buehler**, F. Herzog and A. Lazopoulos,
  "Inclusive Higgs boson cross-section for the LHC at 8 TeV,"
  JHEP **1204** (2012) 004, [arXiv:1202.3638 [hep-ph]].

- **S. Buehler**,
  "Precise inclusive Higgs predictions using iHixs,"
  PoS RADCOR **2011** (2011) 021, [arXiv:1201.0985 [hep-ph]].

- C. Anastasiou, **S. Buehler**, F. Herzog and A. Lazopoulos,
  "Total cross-section for Higgs boson hadroproduction with
  anomalous Standard Model interactions,"
  JHEP **1112** (2011) 058, [arXiv:1107.0683 [hep-ph]].

- **S. Buehler** and C. Duhr,
  "CHAPLIN - Complex Harmonic Polylogarithms in Fortran,"
  arXiv:1106.5739 [hep-ph].

- C. Anastasiou, **S. Buehler**, E. Furlan, F. Herzog and A. Lazopoulos,
  "Higgs production cross-section in a Standard Model with four generations
  at the LHC,"
  Phys. Lett. B **702** (2011) 224, [arXiv:1103.3645 [hep-ph]].